

Greenhouse gas cycling
in
experimental boreal reservoirs

by

Jason James Venkiteswaran

A thesis
presented to the University of Waterloo
in fulfillment of the
thesis requirement for the degree of
Doctor of Philosophy
in
Earth Sciences

Waterloo, Ontario, Canada, 2008

© Jason James Venkiteswaran 2008

Author's declaration

I hereby declare that I am the sole author of this thesis. This is a true copy of the thesis, including any required final revisions, as accepted by my examiners.

I understand that my thesis may be made electronically available to the public.

Abstract

Hydroelectric reservoirs account for 59% of the installed electricity generating capacity in Canada and 26% in Ontario. Reservoirs also provide irrigation capacity, drinking water, and recreational opportunities. Further, they continue to be built in northern Canada, neighbouring boreal countries, and around the world. Yet given their socio-economic importance, they are understudied with respect to greenhouse gas emissions, nutrient and mercury cycling, and aquatic metabolism.

As one of many electricity generating options, hydroelectricity is viewed as well-tested because of its long history and diverse applications in mega-projects, run-of-the-river dams, and small, local applications. It is also considered renewable from a fuel stand-point because an adequate long-term supply of water is assumed. One of several significant criticisms of hydroelectric development is that reservoirs may be a significant source of greenhouse gases to the atmosphere relative to the amount of electricity produced due to flooding the landscape.

As a result of the dearth of information on reservoir development and both greenhouse gases and aquatic metabolism, a pair of whole-ecosystem reservoir experiments were conducted starting in 1991. Three upland boreal forest reservoirs with differing amounts of pre-flood stored organic carbon were built in northwestern Ontario and flooded for five years. The rates of net greenhouse gas production in these reservoirs were determined by calculating mass budgets for carbon dioxide and methane. Additionally, rates of biological processes were determined by combining the mass budgets with measurements of the stable isotopes of carbon and oxygen.

Assembling mass and isotope-mass budgets required three related projects on gas exchange, methane oxidation, and oxygen isotopes. To estimate the gas exchange coefficient for each of the upland reservoirs, a comparative-methods study was undertaken. Methane oxidation enrichment factors were determined in upland and wetland boreal reservoirs so that the importance of methane oxidation in these ecosystems could be assessed. In order to interpret the diel changes in both oxygen concentrations and their isotopic ratios, a dynamic model was developed. This model, PoRGy, was successfully applied to the upland boreal reservoirs as well as prairie rivers and ponds.

Further, PoRGy was used to understand the interplay between the key parameters that control oxygen concentrations, to compare aquatic ecosystems, to make quantitative estimates of ecosystem metabolism, and to assess the vulnerability of aquatic ecosystems under various environmental stressors.

Carbon isotope-mass budgets were used to conclude that community respiration rates declined quickly in the upland reservoirs and had declined by half over five years. This suggested that the most labile organic carbon is quickly consumed but decomposition continued for the five-year life of the project. Net primary production rates were similar for three years, with a small peak in the second or third year, before declining by half by the fifth year. Together, these results indicated that aquatic metabolism slowed over five years while the reservoirs remained a source of greenhouse gases to the atmosphere each year.

Net methane production was greatest in the third year of flooding then decreasing by about half by the fifth year. Methane ebullition also peaked in the third year and declined by two-thirds by the fifth year. Together, these results indicated that methanogenesis was greatest in the third year of flooding. The flux of methane to the atmosphere grew in importance relative to that of carbon dioxide over the five years of the experiment.

Community respiration and primary production could not be estimated directly from the oxygen isotope-mass budgets since the oxygen respiration enrichment factor remains poorly constrained. Instead, three estimates were made, each based on a different assumption. In general, these estimates suggested that rates of community respiration and primary production decreased slightly for three years and most rapidly in the final two years. The oxygen isotope-mass budgets provided a new method for assessing and constraining community metabolism and greenhouse gas fluxes to the atmosphere.

One of the major hypotheses of the whole-ecosystem reservoir experiments was that pre-flood organic carbon stores less tree boles were positively related to greenhouse gas fluxes. Within the three upland boreal forest reservoirs, this hypothesis did not hold true. Over five years, community respiration in the three reservoirs was within 5% of each other. When methane is included, to assess total greenhouse gas fluxes to the atmosphere, the reservoirs were within 1% of each other. Organic carbon stores were therefore poor short-term predictors of carbon lability and greenhouse gas fluxes.

This research presented two methods for determining biological rates at the whole-ecosystem scale: one using carbon isotopes and one using oxygen isotopes. Temporal evolution of greenhouse gas cycling within the upland reservoirs was different than in the wetland reservoir and should inform how reservoir development is done vis-à-vis the amount of flooded land of each type versus electricity production. Medium-term estimates of greenhouse gas fluxes suggest that upland reservoirs do not have adequate pre-flood organic

carbon stores to sustain elevated levels of decomposition the way wetlands do. The strong evidence of continued production of dissolved organic carbon in the upland reservoirs should concern operators of municipal drinking water reservoirs since elevated dissolved organic carbon can make disinfection difficult.

Reservoir modellers, who use decomposition to drive mercury methylation, now have real-world data to use when ‘calibrating’ their models. This research clearly demonstrates that as a direct result of flooding both boreal uplands and wetlands, these ecosystems changed from greenhouse gas sinks to net sources of greenhouse gases, especially methane, to the atmosphere. Further, the decomposition of flooded organic carbon in the upland reservoirs—carbon that was fixed from the atmosphere over just 20 years—was the source of the carbon dioxide and methane flux from those reservoirs to the atmosphere.

Acknowledgements

The considered advice and scientific insights of my advisor Sherry Schiff are appreciatively acknowledged. My research questions, manuscripts, and thesis have all been significantly improved by her knowledge and experience.

I am grateful to the principal investigators of both FLUDEX and ELARP for having proposed, secured funding for, and executed both of these whole-ecosystems experiments. Further, many principal investigators have offered encouragement and helpful advice on the research strategies employed in this thesis. The staff at the Experimental Lakes Area always provided an excellent place in which to conduct research by their eagerness to share ideas, advice, and data. This is particularly true of Marnie Potter who has fed a generation of graduate students, Ken Beaty whose ability to measure and predict the hydrology of even the oddest catchment is impressive, and Mark Lyng whose equipment and willingness to collect hundreds of lake samples helped me complete projects not even part of this thesis.

Without the patient assistance of my brother Kevin, there would have been little chance that the basic model presented in Chapter 4 could have been successfully ported to MATLAB. The interplay of the different community metabolism variables and concepts of co-constraining became clear after watching the MATLAB-based model fit the field data.

Financial support for the research in this thesis was provided by the Natural Sciences and Engineering Research Council of Canada through Discovery and Strategic Grants, the Canadian Foundation for Climate and Atmospheric Sciences, Environment Canada's Science Horizons program, the Centre for Research in Earth and Space Technology, and the Climate Change Action Fund. Operational funding for FLUDEX reservoirs was provided by Fisheries and Oceans Canada, Manitoba Hydro, and Hydro-Québec. Scholarship and bursary funding was awarded by the Ontario Graduate Scholarship program and the University of Waterloo. The support of all funding agencies is appreciated.

The depth of patience exhibited by my spouse is lovingly confessed.

Dedication

To my darlings, who never fail

Contents

List of Tables	xv
List of Figures	xvii
1 Introduction	1
1.1 A brief history of reservoir research	1
1.2 Experimental Lakes Area Reservoir Project: ELARP	4
1.3 Flooded Upland Dynamics Experiment: FLUDEX	5
1.4 Experimental Lakes Area: ELA	6
1.5 Global reservoir research	7
1.6 Thesis objectives	7
2 Processes affecting greenhouse gas production in experimental boreal reservoirs	9
2.1 Introduction	10
2.2 Material and Methods	11
2.3 Results	14
2.4 Discussion	16
2.5 Conclusions	25
3 Importance of ebullition and sediment storage to greenhouse gas emissions from shallow boreal forest reservoirs	37
3.1 Introduction	38
3.2 Methods	38
3.3 Results and Discussion	40
3.4 Conclusions	48
4 Dynamics of dissolved oxygen isotopic ratios: a transient model to quantify primary production, community respiration, and air–water exchange in aquatic ecosystems	65
4.1 Introduction	66
4.2 Materials and Methods	70
4.3 Results and Discussion	75

4.4	Conclusion	79
5	Aquatic metabolism and ecosystem health assessment using dissolved O₂ stable isotope diel curves	87
5.1	Introduction	88
5.2	Methods	90
5.3	Results	92
5.4	Discussion	97
5.5	Conclusions	99
6	Determining community respiration and primary production in shallow boreal forest reservoirs with dissolved oxygen isotopes	115
6.1	Introduction	116
6.2	Methods	117
6.3	Results	121
6.4	Discussion	122
6.5	Conclusions	130
7	Methane oxidation: isotopic enrichment factors in freshwater boreal reservoirs	147
7.1	Introduction	148
7.2	Theory	150
7.3	Methods	150
7.4	Results and discussion	152
7.5	Conclusions	156
8	Direct comparison of two diffusive gas exchange methods in a low-wind environment	161
8.1	Introduction	161
8.2	Site description and methods	163
8.3	Results	167
8.4	Discussion	168
9	Greenhouse gas and dissolved organic carbon production in shallow zones of boreal reservoirs	179
9.1	Introduction	180
9.2	Methods	181
9.3	Results	184
9.4	Discussion	188
10	Conclusions and recommendations	213
10.1	General comments	213
10.2	Main conclusions and contributions to research	213
10.3	Questions for Future Research	217

Appendices	221
A Determining water-column metabolism with carbon and oxygen isotopes	223
A.1 Introduction	224
A.2 Methods	224
A.3 Results and discussion	227
A.4 Conclusions	229
B Permission to include and republish copyrighted materials	235
B.1 Permission to include and republish Chapter 4	236
B.2 Permission to include and republish Chapter 5	241
B.3 Permission to include and republish Chapter 7	243
References	245

List of Tables

2.1	FLUDEX reservoir physical characteristics, forest type, dominant vegetation and soil communities, and carbon stores.	32
2.2	The hydrology budgets for FLUDEX reservoirs for 1999–2003. . . .	33
2.3	Summary of $\delta^{13}\text{C}$ of DIC, CH_4 , soil, vegetation, and periphyton. . .	34
2.4	The volume- and mass-weighted $\delta^{13}\text{C}$ -DIC budgets for FLUDEX Reservoirs for 1999–2003.	35
2.5	The volume- and mass-weighted $\delta^{13}\text{C}$ - CH_4 budgets for FLUDEX reservoirs for 1999–2003.	36
3.1	Flood-season and drawdown CH_4 ebullition from FLUDEX reservoirs to the atmosphere for 1999–2003.	61
3.2	Flood-season and drawdown CO_2 ebullition from FLUDEX reservoirs to the atmosphere for 1999–2003.	62
3.3	Flood-season and drawdown CH_4 ebullition and net CH_4 production in FLUDEX reservoirs for 1999–2003.	63
3.4	Flood-season and drawdown CO_2 ebullition and net DIC production in FLUDEX reservoirs for 1999–2003.	64
4.1	PoRGy model input parameters and results for examples shown in Figures 4.3, 4.4, and 4.5	86
5.1	Summary of the effect the six key parameters on saturation and values.	110
5.2	Stream clusters as described by <i>Wilcock et al. (1998)</i>	111
5.3	Model input parameters and results for field examples shown in Figure 5.9.	112
5.4	Summary of P , R , and k ranges for different ecosystems	113
6.1	The volume- and mass-weighted $\delta^{18}\text{O}$ - O_2 budgets for FLUDEX reservoirs for 1999–2003.	140
6.2	The CR and PP rates calculated from volume- and mass-weighted $\delta^{18}\text{O}$ - O_2 budgets and diffusion-limited estimates of ϵ_{CR} for FLUDEX reservoirs for 1999–2003.	141

6.3	The <i>CR</i> and <i>PP</i> rates calculated from volume- and mass-weighted $\delta^{18}\text{O-O}_2$ budgets and diffusion-limited estimates of ϵ_{CR} for FLUDEX reservoirs for 1999–2003.	142
6.4	PoRGy model input parameters and results for diel O_2 and $\delta^{18}\text{O-O}_2$ modelling of FLUDEX reservoirs in July-2003.	143
6.5	The <i>CR</i> and <i>PP</i> rates calculated from volume- and mass-weighted $\delta^{18}\text{O-O}_2$ budgets and diel estimates of ϵ_{CR} for FLUDEX reservoirs for 1999–2003.	144
6.6	Diel and seasonal <i>CR</i> and <i>PP</i> rates in FLUDEX reservoirs 2003. . .	145
6.7	The <i>CR</i> and <i>PP</i> Rates calculated from volume- and mass-weighted $\delta^{18}\text{O-O}_2$ budgets and DIC-based <i>NPP</i> rates for FLUDEX reservoirs for 1999–2003.	146
7.1	Reservoir enrichment factors and fraction of CH_4 oxidised in ELARP and FLUDEX	160
8.1	Physical characteristics of FLUDEX reservoirs in 2003.	176
8.2	FLUDEX reservoir k_{600} values.	177
9.1	Pre-flood organic carbon stores in ELARP and FLUDEX reservoirs.	208
9.2	Pre- and post-flood GHG and DOC flux rates and equations from FLUDEX reservoirs.	209
9.3	Pre- and post-flood GHG and DOC flux rates from ELARP.	210
9.4	Predictions of 10- and 20-year greenhouse gas and DOC post-flood flux rates from ELARP and FLUDEX reservoirs.	211
9.5	Predictions of 10- and 20-year net greenhouse gas and DOC flux rates from ELARP and FLUDEX reservoirs.	212

List of Figures

2.1	Schematic hydrological budget for the FLUDEX reservoirs.	27
2.2	DIC concentrations and $\delta^{13}\text{C}$ -DIC of FLUDEX reservoir inflow and outflows for 1999–2003.	28
2.3	CH_4 concentrations and $\delta^{13}\text{C}$ - CH_4 of FLUDEX reservoir inflow and outflows for 1999–2003.	29
2.4	Rates of <i>CR</i> and <i>NPP</i> in FLUDEX reservoirs from 1999–2003 calculated from $\delta^{13}\text{C}$ -DIC budgets.	30
2.5	Community respiration, net CH_4 production, and CH_4 ebullition in FLUDEX reservoirs for 1999–2003 expressed as $\text{kg CO}_2 \text{ ha}^{-1}$ of global warming potential (GWP)	31
3.1	Flood-season bubble CH_4 concentrations in FLUDEX reservoirs for 1999–2003.	49
3.2	Flood-season bubble CO_2 concentrations in FLUDEX reservoirs for 1999–2003.	50
3.3	Flood season versus drawdown CH_4 ebullition from FLUDEX reservoirs to the atmosphere in 2001 and 2003.	51
3.4	Flood season versus drawdown CO_2 ebullition from FLUDEX reservoirs to the atmosphere in 2001 and 2003.	52
3.5	Flood-season bubble molar CH_4 : CO_2 ratio in FLUDEX reservoirs for 1999–2003.	53
3.6	Flood-season bubble $\delta^{13}\text{C}$ - CH_4 values in FLUDEX reservoirs for 1999–2003.	54
3.7	Flood-season bubble $\delta^{13}\text{C}$ - CO_2 values in FLUDEX reservoirs for 1999–2003.	55
3.8	Cross-plot of flood-season bubble $\delta^{13}\text{C}$ - CH_4 and $\delta^{13}\text{C}$ - CO_2 in FLUDEX reservoirs for 1999–2003.	56
3.9	Flood season CH_4 ebullition rates from FLUDEX reservoirs to the atmosphere for 1999–2003.	57
3.10	Flood season CO_2 ebullition rates from FLUDEX reservoirs to the atmosphere for 1999–2003.	58
3.11	Flood season $\delta^{13}\text{C}$ - CH_4 values of flood-season ebullition from FLUDEX reservoirs to the atmosphere for 1999–2003.	59

3.12	Flood season $\delta^{13}\text{C-CO}_2$ values of flood-season ebullition from FLUDEX reservoirs to the atmosphere for 1999–2003.	60
4.1	A graphical depiction of O_2 processes on a plot of O_2 saturation versus $\delta^{18}\text{O-O}_2$	81
4.2	Comparison of the <i>Knox et al. (1992)</i> kinetic isotopic fractionation factor laboratory experiments and photosynthesis–respiration–gas exchange (<i>PoRGy</i>) model output	82
4.3	Field data and <i>PoRGy</i> model diel data from the Flooded Upland Dynamics Experiment Medium C reservoir from 23 to 25 July 2003.	83
4.4	Field data and <i>PoRGy</i> model diel data from the pond 50 in St. Denis National Wildlife Area from 28 to 29 July 2000.	84
4.5	Field data and <i>PoRGy</i> model diel data from the South Saskatchewan River near Saskatoon from from 14 to 15 July 2004	85
5.1	A graphical depiction of the primary O_2 processes versus the $\delta^{18}\text{O-O}_2$ showing several <i>P:R</i> ratio lines (dashed grey lines) calculated with the steady-state model of <i>Quay et al. (1993)</i> and $\alpha_R = 0.982$ and $\delta^{18}\text{O-H}_2\text{O} = -7 \text{‰}$	101
5.2	Diel curves show how different rates of <i>P</i> and <i>R</i> affect the shape, size, and location of the curves when the <i>P:R</i> ratio is held constant.	102
5.3	Diel curves show how different rates of <i>R</i> affect the shape, size, and location of the curve when the <i>P:R</i> ratio is increased and <i>P</i> and <i>k</i> are held constant.	103
5.4	Diel curves show how different gas exchange coefficients (<i>k</i>) affect the shape, size, and location of the curve when the <i>P:R</i> ratio and <i>P</i> and <i>R</i> are held constant.	104
5.5	Diel curves show how O_2 isotopic fractionation factors (α_R) affect the shape, size, and location of the curve when the <i>P:R</i> ratio, <i>P</i> , <i>R</i> , and <i>k</i> are held constant.	105
5.6	Diel curves show how different $\delta^{18}\text{O-H}_2\text{O}$ values affect the shape, size, and location of the curve when the <i>P:R</i> ratio, <i>P</i> , <i>R</i> , and <i>k</i> are held constant.	106
5.7	Diel curves show how different temperatures affect the shape, size, and location of the curve when the <i>P:R</i> ratio, <i>P</i> , <i>R</i> , and <i>k</i> are held constant.	107
5.8	Based on a synoptic study of New Zealand streams, <i>Wilcock et al. (1998)</i> organised the ecosystem health of their streams into five clusters based on complete linkage cluster analysis of their <i>P</i> , <i>R</i> , and <i>k</i> values. Using average <i>P</i> , <i>R</i> , and <i>k</i> for these clusters, <i>PoRGy</i> was employed to generate diel O_2 saturation and $\delta^{18}\text{O-O}_2$ curves for each cluster.	108
5.9	Cross-plots of diel O_2 saturation and $\delta^{18}\text{O-O}_2$ and <i>P:R:G</i> ratios in three North American rivers and one prairie wetland.	109

6.1	O ₂ saturation and $\delta^{18}\text{O}\text{-O}_2$ of FLUDEX reservoir inflow and outflows.	132
6.2	O ₂ concentrations and $\delta^{18}\text{O}\text{-O}_2$ of FLUDEX reservoir inflow and outflows.	133
6.3	Net DIC production versus net O ₂ consumption in FLUDEX reservoirs.	134
6.4	Diel field data and PoRGy results from the FLUDEX High C reservoir from 21 to 23 July 2003.	135
6.5	Diel field data and PoRGy results from the FLUDEX Medium C reservoir from 23 to 25 July 2003.	136
6.6	Diel field data and PoRGy results from the FLUDEX Low C reservoir from 25 to 27 July 2003.	137
6.7	Rates of <i>PP</i> and <i>CR</i> in FLUDEX reservoirs from 1999–2003 calculated with ϵ_{CR} determined by diel modelling.	138
6.8	Rates of <i>PP</i> and <i>CR</i> in FLUDEX reservoirs from 1999–2003 calculated by converting <i>NPP</i> from the $\delta^{13}\text{C}\text{-DIC}$ budgets into O ₂ with $PQ = 1.25$	139
7.1	Rayleigh fractionation plot of the CH ₄ oxidation incubations from ELARP and FLUDEX.	158
7.2	Temperature dependency of the CH ₄ oxidation enrichment factor in ELARP, and FLUDEX High and Medium C reservoirs.	159
8.1	Surface water SF ₆ concentrations in the three FLUDEX reservoirs in July 2003.	174
8.2	Surface water SF ₆ concentration in the High C FLUDEX reservoir in July 2003.	175
9.1	Community respiration rates in FLUDEX reservoirs.	194
9.2	Net primary production rates in FLUDEX reservoirs.	195
9.3	Net DIC production rates in FLUDEX reservoirs.	196
9.4	Net CH ₄ production rates in FLUDEX reservoirs.	197
9.5	CH ₄ ebullition rates in FLUDEX reservoirs	198
9.6	Net DOC production rates in FLUDEX reservoirs.	199
9.7	Net DIC production rates in the ELARP pond.	200
9.8	p_{CO_2} values in the ELARP pond.	201
9.9	CO ₂ flux rates from the ELARP pond to the atmosphere.	202
9.10	p_{CH_4} values in the ELARP pond.	203
9.11	CH ₄ flux rates from the ELARP pond to the atmosphere.	204
9.12	Net DOC production rates in the ELARP pond.	205
9.13	CO ₂ flux rates from the ELARP peatland to the atmosphere.	206
9.14	CH ₄ flux rates from the ELARP peatland to the atmosphere.	207

A.1	Change in O ₂ and DIC concentrations and $\delta^{18}\text{O-O}_2$ and $\delta^{13}\text{C-DIC}$ values of the FLUDEX light and dark sealed chambers in late-July and late-August 2002.	231
A.2	DIC- and O ₂ -based CR rates in dark, sealed chambers in FLUDEX in late-July and late-August 2002.	232
A.3	Respiratory $\delta^{18}\text{O-O}_2$ enrichment factors ($\epsilon_{\text{CR-O}_2}$) in sealed chambers in FLUDEX as a function of CR rate in late-July and late-August 2002.	233
A.4	Photosynthetic $\delta^{13}\text{C-DIC}$ enrichment factors ($\epsilon_{\text{PP-DIC}}$) in sealed chambers in FLUDEX as a function of PP rate in late-July and late-August 2002.	234

Chapter 1

Introduction

1.1 A brief history of reservoir research

The estimate of global reservoir surface area is 1.5×10^6 km² (*St.Louis et al., 2000*). Impoundments of water are used for, in order of primary use, irrigation, hydroelectricity generation, water supply, flood control, and recreation. Hydroelectricity provides 22% of global energy production but only represents 20% of the primary use of reservoirs worldwide (*Tremblay et al., 2005*). Determining the effects of dam creation and operation is thus important for both hydroelectric and non-hydroelectric reservoirs and is of importance for both national and international greenhouse gas (GHG) inventories. This is particularly true in Canada where 59% of installed electricity generating capacity is from hydroelectric reservoirs (*Statistics Canada, 2005*), which comprise more than 73 000 km² in surface area (*St.Louis et al., 2000*).

Rosenberg et al. (1995, 1997, 2000) have extensively reviewed the large-scale social and environmental impacts of reservoirs. Landscapes are significantly altered by reservoir creation. Vast areas are flooded, water bodies are dewatered by diversion, and erosion and deposition are caused by altered flows. Wetlands along river margins are dessicated, the natural flood control of levées is lost, and a reduction in spring nutrient inputs to estuaries result from the regulation of river water for hydroelectricity (e.g., *Dudgeon, 2000; Nilsson and Berggren, 2000*).

Using the river continuum concept of *Vannote et al. (1980)*, biological communities are structured along resource gradients and downstream communities rely, in part, upon upstream processes. River impoundment and diversion alters and can completely interrupt these longitudinal gradients. For example, the biogeochemical cycling of nutrients and sediment from headwaters to higher-order rivers is interrupted by reservoirs and their erosion control measures, affecting downstream carbon (C) and nutrient cycling. Habitat outside of the river's main channel can be lost by dessication during low flow periods or destroyed by very high-flow flushing events. Natural flood cycles

and their associated nutrient dispersal and secondary production are significantly altered. Habitat fragmentation and impediments to free passage of fauna can cause extirpations.

Early research on Canadian reservoirs was largely related to mercury dynamics (e.g., *Bodaly et al., 1984*) (cf. *Hecky et al., 1991*). Bioaccumulation of methylmercury by fish and the subsequent consumption of fish by people is a major concern of reservoir creation (*Rosenberg et al., 1997*). Naturally present inorganic mercury is methylated by sulphate-reducing bacteria (*Compeau and Bartha, 1985; Gilmour and Henry, 1991*) in the anoxic flooded soils after reservoir creation (*Bodaly et al., 1984; Hecky et al., 1991; Kelly et al., 1997*). Consumption of sufficiently high amounts of methylmercury may cause teratogenic effects and methylmercury is also a strong neurotoxin (*Myers et al., 2000*). Mercury contamination of fisheries, while spatially restricted to the reservoir and its immediate downstream environment can be long-lived. Data from Canadian and Finnish reservoirs indicate that methylmercury levels in predatory fish can last 20–30 a or more (*Bodaly et al., 1997, 2007; St.Louis et al., 2004*).

In addition to the physical health effects of mercury contamination and poisoning, there are many social effects of reservoir development. The social effects of mercury contamination of fisheries in Canadian aboriginal communities (mainly Cree) have previously been described by others (e.g., *Chevalier et al., 1997; Hornig, 1999; Rosenberg et al., 1997*). However, *Rosenberg et al. (1997)* note that it is difficult to distinguish between the effects of a wide range of social changes caused by hydroelectric development. These include relocation away from flooded areas, increased access by outsiders to traditional territorial land, disruption of fisheries harvests and food sources, and general anxiety caused by the threat of methylmercury exposure (*Roebuck, 1999; Warner, 1999*).

Related to changes in mercury cycling are the changes in C cycling that result from flooding wetlands and uplands. Microbial decomposition of flooded organic C (OC) is the root cause of GHG emissions from reservoirs. Temporally, GHG emissions from reservoirs should decrease with time, as the sources of easily decomposable OC are depleted, but may last for decades or centuries (*Rosenberg et al., 1997*). *Rudd et al. (1993)* reason that the net greenhouse effect of boreal forests is close to zero: forests are neutral for CO₂ and small CH₄ sinks, and wetlands are CO₂ sinks and small sources of CH₄. Flooding forests and wetlands places the stored OC into a net decompositional ecosystem with a net flux of GHGs to the atmosphere. *Kelly et al. (1994)* outline four factors that may control the magnitude and duration of GHG emissions after flooding:

- amount of flooded land: a broadly positive relationship;
- reservoir age: a negative relationship similar to an exponential decline

because of the initial rapid decomposition of labile OC followed by slower decomposition of refractory OC until the GHG flux rate approaches that of undisturbed lakes, which are greater than the original, undisturbed ecosystem ([Rudd et al., 1993](#));

- flooded OC: a positive relationship though plant and soil OC stores vary between ecosystems such as boreal, temperate, and tropical, as well as between forest and wetland; and
- geographic location: with potentially greater GHG fluxes from tropical reservoirs because temperature varies latitudinally and temperature positively affects both decomposition rate and the CH₄:CO₂ ratio.

The CH₄:CO₂ ratio is important because the global-warming potential of CH₄ is greater than CO₂. The 20-, 100-, and 500-year time horizon global warming potentials (GWPs) for CH₄ are 62, 23, and 7 ([Ramaswamy et al., 2001](#)). Details on GWP calculations are found in [Ramaswamy et al. \(2001\)](#) where GWP is defined as the ratio of the time-integrated radiative forcing from the instantaneous release of 1 kg of the compound relative to that of 1 kg of CO₂. Incidentally, in 1998 ([UNFCCC, 1988](#)), the Conference of the Parties decided that calculations under the Kyoto Protocol would follow the GWP values from the Intergovernmental Panel on Climate Change (IPCC) Second Annual Report ([Houghton et al., 1995](#)) and not the more widely cited IPCC Third Annual Report ([Houghton et al., 2001](#)).

At the 50- to 100-year timescale, all of the plant and soil OC will have been fixed from CO₂ and release of that C as CO₂ through a forest fire would result in overall net zero emissions. Release of some of that C as CH₄ would result in a net increase in the GWP of the GHG fluxes from that ecosystem. [Cullenward and Victor \(2006\)](#) note that simple GWP comparisons are 'not sufficient for reservoir studies' since GHG emissions today have a much stronger warming effect than did emissions a decade ago and suggest neither the methods to do the calculation nor the policy implications required have been resolved. A running tab on the cumulative warming effect would be appropriate, since GWPs are non-linear, and would include a decreasing rate of emissions and a decreasing effect of a CH₄ relative to CO₂ over time ([Cullenward and Victor, 2006](#)). A means of time-preference such that the same GWP a decade in the future is worth less than the same GWP now is also required.

In an early assessment of the GHG fluxes from hydroelectric reservoir surfaces, [Rudd et al. \(1993\)](#) concluded that microbial decomposition of soil and vegetation into CO₂ and CH₄ would result from flooding. The GHGs would be released to the atmosphere via diffusion and ebullition. In addition, they proposed that the loss of the wetland-and-forest ecosystem would increase the net GHG emissions of reservoirs. To compare the reservoirs in their study to other sources of electricity, they calculated values for GHG per unit of

energy. Although this 'cost' does not include other reservoir functions, such as flood control, it remains a common method of comparing energy sources for policy purposes (cf. *Cullenward and Victor, 2006*).

1.2 Experimental Lakes Area Reservoir Project: ELARP

Based on studies of reservoirs in northern Manitoba and Québec, *Rudd et al. (1993)* and *Kelly et al. (1994)* hypothesised that the net flux of GHGs to the atmosphere from a reservoir surface (1) is positively correlated to the quantity of flooded OC, (2) peaks in the first year of flooding, and (3) declines thereafter. To test this hypothesis, ELARP was established at the Experimental Lakes Area (ELA). ELARP represented a worst-case scenario for reservoir creation as it flooded a large amount of stored OC in a peatland and pond complex (*Kelly et al., 1997; St.Louis et al., 2004*).

ELARP consisted of a 2.39 ha pond (L979) and its surrounding 14.4 ha peatland (*Kelly et al., 1997*). After 2 years of pre-flood study, the water level was raised 1.3 m by damming the outflow in early June 1993. The water level was reduced each fall to simulate the seasonal fluctuations of many boreal reservoirs. In subsequent years, the water level was again raised by capturing the spring freshet.

Initially, the wetland changed from being a small net C sink to a large net source of C to the atmosphere. The low rates of net C fixation by vegetation on the wetland surface was lost and the surface became a source of CO₂ to the atmosphere; the CH₄ flux increased about 60-fold. The CO₂ and CH₄ flux from the pond increased three- and six-fold, respectively. After more than a decade, CO₂ and CH₄ concentrations in the pond remained as high as in the first few years of flooding (*St.Louis et al., 2004*). Net fluxes from the peat surface also remained as high as in the first three years of flooding (*Saquet, 2003*).

As the peat surface detached from the underlying strata (cf. *Koskenniemi, 1987*), floating peat formed during the first year of flooding (*Scott et al., 1999*). In addition to the elevated GHG fluxes from the pond and flooded peat, CH₄ flux rates from floating peat in the third year of flooding were about 6–7 times greater than from flooded peat (*Scott et al., 1999*). Flux rates were comparably high in the tenth year of flooding (*Saquet, 2003*) and in the subsequent three or four years (J. J. Venkiteswaran, S. L. Schiff, unpublished data).

Dyck and Shay (1999) identified four treed-bog and two open-bog vegetation communities on the wetland surface and quantified the OC therein. Recently fixed OC was expected to play a large role in the post-flood production of GHGs. *Asada et al. (2005)* studied the changes in vegetation communities and OC pool from pre-flood to 10 a post-flood. They found that wetland types had diversified into one open-bog, four open-fen, and one marsh vegetation communities. This change was accompanied by rapid species turnover

and the new OC stores accumulated in plant biomass over 10a was comparable to the pre-flood above-ground biomass. Thus, only one decade was required to re-establish a vegetative community with a similar standing stock of OC. But the underlying peat continued to be a large source of CO₂ and CH₄ to the atmosphere.

1.3 Flooded Upland Dynamics Experiment: FLUDEX

Given the results of ELARP, it was hypothesised that GHG emissions would be positively correlated to pre-flood OC stores in ecosystems with two orders of magnitude less OC than ELARP. To test this hypothesis, a second whole-ecosystem project, FLUDEX, was established to assess upland flooding since actual reservoirs flood both lowland and upland areas. Together two whole-ecosystem experiments (ELARP and FLUDEX) would assess how reservoirs evolve in term of GHG emissions and biological processes.

Bodaly et al. (2004) summarised the experimental design and initial results of FLUDEX. Three reservoirs with differing amounts of stored OC were built near and along the height-of-land of the neighbouring L239 and L468 catchments: the High, Medium, and Low C reservoirs. They were designed to mimic the shallow areas of boreal reservoirs where microbial rates of decomposition and mercury cycling are believed to be greatest. The reservoirs were drawn down each fall to follow the seasonal water level fluctuations of larger reservoirs and characteristic of the shallow zones of boreal reservoirs.

In 1980, a forest fire extensively burnt the sites that became the FLUDEX reservoirs. As a result, the reservoirs contained dense, even-aged jack pine (*Pinus banksiana* Lamb.) and paper birch (*Betula papyrifera* Marsh.) forests and have accumulated soil for only 20 a (*Boudreau, 2000*). Reservoirs were enclosed on the lower three sides by wooden and gravel dikes and were open to catchment input on the fourth side. Water was pumped continuously from a nearby soft water lake (L468) with low concentrations of dissolved OC (DOC) and mercury. Flooding occurred for an average of 113 d a⁻¹ for five consecutive years (1999–2003). Water renewal times ranged from 6 d to 9 d depending on reservoir and year. Reservoirs had a surface area of 0.5 ha to 0.7 ha, a mean depth of about 1 m, and maximum depth of about 2 m.

Several publications have reported FLUDEX results. *Matthews et al. (2005)* reported three years of GHG concentrations demonstrating that surface fluxes of CO₂ and CH₄ were not related to pre-flood OC stores. *Hendzel et al. (2005)* reported that the reservoir surfaces were, contrary to expectations, very small N₂O sinks. They suggested that N₂O consumption was the result of excess labile C and a deficiency of reductants (mainly O₂ and NO₃⁻). *Hall et al. (2005)* found that rates of methylmercury production were generally related to pre-flood OC stores. *Hall and St.Louis (2004)* and *Hall et al. (2004)* used litterbag and enclosure experiments to examine the link between OC decomposition

and methylmercury production. Additionally, several mercury mitigation strategies were explored as part of FLUDEX. These indicated that substantial loss of C, total mercury, and methylmercury was caused by burning (*Mailman and Bodaly, 2005*), but that ecological and logistical problems would limit the usefulness of large-scale controlled burns (*Mailman and Bodaly, 2006*). Further, they suggested that the most promising strategies for lowering methylmercury concentrations in fish in boreal reservoirs are ultimately site selection and project operation including intensive fishing, removal of some of the standing trees, and potential selenium additions.

During the years after ELARP began (pre-flood research was conducted in 1991 and 1992, flooding occurred from 1993 to 2006) and before FLUDEX (flooded from 1999 to 2003), greater availability of continuous flow mass spectrometry made analysis of stable carbon isotopic ratios ($^{13}\text{C}/^{12}\text{C}$; hereafter as $\delta^{13}\text{C}$) much more rapid and significantly reduced the sample size requirements compared to dual-inlet mass spectrometry (cf. *Brenna et al., 1997*). As a result of more efficient analysis, calculating isotope-mass budgets became more feasible than before (see Chapter 2). While mass budgets, based on concentrations and flow rates, are useful for determining the net production of DIC and CH_4 (see *Matthews et al., 2005*), isotope-mass budgets using concentrations, flow rates, and isotopic ratios can be used to calculate rates of biological processes (see Chapters 2 and 3). By determining community metabolism rates in the FLUDEX reservoirs, the dynamic sources and sinks of CH_4 and CO_2 can be determined. Further comparisons between C-based and O_2 -based metabolic rates can be used to describe reservoir evolution year-after-year. FLUDEX offered an excellent opportunity to study C and O_2 cycling in freshwater ecosystems and specifically in boreal reservoirs.

1.4 Experimental Lakes Area: ELA

The ELA is located on the Canadian Shield in northwestern Ontario, Canada ($49^{\circ}40' \text{ N } 93^{\circ}45' \text{ W}$) (*Brunskill and Schindler, 1971*; *Cleugh and Hauser, 1971*). Long-term meteorologic records indicate that ELA climate is humid continental, with a mean annual precipitation of 703 mm (1969–2001) and a mean annual temperature of 2.6°C (1970–2001). Soils at ELA are typically thin, discontinuous, and often capped by mosses such as *Sphagnum* and *Polytrichum*. Some low-lying areas have accumulated *Sphagnum* to depths greater than 0.5 m and hilltops are often exposed bedrock or forested islands (*Lamontagne et al., 2000*; *Schindler et al., 1996a*). Wetlands at ELA contain peat, typically ≤ 10 m, and are usually bogs or poor fens. Forest fires burned portions of the catchments of ELARP and FLUDEX in 1974 and practically their entire catchments in 1980. *Bayley et al. (1992a,b)* described the effects of the forest fires on stream and lake chemistry. As a result of the fires, the upland and wetland forests have largely regrown as an even-aged forest of jack pine,

black spruce (*Picea mariana* (Mill.) BSP), paper birch, and to a much lesser extent alders (*Alnus* spp.) and trembling aspen (*Populus tremuloides* Michx.).

1.5 Global reservoir research

Notable hydroelectric reservoir GHG research outside of Canada includes studies in Finland (e.g., [Huttunen et al., 2002](#)), French Guyana (e.g., [Abril et al., 2005](#); [Galy-Lacaux et al., 1997, 1999](#)), and a smaller amount of research in Panama (e.g., [Keller and Stallard, 1994](#)). [Cullenward and Victor \(2006\)](#) recently summarised much of the controversy associated with hydroelectric reservoir research. Research on GHGs in Brazilian reservoirs has been particularly antagonistic (e.g., [Fearnside, 2006](#); [Rosa et al., 2006](#)). The arguments and counter-arguments have involved the appropriateness of GWP calculations ([Fearnside, 1995](#); [Rosa et al., 1996](#)), 'turbine emissions' (i.e., the CH₄ emitted to the atmosphere from the water that falls through the turbines and not directly from the reservoir surface and sometimes called 'spillway' or 'sluiceway' emissions) ([Fearnside, 2004](#)), citizenship, and conflicts of interest ([Fearnside, 2006](#); [Rosa et al., 2006](#)). In any case, the methods by which to compare the GHG production per unit electricity output have not been fully settled in more than one decade of publications (e.g., [Fearnside, 2002](#); [Rosa and Schaeffer, 1994](#); [Rosa et al., 2006](#); [Rudd et al., 1993](#)).

Regulatory agencies in Canada and the USA consider hydroelectricity to be 'GHG-neutral' and as such reservoirs are not included in the national inventory of GHG emissions ([Bodaly et al., 2004](#)). While few have suggested that they are a GHG sink ([Rosa and Schaeffer, 1994](#)), most have suggested they are a net source to the atmosphere (see data contained within [St.Louis et al., 2000](#)). The omission of reservoirs from GHG inventories is of major significance since it has been estimated that reservoirs comprise about 7% of total anthropogenic GHG emissions (in GWP CO₂ equivalents) ([St.Louis et al., 2000](#)). Results from both ELARP and FLUDEX are of national and international importance because they provide information on GHG cycling within and GHG release from reservoirs.

1.6 Thesis objectives

The overall objective of this thesis was to describe the temporal evolution of upland boreal reservoirs in terms of community respiration (CR) and primary production (PP) rates using carbon (C) and O₂. Given the need for information on GHGs and reservoirs, a series of experiments was designed to:

- quantify the temporal evolution of biological processes in three experimental upland boreal reservoirs (Chapter 2);

- describe the importance of ebullition as a source of CH₄ from three experimental upland boreal reservoirs to the atmosphere (Chapter 3);
- develop and apply an oxygen model that quantifies metabolic and gas exchange rates by accounting for diel changes in oxygen concentrations and isotopic ratios (Chapter 4);
- examine the key environmental parameters that control diel changes in oxygen concentrations and isotopic ratios since these diel curves are intrinsic indicators of ecosystem health (Chapter 5);
- quantify, for the first time in any reservoirs, O₂ and δ¹⁸O-O₂ budgets and biological processes at the reservoir scale (Chapter 6);
- determine CH₄ oxidation fractionation factors for upland and wetland boreal reservoirs at the ELA so that CH₄ production and oxidation processes can be individually quantified (Chapter 7);
- determine the gas exchange coefficients in low-wind speed environments to calculate rates of gas flux from FLUDEX reservoir surfaces to the atmosphere (Chapter 8);
- compare the results of upland and wetland reservoir experiments at the ELA (Chapter 9).

Chapter 2

Processes affecting greenhouse gas production in experimental boreal reservoirs: A stable carbon isotopic ratio approach

Abstract

The Flooded Upland Dynamics Experiment (FLUDEX) involved the creation of three experimental reservoirs in boreal forest uplands differing in their amounts of organic matter stored on the landscape. The biological processes that control net GHG fluxes from the reservoirs to the atmosphere were quantified for five years by constructing stable carbon isotopic ratio mass budgets to study changes in greenhouse gas (GHG) cycling due to flooding. These budgets indicated that primary production consumed 0% to 44% (range of three reservoirs over five years) of the dissolved inorganic carbon produced by community respiration of flooded organic matter, thereby reducing the diffusive flux of CO_2 to the atmosphere. Community respiration declined more quickly than net primary production, year-after-year. Net CH_4 production more than doubled during the first half of the experiment, yet isotopic ratios showed that CH_4 production in the flooded soils increased nearly 10-fold. CH_4 oxidation near the flooded soil-water interface greatly decreased the CH_4 flux to the atmosphere. Isotopic ratios measured in light-exposed and darkened benthic chambers indicated that CH_4 oxidation was light-mediated. Bubbles with high CH_4 concentrations formed in the uppermost portion of the flooded soils where CH_4 oxidation was occurring, and were the most important conduit of CH_4 to the atmosphere after three years. Understanding within-reservoir factors affecting CH_4 oxidation is critical to determining total GHG flux. Although CH_4 production increased over time, the total GHG flux, expressed in CO_2 equivalents, from flooding boreal upland forests declined over five years. Contrary to expectations,

neither community respiration nor total GHG fluxes from the reservoirs were directly related to the quantity of organic carbon flooded.

2.1 Introduction

Construction of water-filled reservoirs alters the storage of organic carbon (OC) on the landscape and thus causes flooded vegetation and soils to decompose. Reservoir creation results in net emissions of the greenhouse gases (GHGs) carbon dioxide (CO₂) and methane (CH₄) to the atmosphere for decades and possibly centuries (*Duchemin et al., 1995; Kelly et al., 1997; St.Louis et al., 2000*). To predict the magnitude of GHG fluxes from reservoirs, the rates and relative importance of biological processes driving carbon (C) cycling on flooded landscapes need to be quantified.

In the Flooded Upland Dynamics Experiment (FLUDEX), three upland areas with differing amounts of OC stores in vegetation and soils were flooded (*Bodaly et al., 2004*). Forests that had been net sinks of CO₂ and CH₄ became sources of both GHGs to the atmosphere (*Matthews et al., 2005*). CO₂ flux to the atmosphere declined markedly from the first to the third year of flooding. However, in total, the global warming potential (GWP) of net GHG production remained relatively constant over three years of flooding because of an increase in net CH₄ emission, which has a GWP 23 times that of CO₂ (*Ehhalt et al., 2001*).

While flux measurements are important in constraining the net flux of GHGs to the atmosphere, they cannot characterise the biological processes affecting these emissions. This study extends beyond flux measurements to quantify the rates of biological processes controlling GHG fluxes. Processes such as CH₄ oxidation and primary production result in a difference between gross GHG production and net loss of GHGs to the atmosphere. To determine the rates of these within-reservoir processes, stable carbon isotopic ratios (¹³C/¹²C; hereafter as δ¹³C) were used because δ¹³C can yield carbon cycling information unavailable from concentration data alone. The δ¹³C of dissolved inorganic C (DIC) gives information about rates of DIC production via community respiration (CR) and DIC loss via net primary production (NPP) (e.g., *Hecky and Hesslein, 1995; Quay et al., 1986*). The δ¹³C can also quantify CH₄ oxidation and assess the contribution of different methanogenic pathways (*Whiticar, 1999; Whiticar et al., 1986*). Extending results from experimental reservoirs to other landscapes requires predictive capability and knowledge of biological processes. The objective of this chapter was to use δ¹³C to examine and quantify four important processes (CR, NPP, CH₄ production, and CH₄ oxidation) affecting net GHG production in the five years of flooding the FLUDEX reservoirs. The final two years of CO₂ and CH₄ production for this five-year experiment are also reported.

2.2 Material and Methods

Study Site

Three FLUDEX reservoirs were built on the Canadian Shield at the Experimental Lakes Area (ELA), northwestern Ontario, Canada (49°40' N 93°45' W). ELA climate is humid continental, with mean annual precipitation of 703 mm (1969–2001) and mean annual temperature of 2.6 °C (1970–2001). The reservoir sites were chosen based on the quantity of OC in vegetation and soil, and designated High, Medium, or Low C (Table 2.1) (Hall *et al.*, 2005). All vegetation and organic soil was completely burned during a forest fire in 1980 and regrowth was dominated by a dense, even-aged jack pine (*Pinus banksiana* Lamb.) and paper birch (*Betula papyrifera* Marsh.) forest. At the time of initial flooding, overburden within the FLUDEX reservoirs ranged from nil on exposed bedrock to more than 1 m of soil. Soil C pools were estimated from soil cores collected at six or seven locations per reservoir. Each soil horizon (litter, fungal–humic, charcoal, and mineral) was measured for bulk density and analysed for C concentration and $\delta^{13}\text{C}$. Twenty to 25 additional soil cores were collected at 20 m intervals along sampling transects in each reservoir, separated into horizons, and analysed for C concentration and $\delta^{13}\text{C}$. Biomass of low shrubs, herbs, mosses, and lichens was estimated by collecting material from 5 to 10 quadrats per reservoir (Heubert, 1999). Woody biomass in tall shrubs and trees was estimated from trunk diameter measurements using allometric equations (cf. Dyck and Shay, 1999). Forest canopy biomass was estimated from monthly collections of litterfall from three locations per reservoir (Matthews *et al.*, 2005). The High C reservoir had 45 900 kg C ha⁻¹ in OC stores and two vegetation and soil communities. The Medium C reservoir had 34 900 kg C ha⁻¹ in OC stores in a dry forest community. The Low C reservoir had 30 900 kg C ha⁻¹ in OC stores and three vegetation and soil communities (Table 2.1).

Reservoir Construction and Hydrology

Reservoirs were built against natural slopes on the landscape and water was contained on the lower sides by wooden walls and gravel dikes. Where water depth was expected to be 1 m or more, polyethylene-lined wooden walls, anchored and sealed directly to bedrock, were constructed. Polyethylene-lined gravel dikes were constructed where water depth was expected to be less than 1 m. Areas above the height of flooding were not diked, leaving regions open to input from the upslope catchment (Table 2.1). Water was continuously pumped into the reservoirs for about 15–16 weeks each year from nearby Roddy Lake beginning in May or June each year from 1999 to 2003. Hydrologic budgets (Figure 2.1; Table 2.2) were calculated for each reservoir each year by measuring the daily inputs (inflow, precipitation, and catchment

input) and outputs (outflow, seepage, and evaporation) with standard equipment (Mattheews *et al.*, 2005). Storage was the volume of water left standing at the end of each flood season. Roddy Lake is oligotrophic (total phosphorus, $6.0 \pm 2.5 \mu\text{g L}^{-1}$, mean $\pm 1SD$, $n = 41$). Each autumn, the reservoirs were drained of water to simulate seasonal water level fluctuations characteristic of boreal hydroelectric reservoirs.

Field Sampling

Mattheews *et al.* (2005) presents detailed field sampling procedures for DIC and CH_4 concentrations. Briefly, reservoir inflow and outflows were sampled weekly for DIC, CO_2 , and CH_4 concentrations. Samples for $\delta^{13}\text{C}$ were collected weekly in Wheaton serum bottles at the main inflow and each reservoir outflow. Samples were sealed with a pre-baked Vacutainer stopper (60 °C for 12 h) punctured by a needle to eliminate any air trapped in the stopper. Saturated sodium azide solution (0.3% of bottle volume) was added within two hours of collection to preserve the samples.

Inflow water volumes were quantified by an in-line flow meter. Continuous stage-level recorders and V-notch weirs were used to calculate outflow volumes. Seepage and fracture flow were canalized and their rates were measured once per season. Precipitation was recorded at the ELA meteorological station (less than 1 km from the reservoirs) and evaporation was estimated with a Class A evaporation pan per reservoir.

Five to ten bubble traps per reservoir were continuously deployed. Accumulated bubble volumes were measured weekly and converted into aerial flux rates. Fresh gas bubbles for concentration and $\delta^{13}\text{C}$ were collected by probing reservoir flooded soils and trapping the bubbles in an inverted funnel. The gas was transferred to serum bottles for concentration analysis or to pre-evacuated tubes (12 mL of gas in a 10 mL tube) for $\delta^{13}\text{C}$ analysis.

To independently assess the GHG flux across the flooded soil-water interface (SWI), benthic chambers ($\approx 13\text{ L}$) were deployed on the flooded soil. Before flooding, fifteen plastic collars (30 cm diameter) per reservoir, in groups of three, were inserted into the soil. After flooding, chambers equipped with a motor and propeller, and a sampling port were deployed from a boat onto the collars for four to six hours every two weeks. Darkened chambers, covered with foil, were deployed alongside the light-exposed chambers. Chambers were sampled from a boat via tubing attached to the sampling port. Pore water was sampled with a permanently emplaced profiler with screened ports at regular intervals.

$\delta^{13}\text{C}$ -mass budgets

To construct the $\delta^{13}\text{C}$ -mass budgets, daily $\delta^{13}\text{C}$ values were multiplied by their respective DIC or CH_4 concentrations and by water volumes entering

and exiting the reservoirs. The difference between inputs and outputs in the $\delta^{13}\text{C}$ mass budget divided by the DIC or CH_4 mass yields the $\delta^{13}\text{C}$ of the net DIC or CH_4 production,

$$net = \sum_{i=1}^j (Q_{out} \times C_{out})_i - \sum_{i=1}^j (Q_{in} \times C_{in})_i \quad (2.1)$$

$$\delta_{net} = \frac{\sum_{i=1}^j (Q_{out} \times C_{out} \times \delta_{out})_i - \sum_{i=1}^j (Q_{in} \times C_{in} \times \delta_{in})_i}{net} \quad (2.2)$$

where net is net production, Q the water flow rates, C the concentration, δ the $\delta^{13}\text{C}$, i day, j the number of flood days, and the subscripts net , out and in denote the net, outputs, and inputs.

Many components in the hydrology (Figure 2.1) and $\delta^{13}\text{C}$ -mass budgets were measured directly (inflow from Roddy Lake, outflow, and storage). Inflow and outflows were sampled for DIC and CH_4 concentrations and $\delta^{13}\text{C}$ weekly to capture changes in concentrations and $\delta^{13}\text{C}$ values throughout the flood season. The $\delta^{13}\text{C}$ -mass budgets must be calculated day-by-day rather than using average values because concentrations, $\delta^{13}\text{C}$ values, and water flow rates changed over the flood season. The day-by-day values were summed into seasonal inputs and outputs. For $\delta^{13}\text{C}$ -mass budgets, weekly values were linearly interpolated to calculate daily values. Storage was calculated by measuring vertical profiles of DIC and CH_4 concentrations and $\delta^{13}\text{C}$ one day before drawdown and multiplying these data by water-volume-to-water-depth curves. To determine DIC, CH_4 , and $\delta^{13}\text{C}$ values in catchment input from the undiked upslope areas of the reservoirs, samples were collected from small runoff channels that formed during and after large rain events. The hydrologically gauged Lake 114 (L114) inflow stream was also sampled as a proxy for the $\delta^{13}\text{C}$ of catchment input since the L114 stream could be sampled throughout the flood season due to its relatively larger area and water storage capacity. The vegetation and soil characteristics of the FLUDEX and L114 catchments were similar (logged in the 1970s, extensively burned in 1980) so the $\delta^{13}\text{C}$ values should be similar.

The $\delta^{13}\text{C}$ of other budget items (gas exchange, seepage, and precipitation) had to be estimated because they could not be directly measured. The $\delta^{13}\text{C}$ - CO_2 lost via gas exchange was calculated from $\delta^{13}\text{C}$ -DIC, pH, reservoir surface-water temperature and isotopic enrichment factors for DIC species (Clark and Fritz, 1997). Gas exchange coefficients were determined experimentally (Matthews et al., 2003, Chapter 8). The pH of all reservoirs was relatively constant (6.2 ± 0.3 , $n = 140$ for all reservoirs in all years). To calculate the $\delta^{13}\text{C}$ -DIC in precipitation, the pH of precipitation was measured and combined with an average atmospheric CO_2 concentration and $\delta^{13}\text{C}$ - CO_2 value (Battle et al., 2000). Isotopic enrichment factors for CH_4 dissolution were smaller than measurement precision (Knox et al., 1992). CH_4 concen-

tration and $\delta^{13}\text{C}\text{-CH}_4$ of precipitation were assumed to be equilibrated with atmospheric CH_4 (Quay *et al.*, 1999).

Analysis of DIC, CO_2 , and CH_4 concentrations and $\delta^{13}\text{C}$ values

Liquid samples were analysed via headspace equilibration and gas samples were analysed directly on the same gas chromatograph as Matthews *et al.* (2005). All analyses for $\delta^{13}\text{C}\text{-DIC}$, CO_2 , and CH_4 were performed on the same gas chromatograph–combustion–isotopic ratio mass spectrometer (GC–C–IRMS) at the Environmental Isotope Laboratory (EIL) as per (Venkiteswaran and Schiff, 2005). Precision of $\delta^{13}\text{C}\text{-DIC}$ and $\delta^{13}\text{C}\text{-CO}_2$ analysis was $\pm 0.3\text{‰}$ and of $\delta^{13}\text{C}\text{-CH}_4$ analysis was $\pm 0.5\text{‰}$.

Analysis of $\delta^{13}\text{C}$ and C/N Ratios of Periphyton, Soil, Vegetation, and DOC

Periphyton, soil, and vegetation samples were freeze-dried and ball-milled. Periphyton samples were freeze-dried and cut to fit sample cups. Dissolved OC (DOC) samples were filtered through pre-combusted Whatman GF/F filters, acidified to pH=2 (37% hydrochloric acid), and freeze-dried. Analysis of $\delta^{13}\text{C}$ and C/N ratios were performed on an elemental analyser–isotopic ratio mass spectrometer (EA–IRMS) (Carlo Erba EA1108 coupled to a Micromass Isochrom) at EIL. Precision of $\delta^{13}\text{C}$ analysis was $\pm 0.2\text{‰}$ and was $< \pm 1\text{‰}$ on C and N.

2.3 Results

$\delta^{13}\text{C}\text{-DIC}$ Values and Budgets

DIC concentrations in the inflow from Roddy Lake were similar every year ($134 \pm 26 \mu\text{mol L}^{-1}$, $n = 80$, Table 2.3, Figure 2.2). Catchment input was only important in the High C reservoir (8–40% of total DIC inputs depending on year) because only this reservoir had a significant area of upslope catchment (Table 2.1). DIC concentration of High C catchment input was $690 \pm 140 \mu\text{mol L}^{-1}$ (geometric mean, $n = 16$). Reservoir outflow DIC concentrations varied greatly ($110\text{--}590 \mu\text{mol L}^{-1}$; all reservoirs, all years) and were always greater than inflow DIC concentrations even though the residence time of the water in the reservoirs was short (6–9 days). Therefore, DIC production was substantial within all reservoirs in all five years. On average, one-third of DIC leaving the reservoirs was lost to the atmosphere and, on average, more than one-half of DIC was lost to outflow and seepage (Table 2.4)

Net DIC production was greatest in the first year and generally declined over five years (Table 2.4). The largest decline was from the first to second

year. Net DIC production was similar in the second and third years and declined modestly to the fifth year. Over five years, net DIC production declined by 45 %, 46 %, and 65 % in the High, Medium, and Low C reservoirs.

Although the DIC concentrations of the inflow were steady, the $\delta^{13}\text{C}$ -DIC values ranged from -18.0‰ to -2.2‰ (Figure 2.2). During summer, gas exchange and photosynthesis increased the $\delta^{13}\text{C}$ -DIC of Roddy Lake by 3 ‰ to 7 ‰ from the lower $\delta^{13}\text{C}$ -DIC, characteristic of vernal turnover. The $\delta^{13}\text{C}$ -DIC of the L114 stream, used as a proxy for catchment input, was different than Roddy Lake input at $-25.7 \pm 0.8\text{‰}$ ($n = 4$).

Outflow $\delta^{13}\text{C}$ -DIC peaked between mid-July and early August each year and ranged from -21.7‰ to -10.3‰ . The $\delta^{13}\text{C}$ -DIC was always more negative than the inflow (Figure 2.2). Therefore $\delta^{13}\text{C}$ -DIC more negative than reservoir outflows was added within the reservoirs.

Net $\delta^{13}\text{C}$ -DIC production values ranged between -28.5‰ and -18.8‰ and did not follow the pattern of net DIC production (Table 2.4). In the first year, net $\delta^{13}\text{C}$ -DIC production was about -24.2‰ in all reservoirs. In the High C reservoir, net $\delta^{13}\text{C}$ -DIC production decreased 2 ‰ over five years. In the Medium C reservoir $\delta^{13}\text{C}$ -DIC increased 2 ‰ over the first to third years and then declined by 2.5 ‰ in total from the third to fifth years. The year-to-year change in net $\delta^{13}\text{C}$ -DIC production was most pronounced in the Low C reservoir: increasing by 4.7 ‰ over the first three years and then decreasing by 9.7 ‰ over the last three years.

$\delta^{13}\text{C}$ -CH₄ Values and Budgets

CH₄ was also produced in all reservoirs in all years (Table 2.5). CH₄ concentrations in the inflow and catchment input were very low ($< 0.2\ \mu\text{mol L}^{-1}$). Outflow CH₄ concentrations peaked during August each year and, on average, increased through the first three years and declined modestly in the fourth and fifth years (Figure 2.3).

Net CH₄ production was lowest in the first year (Figure 2.3; Table 2.5). By the third year, net CH₄ production had increased by two- to four-fold (Figure 2.3; Table 2.5). In the subsequent two years, net CH₄ production declined but remained greater than in the first year. In the last year of flooding, net CH₄ production was greater than in the first year but lower than the interim years. CH₄ was lost to the atmosphere via gas exchange, ebullition and from downstream degassing of reservoir outflows.

Outflow $\delta^{13}\text{C}$ -CH₄ exhibited different trends each year. In the first year, outflow $\delta^{13}\text{C}$ -CH₄ (-89.3‰ to -65.9‰) remained more negative than CH₄ in most freshwater systems (Whiticar, 1999). In the second year, outflow $\delta^{13}\text{C}$ -CH₄ became more positive as the flood season progressed (-99.4‰ to -35.9‰). In the third year, the $\delta^{13}\text{C}$ -CH₄ in the Medium and Low C reservoir outflow remained steady at -50‰ to -45‰ after 8 weeks; however, CH₄ in the High C reservoir continued to increase as outflow became

more positive, increasing to -17‰ (Figure 2.2). In the final two years, the $\delta^{13}\text{C-CH}_4$ in the Medium and Low C reservoir outflows was consistently around -50‰ to -40‰ for the entire flood season. Similar to the third year, the High C reservoir outflow was generally much more positive than the other reservoirs and peaked in mid- to late-August (at -11.4‰ and -12.7‰ in the fourth and fifth years respectively). The increase in the High C reservoir $\delta^{13}\text{C-CH}_4$ occurred concomitantly with a decline in CH_4 concentration.

Net $\delta^{13}\text{C-CH}_4$ production values were lowest in the first year at -73.0‰ , -92.1‰ , and -82.0‰ in the High, Medium, and Low C reservoirs (Figure 2.3; Table 2.5). Net $\delta^{13}\text{C-CH}_4$ production values increased each year from the first to fourth year (to -25.9‰ , -46.3‰ , and -46.8‰ in the High, Medium, and Low C reservoirs). In the fifth year, net $\delta^{13}\text{C-CH}_4$ production values decreased to -45.2‰ , -50.2‰ , and -50.6‰ in the High, Medium, and Low C reservoirs.

2.4 Discussion

Hydroelectric reservoir creation results in flooding of vast areas of land and submerges large stores of soil carbon. The fate of this submerged C in FLUDEX reservoirs was varied. Some was decomposed leading to increased DIC concentrations and CO_2 fluxes to the atmosphere; however, some DIC was consumed by autotrophs. CH_4 fluxes from reservoirs can also be an important part of the GHG budgets of these systems (*St.Louis et al., 2000*). Flooded OC and CO_2 may be reduced to CH_4 , but some CH_4 produced was consumed by methanotrophs, thus reducing potential CH_4 fluxes. As a result, the processes controlling the within-reservoir production and consumption of DIC and CH_4 were quantified.

Partitioning changes in DIC concentrations and $\delta^{13}\text{C-DIC}$ values

In order to transfer results from FLUDEX to other systems, *NPP* and *CR* must be determined separately. *CR* is the decomposition of flooded OC to CO_2 but some of this CO_2 production is consumed by *NPP*. Thus net DIC production cannot be used to compare reservoirs and assess *CR* from flooding. The effect of *NPP* on net DIC production must be determined for each reservoir in each year. *CR* depends largely on substrate and temperature (*Wetzel, 2001*), while *NPP* depends on many diverse factors such as nutrient concentrations, mixing, light, mean depth, and DOC (*Falkowski and Raven, 1997*). Traditional incubation-based techniques of determining *CR* and *NPP* rates would not have been able to easily capture *CR* in the flooded soils and *NPP* in attached algae. The $\delta^{13}\text{C-DIC}$ mass budgets can be used to quantify *NPP* and *CR* separately because each process affects the $\delta^{13}\text{C-DIC}$ quite differently. To determine *NPP* and *CR*, the effect of *NPP* and *CR* on the $\delta^{13}\text{C-DIC}$ must each be assigned a priori because they cannot be measured directly.

Assigning end-member $\delta^{13}\text{C}$ values to *NPP*

For *NPP*, photosynthetic organisms preferentially use ^{12}C over ^{13}C by a photosynthetic enrichment factor of about -19‰ in environments where CO_2 is not limiting (Hecky and Hesslein, 1995). The $\delta^{13}\text{C}\text{-CO}_2$ used by *NPP* was calculated from measured DIC concentration, pH, temperature, and $\delta^{13}\text{C}\text{-DIC}$. The $\delta^{13}\text{C}\text{-NPP}$ was independently evaluated by comparison with the $\delta^{13}\text{C}$ of periphyton. Pairs of pine dowels were hung at five sites in each reservoir as a surrogate substrate for periphyton (attached algae and associated organisms), the major form of *NPP* in the reservoirs. Independent sampling indicates phytoplankton were less than 1% of *NPP* (D. Findlay, unpublished data). Emergent macrophytes were not observed in the reservoirs until the third year of flooding and numbered less than 20. Periphyton was also collected after drawdown as a second method of evaluating $\delta^{13}\text{C}\text{-NPP}$. Periphyton $\delta^{13}\text{C}$ in August and September was expected to range from -39‰ to -34‰ based on $\delta^{13}\text{C}\text{-DIC}$ of the outflow and water column, pH, and calculated photosynthetic enrichment. Periphyton grown on dowels could be contaminated with bacteria feeding on non-periphyton carbon such as DOC or detritus (floating litter comprised mostly of needle and leaf remnants). The $\delta^{13}\text{C}$ of bacteria feeding on DOC would have been approximately equal to $\delta^{13}\text{C}\text{-DOC}$ (-29‰ to -26‰) or detrital carbon (-30‰ to -27‰) and thus more positive than the periphyton. Periphyton $\delta^{13}\text{C}$ (-39‰ to -29‰) indicated detritus and bacteria in the matrix were sufficient to alter the $\delta^{13}\text{C}$.

Periphyton collected after the flood season were more negative (-39‰ to -35‰) than periphyton grown on pine dowels (-36‰ to -29‰) and were within the expected range of $\delta^{13}\text{C}$ predicted by $\delta^{13}\text{C}\text{-DIC}$, pH, and the photosynthetic enrichment (-39‰ to -34‰). Sample collection after flood season likely avoided visible detritus better than the pine dowels. Bacteria using vegetation and soil C may have also been more common on the outside of periphyton and thus more prone to loss during reservoir drawdown.

To determine if periphyton samples on dowels contained a significant amount of detritus, these samples were also analysed monthly for $\delta^{13}\text{C}$ and C/N ratios because detritus would also alter these values. Samples with significant detritus would have had larger C/N ratios than samples without detritus because litter, the main component of detritus, had large C/N ratios (mean of 47, $n = 19$). The expected C/N ratios of FLUDEX periphyton should have been greater than those of ELA lakes due to increased C-rich structural components of filamentous algae. Periphyton in non-manipulated ELA lakes had a mean C/N ratio of 14 ($n = 11$) (Turner *et al.*, 1994). Periphyton samples collected on dowels had a mean C/N ratio of 20 ($n = 21$) in 2000, and 32 ($n = 13$) in 2001. Both $\delta^{13}\text{C}$ and C/N ratios indicated that periphyton samples were mostly algal, although detritus and bacteria may have been the cause of the more positive than expected $\delta^{13}\text{C}$ of some periphyton samples.

This confirms the estimated photosynthetic enrichment factor of -19‰

because (1) periphyton samples matched the calculated photosynthetic enrichment factor model, and (2) it was likely that periphyton samples included small amounts of detritus and bacteria. Because $\delta^{13}\text{C-DIC}$, pH, and temperature changed throughout the flood seasons, when calculated for each reservoir and year, the $\delta^{13}\text{C-NPP}$ ranged from -44‰ to -37‰ . If the magnitude of the enrichment factor was slightly overestimated, then estimates of NPP were minima.

Assigning end-member $\delta^{13}\text{C}$ values to CR

Compared to NPP , assigning a $\delta^{13}\text{C}$ value to CR ($\delta^{13}\text{C-CR}$) was much simpler. The $\delta^{13}\text{C-CR}$ was assigned based on two lines of evidence. First, laboratory incubations of FLUDEX vegetation and soils indicated that early stages of soil decomposition produced DIC that is 2‰ to 3‰ more positive than bulk OC (Baril, 2001; Boudreau, 2000; Oelbermann and Schiff, 2008, J. J. Venkiteswaran, unpublished data). Second, selective decomposition of vegetation and soil components and/or enrichment during early stages of decomposition have been reported to increase the $\delta^{13}\text{C-DIC}$ by 1‰ to 2‰ (Fogel and Cifuentes, 1993; Nadelhoffer and Fry, 1988). Thus vegetation and soil $\delta^{13}\text{C}$ (-30‰ to -27‰ ; Table 2.3) was adjusted to account for a small alteration and the $\delta^{13}\text{C-CR}$ was assigned a value of -27‰ . If the $\delta^{13}\text{C-CR}$ assigned is slightly overestimated, then estimates of CR are maxima and NPP are minima.

Once the $\delta^{13}\text{C}$ of NPP (δ_{NPP}) and CR (δ_{CR}) were assigned, NPP and CR were calculated from a two end-member mixing model,

$$\text{net DIC production} = CR - NPP \quad (2.3)$$

$$\text{net DIC production} \times \delta_{\text{net DIC production}} = CR \times \delta_{CR} - NPP \times \delta_{NPP} \quad (2.4)$$

where net DIC production is from Equation 2.1 and $\delta_{\text{net DIC production}}$ is net $\delta^{13}\text{C-DIC}$ production (Equation 2.2). NPP and CR are seasonal values calculated from the $\delta^{13}\text{C-DIC}$ mass budgets (Equations 2.3 and 2.4); these values and their assigned $\delta^{13}\text{C}$ values were confirmed with independent data.

Net primary production

While decomposition of vegetation and soil (as CR) added DIC to the reservoirs, NPP consumes CO_2 thereby reducing the DIC concentration and drove the remaining $\delta^{13}\text{C-DIC}$ to become more positive. Vegetation and soil were expected to be the main source of OC for decomposition, but net $\delta^{13}\text{C-DIC}$ production values (mean of -22.4‰ , range of -23.9‰ to -18.8‰ , $n = 15$, for all reservoirs, all years) were not similar to $\delta^{13}\text{C}$ of soil or vegetation (-30‰ to -27‰ ; Table 2.3). Thus NPP rates were sufficiently large to alter the $\delta^{13}\text{C-DIC}$ values. Although net DIC production declined in each reservoir by 55%, 54%, and 35% over five years in the High, Medium, and Low

C reservoirs, the $\delta^{13}\text{C}$ did not exhibit a trend during the same time. *NPP* varied between reservoirs and was dependant on mean depth and flow, as well as differences in nutrients supplied by different decomposing vegetation and soil communities. Therefore to compare *CR* in reservoirs and make predictive models that include *NPP*, contributions of *CR* and *NPP* to net DIC production need to be separated.

On a reservoir scale, 0% to 44% of *CR* was removed by *NPP* (Table 2.4). Year-to-year, *NPP* exhibited similar temporal patterns in the High C (48–195 kg C ha⁻¹) and Medium C (87–207 kg C ha⁻¹) reservoirs where *NPP* was similar for three years and declined in the final two years. *NPP* was most variable in the Low C reservoir (0–322 kg C ha⁻¹) increasing from the first to third years and then declining to zero by the fifth year (Figure 2.4).

The fate of periphyton C in the FLUDEX reservoirs was unknown. Large periphyton sheets, visible during flooding and following drawdown, were not present after snowmelt the following spring. Since a significant portion of periphyton biomass was likely decomposed between flood seasons, periphyton may have been a temporary C sink. Periphyton held over from one year to the next would have been orders of magnitude smaller than vegetation and soil OC (Tables 2.1 and 2.3). Thus net DIC production and gas exchange during the flood season may underestimate the total loss of GHGs to the atmosphere as a result of flooding upland landscapes. However, *CR* captured this.

Community Respiration

CR was from the decomposition of OC stores within the reservoirs. There was enough stored OC in the recently burnt boreal forest catchments, even in the sparsely treed areas, to support GHG fluxes to the atmosphere for the five-year span of this experiment.

CR rates generally declined year-after-year in all reservoirs (Figures 2.4 and 2.5; Table 2.4). Similar to *NPP*, the five-year decline in *CR* was tempered in the third year. In the first year, *CR* rates were the same in the High and Low C reservoirs at 876 and 877 kg C ha⁻¹ and greater in the Medium C reservoir at 965 kg C ha⁻¹. *CR* dropped by about one-third in the second year. In the third year, *CR* was unchanged in the High C reservoir and increased slightly in the Medium and Low C reservoirs. Again in the fourth year, *CR* was unchanged in the High C reservoir, but it declined in both the Medium and Low C reservoirs. In the last year, *CR* in the High C reservoir declined moderately to 425 kg C ha⁻¹, increased slightly in the Medium C reservoir to 510 kg C ha⁻¹, and declined substantially to 216 kg C ha⁻¹.

CR in the Medium and Low C reservoirs was within 30% of the High C reservoir despite differences in OC stores except in the final year in the Low C reservoir. *CR* was about 25% to 50% higher in the first year than in the second and third years of flooding. *CR* over five years declined by half in the

High C (51 %) and Medium C (47 %) reservoirs and by three-quarters in the Low C reservoir (75 %).

CR was 0 % to 75 % (mean of 29 %) greater than net DIC production, across all reservoirs and years, and this reconfirms that *NPP* is important in these reservoirs and must be included in assessments of OC stores and GHG production. Year-to-year trends were different and CR declined more quickly than *NPP*.

Mineralization of DOC from reservoir inflow from Roddy Lake was not a significant source of DIC for several reasons. Reservoir residence times were short (6–9 d). ELA lakes similar to Roddy Lake have residence times greater than 15–20 a and thus Roddy Lake DOC had been subjected to extensive microbial and photolytic degradation prior to entering the reservoirs. Light penetration in the reservoirs is much lower than in ELA lakes and would have led to lower photolytic loss rates of the refractory lake DOC. In the short reservoir residence times, degradation of recalcitrant DOC would have been small. Reservoir DOC concentrations were greater (mean of $660 \mu\text{mol CL}^{-1}$, $n = 128$, all reservoirs in all years) than in Roddy Lake ($440 \pm 40 \mu\text{mol CL}^{-1}$, $n = 43$) due to decomposition of vegetation and soil. Roddy Lake $\delta^{13}\text{C}$ -DOC was -26.9‰ (± 0.2 , $n = 27$) and thus cannot be distinguished from vegetation and soil decomposition in the reservoirs. However, DOC produced within the reservoirs and subsequently converted to DIC was included in CR.

Error assessment

The potential error on the CR and *NPP* estimates can be assessed by adjusting the $\delta^{13}\text{C}$ values assigned to CR and *NPP*. Using combinations of $\pm 1 \text{‰}$ for the assigned $\delta^{13}\text{C}$ CR and *NPP* values (a range that is $> 2SD$ on $\delta^{13}\text{C}$ -DIC measurements) affects CR by only ± 6 –13 % in the High and Medium C reservoirs and ± 6 –17 % in the Low C reservoir for all years and is equal to an average of $\pm 60 \text{ kg C ha}^{-1}$ on both CR and *NPP*. This error is comparable to the errors associated with other budget items such as concentrations, gas exchange, and volumetric measurements of inflow and outflow water (cf. [Matthews et al., 2005](#)).

CH₄ production and CH₄ oxidation

Different microbial pathways produce CH₄ with different $\delta^{13}\text{C}$ -CH₄ values. Methyl-type fermentation has an enrichment factor of -25‰ to -35‰ between source compounds and CH₄. Fermentation differs from CH₄ produced via CO₂ reduction that has an enrichment factor more negative than -55‰ ([Whiticar, 1999](#)). Thus $\delta^{13}\text{C}$ -CH₄ of unoxidised CH₄ can be used to infer the dominant microbial pathway in the flooded soils. However, CH₄ oxidation causes $\delta^{13}\text{C}$ -CH₄ to progressively increase as a greater fraction of CH₄ is consumed. The amount of oxidation can be calculated using a Rayleigh equation

if the $\delta^{13}\text{C-CH}_4$ prior to oxidation can be measured and the CH_4 oxidation enrichment factor is known (Clark and Fritz, 1997),

$$\text{fraction of CH}_4 \text{ oxidised} = 1 - \left(\frac{\delta_{\text{oxidised}} + 1000}{\delta_{\text{unoxidised}} + 1000} \right)^{\frac{1000}{\epsilon}} \quad (2.5)$$

where δ is $\delta^{13}\text{C}$, subscripts residual and unoxidised denote CH_4 remaining after partial oxidation, the initial unoxidised CH_4 , and ϵ is the CH_4 oxidation enrichment factor (calculated so that ϵ values are below 0 ‰ and α values are below 1). Anoxic pore water provided the most representative source of unoxidised CH_4 and was measured throughout the flood season. Although a wide range of CH_4 oxidation enrichment factors have been reported (cf. Whiticar, 1999) (on average about -10 ‰, but some values down to -30 ‰), incubations of methanotrophs from the FLUDEX reservoirs yielded enrichment factors within a narrow range (High C reservoir, -13.9 ‰ at 22 °C and -12.5 ‰ at 30 °C; Medium C reservoir, -14.3 ‰ at 22 °C and -14.0 ‰ and 30 °C (Venkiteswaran and Schiff, 2005)).

Net CH_4 and $\delta^{13}\text{C-CH}_4$ production is calculated from the $\delta^{13}\text{C-CH}_4$ budgets and was thus the residual CH_4 remaining after oxidation and release to the reservoir water column. Net $\delta^{13}\text{C-CH}_4$ production increased for the first four years and declined slightly in the fifth year (Figure 2.3; Table 2.5). In the first year, the main CH_4 production pathway was CO_2 reduction with little subsequent CH_4 oxidation because the measured $\delta^{13}\text{C-CH}_4$ (more negative than -72 ‰) were similar to expected values of -75 ‰ to -85 ‰ for CO_2 reduction with measured pore water $\delta^{13}\text{C-CO}_2$ of about -20 ‰. CH_4 from methyl-type fermentation would have $\delta^{13}\text{C-CH}_4$ between -65 ‰ and -51 ‰ since source compounds would be approximately -30 ‰ to -26 ‰ (range of vegetation, soil, and DOC). In the second and third years, CH_4 was initially produced by CO_2 reduction (more negative than -80 ‰ in the first month of flooding). Thereafter, most CH_4 was produced by methyl-type fermentation because the $\delta^{13}\text{C-CH}_4$ of anoxic pore water (more positive than -55 ‰ after the first month of flooding). In addition, CH_4 oxidation must have occurred because water column values (typically -50 ‰ to -20 ‰) were more positive than anoxic pore water. In the fourth and fifth years, most CH_4 was produced by methyl-type fermentation because the $\delta^{13}\text{C-CH}_4$ of anoxic pore water was always more positive than -55 ‰. Similarly, CH_4 oxidation must have occurred because water column values were more positive than anoxic pore water.

The $\delta^{13}\text{C-CH}_4$ mass budgets captured the net $\delta^{13}\text{C-CH}_4$ production after partial oxidation and, in these reservoirs, this corresponds to the CH_4 that enters the water column. To separate CH_4 production from oxidation, the water column (residual CH_4 after partial oxidation) was compared to anoxic pore water (before oxidation). CH_4 oxidation occurred strictly in the flooded soils. Unlike other reservoirs or many lakes (e.g., Duchemin et al., 1995; Rudd

and Hamilton, 1975), the oxic-anoxic boundary was at the SWI and not in the water column. Water column and pore water data indicated that $\delta^{13}\text{C-CH}_4$ increased only across the SWI (by 3 ‰ to 9 ‰ from pore water to water column). Upper water columns exhibited little or no variation in $\delta^{13}\text{C-CH}_4$. Water column $\delta^{13}\text{C-CH}_4$ matched the $\delta^{13}\text{C-CH}_4$ added to benthic chambers. Agreement between light-exposed chamber and water column data shows that oxidation occurred below the SWI. Thus in absence of light, the unoxidised CH_4 ($\delta^{13}\text{C-CH}_4$ of pore water) was added to darkened chambers, and in the presence of light, residual CH_4 (same $\delta^{13}\text{C-CH}_4$ as the water column) was added to light-exposed chambers. The diffusion of photosynthetically derived O_2 into the anoxic flooded soil appears to have played a role in CH_4 oxidation.

A large fraction of the CH_4 produced in the anoxic soils was oxidised before being released to the water column as net CH_4 production. The fraction of CH_4 oxidised increased from the first to third years. In the second year, 69%, 26%, and 64% of the CH_4 produced was oxidised in the High, Medium, and Low C reservoirs. In the third year, when CH_4 concentrations (Figure 2.2) and loss of CH_4 via gas exchange were generally greatest (Table 2.5), 91%, 77%, and 78% was oxidised in the High, Medium, and Low C reservoirs. This fraction increased to 96%, 83%, and 79% in the High, Medium, and Low C reservoirs in the fourth year. In the fifth year, the fraction of the CH_4 produced that was oxidised was 85%, 77%, and 76% in the High, Medium, and Low C reservoirs. In order for net CH_4 production to have increased from the first to third years and for the fraction of CH_4 oxidised to also have increased, CH_4 production in the flooded soils (methanogenic activity) must have increased by about 10-fold.

The $\delta^{13}\text{C-CO}_2$ produced during CH_4 oxidation was more negative than the source $\delta^{13}\text{C-CH}_4$ because CH_4 oxidation was incomplete and also very much more negative than the pre-existing $\delta^{13}\text{C-DIC}$. If enough CO_2 were to have been produced, the $\delta^{13}\text{C-DIC}$ could have been changed. However, the amount of CH_4 oxidised to CO_2 was very much smaller ($< 10 \mu\text{mol L}^{-1}$) than the DIC pool in these reservoirs ($> 100 \mu\text{mol L}^{-1}$). Therefore any change in $\delta^{13}\text{C-DIC}$ due to CO_2 from CH_4 oxidation was too small to have been detected in the reservoirs.

The importance of ebullition

CO_2 ebullition was very small in all years and all reservoirs, less than 0.5% of DIC output (Table 2.4). Ebullitive $\delta^{13}\text{C-CO}_2$ values were similar to $\delta^{13}\text{C-CO}_2$ pore water values calculated from $\delta^{13}\text{C-DIC}$ and pH.

Ebullition rates of CH_4 were consistently low in all reservoirs in the first year. CH_4 ebullition increased sharply 8–10 weeks after flooding in each of the second to fifth years. Ebullition, as a portion of total CH_4 emissions to the atmosphere (ebullition and gas exchange) also increased from the first

to third year. In the first year, ebullition accounted for 0 % to 15 % of total surface emissions. In the second year, this increased to 50 % to 80 % of total surface emissions. In the third year, this further increased to 75 % to 90 % of total surface emissions. This led to a higher proportion of CH₄ loss via ebullition because of the low solubility of CH₄ in water. In the fourth and fifth years, this remained at 70 % to 80 % in the High C reservoir but declined to 44 % to 50 % in the Medium and Low C reservoirs (Table 2.5). CH₄ ebullition increased (first to third year) and decreased (fourth and fifth year) concomitantly with net CH₄ production also indicating increasing then decreasing activity by methanogens.

During periods of high rates of ebullition in the second to fifth years, $\delta^{13}\text{C-CH}_4$ in gas bubbles ranged from -65‰ to -45‰ . The $\delta^{13}\text{C-CH}_4$ of ebullition increased during flood season and followed outflow $\delta^{13}\text{C-CH}_4$, -93‰ to -43‰ in the second year, and -64‰ to -50‰ in the third year (Figure 2.2). Similarly in the fourth and fifth years the $\delta^{13}\text{C-CH}_4$ of ebullition was similar to out flow $\delta^{13}\text{C-CH}_4$ values between -60‰ and -50‰ . One notable exception to this pattern was the High C reservoir in the fourth and fifth years when $\delta^{13}\text{C-CH}_4$ outflow values increased to -11‰ but the $\delta^{13}\text{C-CH}_4$ of ebullition remained between -60‰ and -50‰ . Although ebullition $\delta^{13}\text{C-CH}_4$ was more negative than water column $\delta^{13}\text{C-CH}_4$, ebullitive CH₄ was more positive than anoxic pore water and thus affected by oxidation. CH₄ in bubbles was the residual after 50 % to 75 % of the CH₄ had been oxidised. Therefore bubble formation must have occurred within the top of the soil because CH₄ in bubbles was partially oxidised and pore water at 2 cm below the SWI was anoxic.

The depth to which O₂ from benthic photoautotrophs diffused into the soil must have been severely limited by O₂ consumption due to CR. Because CH₄ in bubbles was subject to less oxidation than the diffusive flux across the SWI, in general, a increasing fraction of CH₄ production was released to the atmosphere from the first to fifth years of flooding in all reservoirs. Thus total (or gross) CH₄ production must have been highest in the third or fourth year given that a greater fraction was oxidised and net CH₄ production was greater than other years.

Organic carbon stores as predictors of GHG production

Decomposition of OC stores, as measured by CR, ultimately differed little between reservoirs: the five-year sum of CR for each reservoir was within 5 % (Figure 2.5). The initial hypothesis of ELARP (the Experimental Lakes Area Reservoir Project) (cf. Kelly *et al.*, 1997; St.Louis *et al.*, 2004) and FLUDEX (cf. Bodaly *et al.*, 2004) was that long-term GHG production was positively related to the quantity of OC stored in vegetation and soils. Within the FLUDEX reservoirs, this hypothesis did not hold true. While the differences between CR in the reservoirs increased in each year (CR in the reservoirs differed by

9 %, 16 %, 23 %, 24 %, and 58 % in each of the five years), the reservoirs with the greatest and least CR in each year were seldom the High and Low C reservoir. Within FLUDEX, OC stores were therefore not good short-term predictors of carbon lability.

All reservoirs contained a dry forest community, but the High C also had a moist forest community and the Low C reservoir also had a moss-lichen and a bedrock community. The five-year decline in CR was greatest in the Low C reservoir and similar in the High and Medium C reservoirs indicating that, after five years, CR was lowest in the moss-lichen community and CR was similar in the moist and dry forest communities. Litterbag and laboratory incubations of vegetation and soil indicated that the dry forest communities have a greater OC decomposition rate than the moist forest community (Baril, 2001; Hall and St.Louis, 2004) suggesting that carbon lability is different in each community. Further, DOC leachability (ability to leach DOC from parent material) and DOC lability from vegetation and soils likely differed between community types (Ferguson, 2000). Nevertheless, the five-year total CR was very similar among reservoirs. Long-term CR may become more related to OC stores if leachability and lability become less important with time as more easily decomposable components are consumed.

The 100-year time horizon GWP of CH₄ is 23 times that of CO₂ (Ehhalt et al., 2001) and thus the increase in CH₄ production and the shift from gas exchange (CH₄ more susceptible to oxidation) to ebullition (CH₄ less susceptible to oxidation) resulted in moderating the decline in CR. Nevertheless, the total GHG GWP per year declined by 42 %, 40 %, and 68 % in the High, Medium, and Low C reservoirs over five years (Figure 2.5). This annual rate of decline was similar in the High and Medium C reservoirs and greatest in the Low C reservoir. When summed across five years, the five-year GHG GWP of each reservoir was within 1 % of each other. Thus after 5 years, the relationship between GHG emissions and pre-flood OC stores did not hold. However, the medium- and long-term, e.g., 10–50 years, relationship between GHG emissions and pre-flood OC stores may hold if the trends in CR, net CH₄ production, and CH₄ ebullition continue.

Rudd et al. (1993) and St.Louis et al. (2000) suggested that GHG emissions from reservoirs should be directly related to OC stores not including tree boles. This may hold true if the following confounding factors are constant between reservoirs: lability of OC stores, photosynthetic consumption of DIC, gas exchange coefficient, and water residence time. Comparing CR rather than surface GHG fluxes to OC stores not including tree boles will eliminate these confounding factors. GHG emissions from different reservoirs can only be easily predicted and compared from measures of OC stores if these other factors are similar.

2.5 Conclusions

To compare processes between years and reservoirs, $\delta^{13}\text{C}$ was used to separate and quantify *CR*, *NPP*, CH_4 production, and CH_4 oxidation. *Matthews et al.* (2005) observed a general DIC concentration decline and a general CH_4 concentration increase in the FLUDEX reservoirs over three years. However, changes in the processes controlling DIC and CH_4 production could not have been determined without $\delta^{13}\text{C}$.

After five years of $\delta^{13}\text{C}$ research, results from FLUDEX conclude that: (1) *NPP* consumed 0% to 44% of the DIC produced by *CR*, depending on year and reservoir; (2) year-to-year, *CR* declined more quickly than *NPP*; (3) CH_4 production in the flooded soils increased 10-fold; (4) CH_4 oxidation greatly reduced the net CH_4 flux to the atmosphere; (5) CH_4 oxidation was light mediated; (6) bubble formation occurred in the upper portion of flooded soils where CH_4 oxidation occurred; (7) *CR* and CH_4 production combined indicate that the GWP of the total GHG flux from the FLUDEX reservoirs declined markedly from the first to fifth year; and (8) neither *CR* nor total GHG fluxes were directly related to the quantity of flooded OC.

CR, *NPP*, CH_4 production, and CH_4 oxidation rates were specific to these reservoirs. However, FLUDEX results can be used in other systems when scaling up GHG production estimates to larger reservoirs since processes affecting GHGs must be modelled independently. For example, *NPP* may be less important in large reservoirs because of dilution of SWI-derived nutrients, and differences in reservoir shape and hydrology. Also, inflow water from Roddy Lake was clear compared to reservoirs with inflows from surrounding forested catchments and DOC in inflows must be accounted for in a similar fashion to catchment input in these budgets. *CR* estimates can be scaled to shallow areas of large reservoirs where temperature regimes are similar. Further work on the temperature dependence of *CR* and CH_4 production and oxidation is needed to extend the applicability of FLUDEX. The combination of DIC and CH_4 concentrations and their $\delta^{13}\text{C}$ values: (1) provided a method for separating processes, (2) described reservoir evolution by the year-to-year changes in processes, and (3) illuminated the importance of different within-reservoir processes that affect both gross GHG production and net GHG emission.

Acknowledgements

R. J. Elgood provided important logistical support. We thank at least ten students who provided field assistance. W. A. Mark provided excellent EA-IRMS analysis and IRMS assistance. This research was funded by the Centre for Research in Earth and Space Technology, Canadian Foundation for Climate and Atmospheric Sciences, Climate Change Action Fund, and Nat-

ural Sciences and Engineering Research Council of Canada. Environment Canada's Science Horizons Youth Internship Program funded a laboratory assistant. Keith K. Venkiteswaran generated Figure 2.1. FLUDEX was funded by Fisheries and Oceans Canada, Manitoba Hydro, and Hydro-Québec.

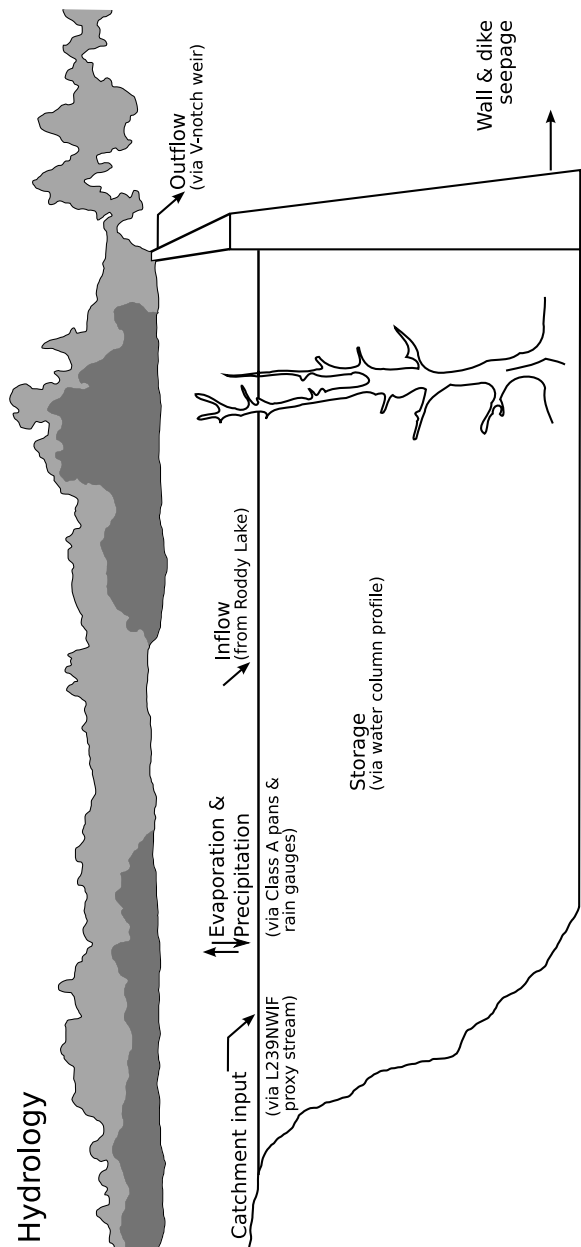


Figure 2.1: Schematic hydrological budget for the FLUDEX reservoirs. Each of the inputs and outputs are measured or estimated for each reservoir each year. The north-west inflow stream of L239 served as a well-studied hydrological proxy for catchment input. Grey sections at the top of this pictorial are forests at the far shore of the reservoir.

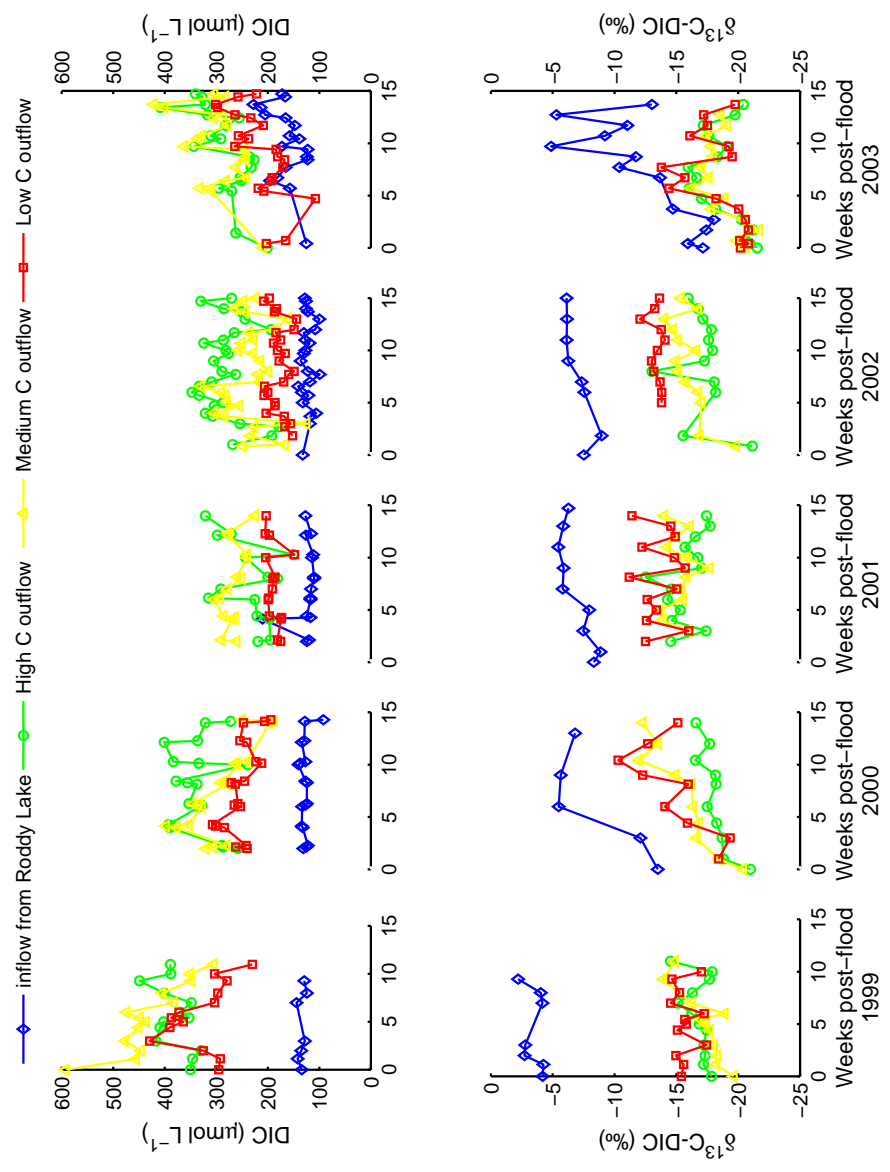


Figure 2.2: DIC concentrations and $\delta^{13}\text{C-DIC}$ of FLUDEX reservoir inflow and outflows. Flooding began on 22 June 1999, 30 May 2000, 29 May 2001, 02 June 2002, and 04 June 2003.

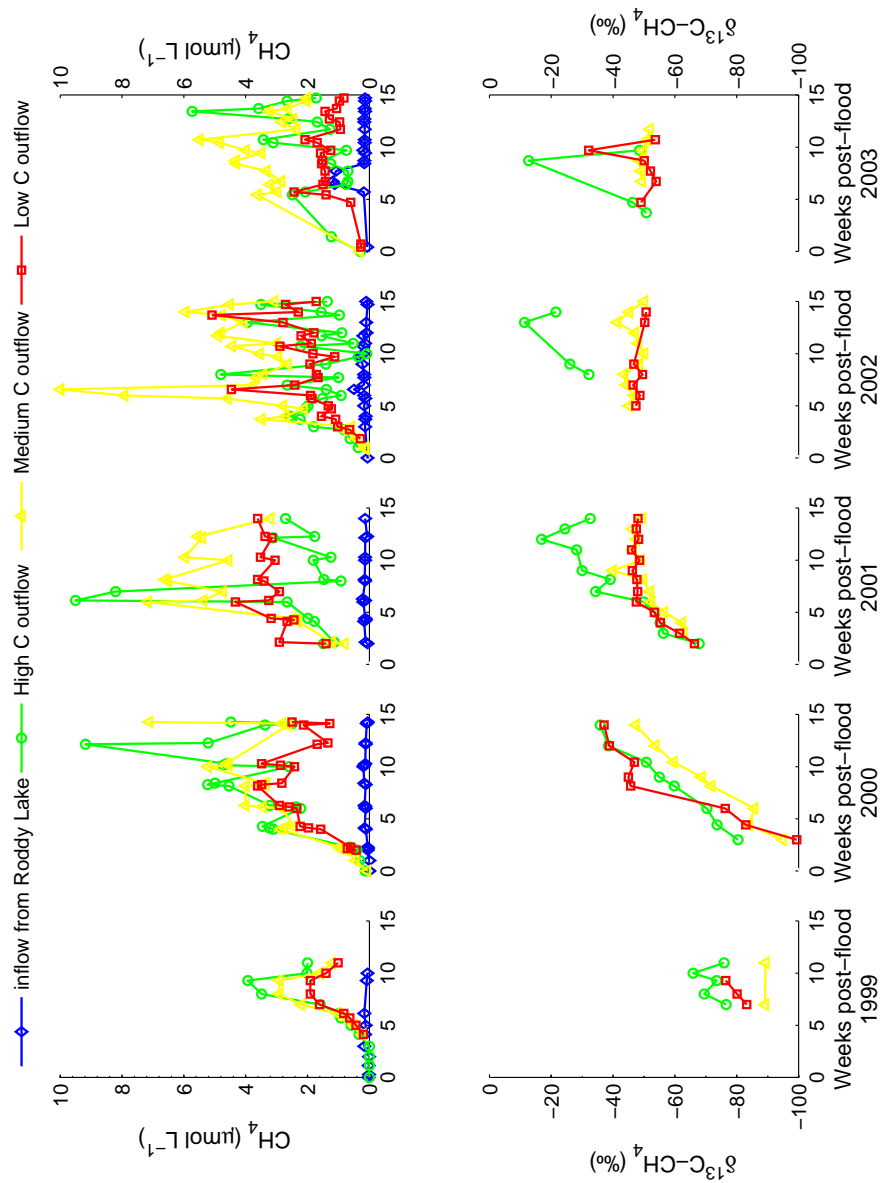


Figure 2.3: CH_4 concentrations and $\delta^{13}\text{C}-\text{CH}_4$ of FLUDEX reservoir inflow and outflows. Flooding began on 22 June 1999, 30 May 2000, 29 May 2001, 02 June 2002, and 04 June 2003. CH_4 concentrations were insufficient for $\delta^{13}\text{C}-\text{CH}_4$ analysis in reservoir inflow from Roddy Lake and reservoir outflow prior to the seventh week of flooding in 1999.

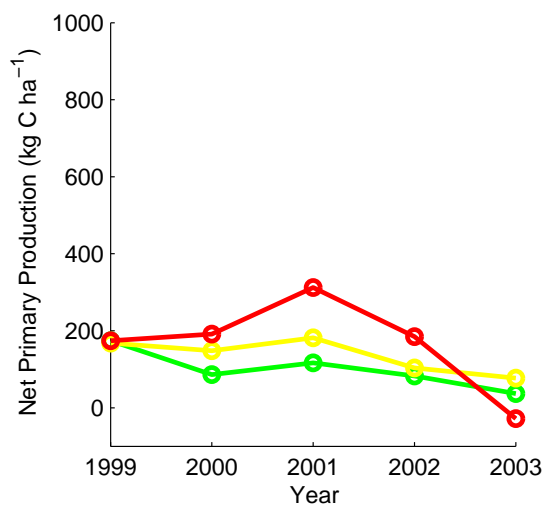
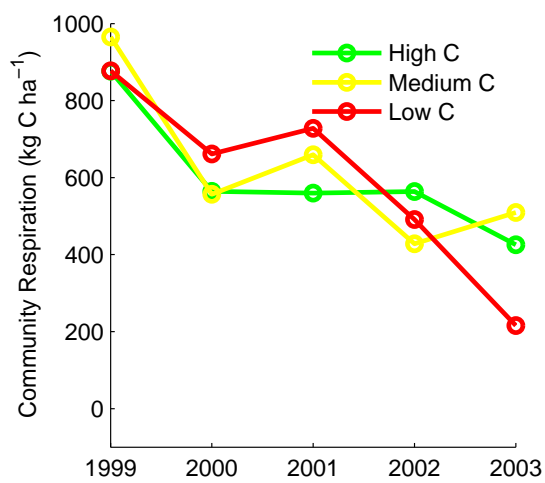


Figure 2.4: Rates of CR and NPP in FLUDEX reservoirs from 1999–2003 calculated from $\delta^{13}\text{C}$ -DIC budgets.

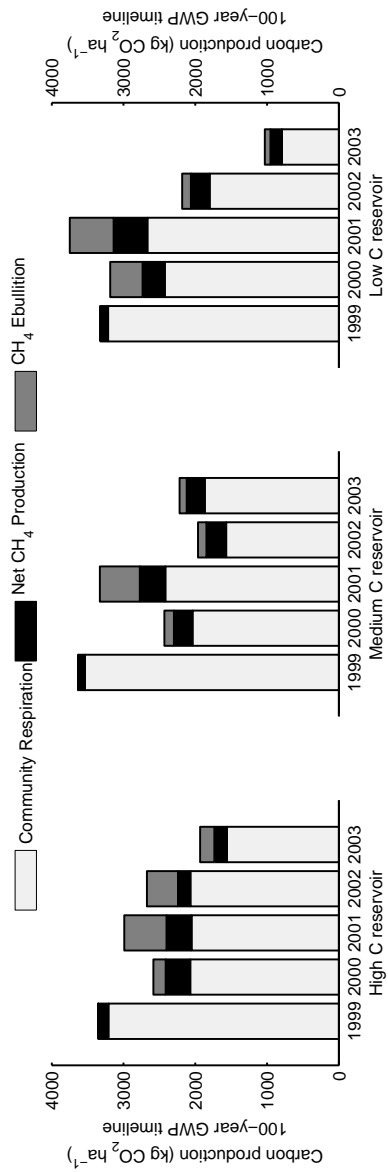


Figure 2.5: Community respiration, net CH₄ production, and CH₄ ebullition in FLUDEX reservoirs for 1999–2001 expressed as kg CO₂ ha⁻¹ of global warming potential (GWP). The 100-year time horizon GWP of CH₄ is 23 times that of CO₂, hence net CH₄ production and CH₄ ebullition have been multiplied by 23 to allow direct comparison of GWP by all these sources of GHGs.

Table 2.1: FLUDEX reservoir physical characteristics, forest type, dominant vegetation and soil communities, and carbon stores.

	High C reservoir	Medium C reservoir	Low C reservoir
Water surface area (m ²)	7400	5000	6300
Upland catchment area (m ²)	47800	7300	900
Reservoir volume (m ³)	6870	4270	7170
Mean depth (m) ^a	0.9	0.9	1.1
Total soil carbon (kg C ha ⁻¹) (litter, fungal-humic, and mineral layers)	18300	7200	11100
Total carbon in above ground vegetation (kg C ha ⁻¹)	27600	27700	19800
Total carbon (kg C ha ⁻¹)	45900	34900	308900
Dominant vegetation and soil communities (percentage of area)	<ol style="list-style-type: none"> wet forest community (53 %): jack pine (<i>Pinus banksiana</i> Lamb.), Labrador tea (<i>Ledum groenlandicum</i> (Oeder)), leatherleaf (<i>Chamaedaphne calyculata</i> (L.) Moench), <i>Sphagnum</i> spp. dry forest community (47 %): jack pine, <i>Polytrichum</i> spp. 	<ol style="list-style-type: none"> dry forest community (47 %): jack pine, <i>Polytrichum</i> spp. 	<ol style="list-style-type: none"> dry forest community (73 %): jack pine, blueberry (<i>Vaccinium</i> spp.) lichen and exposed bedrock community (22 %) lichen-moss pillow community (5 %): reindeer lichen (<i>Cladonia</i> spp.), cup lichen (<i>Cladonia</i> spp.), <i>Polytrichum</i> spp., <i>Racomitrium macrocarpon</i> (Hedw.) Brid., grasses (<i>Poa</i> spp.)

^a Reservoir Volume ÷ Water Surface Area

Table 2.2: The hydrology budgets for FLUDEX reservoirs for 1999–2003. All volumes are in m³.

	High C reservoir					Medium C reservoir					Low C reservoir				
	1999	2000	2001	2002	2003	1999	2000	2001	2002	2003	1999	2000	2001	2002	2003
Inflow	78 600	93 300	84 800	83 600	88 500	76 700	69 600	74 700	53 400	56 900	89 900	108 600	106 900	98 400	115 200
Precipitation	1 340	1 840	1 310	1 380	1 130	900	1 240	880	920	760	1 260	1 730	1 230	1 290	1 060
Throughfall	790	1 020	1 300	1 360	1 120	530	690	880	920	760	620	800	1 020	1 070	880
Catchment Input	4 680	12 220	4 950	4 200	1 900	710	1 850	780	980	290	60	150	90	40	40
Total Inputs	85 410	108 380	92 360	90 540	92 650	78 840	73 380	77 240	56 220	58 710	91 840	111 280	109 240	100 800	117 180
V-notch Outflow	60 200	80 200	64 000	65 900	60 400	60 800	57 200	63 700	46 300	44 700	33 500	42 500	51 500	37 400	43 800
Wall Seepage	16 000	15 900	13 000	11 200	11 700	15 400	13 900	14 500	12 000	11 600	23 100	19 100	12 200	18 900	11 200
Fracture											36 900	43 400	40 800	30 700	45 500
Storage	6 870	6 870	6 870	6 870	6 870	4 260	4 260	4 260	4 260	4 260	7 120	7 120	7 120	7 120	7 120
Evaporation	1 620	1 800	1 900	1 820	2 240	1 350	1 300	1 350	1 520	1 600	1 380	1 650	1 570	1 930	1 860
Canopy interception	920	1 316	370	390	320	620	890	250	260	220	720	1 030	290	300	250
Total Outputs	85 610	106 086	86 140	86 180	81 530	82 430	77 550	84 060	64 340	62 380	102 720	114 800	113 480	96 350	109 730
Water yield (%) ^a	100.2	97.9	93.3	95.2	88.0	104.6	105.7	108.8	114.4	106.3	111.8	103.2	103.9	95.6	93.6
Residence time (d) ^b	8.4	7.3	8.6	8.3	8.3	5.6	6.7	6.5	8.3	8.1	8.1	7.4	7.6	7.6	6.8
Exchanges ^c	12.5	15.4	12.5	12.5	11.9	19.3	18.2	19.7	15.1	14.6	14.4	16.1	15.9	13.5	15.4
Days of weir outflow	96	105	103	99	100	95	104	108	102	98	91	100	100	87	94
Days to fill	8	10	13	10	12	9	11	9	7	14	13	15	17	21	18

^a Total Outputs ÷ Total Inputs

^b Reservoir Volume ÷ (Total Inputs ÷ Total Days)

^c Total Outputs ÷ Reservoir Volume

Table 2.3: Summary of $\delta^{13}\text{C}$ of DIC, CH_4 , soil, vegetation, and periphyton.

	$\delta^{13}\text{C-DIC}$ (‰)	$\delta^{13}\text{C-CH}_4$ (‰)	$\delta^{13}\text{C}$ of total C (‰)
Inflow from Roddy Lake	-18.0 to -2.2 ^a -8.3 \pm 4.2 (<i>n</i> = 42) ^b		
High C reservoir outflow	-21.6 to -12.5 ^a -17.4 \pm 1.9 (<i>n</i> = 64) ^b	-80.4 to -11.4 ^a -47.4 \pm 20.1 (<i>n</i> = 33) ^b	
Medium C reservoir outflow	-21.7 to -12.0 ^a -16.7 \pm 2.1 (<i>n</i> = 61) ^b	-94.8 to -39.9 ^a -55.6 \pm 14.5 (<i>n</i> = 39) ^b	
Low C reservoir outflow	-20.8 to -10.3 ^a -15.4 \pm 2.7 (<i>n</i> = 61) ^b	-99.4 to -32.1 ^a -54.2 \pm 14.4 (<i>n</i> = 37) ^b	
Catchment input	-25.7 \pm 0.8 (<i>n</i> = 4) ^b		
Periphyton during flooding			2000: -32.7 \pm 2.4 (<i>n</i> = 22) ^{b,c} 2001: -32.6 \pm 1.7 (<i>n</i> = 13) ^{b,c}
Periphyton after flooding			2000: -36.6 \pm 1.9 (<i>n</i> = 3) ^{b,c} 2001: -33.3 \pm 1.7 (<i>n</i> = 6) ^{b,c} 2002: -34.3 \pm 2.3 (<i>n</i> = 12) ^{b,c}
Vegetation (11 species)			-29.4 \pm 2.1 (<i>n</i> = 16) ^{b,c,d}
Litter soil layer			-28.1 \pm 1.3 (<i>n</i> = 17) ^{b,c,d}
Fungal-humic soil layer			-27.3 \pm 1.0 (<i>n</i> = 18) ^{b,c,d}

^a range in all years

^b mean \pm *SD*

^c combined data for all reservoirs

^d prior to flooding

Table 2.4: The volume- and mass-weighted $\delta^{13}\text{C}$ of dissolved inorganic carbon (DIC) budgets for FLUDEX reservoirs for 1999–2003 (DIC in kgCh^{-1} and $\delta^{13}\text{C}$ in ‰).

	High C reservoir												Medium C reservoir												Low C reservoir															
	1999				2000				2001				2002				2003				1999				2000				2001				2002				2003			
	DIC	$\delta^{13}\text{C}$	DIC	$\delta^{13}\text{C}$	DIC	$\delta^{13}\text{C}$	DIC	$\delta^{13}\text{C}$	DIC	$\delta^{13}\text{C}$	DIC	$\delta^{13}\text{C}$	DIC	$\delta^{13}\text{C}$	DIC	$\delta^{13}\text{C}$	DIC	$\delta^{13}\text{C}$	DIC	$\delta^{13}\text{C}$	DIC	$\delta^{13}\text{C}$	DIC	$\delta^{13}\text{C}$	DIC	$\delta^{13}\text{C}$	DIC	$\delta^{13}\text{C}$	DIC	$\delta^{13}\text{C}$	DIC	$\delta^{13}\text{C}$	DIC	$\delta^{13}\text{C}$	DIC	$\delta^{13}\text{C}$	DIC	$\delta^{13}\text{C}$		
Inflow	169	-3.4	194	-8.7	167	-7.0	167	-7.5	223	-12.6	248	-3.4	217	-8.7	222	-6.9	158	-7.4	216	-12.3	248	-3.4	268	-8.8	251	-6.9	231	-7.4	340	-12.6	0	-8.0	1	-8.0	0	-8.0	1	-8.0	0	-8.0
Precipitation ^a	0	-8.0	1	-8.0	0	-8.0	0	-8.0	0	-8.0	0	-8.0	0	-8.0	0	-8.0	0	-8.0	0	-8.0	0	-8.0	1	-8.0	0	-8.0	0	-8.0	0	-8.0	0	-8.0	0	-8.0	0	-8.0	0	-8.0		
Catchment Input	41	-25.7	128	-25.7	56	-25.7	45	-25.7	20	-25.7	8	-25.7	29	-25.7	13	-25.7	16	-25.7	16	-25.7	5	-25.7	2	-25.7	1	-25.7	0	-25.7	0	-25.7	0	-25.7	0	-25.7	0	-25.7	0	-25.7	0	-25.7
Total Inputs	211	-7.8	324	-15.5	223	-11.6	213	-11.3	244	-13.7	256	-4.1	246	-10.7	235	-8.0	175	-9.1	221	-12.6	249	-3.5	271	-8.9	253	-7.0	232	-7.5	341	-12.6	0	-8.0	1	-8.0	0	-8.0	1	-8.0	0	-8.0
V-notch Outflow	378	-16.5	407	-17.9	249	-15.9	298	-17.3	288	-18.5	602	-16.9	369	-15.5	406	-15.3	261	-16.1	333	-18.2	194	-15.7	196	-14.9	186	-13.6	127	-13.5	172	-17.5	0	-8.0	0	-8.0	0	-8.0	0	-8.0	0	-8.0
Gas Exchange ^b	389	-23.9	278	-25.8	324	-23.0	317	-24.2	242	-24.5	263	-24.8	162	-23.6	188	-22.5	145	-22.4	195	-24.6	337	-22.9	216	-21.7	210	-16.4	202	-18.3	165	-22.6	0	-8.0	0	-8.0	0	-8.0	0	-8.0	0	-8.0
Wall Seepage	101	-16.6	84	-17.9	58	-15.9	53	-17.4	55	-18.7	155	-17.1	101	-15.9	89	-15.3	73	-16.4	92	-18.5	147	-15.7	88	-15.3	52	-13.6	68	-13.5	43	-18.0	0	-8.0	0	-8.0	0	-8.0	0	-8.0	0	-8.0
Fracture Storage	45	-17.0	33	-15.0	35	-17.0	26	-17.0	47	-17.0	33	-16.0	23	-16.7	30	-14.0	20	-14.0	34	-17.0	233	-15.7	199	-15.3	174	-13.6	116	-13.5	174	-18.0	0	-8.0	0	-8.0	0	-8.0	0	-8.0	0	-8.0
Total Outputs	912	-19.7	802	-20.5	666	-19.4	694	-20.4	632	-20.7	1053	-18.9	655	-17.6	713	-17.2	500	-17.9	653	-20.1	952	-18.3	740	-17.1	668	-14.4	538	-15.2	585	-18.9	0	-8.0	0	-8.0	0	-8.0	0	-8.0	0	-8.0
Net DIC Production	702	-23.3	478	-23.9	444	-23.3	481	-24.4	388	-25.1	797	-23.6	408	-21.8	478	-21.7	325	-22.6	432	-23.9	703	-23.5	470	-21.9	415	-18.8	306	-21.1	244	-27.5	0	-8.0	0	-8.0	0	-8.0	0	-8.0	0	-8.0
Community Respiration ^c	897	-27.0	578	-27.0	572	-27.0	568	-27.0	437	-27.0	993	-27.0	579	-27.0	684	-27.0	434	-27.0	519	-27.0	898	-27.0	673	-27.0	737	-27.0	480	-27.0	235	-27.0	0	-8.0	0	-8.0	0	-8.0	0	-8.0	0	-8.0
Net Primary Production ^c	195	-40.4	100	-41.8	129	-39.8	87	-41.2	48	-42.4	196	-40.8	171	-39.4	207	-39.3	109	-40.0	87	-42.2	195	-39.7	203	-38.9	322	-37.5	174	-37.4	-9	-41.4	0	-8.0	0	-8.0	0	-8.0	0	-8.0	0	-8.0
Flood Season Ebullition	0.01	-23.6	0.48	-16.4	1.77	-13.6	1.01	-19.2	0.3	-13.6	0.07	-25.3	0.43	-17.5	1.48	-14.2	0.34	-17.2	0.3	-14.2	0.00	0.84	-14.7	1.46	-16.4	0.31	-17.8	0.18	-16.4	0	-8.0	0	-8.0	0	-8.0	0	-8.0	0	-8.0	
Drawdown Ebullition																																								

^a DIC input from precipitation is less than 1% that of the inflow; pH of rain at ELA from May to November-2001 was 5.48 ± 0.37 (mean \pm SD, $n = 42$, range 4.35–6.65).

^b $\delta^{13}\text{C}$ values are calculated from surface $\delta^{13}\text{C}$ -DIC values, pH, temperature, and carbonate species isotope fractionation (Clark and Fritz, 1997).

^c $\delta^{13}\text{C}$ values are assigned: -27‰ for CR and based on calculated $\delta^{13}\text{C}$ -CO₂ with $\epsilon = -19$ ‰ for NPP.

Table 2.5: The volume- and mass-weighted $\delta^{13}\text{C}$ of methane (CH_4) budgets for FLUDEX reservoirs for 1999–2003 (CH_4 in kg Ch a^{-1} and $\delta^{13}\text{C}$ in ‰).

	High C reservoir												Medium C reservoir												Low C reservoir											
	1999			2000			2001			2002			2003			1999			2000			2001			2002			2003								
	CH_4	$\delta^{13}\text{C}$		CH_4	$\delta^{13}\text{C}$		CH_4	$\delta^{13}\text{C}$		CH_4	$\delta^{13}\text{C}$		CH_4	$\delta^{13}\text{C}$		CH_4	$\delta^{13}\text{C}$		CH_4	$\delta^{13}\text{C}$		CH_4	$\delta^{13}\text{C}$		CH_4	$\delta^{13}\text{C}$										
Inflow	0.1	-47.4		0.1	-47.4		0.2	-47.4		0.2	-47.4		0.2	-47.4		0.2	-47.4		0.2	-47.4		0.2	-47.4		0.2	-47.4		0.2	-47.4							
Precipitation ^a																																				
Catchment Input																																				
Total Inputs	0.1	-47.4		0.1	-47.4		0.2	-47.4		0.2	-47.4		0.2	-47.4		0.2	-47.4		0.2	-47.4		0.2	-47.4		0.2	-47.4		0.2	-47.4							
V-notch Outflow	1.4	-72.3	4.3	-53.9	2.8	-40.7	1.9	-26.0	2.2	-45.4																										
Gas Exchange	2.7	-72.3	5.7	-55.2	7.3	-37.7	3.5	-27.1	3.0	-44.7																										
Wall Seepage	0.3	-72.3	0.9	-55.1	0.9	-36.8	0.3	-26.6	0.4	-45.4																										
Fracture																																				
Storage	0.3	-72.3	0.4	-50.0	0.6	-37.0	0.2	-37.0	0.5	-37.0																										
Total Outputs	4.8	-72.3	11.4	-54.5	11.6	-38.3	5.9	-27.0	6.1	-44.3																										
Net CH_4 production	4.6	-73.0	11.2	-54.6	11.4	-38.2	5.7	-26.3	5.8	-44.1																										
Flood Season Ebullition	0.0	-72.3	5.6	-54.2	19.1	-55.4	14.1	-57.1	6.5	-55.4																										
Drawdown Ebullition																																				

^a CH_4 input from precipitation is assigned a $\delta^{13}\text{C}$ value of -47.4 ‰.

Chapter 3

Importance of ebullition and sediment storage to greenhouse gas emissions from shallow boreal forest reservoirs

Abstract

The diffusive fluxes of CO₂ and CH₄ from reservoir surfaces to the atmosphere have been characterised for some temperate, northern, and tropical reservoirs. The ebullitive flux of these gases during the flood season has been less well documented and the ebullitive flux released when reservoirs are drained of water each autumn has not previously been quantified. The Flooded Upland Dynamics Experiment (FLUDEX) involved the creation of three experimental reservoirs, in boreal forest uplands, differing in their amount of stored organic carbon. Although these reservoirs are shallow, they share similar characteristics with larger reservoirs and represent the shallow zones of larger boreal reservoirs. The reservoirs were flooded for five consecutive years, to study changes in greenhouse gas cycling due to flooding. Soil gas surveys were performed in FLUDEX reservoirs at the end of two flood seasons. Stores of soil gas (predominantly CH₄) available to flux to the atmosphere at the end of the flood season were almost as large as the ebullitive flux for the entire flood season and generally as large as whole-reservoir net CH₄ production for the entire flood season. In the shallow zones of reservoirs, this large flux of CH₄ is seldom measured or considered in greenhouse gas flux inventories and, as a result, current calculations of greenhouse gas fluxes from reservoirs are underestimates.

3.1 Introduction

When soils and vegetation are flooded during reservoir creation, landscape-scale carbon (C) cycling is significantly altered and results in a net flux of the greenhouse gases (GHGs) carbon dioxide (CO₂) and methane (CH₄) to the atmosphere for decades and possibly centuries (*St.Louis et al., 2000*). However, GHG emissions from reservoir surfaces to the atmosphere are understudied and relative to their surface area there are few data for CO₂ and CH₄ (*Abril et al., 2005; Delmas et al., 2001; Duchemin et al., 1995; Galy-Lacaux et al., 1997, 1999; Huttunen et al., 2002; Keller and Stallard, 1994; Kelly et al., 1994, 1997; Matthews et al., 2005; McKenzie et al., 1998; Rudd et al., 1993; Scott et al., 1999; St.Louis et al., 2000; Tremblay et al., 2004, Chapter 2*) and very little for N₂O (*Hendzel et al., 2005; Huttunen et al., 2002*). The ebullitive flux of GHGs from reservoir surfaces has received still less study (e.g., *Huttunen et al., 2002; Keller and Stallard, 1994; Matthews et al., 2005*). A recent review suggests that 6–16 % of all natural CH₄ emissions come from lakes and about half of that CH₄ flux is estimated to be from ebullition (*Bastviken et al., 2004*). As such, ebullition from reservoirs deserves further study.

Bubble CH₄ and CO₂ concentrations and their molar and isotopic ratios were used to determine the importance of ebullition, both flood-season ebullition and bubble storage, relative to total GHG fluxes from three experimental upland boreal reservoirs. Flood-season ebullition is the flux of bubbles from the flooded soils to the atmosphere during the flood season. Bubble storage are the bubbles trapped in the soil matrix that are released directly to the atmosphere as reservoir levels are lowered in the autumn.

3.2 Methods

Field site

Three FLUDEX (Flooded Uplands Dynamic Experiment) reservoirs were built at the Experimental Lakes Area (ELA) in northwestern Ontario (49°40' N 93°45' W) to study the effects of upland flooding on GHG and mercury cycling (*Bodaly et al., 2004*). The reservoirs were flooded seasonally from 1999 to 2003 for about 113 d a⁻¹. Reservoirs were named according to their amount of pre-flood organic carbon (OC) as High, Medium, and Low C reservoirs (Table 2.1). Details of FLUDEX construction, site selection, and pre-flood forest conditions have been reported elsewhere (*Bodaly et al., 2004; Matthews et al., 2005, Chapter 2*). A brief description follows.

Each reservoir of 0.5 to 0.8 ha surface area flooded a hill slope and was contained on three sides by wooden walls and gravel dikes and the fourth side was left open to the upslope catchment. Wooden walls, lined with polypropylene, were built where flood depth was expected to be 1 m or greater. Polypropylene-lined gravel dikes were built where flood depth was expected

to be less than 1 m.

Pre-flood C in low shrubs, herbs, mosses, and lichens was estimated by collecting material from quadrats in each reservoir (Heubert, 1999). Pre-flood C in woody biomass in tall shrubs and trees was estimated from trunk diameter measurements and standard regression equations (cf. Dyck and Shay, 1999). Pre-flood C in the canopies of tall shrubs and trees was estimated from monthly collections of litter fall from three locations per reservoir (Matthews et al., 2005). Pre-flood soil C was estimated from soil cores collected from six or seven locations per reservoir. Soil horizons (litter, fungal-humic, charcoal, and mineral) were measured for bulk density and analysed for C concentration and C stable isotopic ratio ($^{13}\text{C}/^{12}\text{C}$; hereafter referred to as $\delta^{13}\text{C}$). Spatial variability in pre-flood carbon was estimated by collecting an additional 20–25 soil cores at 20 m intervals along sampling transects. These cores were separated in organic (litter, fungal-humic), charcoal, and mineral layers and analysed for C concentration and $\delta^{13}\text{C}$.

Flood season bubble traps

As described in Chapter 2, five to ten inverted 30 cm diameter plastic funnels were held afloat below the surface of each reservoir to trap bubbles released from the flooded soil. Bubble traps were deployed continuously each flood season and the volume of accumulated gas measured weekly or biweekly. Fresh bubbles were collected for concentration and $\delta^{13}\text{C}$ analyses by probing the flooded soils. Volumetric flux rates were combined with the concentrations and $\delta^{13}\text{C}$ to determine the flux of CO_2 and CH_4 and their $\delta^{13}\text{C}$ values.

Joyce (2001) reported ebullition concentrations and rates from the first year and Matthews (2002) from the second and third years. Ebullition rates for the first three years of FLUDEX were reported together in Matthews et al. (2005). Ebullition rates from the fourth and fifth years are previously unpublished.

Flood season $\delta^{13}\text{C}$ - CH_4 data from the first year were reported by Boudreau (2000). Flood season $\delta^{13}\text{C}$ data from the second year were previously reported by Venkiteswaran (2002). Flood season $\delta^{13}\text{C}$ data from the fourth and fifth years and drawdown $\delta^{13}\text{C}$ data are previously unpublished.

Drawdown bubble traps

To estimate the storage of CO_2 and CH_4 in bubbles trapped in the flooded soils, a soil gas survey was conducted as the water level declined at the end of the third and fifth flood seasons. When the water depth was about 0.5 m, a water-filled funnel was placed on the soil and the soil below the funnel was disturbed to collect all the trapped soil gas. Samples were collected from 10–15 locations per reservoir in previously undisturbed areas. Gas volumes were combined with the concentrations and $\delta^{13}\text{C}$ values to determine the flux of CO_2 and CH_4 and their $\delta^{13}\text{C}$ values. Soil gas samples for CO_2 and CH_4

concentrations and $\delta^{13}\text{C}$ were collected and analysed in the same manner as the other bubble samples.

Analysis of concentration and $\delta^{13}\text{C}$

CO_2 and CH_4 concentration analyses were performed at the ELA via gas chromatography as per Chapter 2. Precision on concentration measurements was $\pm 5\%$. The $\delta^{13}\text{C}$ analyses were performed via isotope ratio mass spectrometry at the Environmental Isotope Laboratory at the University of Waterloo as per Chapter 2. Precision of $\delta^{13}\text{C}\text{-CO}_2$ analysis was $\pm 0.3\%$ and of $\delta^{13}\text{C}\text{-CH}_4$ analysis was $\pm 0.5\%$.

3.3 Results and Discussion

Concentrations and $\delta^{13}\text{C}$ values of flood-season bubbles

The concentrations of CH_4 and CO_2 in flood-season bubbles varied widely in all reservoirs and in all years. Concentration data from individual bubbles traps was not available from the first year of flooding. CH_4 concentrations tended to increase during each flood season (Figure 3.1) and concentrations ranged from 4900 to 870 000 $\mu\text{mol mol}^{-1}$. CH_4 concentrations did not reach values above 500 000 $\mu\text{mol mol}^{-1}$ in the fifth year of flooding and were, in general, lower than in other years. CO_2 concentrations did not exhibit seasonal trends (Figure 3.2) and concentrations ranged from 1300 to 124 000 $\mu\text{mol mol}^{-1}$. CO_2 concentrations were lower in the fifth year than in other years and were, except for two samples, less than 30 000 $\mu\text{mol mol}^{-1}$.

The $\text{CH}_4\text{:CO}_2$ molar ratio can provide information about decomposition and redox. The relative fluxes of CH_4 and CO_2 are important because the 100-year timeline GWP of CH_4 is 23 times that of CO_2 on a per mass basis, i.e., comparing 1 kg CO_2 to 1 kg CH_4 , 31 times on a per kg C basis, and 63 times on a per mole C basis (Ehhalt *et al.*, 2001). The molar ratio of $\text{CH}_4\text{:CO}_2$ in flood-season bubbles also varied widely in all reservoirs and in all years. In general, $\text{CH}_4\text{:CO}_2$ ratios were less than 40:1 (Figure 3.5). In the second, third, and fourth years, the increasing trend in CH_4 concentrations was evident in the increase in average $\text{CH}_4\text{:CO}_2$ ratios. However, in the fifth year of flooding there appears to have been no trend in $\text{CH}_4\text{:CO}_2$ ratios. Given the very high concentrations of CH_4 in flood-season bubbles, ebullition was expected to have been a large loss vector for CH_4 from the reservoirs

The range of $\delta^{13}\text{C}\text{-CH}_4$ values measured in flood-season bubbles was larger than in most ecosystems (cf. Whiticar, 1999), ranging from -93% to -43% (Figure 3.6). The very low $\delta^{13}\text{C}\text{-CH}_4$ values were only measured in the first year of flooding and the first-half of the second year of flooding. From mid-summer in the second year to the end of the fifth year, all $\delta^{13}\text{C}\text{-CH}_4$ values were between -65% and -45% . Only data in the second

year exhibited a seasonal trend when $\delta^{13}\text{C-CH}_4$ values increased by more than 50 ‰. The overall range of $\delta^{13}\text{C-CO}_2$ values measured (–26 ‰ to –7 ‰) was much smaller than the $\delta^{13}\text{C-CH}_4$ (Figure 3.7). Both the second and fifth years exhibited increasing seasonal trends in $\delta^{13}\text{C-CO}_2$. For both $\delta^{13}\text{C-CH}_4$ and $\delta^{13}\text{C-CO}_2$, the range of δ values measured in one reservoir on the same day was up to 10 ‰.

Soil processes affecting CH_4 and CO_2 in bubbles

Using CH_4 and CO_2 concentration in bubbles to estimate soil processes requires understanding how soil pore water concentrations develop and are related to bubbles. Many factors control both the volume of ebullition and its $\text{CH}_4:\text{CO}_2$ ratio. These include:

- $\text{CH}_4:\text{CO}_2$ production ratio; this would be 1 under ‘traditional’ anaerobic decomposition dynamics where $2\text{CH}_2\text{O} \rightarrow \text{CH}_4 + \text{CO}_2$ but could be > 1 or nonsensical in other scenarios such as CO_2 reduction, or < 1 if there are other electron acceptors (Thauer, 1998);
- how much, if any, of the CH_4 is oxidised to CO_2 ;
- how quickly dissolved pore-water gases equilibrate with the bubbles, i.e., the gas exchange coefficient across the bubble–pore water interface;
- what the ‘sphere of influence’ is of each bubble, i.e., how much of the dissolved gas is actually available for equilibration with the bubbles; this is related to pore water dissolved concentrations and diffusion coefficients in the pore water, and the gas exchange coefficient across the bubble–pore water interface if it controls the diffusion gradient;
- Henry’s constants of CH_4 and CO_2 ;
- soil pore water pH because of dissolved inorganic C (DIC) speciation; and
- the bubble storage-time in the soils, i.e., how long do the bubbles stay in the soil before they are released; this would be controlled by several variables such as sediment structure and preferred pathways, bubble depth, and bubble size.

Several modelling approaches have been used to tease apart the production and ebullitive release of CH_4 and CO_2 . Bubble growth models include a variety of simplifying assumptions (e.g., Boudreau *et al.*, 2001a,b). Boudreau *et al.* (2001a) present a model of the growth of a bubble’s radius using porosity, tortuosity-corrected diffusivity, concentration of the gas in the bubble, rate of methanogenesis near the bubble, separation distance between bubbles, CH_4 concentration at the bubble surface, and pore water CH_4 concentration.

This model, however, does not assume that the surrounding pore water dissolved gas concentrations are supersaturated, since this does not appear to be a requirement for bubble growth in some sediment types (e.g., *Chanton et al., 1989*). Whereas, *Fechner-Levy and Hemond (1996)* start with the assumption that adequate amounts of CH₄ are required in the soil pore water (20% of total gases) since about 80% will already be N₂. Using changes in the elevation of a peat mat relative to its water table (i.e., a measure of the buoyant force of the trapped bubbles) and a simple buoyancy model to estimate gas bubble volume, *Fechner-Levy and Hemond (1996)* concluded that CH₄ ebullition was controlled by atmospheric pressure, temperature, and water-table elevation in addition to the physical disturbance of the wetland. However, this hydrostatic model does not address whether or how quickly the dissolved pore water concentrations equilibrate with the bubbles.

The CH₄:CO₂ ratio of Henry's constants

To use measured bubble concentrations to estimate soil processes, the effects of the CH₄:CO₂ ratio of Henry's constants must be explored. Imposed on the CH₄:CO₂ ratio of flood-season bubbles is the ratio of the Henry's constants of CH₄ and CO₂; this ratio is about 24:1 where CH₄ is 24-times more likely to be in the gas phase than CO₂ (*Sander, 1999*). For example, mid-summer pore water concentrations were typically about 500 μmol CH₄ L⁻¹ and 4500 μmol DIC L⁻¹. Measured pH values of the bottom of the water column were about 6 and assuming the pH of the flooded soils was at least as acidic as this, more than 60% of the DIC would have been as free CO₂. Thus the dissolved CH₄:CO₂ ratio would have been at most 0.2 and the bubble CH₄:CO₂ ratio would have been at most 4.4 assuming that the bubbles were not diffusion limited and there was adequate time for equilibration. This would have resulted in the preferential stripping of CH₄ from soil pore water by ebullition and would have reduced the soil pore water CH₄:CO₂ ratio with time relative to the production ratio.

When the ebullition CH₄:CO₂ ratio was greater than about 24 and assuming that CH₄ and CO₂ were equally distributed in the soil, then the soil pore water and thus the decomposition CH₄:CO₂ ratio must have been much greater than 1 in order to maintain an adequately large pore water CH₄ concentration. In this case, the volumetric rate of ebullition would have strongly controlled the CH₄:CO₂ ratio in the pore water and thus in the bubbles.

When the ebullition CH₄:CO₂ ratio was much less than 24 then the soil pore water CH₄:CO₂ ratio must have been low and thus the decomposition CH₄:CO₂ ratio was likely to have been at or below 1. Alternatively, the volumetric ebullition rate was high and/or diffusion of the ambient CH₄ and CO₂ to the bubbles was limited by diffusion.

CH₄:CO₂ production ratio

Different decomposition processes produce CH₄ and CO₂ at different ratios. While a CH₄:CO₂ of 1 is often cited for net anaerobic decomposition of carbohydrates, other processes produce different CH₄:CO₂ ratios. Anaerobic decomposition of plant material such as glucose typically produces acetate, formate, CO₂ and H₂. These organic compounds, more reduced than carbohydrates, typically yield a CH₄:CO₂ ratio less than 1 when fermented (*Ingvorsen and Brock, 1982*) since the reduction of acetate yields a CH₄:CO₂ ratio of 1 and the reduction of formate yields a CH₄:CO₂ ratio of 1:4. However, methanol reduction produces CH₄ with a CH₄:CO₂ ratio of 3:1 or 4:1 (*Thauer, 1998*). The net result of decompositional and fermentative methanogenesis is typically to reduce the ambient CH₄:CO₂ ratio.

Reduction of CO₂ (i.e., oxidation of H₂) to CH₄ will increase the CH₄:CO₂ ratio. Conversely, CH₄ oxidation, would reduce the CH₄:CO₂ ratio. Consumption of CH₄ by anaerobic oxidation, e.g., denitrification with CH₄ as the electron donor and without O₂, will cause the CH₄:CO₂ ratio to decrease (*Raghoebarsing et al., 2006*); although, rates of N₂O consumption in the soils of the FLUDEX reservoirs (*Hendzel et al., 2005*) were very low and thus this process is not likely to contribute much to the CH₄:CO₂ ratio.

A high CH₄:CO₂ production ratio would be indicative of highly reducing conditions in the flooded soil where methanogenesis greatly outpaces methanotrophy and CO₂ production and suggests that there were low concentrations of alternate electron acceptors such as NO₃⁻ and SO₄²⁻. Also, a high CH₄:CO₂ ratio is important at the reservoir scale because soil C originating as atmospheric CO₂, fixed by photosynthesis, and released back to the atmosphere as CH₄ is clearly a net increase in the GWP on a C basis.

Differences between δ¹³C-CH₄ and δ¹³C-CO₂

The difference between δ¹³C-CH₄ and δ¹³C-CO₂ in bubbles can sometimes be used to identify production processes (*Whiticar, 1999*). The ε_{CO₂-CH₄} value is characteristic for different methanogenic pathways and, as a result, even if δ¹³C-CH₄ values increase as a result of changes in the source compounds, the pair (δ¹³C-CH₄ and δ¹³C-CO₂) will shift together. The effect of CH₄ oxidation is to reduce the difference between δ¹³C-CH₄ and δ¹³C-CO₂. However, combinations of processes may yield non-unique δ¹³C-CH₄-δ¹³C-CO₂ pairs.

The δ¹³C-CO₂ from decomposition should be similar to the soil, -27 ‰ (Chapter 2). This CO₂ will be added to the existing DIC pool, shifting the δ¹³C-DIC value toward -27 ‰. Since pH controls DIC speciation, pH will also affect the pore water δ¹³C-CO₂ value available for equilibration with bubbles (*Clark and Fritz, 1997*). The net effect of adding H⁺ from decomposition is to decrease the pore water δ¹³C-CO₂ as DIC speciation is shifted from HCO₃⁻ to dissolved CO₂. The CO₂ produced from CH₄ oxidation will have a

$\delta^{13}\text{C-CO}_2$ value more negative than the co-extant $\delta^{13}\text{C-CH}_4$ and the co-extant $\delta^{13}\text{C-CH}_4$ will be more negative than -27‰ . Only CO_2 reduction will cause the residual dissolved CO_2 to become more positive than expected. [Whiticar \(1999\)](#) summarised these dynamics as the difference between the $\delta^{13}\text{C-CH}_4$ and $\delta^{13}\text{C-CO}_2$ values, where a difference more negative than about -55‰ being exclusively the result of CO_2 reduction and differences more positive than about -30‰ being the result of significant CH_4 oxidation.

Most flood-season bubble $\delta^{13}\text{C}$ data falls in the centre of a cross-plot of $\delta^{13}\text{C-CH}_4$ and $\delta^{13}\text{C-CO}_2$ (Figure 3.8). This region was identified by [Whiticar \(1999\)](#) as indicative of both methanogenic fermentation and some degree of CH_4 oxidation. Bubble data with very low $\delta^{13}\text{C-CH}_4$ values, are suggestive of CO_2 reduction and thus very reducing conditions in the flooded soils. Together, these data indicate that multiple CH_4 -related processes were occurring in FLUDEX soils.

Rates of field-season ebullition

Bubble concentrations were combined with measured volumetric flux rates to determine the ebullitive flux of CH_4 and CO_2 to the atmosphere. This loss of CO_2 and CH_4 was in addition to the diffusive fluxes from reservoir surfaces, which are typically determined with surface water concentrations and gas exchange coefficients (Chapter 2). Ebullitive fluxes depend on factors such as pore water dissolved gas partial pressures, temperature, depth of flooding (i.e., hydrostatic pressure), soil depth, soil matrix, diffusion rates of pore water dissolved gases, and the development of preferential pathways in the flooded soils.

Ebullition rates were highly spatially and temporally variable (Figures 3.9 and 3.10) (e.g., [Fechner-Levy and Hemond, 1996](#); [Walter et al., 2006](#)). Bubble traps in some locations consistently measured a greater flux rate than in other areas. Other than in the first year of flooding, when ebullition was always very low, ebullition rates tended to increase rapidly after the sixth week of flooding, peaked by the tenth or twelfth week when water temperatures were greatest, and declined markedly thereafter. In general, there was a decrease in the lag before ebullition rates increased in each subsequent year.

Ebullition rates were negligible in the first year; no bubbles were captured in the Low C reservoir at all. Ebullition rates were very low in the first half of the second year and increased greatly by the tenth week of flooding. This pattern was similar to the rapid increase in water column CH_4 concentrations observed in that year (Figure 2.3). DIC concentrations did not exhibit this pattern suggesting that DIC and CH_4 production patterns in the flooded soils were different. Ebullition rates were greatest in the third year when there were two measured peaks: first at week nine and again at weeks eleven and twelve. Ebullition in the fourth year of flooding increased rapidly and peaked in the seventh and eight weeks but never reached the high flux rates

of year three. Ebullition rates in the fifth year were lower than in the fourth year and peaked much later in the flood season, around the eighth to tenth weeks.

Isotopic ratios of field-season ebullition

The $\delta^{13}\text{C-CH}_4$ values of ebullition, essentially, the flux-weighted $\delta^{13}\text{C-CH}_4$ value, generally followed temporal trends of the $\delta^{13}\text{C-CH}_4$ of the reservoir outflow (Figures 3.11 and 2.3). However, bubble $\delta^{13}\text{C-CH}_4$ values were more negative than those of reservoir outflow. This suggested a relationship between the pore water CH_4 that diffused into the water column and into bubbles. Since the $\delta^{13}\text{C-CH}_4$ values tended to be offset by up to 10 ‰ this indicated that pore water CH_4 that diffuses to the water column was subject to more oxidation than CH_4 in bubbles.

When ebullitive flux rates were very low in the first year, only ebullition $\delta^{13}\text{C-CH}_4$ values were measured (Boudreau, 2000). From weeks five to eight, the $\delta^{13}\text{C-CH}_4$ values declined from about -57 ‰ to about -75 ‰. The greatest within-season change in $\delta^{13}\text{C-CH}_4$ occurred in the second year when $\delta^{13}\text{C-CH}_4$ increased through much of the flood season and mirrored the trend in water-column $\delta^{13}\text{C-CH}_4$ values. Initially, when flux rates were low, $\delta^{13}\text{C-CH}_4$ was -90 ‰ to -80 ‰, increasing to about -55 ‰ to -40 ‰ by the end of the flood season. Along with the increase in $\delta^{13}\text{C-CH}_4$, the $\delta^{13}\text{C-CO}_2$ values increased from -25 ‰ to -20 ‰ in weeks three to eight to -15 ‰ to -10 ‰ in week 12 (Figure 3.11).

In the third, fourth, and fifth years, $\delta^{13}\text{C-CH}_4$ of flood-season ebullition was generally between -60 ‰ and -50 ‰. Concurrent $\delta^{13}\text{C-CO}_2$ values were -25 ‰ and -10 ‰. In the fourth and fifth years, which have more data than the third year, the range of $\delta^{13}\text{C-CO}_2$ measured on any given day was about 10 ‰.

Annual summaries of field-season ebullition

The total amount of CH_4 or CO_2 that fluxed to the atmosphere from each reservoir in a given flood season was calculated by summing the flood-season ebullition rates (Figures 3.9 and 3.10, Table 3.1). Flood-season CH_4 ebullition was very low in the first year. It was a negligible flux of CH_4 relative to other sources and sinks that year (Chapter 2). CH_4 ebullition increased by two orders of magnitude in the second year in all reservoirs. The greatest ebullitive flux of CH_4 was in the third year. The flux from the High C reservoir remained relatively high in the fourth year while it declined by 70 % to 80 % in the Medium and Low C reservoirs. Flood season CH_4 ebullition further declined in the fifth year but was still more than one order of magnitude greater than in the first year.

When flood-season CH₄ ebullition was very low in the first year of flooding, the $\delta^{13}\text{C-CH}_4$ of that ebullition was also very low: -72‰ and -89‰ in the High and Medium C reservoirs. Thereafter, flood-season $\delta^{13}\text{C-CH}_4$ ebullition was between -60‰ and -50‰ . This large change in $\delta^{13}\text{C-CH}_4$ values indicated that: (1) when CH₄ ebullition was low and $\delta^{13}\text{C-CH}_4$ ebullition was low, CH₄ must have been produced in the soils by CO₂ reduction; and (2) when CH₄ ebullition was high and $\delta^{13}\text{C-CH}_4$ between -60‰ and -50‰ , the ratio of CH₄ production to oxidation must have been similar during those years despite the five- to six-fold difference in CH₄ ebullition rates. After the third year, CH₄ oxidation rates must have declined at the same relative rate as CH₄ production rates in order for the total ebullitive flux to have decreased and the $\delta^{13}\text{C-CH}_4$ values to have remained about the same.

Flood-season CO₂ ebullition was never greater than 2 kg C ha^{-1} in any reservoir or year. This was more than two orders of magnitude smaller than both the diffusive CO₂ flux and net DIC production (Chapter 2). Although the magnitude of CO₂ ebullition may be negligibly small, its $\delta^{13}\text{C-CO}_2$ value provided some detail about carbon cycling within the flooded soils.

In the first year when flood-season CO₂ ebullition was very low, the $\delta^{13}\text{C-CO}_2$ values were also low, -24‰ and -25‰ in the High and Medium C reservoirs. In all other years, the $\delta^{13}\text{C-CO}_2$ was between -20‰ and -12‰ . While difficult to ascribe to single changes in flooded-soil processes, the change in both $\delta^{13}\text{C-CH}_4$ and $\delta^{13}\text{C-CO}_2$ between the first and other years both support a change in the production and consumption pathways of CH₄ and CO₂.

Drawdown ebullition

The storage of CO₂ and CH₄ trapped in bubbles in the flooded soils was estimated at the end of the third and fifth years. As the reservoirs were drained of water, typically taking 7–10 d, reservoir shorelines moved tens of metres per day. Drawdown was rapid enough that bubbles trapped in the waterlogged soils were observed to effervesce as the hydrostatic pressure was reduced and the soils exposed. This gas was released directly to the atmosphere. The relative importance of drawdown ebullition to flood-season ebullition is shown in Figures 3.3 and 3.4. For the two sampling years, both drawdown CH₄ and CO₂ ebullition were remarkably similar to but generally less than their corresponding flood-season ebullition ($r^2 = 0.68$ for CH₄, Figure 3.3; $r^2 = 0.31$ for CO₂, Figure 3.4).

In the third year of flooding, drawdown CH₄ ebullition was of the same order of magnitude as flood-season ebullition; it was about half of the flood-season ebullition in the High C reservoir, about three-quarters in the Medium C reservoir, and about 25% greater in the Low C reservoir. In the fifth year of flooding, it was also of the same order of magnitude as flood-season ebulli-

tion: 18 % and 2 % less in the High and Medium C reservoirs and 39 % higher in the Low C reservoir.

The average drawdown $\text{CH}_4:\text{CO}_2$ ratio in bubbles was 15:1 in the third year of flooding. Data from the last two weeks of that year indicate that the ebullitive $\text{CH}_4:\text{CO}_2$ ratio was between 13:1 and 20:1. This indicates that stored bubbles were similar to the released bubbles in the third year of flooding. At the end of the fifth year of flooding, the drawdown $\text{CH}_4:\text{CO}_2$ ratio was 7:1. During the last two weeks of flooding that year, the ebullitive $\text{CH}_4:\text{CO}_2$ ratio was between 19:1 and 23:1 in the High C reservoir, between 9:1 and 10:1 in the Medium C reservoir, and between 9:1 and 32:1 in the Low C reservoir. This indicates that stored bubbles were not similar to the released bubbles in the fifth year. Together, these data suggest that bubble storage and released mechanisms may have been different in those two years. Bubbles collected at drawdown were from the entire flooded soil profile whereas bubbles collected during the flood season may have represented bubbles closer to the top of the flooded soil profile.

Drawdown $\delta^{13}\text{C}-\text{CH}_4$ should have been similar to that collected during the last week of flooding if the bubbles did not undergo further processing as a result of drawdown or an additional week of entrapment in the soil. In all reservoirs and years, drawdown $\delta^{13}\text{C}-\text{CH}_4$ ebullition was within 2.5 % of flood-season $\delta^{13}\text{C}-\text{CH}_4$ ebullition, typically about -55 % (Table 3.1). This suggested that little additional methanotrophy occurred during drawdown.

Similar to flood-season ebullition, drawdown CO_2 ebullition was a very small component of the total GHG flux to the atmosphere and was never greater than 2 kg C ha^{-1} . The $\delta^{13}\text{C}-\text{CO}_2$ value of drawdown ebullition averaged -15 %. These values were within 3 % of total flood-season ebullition and often within 1 %. Together the $\text{CH}_4:\text{CO}_2$ ratio and $\delta^{13}\text{C}-\text{CH}_4$ data, these values suggest that there were no changes to methanogenic or methanotrophic processes during drawdown although the source of bubbles in the flooded soil profile may have been different.

Ebullition as a conduit of GHGs to the atmosphere

A comparison between ebullition rates and diffusive flux rates was tempting, but would not have reflected that FLUDEX reservoirs had very short but different residence times (6–9 d) and different gas exchange coefficients (see Chapters 2 and 8). As a result of the slow gas exchange coefficients and rapid flushing rates, a large portion of the CO_2 and CH_4 produced in the reservoirs was flushed out the outflow and available to be fluxed to the atmosphere from the downstream environment (see Chapter 2). Thus, a comparison between the entire flood-season ebullition and net DIC or CH_4 production was more appropriate since gas exchange coefficients control diffusive fluxes.

Both the fluxes of flood-season CH_4 ebullition and drawdown CH_4 ebullition were similar in size to net CH_4 production and thus important and

large fluxes of CH₄ to the atmosphere (Table 3.3). When net CH₄ production were above about 5 kg C ha⁻¹, CH₄ ebullition became a conduit of CH₄ from the flooded soils to the atmosphere suggesting a minimum requirement for enough CH₄ to accumulate in the flooded soils to trigger comparable levels of ebullition.

The ebullitive fluxes of CO₂ were orders of magnitude smaller than net DIC production (Table 3.4). As net DIC production declined every year, suggesting a general decline in DIC-CO₂ production in the flooded soils, CO₂ ebullition never became a significant source of GHGs to the atmosphere.

3.4 Conclusions

The ebullitive flux of CH₄ was much more important to total GHG production in the FLUDEX reservoirs than was CO₂ ebullition. Ebullition was spatially heterogeneous but exhibited seasonal trends peaking between the seventh and twelfth weeks of flooding each year and coinciding with the seasonal temperature maxima. The greatest rates of ebullition and greatest total ebullition occurred in the third year of flooding; this supports a conclusion drawn from the δ¹³C budgets that CH₄ production was greatest in that year. In the third year, total ebullition was very similar between all three reservoirs. Over five years, the High C reservoir exhibited the slowest decline in year-to-year ebullition and the greatest total flux of ebullition of all FLUDEX reservoirs. In the two years when it was measured, drawdown ebullition, the loss of bubbles from the soils as the water was drained from the reservoirs, was as important a source of CH₄ to the atmosphere as the entire flood-season of ebullition.

Acknowledgements

R. J. Elgood provided important laboratory, field, and logistical support during the FLUDEX years. He and S. L. Schiff were oddly exuberant when sampling drawdown ebullition. W. A. Mark kindly provided IRMS assistance. This research was funded by the Natural Sciences and Engineering Research Council of Canada, Canadian Foundation for Climate and Atmospheric Sciences, Climate Change Action Fund, Environment Canada's Science Horizons program, the Centre for Research in Earth and Space Technology, and an Ontario Graduate Scholarship. FLUDEX was funded by Fisheries and Oceans Canada, Manitoba Hydro, and Hydro-Québec. Field work during the FLUDEX years was also conducted by: E. M. Joyce, C. J. D. Matthews, K. T. Maurice, M. Pinsonneault, M. Puchniak, M. A. M. Saquet, and A. M. Wojtyniak

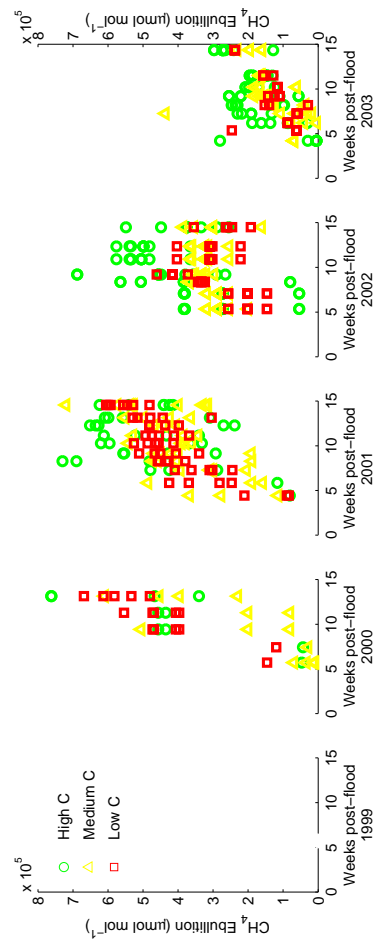


Figure 3.1: Flood-season bubble CH₄ concentrations in FLUDEX reservoirs for 1999–2003. [Matthews \(2002\)](#) published concentrations for the second and third years.

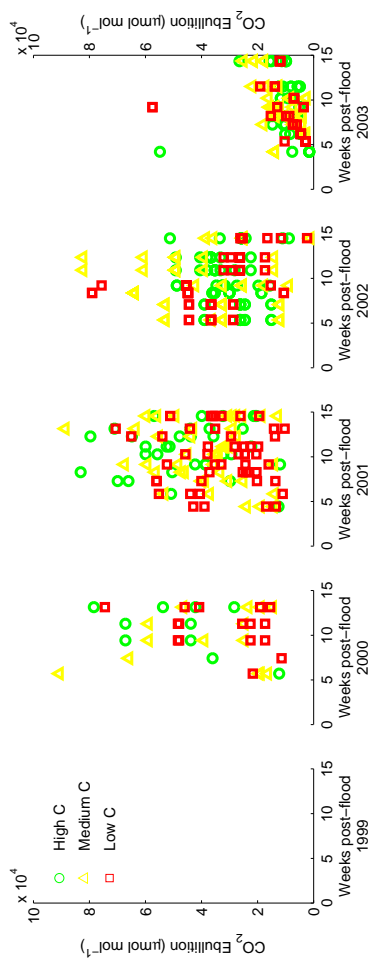


Figure 3.2: Flood-season bubble CO₂ concentrations in FLUDEX reservoirs for 1999–2003. [Matthews \(2002\)](#) published concentrations for the second and third years.

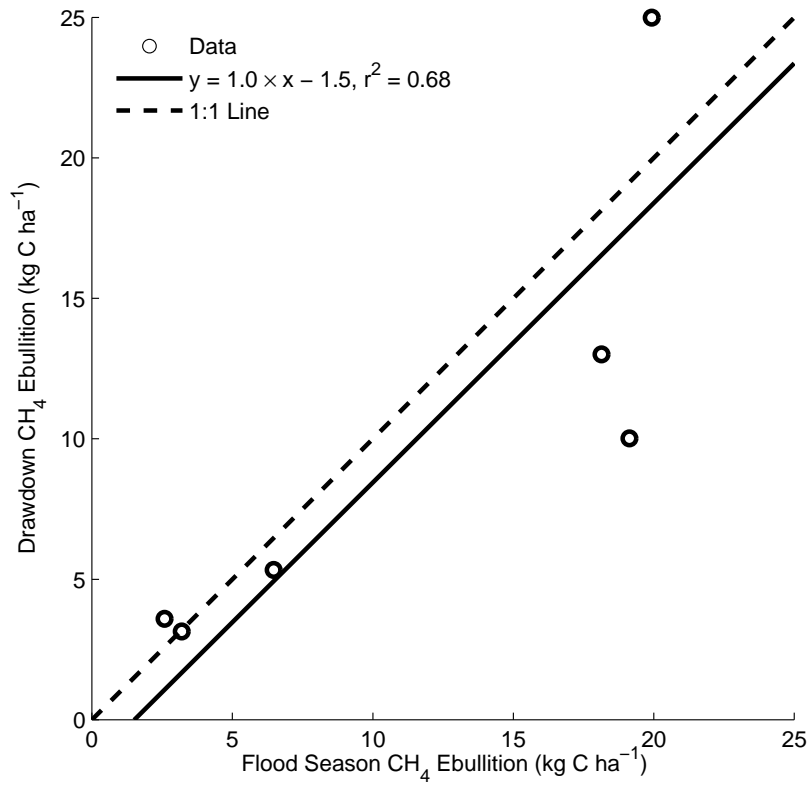


Figure 3.3: Flood season versus drawdown CH₄ ebullition from FLUDEX reservoirs to the atmosphere in 2001 and 2003.

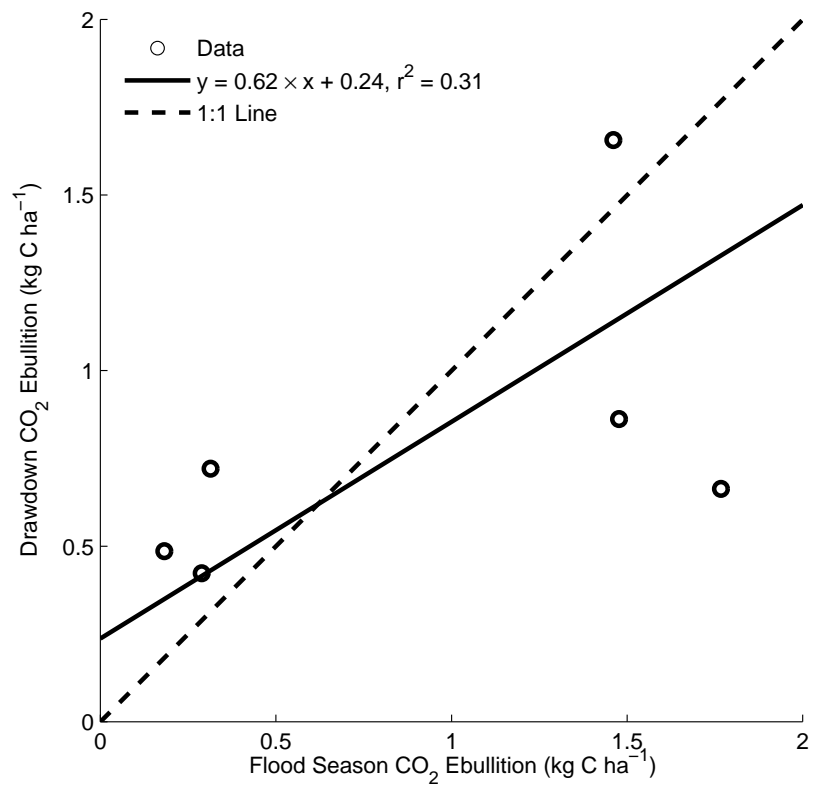


Figure 3.4: Flood season versus drawdown CO₂ ebullition from FLUDEX reservoirs to the atmosphere in 2001 and 2003.

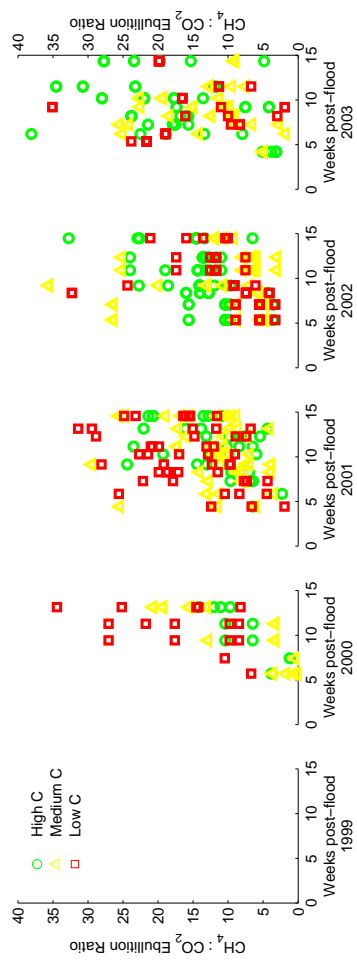


Figure 3.5: Flood-season bubble molar CH₄:CO₂ ratio in FLUDEX reservoirs for 1999–2003. *Matthews* (2002) published concentrations for the second and third years.

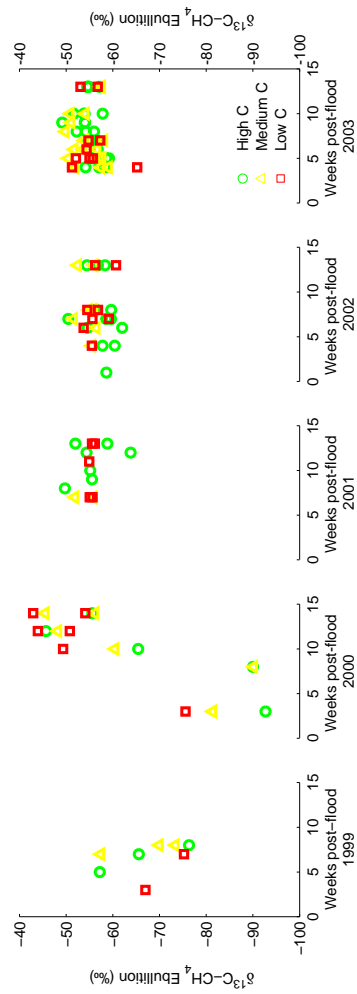


Figure 3.6: Flood-season bubble $\delta^{13}\text{C-CH}_4$ values in FLUDEX reservoirs for 1999–2003. [Boudreau \(2000\)](#) published $\delta^{13}\text{C-CH}_4$ values for the first year.

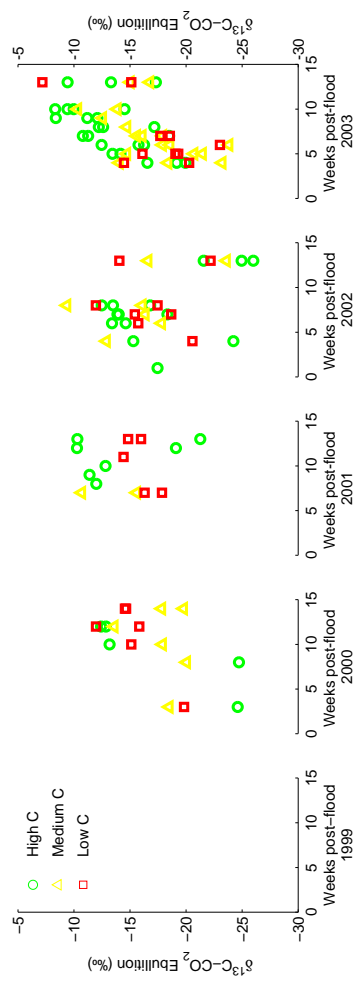


Figure 3.7: Flood-season bubble $\delta^{13}\text{C-CO}_2$ values in FLUDEX reservoirs for 1999–2003.

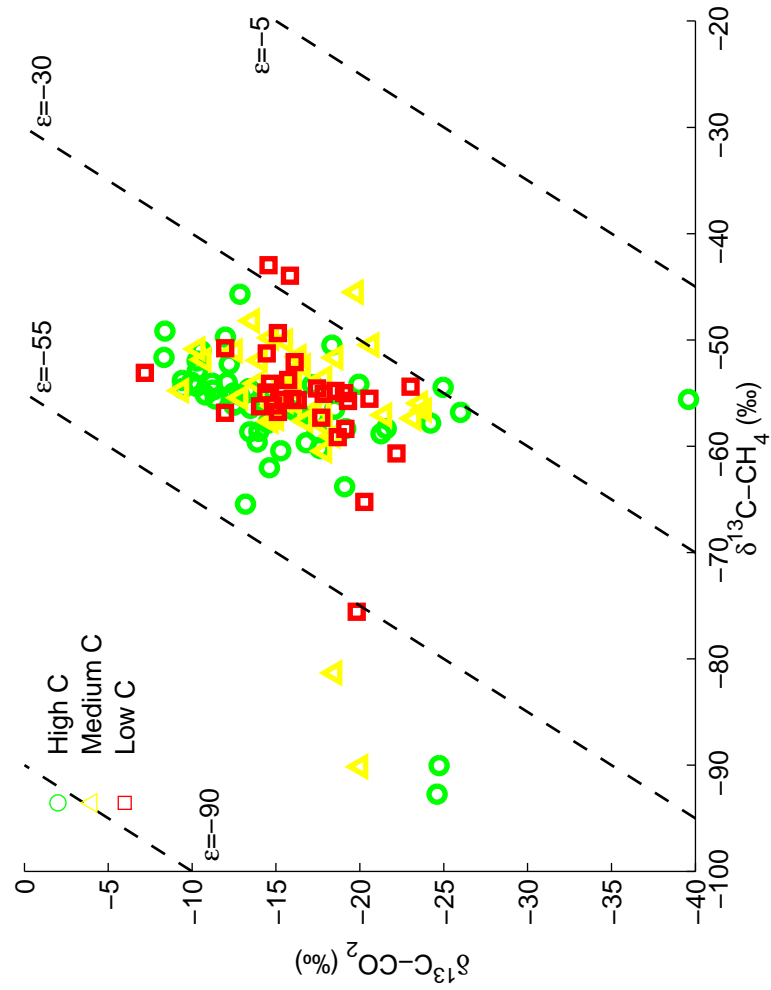


Figure 3.8: Cross-plot of flood-season bubble $\delta^{13}\text{C-CH}_4$ and $\delta^{13}\text{C-CO}_2$ in FLUDEX reservoirs for 1999–2003. Dashed lines are enrichment factors (ϵ) between CO_2 and CH_4 that delineate regions suggested by *Whiticar (1999)* as broadly characteristic of CO_2 reduction (ϵ between -90‰ and -55‰), methanogenic fermentation (ϵ between -55‰ and -32‰), and CH_4 oxidation (ϵ between -30‰ and -5‰). However, CH_4 oxidation will also cross these ϵ -delineations from left-to-right as progressively more CH_4 is consumed.

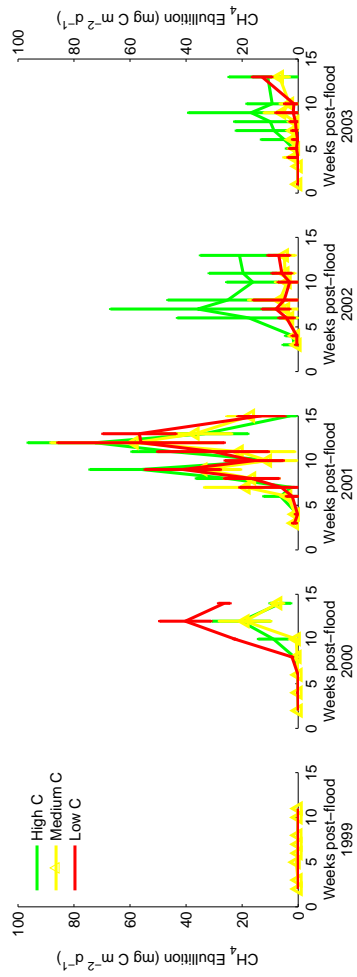


Figure 3.9: Flood season CH_4 ebullition rates from FLUDEX reservoirs to the atmosphere for 1999–2003. Rates are whole-reservoir averages (shown with $1SE$ error bars). [Joyce \(2001\)](#) published ebullition rates from the first year, [Matthews \(2002\)](#) the second and third years.

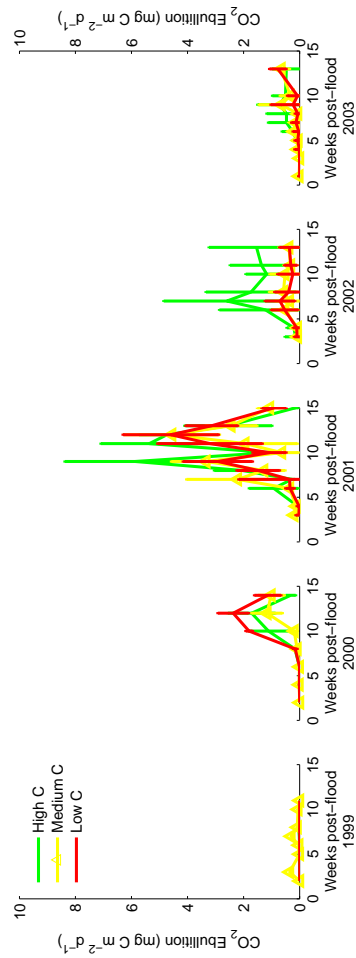


Figure 3.10: Flood season CO₂ ebullition rates from FLUDEX reservoirs to the atmosphere for 1999–2003. Rates are whole-reservoir averages (shown with 1SE error bars). [Joyce \(2001\)](#) published ebullition rates from the first year, [Matthews \(2002\)](#) the second and third years.

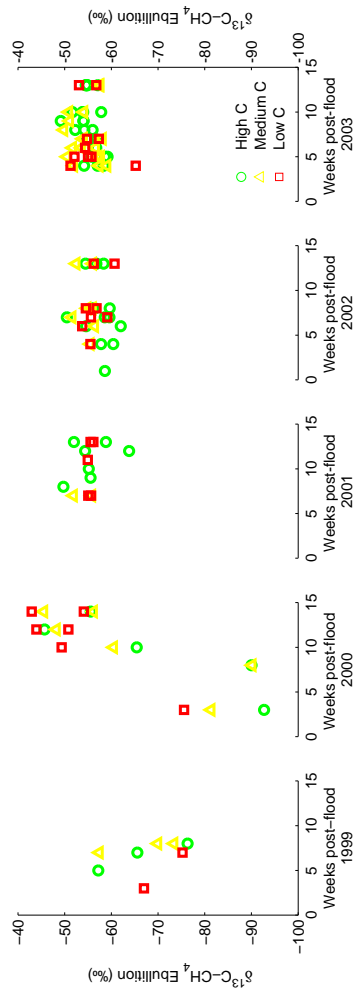


Figure 3.11: Flood season $\delta^{13}\text{C-CH}_4$ values of flood-season ebullition from FLUDEX reservoirs to the atmosphere for 1999–2003. All Data are shown. Flood season $\delta^{13}\text{C-CH}_4$ data from the first year were published by [Boudreau \(2000\)](#).

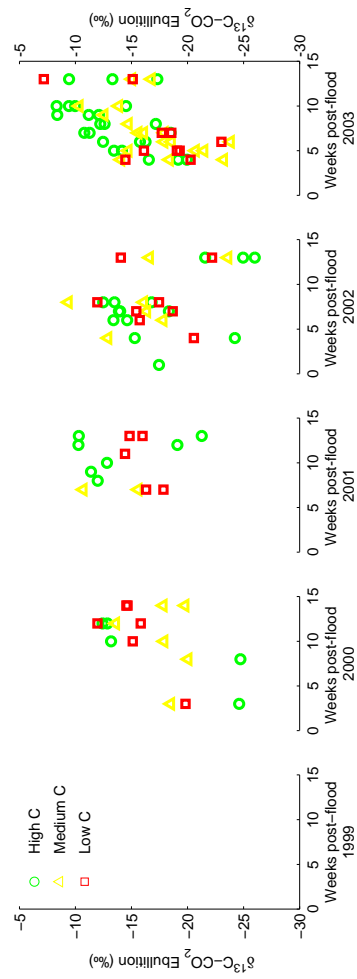


Figure 3.12: Flood season $\delta^{13}\text{C-CO}_2$ values of flood-season ebullition from FLUDEX reservoirs to the atmosphere for 1999–2003. All Data are shown.

Table 3.1: Flood-season and drawdown CH_4 ebullition from FLUDEX reservoirs to the atmosphere for 1999–2003. Each flood-season and drawdown column contains a flux of CH_4 in kgC ha^{-1} and its $\delta^{13}\text{C-CH}_4$ value in ‰.

	High C reservoir		Medium C reservoir		Low C reservoir	
	Flood-season	Drawdown	Flood-season	Drawdown	Flood-season	Drawdown
	Flux	$\delta^{13}\text{C}$	Flux	$\delta^{13}\text{C}$	Flux	$\delta^{13}\text{C}$
1999	0.0	-72.3	0.1	-89.2	0	
2000	5.6	-54.2	4.4	-49.7	14.7	-48.4
2001	19.1	-55.4	18.1	-53.5	19.9	-55.9
2002	14.1	-57.1	3.8	-54.1	4.0	-57.3
2003	6.5	-54.3	3.2	-54.3	2.6	-55.6
					25.0	-58.4
					3.6	-55.5

Table 3.2: Flood-season and drawdown CO₂ ebullition from FLUDEX reservoirs to the atmosphere for 1999–2003. Each flood-season and drawdown column contains a flux of CO₂ in kgC ha⁻¹ and its δ¹³C-CO₂ value in ‰.

	High C reservoir		Medium C reservoir		Low C reservoir	
	Flood-season δ ¹³ C	Drawdown Flux	Flood-season δ ¹³ C	Drawdown Flux	Flood-season δ ¹³ C	Drawdown Flux
1999	0.0	-23.6	0.1	-25.3	0	-14.7
2000	0.5	-16.4	0.4	-17.5	0.8	-16.4
2001	1.8	-13.6	1.5	-14.2	1.5	-17.8
2002	1.0	-19.2	0.3	-17.2	0.3	-16.1
2003	0.3	-12.4	0.0	-14.4	0.2	-15.4

Table 3.3: Flood-season and drawdown CH₄ ebullition and net CH₄ production (NMP) in FLUDEX reservoirs for 1999–2003. Each column contains a flux of CH₄ in kgC ha⁻¹.

	High C reservoir		Medium C reservoir		Low C reservoir	
	Flood-season	Drawdown	Flood-season	Drawdown	Flood-season	Drawdown
1999	0.0	4.6	0.1	3.0	0.0	3.4
2000	5.6	11.2	4.4	8.4	14.7	10.2
2001	19.1	11.4	18.1	11.6	19.9	25.0
2002	14.1	5.7	3.8	9.0	4.0	8.5
2003	6.5	5.3	3.2	8.2	2.6	5.2

Table 3.4: Flood-season and drawdown CO₂ ebullition and net DIC production (NDICP) in FLUDEX reservoirs for 1999–2003. Each flood-season and drawdown column contains a flux of CO₂ or DIC in kg C ha⁻¹.

	High C reservoir		Medium C reservoir		Low C reservoir				
	Flood-season	Drawdown	NDICP	Flood-season	Drawdown	NDICP	Flood-season	Drawdown	NDICP
1999	0.0		702	0.1		797	0		704
2000	0.5		478	0.4		408	0.8		470
2001	1.8	0.7	444	1.5	0.9	478	1.5	1.7	415
2002	1.0		481	0.3		325	0.3		306
2003	0.3	0.7	388	0.0	0.4	433	0.2	0.5	244

Chapter 4

Dynamics of dissolved oxygen isotopic ratios: a transient model to quantify primary production, community respiration, and air–water exchange in aquatic ecosystems

Jason J. Venkiteswaran¹, Leonard I. Wassenaar², Sherry L. Schiff¹

Oecologia 153(2): 385–398 doi: [10.1007/s00442-007-0744-9](https://doi.org/10.1007/s00442-007-0744-9).

© Springer-Verlag 2007, with kind permission from Springer Science and Business Media. The original publication is available at www.springerlink.com. Permission to reproduce and statement from the co-authors is found in Appendix B.

Abstract

Dissolved oxygen (O₂) is an important aquatic ecosystem health indicator. Metabolic and gas exchange rates (G), which control O₂ concentration, are affected by nutrient loading and other environmental factors. Traditionally, aquatic metabolism has been reported as primary production:community respiration (*P:R*) ratios using diel measurements and interpretations of dissolved O₂ and/or CO₂ concentrations, and recently using stable isotopes ($\delta^{18}\text{O}$, $\Delta^{17}\text{O}$) and steady state assumptions.

¹Department of Earth Sciences, University of Waterloo, 200 University Avenue West, Waterloo ON, N2L 3G1, Canada.

²Environment Canada, 11 Innovation Boulevard, Saskatoon SK, S7N 3H5, Canada.

Aquatic ecosystems, such as rivers and ponds, are not at steady state and exhibit diel changes, so steady state approaches are often inappropriate. A dynamic O₂ stable isotope model (photosynthesis–respiration–gas exchange; PoRGy) is presented here, requiring a minimum of parameters to quantify daily averaged P , R , and gas exchange rates under transient field conditions. Unlike steady state approaches, PoRGy can address scenarios with 100% O₂ saturation but with $\delta^{18}\text{O}\text{-O}_2$ values that are not at air equilibrium. PoRGy successfully accounts for isotopic G when applied to an oxygen isotope equilibration laboratory experiment. PoRGy model results closely matched the diel O₂ and $\delta^{18}\text{O}\text{-O}_2$ data from three field sites with different P : R : G ratios and various P , R , and G rates. PoRGy provides a new research tool to assess ecosystem health and to pose environmental impact-driven questions. Using daily averaged rates was successful and thus they can be used to compare ecosystems across seasons and landscapes.

4.1 Introduction

Dissolved oxygen (O₂) is a crucial biogeochemical cycle in aquatic communities (*Odum, 1956; Stumm and Morgan, 1996*) because it sustains aquatic life and maintains biodiversity (*Broecker, 1985; Falkowski and Raven, 1997*). O₂ cycling is particularly sensitive to cultural eutrophication and watershed nutrient loading (*Schindler, 1987; Yan, 2005*) and is therefore a key aquatic health indicator.

Dissolved O₂ concentration is controlled to a large extent by air–water gas exchange (G) and is produced by aquatic primary production (P) and consumed by community respiration (R) at rates driven by nutrient availability, temperature, light, substrate availability, and other environmental conditions (*Odum, 1956; Stumm and Morgan, 1996*). Traditionally, aquatic metabolic status has been reported as the P : R ratio (*Wetzel, 2001; Wilcock et al., 1998*). Ecosystem metabolic balance, whether predominantly heterotrophic (P : R < 1) or autotrophic (P : R > 1), is often determined from summertime diel measurements of dissolved O₂ concentrations (*Chapra and Di Toro, 1991; Hornberger and Kelly, 1975; Marzolf et al., 1994; Mulholland et al., 2005*), by the degree O₂ or CO₂ saturation, or by light and dark bottle-incubation experiments (cf. *Carignan et al., 2000; del Giorgio and Peters, 1994; Prairie et al., 2002*). Dissimilar aquatic ecosystems with differing P and R rates can have the same P : R ratio, casting doubt on whether the P : R ratio is a meaningful indicator of metabolic or ecological status. At the ecosystem level the chief source of error in these approaches is poor quantification of the air–water G rate. This has resulted in the development of alternative approaches to quantifying aquatic metabolism primarily by using stable oxygen isotopic ratios³ of dissolved O₂ as tracers to constrain these three processes (P , R , G).

³The ^{18}O : ^{16}O ratio of O₂ is measured and reported as the parts per thousand deviation from

The study of dissolved O₂ and its ¹⁸O:¹⁶O (dual-isotope) isotopic ratios ($\delta^{18}\text{O}-\text{O}_2$) in various aquatic ecosystems has mainly focused on determining metabolic balance ($P:R$) (Parker et al., 2005; Quay et al., 1995; Russ et al., 2004) under steady state assumptions or examination of the Dole effect (Bender et al., 1994; Hoffmann et al., 2004). Recently, ¹⁷O (triple-isotope) analysis has been proven useful in quantifying gross O₂ production by exploiting the ¹⁷O disequilibrium between dissolved and atmospheric O₂ integrated over multi-week timescales, and in low productivity or high G environments (e.g., Hendricks et al., 2005; Luz and Barkan, 2000; Luz et al., 1999; Sarma and Abe, 2006). The triple-isotope method has the additional advantage of avoiding the uncertainty in isotopic fractionation due to R; however, it requires laborious dual-inlet analysis (Barkan and Luz, 2003), whereas dual-isotope analyses are easily automated using continuous-flow mass spectrometry, a significant cost and technical advantage where large numbers of hourly samples are required in diel studies (Barth et al., 2004; Wassenaar and Koehler, 1999). Both dual- and triple-isotope approaches to date have relied on parameterised empirical models to estimate the gas exchange coefficient (k).

Almost all previously published O₂ dual- and triple-isotope studies have assumed that the aquatic ecosystem was at steady state and that neither the O₂ concentrations nor its isotopic ratios changed significantly over timeframes that ranged from hours to months (Hendricks et al., 2005; Luz and Barkan, 2000; Quay et al., 1993, 1995; Russ et al., 2004; Sarma et al., 2005; Wang and Veizer, 2000, 2004). This steady state assumption implies there is no significant concentration or isotopic response to a diel light cycle. While this may be valid for deep well-mixed oceanic surface studies, most natural and impacted freshwater lake and river ecosystems typically exhibit some degree of diel or seasonal productivity change. Fortunately, diel concentration and isotope dynamics can be used to better account for metabolic dynamics (e.g. Fry, 2006).

Recently, Parker et al. (2005) acknowledged the problem of steady state assumptions in small rivers, but applied traditional curve analysis methods to O₂ concentration data to determine metabolic rates and k (Odum, 1956). Then $\delta^{18}\text{O}-\text{O}_2$ values were predicted using steady state equations (Quay et al., 1995) and compared to field data. Similarly (e.g., Russ et al., 2004; Wang and Veizer, 2000), Parker et al. (2005) assumed an isotope fractionation factor for R. By not using a dynamic process-driven model of O₂ and its isotopes, an opportunity to use $\delta^{18}\text{O}-\text{O}_2$ data to constrain and calculate P, R, and G, and to address the short-comings (steady state assumptions, poorly known R fractionation, poorly constrained k) was missed. The triple-isotope approach has not yet been attempted in smaller aquatic ecosystems having significant

Vienna Standard Mean Ocean Water (VSMOW): $\delta = \left(\frac{R_{\text{sample}}}{R_{\text{VSMOW}}} \right)$ where R is the ¹⁸O:¹⁶O ratio. Isotope fractionation factors for different processes are denoted as α values: $\alpha = \frac{R_b}{R_a}$ where R is the ¹⁸O:¹⁶O ratio of the reactant (a) and product (b).

diel fluctuations.

To advance the application of O₂ isotopes in quantifying metabolic responses in freshwater ecosystems, a dynamic non-steady state O₂ concentration and δ¹⁸O-O₂ (dual-isotope) model was developed. This model incorporates all of the key physical and biological processes, O₂ isotopic fractionation factors, and temporal variables (e.g., light, temperature), while using the minimum number of variables. The objectives of this paper are to: (1) describe a new dynamic O₂ and δ¹⁸O-O₂ model that enables quantification of average *P*, *R*, and *G* rates and allows for predictive modelling; (2) illustrate the importance of quantifying both O₂ and isotopic *G* using experimental laboratory dissolved O₂ and δ¹⁸O-O₂ data; and (3) apply the model to three aquatic ecosystems with different metabolic and *G* rates.

The computer model (photosynthesis–respiration–gas exchange; PoRGy) was developed to perform transient and steady state dissolved O₂ and δ¹⁸O-O₂ modelling calculations and is made available to researchers at <http://www.science.uwaterloo.ca/~jjvenkit/PoRGy/> or from the authors. Detailed discussion of the effect of each variable on the diel O₂ and δ¹⁸O-O₂ curves and on the subsequent assessment of ecosystem health is presented elsewhere (Venkiteswaran *et al.*, 2008).

Isotope Dynamics of *P*, *R*, and *G*

The O₂ generated during aquatic *P* is derived from oxidizing ambient water molecules. This process does not cause significant O₂ isotope fractionation ($\alpha_P = 1.000$) and adds dissolved O₂ to the aquatic ecosystem with δ¹⁸O values identical to that of the water (Guy *et al.*, 1989, 1993; Helman *et al.*, 2005; Stevens *et al.*, 1975). The δ¹⁸O-O₂ of photosynthetic O₂ added to the dissolved O₂ pool is always more depleted in ¹⁸O (typically –30 to 0 ‰) than atmospheric O₂ (+23.5 ‰)⁴. Given the large difference between the δ¹⁸O of atmospheric O₂ and water oxygen, δ¹⁸O-O₂ assays are well suited to detect the addition of small amounts of photosynthetic O₂ to aquatic ecosystems.

The rate at which aquatic photosynthetic O₂ is produced is inherently linked to incident photosynthetically active radiation (PAR). PAR increases and decreases predictably during the day (barring clouds) but in the water column can be affected by other factors (e.g., turbidity change, and variable water velocity and depth). In general, aquatic *P* causes daytime dissolved O₂ concentrations to increase from sunrise to shortly after solar noon and decrease thereafter. At sunset, *P* declines to zero and dissolved O₂ concentrations decrease due to consumption by *R*. A simplified depiction of the

⁴In recent publications, atmospheric δ¹⁸O-O₂ is reported to have a value of +23.8 ± 0.3 ‰ versus VSMOW (Copley *et al.*, 2001), whereas others forgo conventional VSMOW–SLAP standardisation procedures and report dissolved O₂ results as ‰ deviations from local air O₂ (Luz *et al.*, 1999)

key O₂ processes (*P*, *R*, and *G*) versus expected δ¹⁸O-O₂ values is shown in Figure 4.1.

Aerobic microbial *R* is the principal sink for O₂ in most natural aquatic environments (*Stumm and Morgan, 1996; Wetzel, 2001*). Aquatic community *R* is defined as the weighted mean of all O₂ consuming pathways, which include: (1) microbial *R* via the cytochrome oxidase pathway in eukaryotes and the equivalent pathway in prokaryotes; (2) microbial *R* via the alternative oxidase pathway in eukaryotic autotrophs; (3) photorespiration in photoautotrophs (*Osmond, 1981*); (4) the Mehler-peroxidase reaction in photoautotrophs (*Laws et al., 2000*); (5) chlororespiration in eukaryotes (*Bennoun, 2002*); (6) photochemical consumption of O₂ (*Andrews et al., 2000; Miles and Brezonik, 1981*); and (7) geochemical oxidation of reduced species such as Fe²⁺, NH₄⁺, and S. The relative importance of each pathway will likely be different for aquatic systems of differing community structure. The first two pathways are the most prevalent and occur both in light and dark, consuming organic carbon and O₂ while producing CO₂. The next two pathways only occur in the light and short-circuit photosynthetic electron transport prior to carbon fixation.

At the field scale, consumption of dissolved O₂ by the different biological pathways and aquatic organisms is combined into a single community *R* rate for modelling purposes. During aerobic *R*, the lighter O₂ isotopologue (¹⁶O¹⁶O) is preferentially consumed over the heavier O₂ isotopologue (¹⁸O¹⁶O), resulting in O₂ isotope fractionation (α_R) with the residual dissolved δ¹⁸O-O₂ becoming progressively more positive. Community α_R is the weighted mean of all unique isotopic fractionation factors for each of the dissolved-O₂-consuming pathways and organisms present. The α_R values for individual species remain largely unknown; however, α_R for microbial *R* averages around 0.980 for a series of marine organisms, fish, and molluscs (*Kiddon et al., 1993*). The α_R for O₂ consumption by photorespiration and Mehler-peroxidase reactions falls between about 0.979 and 0.985 (*Guy et al., 1993*). Hence, at field scales α_R could range between about 0.979 and 0.985, comparable to ranges of α_R calculated from whole water closed incubations (*Quay et al., 1995*). However, in ecosystems where biological dissolved O₂ consumption rates are high, but where O₂ flux may be diffusion limited (e.g., within substrate), microbes become less discriminating and α_R can range from 0.994 to 1.000 (*Brandes and Devol, 1997; Hartnett et al., 2005; Hendry et al., 2002*). Non-biological dissolved O₂ consumption may occur in aquatic systems by abiotic chemical oxygen demand (COD) as a result of discharging waste. The O₂ isotope fractionation involved in COD is likely small (cf. *Taylor et al., 1984*) and unknown in photochemical O₂ consumption.

Whereas *P* and *R* are unidirectional processes that either add or remove dissolved O₂ from the aquatic environment, air–water *G* is a bi-directional process that continuously adds and removes O₂ (and its isotopologues) from the system. The net flux of O₂ into or out of a water body can be calculated.

The magnitude of the G coefficient (k) determines how quickly G occurs. Although k can be measured directly with tracer experiments, k is typically calculated using empirical models based on a few key parameters. For lakes and oceans, k is often parameterised in terms of wind speed ([Gelda et al., 1996](#)). In streams and rivers, k is often parameterized in terms of channel depth and water velocity ([Moog and Jirka, 1998](#)). Despite dozens of equations that can be used to estimate k for different settings, model-calculated k values can vary by orders of magnitude for the same system ([Jha et al., 2001, 2004; McBride, 2002](#)). Finally, because dissolved O_2 saturation concentrations are strongly temperature dependent ([Weiss, 1970](#)), changes in water temperature will also affect the direction and rate of G . Previous O_2 dual- and triple-isotope approaches have relied on empirical models to estimate k , and this variable remains the greatest source of uncertainty ([Juranek and Quay, 2005](#)).

The $\delta^{18}O$ of atmospheric O_2 is globally constant at +23.5 ‰ ([Kroopnick and Craig, 1972](#)). The air–water equilibrium O_2 fractionation factor ($\alpha_{G-eg} \cong 1.0007$) ([Benson et al., 1979](#)) is the result of the small difference in solubility of each O_2 isotopologue and is not very temperature sensitive between 0 and 30°C. Hence, dissolved O_2 in saturation equilibrium with air at Earth surface temperatures will have a $\delta^{18}O-O_2$ of about +24.2 ‰. The kinetic O_2 fractionation factor ($\alpha_{G-k} = 0.9972$) is the ratio of the k of each isotopologue ([Knox et al., 1992](#)); the k for the light isotopologue is slightly larger than that of the heavy isotopologue. Even when there is no net O_2 G (i.e., at 100% O_2 saturation), if either isotopologue is in disequilibrium, there will be a net flux of that isotopologue into or out of the aquatic ecosystem until isotopic equilibrium with air is also attained. Most studies rely on derived or empirical estimates of k ; however, k can also be constrained and quantified by the shape of the diel O_2 and $\delta^{18}O-O_2$ curves (Chapter 5).

4.2 Materials and Methods

Transient Model of Oxygen Concentration and Isotopic Ratios

To quantify the non-steady state dynamics of dissolved O_2 and $\delta^{18}O-O_2$ in aquatic ecosystems, PoRGy was developed. PoRGy is a dynamic, process-based, computer model that combines rates of P , R , and G with their associated O_2 isotopic fractionation factors, and environmental variables such as temperature, PAR, and $\delta^{18}O-H_2O$. The model produces transient diel curves of dissolved O_2 and $\delta^{18}O-O_2$ that can be compared with field data. PoRGy was constructed as a box model (using Stella software, version 9.0.1, <http://www.iseesystems.com/>) with differential equations computed at any time interval. Thus, the effect of changing single or combined environmental parameters can be explored. PoRGy calculates the movement of the O_2 isotopologues separately, and then recombines them to produce dissolved O_2

concentrations and $\delta^{18}\text{O}-\text{O}_2$ values for every time-step. Each of the variables is discussed below.

Photosynthesis

O_2 evolution by aquatic P is inherently related to incident light (PAR). The conventional approach to estimate P in lakes and oceans is to use a photosynthesis versus irradiance (P–E) curve. The P–E curve is modelled as a rectangular hyperbola or hyperbolic tangent curve that is linear at lower incident light and levels off at higher incident light (*Falkowski and Raven, 1997*). Practically, the time and cost required to generate site specific P–E curves is too great to be easily applied. PoRGy instead uses theoretical daily incident light curves to adjust the rate of photosynthetic O_2 evolution. This simplification assumes that a large number of photoautotrophs are not light saturated for a significant portion of the day. This may be the case for mixed open water ecosystems, but may not be true for shallow or turbid water, or ecosystems with a large number of epiphytes or shaded submerged macrophytes. PoRGy generates daily incident light curves for any latitude, longitude, altitude, and day-of-year combination (*Bird and Hulstrom, 1981; van Dam, 2001*).

The O_2 added to the aquatic ecosystem from P has the same $\delta^{18}\text{O}$ as the water, which can be determined from a small water sample (cf. *Horita and Kendall, 2004*). In summary, PoRGy calculates the photosynthetic addition of O_2 from a photosynthetic rate, selected by the user, modified by an incident light model (based on latitude, longitude, altitude, and date), and the measured $\delta^{18}\text{O}-\text{H}_2\text{O}$ value.

Respiration

Although the consumption of dissolved O_2 by the aquatic community combines all respiratory pathways of various organisms, the influence of α_R from each discrete pathway or group of organisms on the whole community α_R is proportional to the relative rates of O_2 consumption. The impact of fish, for example, is expected to be negligible compared to benthic microbes. PoRGy uses a single community α_R that can be adjusted or varied temporally. In shallow waters the range of α_R may be greater than in the open ocean. In previous steady state models the assumed value of a single community α_R is a limiting variable with a potentially large range (cf. *Brandes and Devol, 1997; Kiddon et al., 1993; Quay et al., 1995*). Fortunately, the presence of a strong diel curve places constraints on α_R . The nighttime plateau (in O_2 and $\delta^{18}\text{O}-\text{O}_2$) constrains α_R because the shapes of the diel curves approaching the plateau are different for O_2 and for $\delta^{18}\text{O}-\text{O}_2$ and depend on α_R and k . The plateau $\delta^{18}\text{O}-\text{O}_2$ value also depends on α_R . Thus community α_R can be determined in two ways: by best-fit modelling of the nighttime plateau and by best-fit

modelling of 24 h diel data. Variance due to uncertainties in α_R is fortunately very small (*Juraneck and Quay, 2005; Parker et al., 2005*, also see below).

Aquatic ecosystems may exhibit daily temperature ranges that exceed 5–10 °C. Because the R rate increases with increasing temperature (R_T) (*Kirschbaum, 1995*), the nominal R rate at 20 °C (R_{20}) is related to water temperature using the van 't Hoff–Arrhenius equation:

$$R_T = R_{20} \times 1.047^{T-20} \quad (4.1)$$

The temperature correction value (1.047) is a widely accepted value from water quality research and BOD₅ experiments (*Borsuk et al., 2004; Bowie et al., 1985*). PoRGy generates a daily water temperature regime from either a measured minimum and maximum (and related to PAR) or from a fifth-order polynomial (useful for summarising field data). In summary, PoRGy calculates O₂ consumption from a user-selected R rate, temperature regime, and α_R .

Gas Exchange

For G , four factors must to be considered: (1) the level of dissolved O₂ saturation which drives the net flux of O₂ into or out of the system; (2) the level of dissolved O₂ isotopologue saturation which drives ¹⁶O¹⁶O or ¹⁸O¹⁶O into or out of the system; (3) the air–water k ; and (4) water temperature, which directly affects the previous three factors. In PoRGy, the flux of each isotopologue is modelled separately for G and is analogous to that described by *Hendry et al. (2002)* for soils. The ¹⁶O¹⁶O concentration can be represented by measured dissolved O₂ concentration because ¹⁶O¹⁶O comprises more than 99.75 % of the dissolved O₂. Therefore, the G equation can be written for ¹⁶O¹⁶O as:

$$G = k \times (\text{O}_2 \text{ saturation} - \text{O}_2) \quad (4.2)$$

where G is the net flux rate of ¹⁶O¹⁶O (O₂), O₂ is the measured dissolved O₂ concentration, and O₂ saturation is the temperature-dependent equilibrium saturation dissolved O₂ concentration. O₂ saturation is a function of temperature (*Weiss, 1970*):

$$\text{O}_2 \text{ saturation} = 1.4276 \times \left[-173.4294 + 249.6339 \times \frac{100}{T} + 143.3483 \times \ln\left(\frac{T}{100}\right) - 21.8392 \times \frac{T}{100} \right] \quad (4.3)$$

where O₂ saturation is concentration in mg L⁻¹ and T is the temperature in kelvins. Diel changes in water temperature directly affect the rate and direction of G by dynamically changing the equilibrium saturation concentration.

G for the ¹⁸O¹⁶O isotopologue can be modelled using the same G equation as for total O₂ and correcting for the difference in saturation and isotope fractionation during G (*Knox et al., 1992*):

$$G_{^{18}\text{O}^{16}\text{O}} = k \times \alpha_{G-k} \times \left(\text{O}_2 \text{ saturation} \times \frac{^{18}\text{O}}{^{16}\text{O}}_{\text{air}} \times \alpha_{G-eg} - \text{O}_2 \times \frac{^{18}\text{O}}{^{16}\text{O}} \right) \quad (4.4)$$

where $G_{^{18}\text{O}^{16}\text{O}}$ is the net flux rate of $^{18}\text{O}^{16}\text{O}$, $k \times \alpha_{G-k}$ is the gas exchange coefficient for $^{18}\text{O}^{16}\text{O}$, $\text{O}_2 \text{ saturation} \times \frac{^{18}\text{O}}{^{16}\text{O}}_{\text{air}} \times \alpha_{G-eg}$ is the equilibrium saturation dissolved $^{18}\text{O}^{16}\text{O}$ concentration, and $\text{O}_2 \times \frac{^{18}\text{O}}{^{16}\text{O}}$ is the $^{18}\text{O}^{16}\text{O}$ concentration. In summary, PoRGy calculates G from k , O_2 saturation (and therefore temperature), $\delta^{18}\text{O}-\text{O}_2$, and appropriate fractionation factors (α_{G-k} , α_{G-eg}).

Mass Balance of P , R , and G

Arithmetically, PoRGy determines the dissolved O_2 ($^{16}\text{O}^{16}\text{O}$) concentration at any time by combining the P , R , and G equations and calculates the rate of O_2 change as:

$$\frac{d\text{O}_2}{dt} = P - R + G \quad (4.5)$$

where P , R , and G are rates as described above. PoRGy determines the $^{18}\text{O}^{16}\text{O}$ isotopologue at any time based on the ratio of isotopologues ($^{18}\text{O}^{16}\text{O}$ to $^{16}\text{O}^{16}\text{O}$) and by combining P , R , and G rates with the appropriate fractionation factors and calculates the rate of $^{18}\text{O}^{16}\text{O}$ change as:

$$\frac{d^{18}\text{O}^{16}\text{O}}{dt} = P \left(\alpha_P \times \frac{^{18}\text{O}}{^{16}\text{O}}_{\text{H}_2\text{O}} \right) - R \left(\alpha_R \times \frac{^{18}\text{O}}{^{16}\text{O}}_t \right) + G_{^{18}\text{O}^{16}\text{O}} \quad (4.6)$$

where $\frac{^{18}\text{O}}{^{16}\text{O}}_{\text{H}_2\text{O}}$ is the isotopic ratio of H_2O .

Surface Area, and Other Model Considerations

PoRGy calculates water volume using a user-specified surface area and depth: a well-mixed, non-steady state box that is open to the atmosphere. All P , R , and G rates are calculated per unit area so all rates are directly comparable. PoRGy assumes the same water ‘stays in the box’ during diel or temporal fluctuations, whether for ponds or rivers. In reality, few water bodies are static so the quasi steady state hydrologic assumption must be considered. For aquatic systems with a rapid flow rates or mixing (e.g., thermocline depth changes in lakes) this assumption may be valid for one or two diel cycles. However, short-term events like diel mixing, storms, or upstream water releases from reservoirs and storm sewers may invalidate this assumption. PoRGy assumes that there are no clouds and no unexpected daytime variability in PAR or P as a result. These factors need to be taken into consideration when collecting representative field data and modelling the results.

Dissolved O₂ and $\delta^{18}\text{O-O}_2$ field sampling for the purposes of PoRGy modelling should be made under the environmental conditions that are as typical as possible for the water body over the study period. In general, the three main factors influencing metabolic rates over diel cycles are: amount of biomass, water temperature, and light conditions. Finally, PoRGy is likely most applicable for productive water bodies (e.g., streams, rivers, and ponds) where turnover times of dissolved O₂ due to P and R are relatively rapid (hours to days) and G is lower than metabolic rates in order to produce $\delta^{18}\text{O-O}_2$ diel patterns that can be modelled. In larger water bodies (e.g., large lakes) incomplete mixing may be a confounding factor. Nevertheless, PoRGy modelling can also be applied to ecosystems that do not exhibit diel cycles (e.g., oligotrophic systems) to obtain P , R , and G rates as long as these ecosystems are not simultaneously at 100% O₂ saturation and isotopic equilibrium with the atmosphere.

Model Output and Sensitivity Analyses

PoRGy calculates each variable (P , R , G , dissolved O₂ concentration and saturation, $\delta^{18}\text{O-O}_2$, temperature, and PAR) for each time-step, summarises the data, and generates two types of output: (1) tables of P , R , and G rates, dissolved O₂ concentration, saturation, and $\delta^{18}\text{O-O}_2$ values, which can then be imported into a spreadsheet for comparison with field data; and (2) plots of the data (O₂ saturation versus $\delta^{18}\text{O-O}_2$), which are useful for graphical comparison with field results and for comparing different model runs. Daily rates of P , R , and G can be calculated, as can the conventional $P:R$ ratio.

Metabolic rates are unlikely to be invariant over 24 h, (even if PAR and temperature are constant). Organisms and cells grow and divide on diel time scales that exhibit circadian rhythms (cf. [Falkowski and Raven, 1997](#); [Pace and Prairie, 2005](#)). Other environmental conditions may change as a result of biological, chemical, or physical activity (nutrient availability, flow rates, cloudiness, etc.). Model results from PoRGy represent a daily average that would not be expected to exactly fit each point of field data.

Results from PoRGy depend on the quality and accuracy of input parameters and assumptions. PoRGy results cannot be directly validated because it is impossible to independently and simultaneously determine all of the variables of interest in a natural system at hourly time frames (cf. [Oreskes et al., 1994b](#)), nor can the three key parameters of P , R , and α_R be measured simultaneously in the same aquatic system. Most often, P and R rates can only be obtained through incubations in bottles or submerged chambers with their associated artefacts. When there is no P at night, the cumulative effect of R and G rates and α_R may be measured simultaneously, but may not be the same as in the day. G is the only rate that can be measured independently by measuring k with another gas in a whole ecosystem tracer addition experiment. For this reason a sensitivity analysis can be used to assess the extent

to which small changes in input parameters generate important changes in model results (O_2 saturation and $\delta^{18}O-O_2$).

To assess the fit between the model-generated results and field data, two approaches were used: (1) coefficient of determination (r^2) between the PoRGy-generated dissolved O_2 and $\delta^{18}O-O_2$ results and field data; and (2) visual comparison of both the shape and extremes of the field data to those generated by the model. An r^2 of about 0.9 or better is suggested for dissolved O_2 and $\delta^{18}O-O_2$ between model and field data as providing an acceptable solution. While the best-fit to field results represents one possible solution for aquatic metabolism, caveats regarding the acceptance and reliability of modelling efforts apply (*Konikow and Bredehoeft, 1992; Oreskes et al., 1994a*).

Since modelling cannot exactly replicate nature, what scientific or resource management benefits can be derived from the simplifications required by a broadly applicable model limited to key input variables? The benefits are the ability to: (1) generate average metabolic rates for the whole ecosystem (bottle incubation rates may be impractical, only short term, or limited to a subset of the ecosystem); (2) assess the influence of small or large environmental changes (akin to a sensitivity analysis); (3) test the simplifying assumptions made in the model; and (4) examine 'what if' scenarios in a predictive mode. Although determining daily average P , R , and G rates is a useful objective in itself, a potential application is to quantify the effect of key metabolic and physical variables on the shape and magnitude of the diel curves in response to imposed ecological or multiple stressors (e.g., change in nutrient loading, water level, climate).

4.3 Results and Discussion

Dynamic Modelling of Isotope Gas Exchange

To assess whether PoRGy could successfully capture the dynamics of O_2 isotopic exchange when O_2 is at saturation, PoRGy was applied to the data of *Knox et al. (1992)*. The laboratory experiment involved measurement of O_2 and $\delta^{18}O-O_2$ for G . In the experiment, a 4 L flask of degassed water was connected to a 12 L ballast via a manometer. Pure O_2 was introduced as headspace into the smaller flask. The water was stirred slowly to minimize disturbance of the water surface. The net G rate was measured as the change in water level in the manometer. Headspace samples were analysed for $\delta^{18}O-O_2$. Initially, the $\delta^{18}O-O_2$ of the headspace increased because the dissolution rate of $^{16}O^{16}O$ was greater than that of $^{18}O^{16}O$ (a result of kinetic isotopic fractionation). After the water reached about 50% saturation the $\delta^{18}O-O_2$ of the headspace began to decline. As 100% saturation was approached, the $\delta^{18}O-O_2$ of the headspace continued to decline below its initial value, because of equilibrium isotopic fractionation, and the $\delta^{18}O$

of the dissolved O_2 must be greater than the $\delta^{18}O-O_2$ of the headspace (set by the equilibrium isotopic fraction factor). Thus isotopic exchange occurs until both O_2 concentration and isotopic equilibrium are reached. The experimental data and PoRGy results are shown in Figure 4.2. The maximum and minimum $\delta^{18}O-O_2$ values of the headspace are a function of the volumes of the headspace and water. The goodness-of-fit yielded an r^2 of 0.94 for $\delta^{18}O-O_2$. Most importantly, PoRGy reproduced the initial increase and subsequent decrease in headspace $\delta^{18}O-O_2$ as isotopic equilibrium was dynamically established.

Steady state models used previously (Quay *et al.*, 1995; Wang and Veizer, 2000) did not allow for diel changes in O_2 or $\delta^{18}O-O_2$ because at steady state the $P:R$ ratio is independent of k . The steady state assumption is especially problematic when O_2 is at 100 % saturation but $\delta^{18}O-O_2$ is not at equilibrium because the steady state equation is indeterminate despite the fact that G (to establish isotopic equilibrium) still occurs. Given that G remains the most problematic and primary source of error for dual- and triple-isotope assessments of aquatic metabolism (Juraneck and Quay, 2005), PoRGy applied to diel curves provides an improved approach. PoRGy can model isotopic G that was ignored in steady state approaches or assumed to occur only when O_2 saturation is not 100 %.

Dynamic modelling of field data for ecological assessment

PoRGy is applied to the field data of three sites to illustrate the potential to derive ecological information. The first example is a diel sampling of an experimental reservoir in northwestern Ontario. The Flooded Upland Dynamics Experiment (FLUDEX) was conducted at the Experimental Lakes Area (49°40' N 93°45' W) to study the effects of reservoir creation on greenhouse gas cycling in boreal reservoirs (cf. Bodaly *et al.*, 2004). The Medium C reservoir was constructed by enclosing about 0.5 ha of upland forest in wooden dykes and gravel walls to a mean water depth of 0.9 m. Water was continuously pumped into the reservoir (water renewal time of 7.4 d in 2003) and the inflow and outflow monitored. In mid-July 2003, the fifth year of flooding, a 2-day diel sampling of O_2 concentration and $\delta^{18}O-O_2$ was performed. Sunrise and sunset occurred at 0530 hours and 2110 hours (local time). Samples were collected from the outflow of the well-mixed reservoir hourly for Winkler O_2 concentration and $\delta^{18}O-O_2$, and at 5-min intervals for O_2 saturation and temperature by a Hydrolab sonde deployed 30 cm below the surface of the water. To determine k directly, SF_6 was added to the reservoir and the decline in SF_6 concentration was monitored. PoRGy was run by using the independently determined k (0.524 cm h^{-1} ; corrected from SF_6 to O_2), a measured $\delta^{18}O-H_2O$ of -6.8 ‰ , measured temperature, and latitude, longitude, and altitude. The field data and PoRGy results are shown in Figure 4.3. The reservoir exhibited a strong diel cycle in both O_2 saturation and $\delta^{18}O-O_2$ that

is adequately captured with three average rates: P , R , G . The goodness-of-fit between PoRGy and the field data yielded an r^2 of 0.96 for O_2 saturation and an r^2 of 0.87 for $\delta^{18}O-O_2$, with daily average rates of P and R of 131 and 168 $mg\ m^{-2}\ h^{-1}$ respectively. The gross G rate (sum of influx and efflux, not their difference) was 14 $mg\ m^{-2}\ h^{-1}$. The diel results yielded a $P:R$ ratio of 0.78:1 and a $P:R:G$ ratio of 9.28:11.9:1. PoRGy was able to successfully reproduce both the O_2 and $\delta^{18}O-O_2$ curves even though the system was evolving with time (i.e., mean O_2 saturation decreasing and mean $\delta^{18}O-O_2$ increasing over two days). The reservoir was consistently well below O_2 saturation (55–85%) with $P < R$ and a low k . However, the $\delta^{18}O-O_2$ was mostly below atmospheric equilibrium because of the large difference between $\delta^{18}O-H_2O$, which yields O_2 for photosynthesis, and $\delta^{18}O$ of atmospheric O_2 .

The second example is a diel sampling of a productive closed basin prairie slough (wetland 50) in the St. Denis National Wildlife Area east of Saskatoon (Woo and Rowsell, 1993). Mean water depth over the sampling period (late September 2000) was 0.165 m. Sunrise and sunset occurred at 07:00 and 18:50 (local time). A Hydrolab sonde recorded O_2 saturation and temperature at 15 min intervals. The sonde was placed mid-depth below the water surface at the centre of the pond. The $\delta^{18}O-O_2$ samples were taken at 60 to 120 min intervals adjacent to the sonde, with sampling frequency increased around sunrise and sunset. To estimate k , wind speed was measured using the on-site meteorological station and used in common empirical models for sites with low wind speed (Crusius and Wanninkhof, 2003) yielding a range of 0.93–1.24 $cm\ h^{-1}$ for k for O_2 . PoRGy was run by using this range of k , an $\delta^{18}O-H_2O$ of 0 ‰ calculated from seasonal changes in $\delta^{18}O-H_2O$ from 2000 (Environment Canada, unpublished data), measured temperature, and known latitude, longitude and altitude. The field data and PoRGy results are shown in Figure 4.4. The goodness-of-fit yielded an r^2 of 0.96 for O_2 saturation and an r^2 of 0.93 for $\delta^{18}O-O_2$, with daily average rates of P and R of 105 and 143 $mg\ m^{-2}\ h^{-1}$ respectively. The gross G rate was 41 $mg\ m^{-2}\ h^{-1}$. The diel results yielded a $P:R$ ratio of 0.73:1 and a $P:R:G$ ratio of 2.5:3.5:1. This productive slough exhibited a large diel change in O_2 saturation from 120 % during the day to 20 % at night. However, $P < R$ and the mean O_2 saturation was < 100 %.

The third example is a diel sampling of the South Saskatchewan River, approximately 50 km downstream of Saskatoon in mid-July 2004. A Hydrolab sonde was deployed mid-depth below the water surface to measure O_2 saturation and temperature at 15-min intervals. The depth of the river was 0.65 m and the average water velocity over the 24 h sampling period was 0.21 $m\ s^{-1}$. Sunrise and sunset occurred at 0500 hours and 2120 hours (local time). Hourly $\delta^{18}O-O_2$ samples were collected adjacent to the sonde. To estimate k , depth and velocity measurements were used in four common river empirical models (Churchill et al., 1962; Langbein and Durum, 1967; O'Connor

and Dobbins, 1958; Owens et al., 1964) yielding a range in k of 4.2 to 7.1 cm h⁻¹. PoRGy was run by allowing k to fluctuate within this range, a measured $\delta^{18}\text{O}\text{-H}_2\text{O}$ of -7‰ , measured temperature, and known latitude, longitude, and altitude. The field data and PoRGy results are shown in Figure 4.5. The goodness-of-fit yielded an r^2 of 0.98 for O_2 saturation and an r^2 of 0.97 for $\delta^{18}\text{O}\text{-O}_2$, with daily average rates of P and R of 425 and 382 mg m⁻² h⁻¹ respectively. The gross G rate was 215 mg m⁻² h⁻¹. The diel results yielded a $P\text{:}R$ ratio of 1.11:1 and a $P\text{:}R\text{:}G$ ratio of 1.97:1.78:1. The river had a large diel in both O_2 saturation and $\delta^{18}\text{O}\text{-O}_2$. The mean O_2 saturation exceeded 100% because $P > R$ but the $\delta^{18}\text{O}\text{-O}_2$ was consistently below atmospheric equilibrium because of the high P rate adding O_2 with the $\delta^{18}\text{O}\text{-H}_2\text{O}$ of -7‰ .

The sensitivity of model results to the input parameters can be easily assessed with PoRGy. A reasonable range for each unknown input parameter can be used and the resulting curves plotted together generating a ‘sensitivity cloud’ or ‘error space’ around the field data. A range of $\pm 5\%$ in metabolic rates is comparable to the measured error in typically laboratory incubations. A range of $\pm 10\%$ in k is representative of the variability in k estimated by empirical wind speed equations or depth and velocity equations (cf. Crusius and Wanninkhof, 2003; Jha et al., 2001). A range of ± 0.003 in α_R is typical of laboratory incubations (e.g., Kiddon et al., 1993; Quay et al., 1995). A range of $\pm 0.3\text{‰}$ in $\delta^{18}\text{O}\text{-H}_2\text{O}$ is comparable to the largest error expected among the commonly used analytical methods summarised by Horita and Kendall (2004). A matrix of all possible combinations of the above ranges in P , R , k , α_R , and $\delta^{18}\text{O}\text{-H}_2\text{O}$ were modelled using PoRGy for the South Saskatchewan River example and presented as the ‘sensitivity cloud’ circumscribing the field data and best-fit results in Figure 4.5. The best-fit results of the South Saskatchewan River involved finding P and R rates, a k value within a specified range, and an α_R value that minimised the difference between model output and field data. Thus any changes in those parameters to create the ‘cloud’ necessarily reduced the goodness-of-fit. Thus the P and R rates, and k and α_R values are together best-fit values (Table 4.1). The r^2 -values of the generated diel curves contained within the cloud ranged from 0.96 to 0.98. The sensitivity of model output to changes in the R fractionation factor (α_R) value was low, confirming the observations of others (Juraneck and Quay, 2005; Parker et al., 2005). Similarly, sensitivity of model results to only one variable or a combination of two or more variables is easily assessed.

PoRGy successfully modelled diel data ($r^2 \geq 87\%$) for three field sites with a large range in P , R , and G , and differing mean O_2 saturation and mean $\delta^{18}\text{O}\text{-O}_2$. PoRGy used daily average input parameters to generate daily average P , R , and G rates. Even though daily rates are used, the overall goodness-of-fit between model output and field data is good even in ecosystems that are evolving over the sampling period. The FLUDEX reservoir and prairie slough have similar P and R rates, $P\text{:}R$ ratio, mean O_2 and mean

$\delta^{18}\text{O}-\text{O}_2$. The prairie slough has a much larger diel range in O_2 (20–120%) and $\delta^{18}\text{O}-\text{O}_2$ (12–30 ‰) than the FLUDEX reservoir. However, k is much higher in the slough and thus the $P:R:G$ ratio (2.5:3.5:1) is also much different than in the reservoir (9.3:11.9:1). Thus the relative magnitude of P and R cannot be immediately assessed by simply comparing diel curves. O_2 diel curves (and $\delta^{18}\text{O}-\text{O}_2$ curves) exhibit the balance between P , R , and G . The South Saskatchewan River has much higher P and R rates than either the slough or reservoir. The magnitude of the diel range, however, is less than the slough due to the much higher G . Ecosystems can be compared with P and R rates or $P:R:G$ ratios; both offer more detail than the $P:R$ ratio. In $P:R$ ratio studies, G is often not determined directly. PoRGy facilitates the comparison by calculating average P , R , and G rates, and thus the $P:R:G$ ratio, over the diel cycle.

Some parameters used to model the field examples were assumed to be fixed or a daily average (e.g., k , flow rates, α_R) although some of these may have changed on hourly timescales. Practically, instantaneous rates are of little broad interest, hence an absolute model fit to field data was neither expected nor required. Nevertheless, the results show that large diel changes are more apparent and easily measurable in lower G environments like ponds compared to higher G environments like rivers (Table 4.1; Figures 4.3, 4.4, and 4.5) since the latter require relatively higher metabolic rates to maintain diel changes in O_2 and $\delta^{18}\text{O}-\text{O}_2$.

Dynamic modelling with PoRGy has captured the main features of the diel O_2 and $\delta^{18}\text{O}-\text{O}_2$ curves: the timings and values of the maxima and minima. The simplifications in PoRGy such as using average values, even though ecosystems do not operate with average values, did not hinder the best-fit modelling. An important benefit derived from average P , R , and G rates is the ability to compare ecosystems seasonally, longitudinally, and with each other. Comparing the three field examples shows that ecosystems can have large diel ranges in O_2 and $\delta^{18}\text{O}-\text{O}_2$ with widely different $P:R:G$ ratios and rates and thus different ecosystem functions.

4.4 Conclusion

Most aquatic systems of interest, and especially human-impacted systems, are not at steady state and exhibit significant diel O_2 cycles. Transient modelling is therefore required if reasonable estimates of $P:R:G$ ratios and P , R , and G rates are needed to quantify the cumulative impact of anthropogenic stressors on community metabolism. The transient model (PoRGy) approach solves dynamic O_2 and $\delta^{18}\text{O}-\text{O}_2$ mass balances using a minimum number of key variables. The model generates dissolved O_2 concentration and $\delta^{18}\text{O}-\text{O}_2$ diel curves that can be compared to field data. By changing rates of biological processes (P and R), G , the O_2 isotopic fractionation factors, light curves,

and temperature, each of the key variables may be further examined for its role and relative importance in the shape of the hysteretic diel curve. PoRGy allows researchers to quickly visualise the sensitivity of small changes in the environmental variables to the overall rates and metabolic balance in aquatic systems.

The PoRGy model provides daily fundamental ecological rates. Users can employ PoRGy to pose impact- and process-driven causal environmental questions, such as: how does a nutrient-driven 5% increase in metabolic rates affect O₂ status under the same *G* regime? Or, how does a 2 °C increase in water temperature affect *R* outcomes? Periodic diel δ¹⁸O-O₂ surveys in conjunction with basic O₂ saturation data can provide river managers with both metabolic rates and a method for deriving *G* rates necessary for watershed models.

Acknowledgements

This work was supported by a Natural Sciences and Engineering Research Council of Canada (NSERC) Strategic grant (S. L. S. and L. I. W.), Environment Canada (L. I. W.), the Canadian Foundation for Climate and Atmospheric Sciences (CFCAS) (S. L. S.), an Ontario Graduate Scholarship (J. J. V.), and Environment Canada's Science Horizons Youth Internship Program (S. L. S.). Analytical development at the University of Waterloo was funded by an NSERC Discovery grant (S. L. S.), CFCAS (S. L. S.), and the Centre for Research in Earth and Space Technology (S. L. S.). Andrea Wojtyniak, Kevin Maurice, and Matthijs Vlaar provided field assistance. Richard Elgood, Geoff Koehler, and Daryl Halliwell provided additional field and laboratory assistance. FLUDEX was funded by Fisheries and Oceans Canada, Manitoba Hydro, and Hydro-Québec.

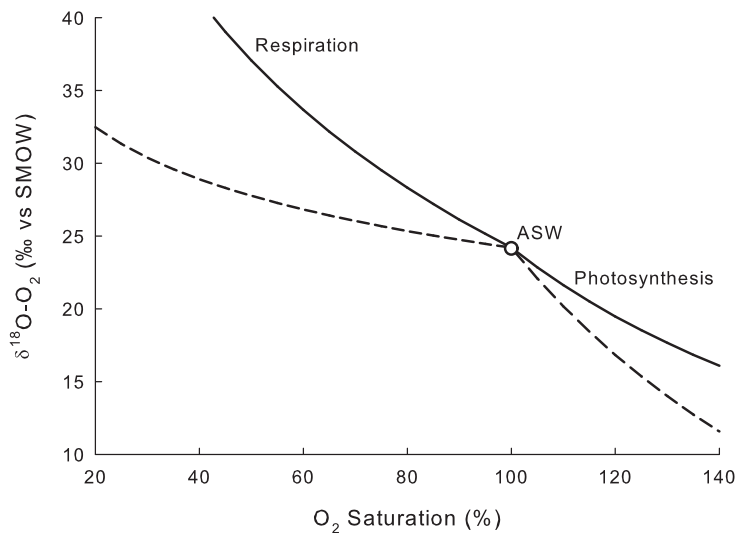


Figure 4.1: A graphical depiction of O_2 processes on a plot of O_2 saturation versus $\delta^{18}O-O_2$. Respiration and photosynthesis are depicted as closed-system trajectories moving away from air-saturated water (ASW). The angles of the respiration and photosynthesis trajectories are controlled by α_R and $\delta^{18}O-H_2O$ respectively. Two respiration trajectories are shown, $\alpha_R = 0.987$ (solid line) and $\alpha_R 0.995$ (dashed line), and were calculated as a unidirectional closed-system Rayleigh fractionation from ASW. Two photosynthesis trajectories are shown, $\delta^{18}O-H_2O = -7\text{‰}$ (solid line) and $\delta^{18}O-H_2O = -15\text{‰}$ (dashed line), and were calculated as a mixing model from ASW. Gas exchange (not shown) exhibits a curved trajectory toward ASW where an under- or super-saturated water approaches isotopic equilibrium slightly faster than approaching 100% saturation. VSMOW Vienna standard mean oceanic water.

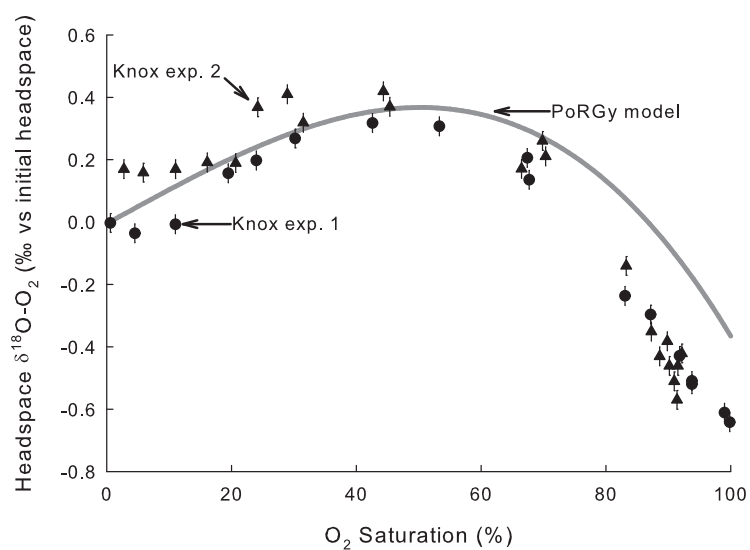


Figure 4.2: Comparison of the *Knox et al. (1992)* kinetic isotopic fractionation factor laboratory experiments (*exp.*) (black dots and triangles) and photosynthesis–respiration–gas exchange (*PoRGy*) (grey line). Axes are the same as those used by Knox et al. (1992) where the *x*-axis is the level of O₂ saturation in the water and the *y*-axis is the δ¹⁸O-O₂ of the headspace versus the isotopic ratio of the initial headspace gas and not versus VSMOW. The δ¹⁸O-O₂ error bars are ± 0.03 ‰ as reported by Knox et al. (1992).

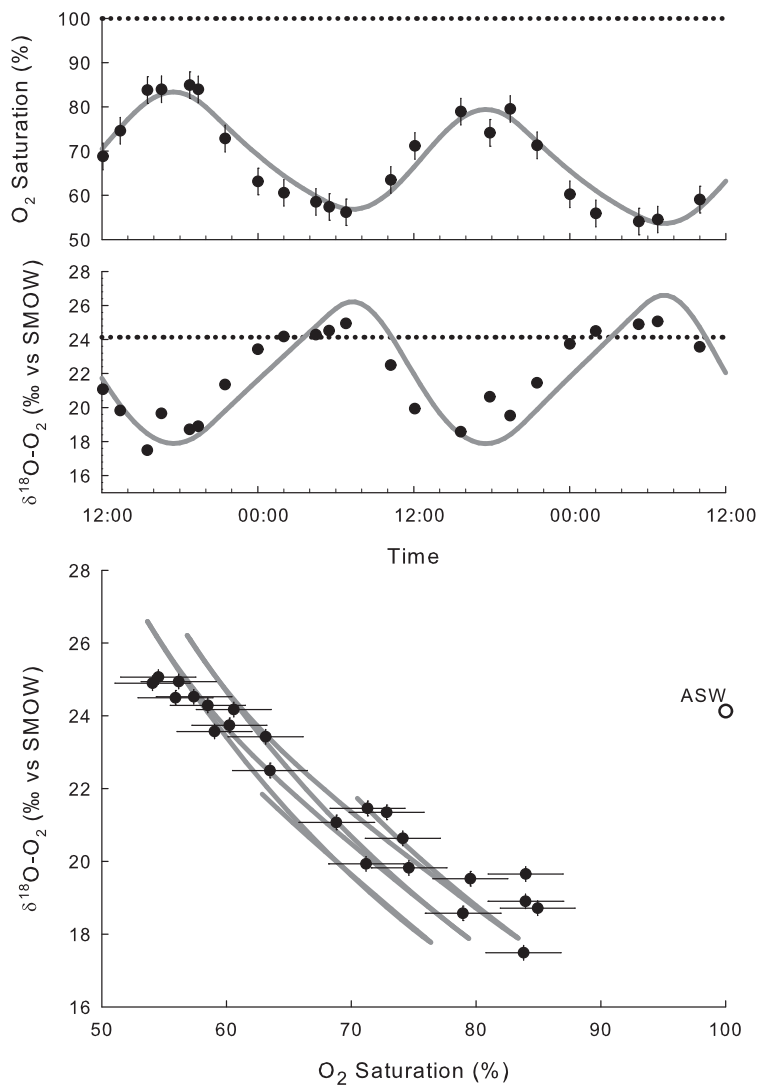


Figure 4.3: Field data (*black dots*) with 1 SD error bars ($\pm 0.2\%$ and $\pm 0.2\text{‰}$) and PoRGy model (*grey line*) diel data from the Flooded Upland Dynamics Experiment Medium C reservoir from 23 to 25 July 2003. The frequency of O₂ saturation data is reduced to match the $\delta^{18}\text{O-O}_2$ data. Equilibrium saturation is shown as dotted lines in the temporal figures and ASW is shown in the cross-plot. For abbreviations, see Figures 4.1 and 4.2.

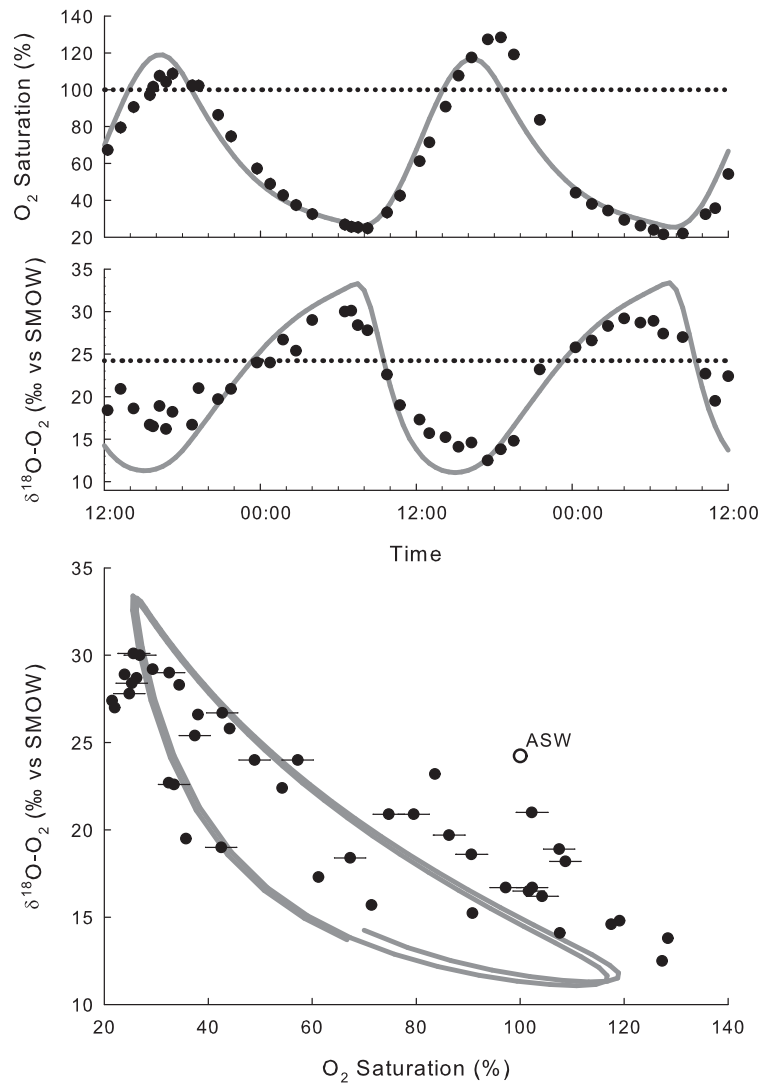


Figure 4.4: Field data (*black dots*) with 1 *SD* error bars ($\pm 0.2\%$ and $\pm 0.2\%$) and PoRGy model (*grey line*) diel data from the pond 50 in St. Denis National Wildlife Area from 28 to 29 July 2000. The frequency of O₂ saturation data is reduced to match the $\delta^{18}\text{O}-\text{O}_2$ data. Equilibrium saturation is shown as dotted lines in the temporal figures and ASW is shown in the cross-plot. For abbreviations, see Figures 4.1 and 4.2.

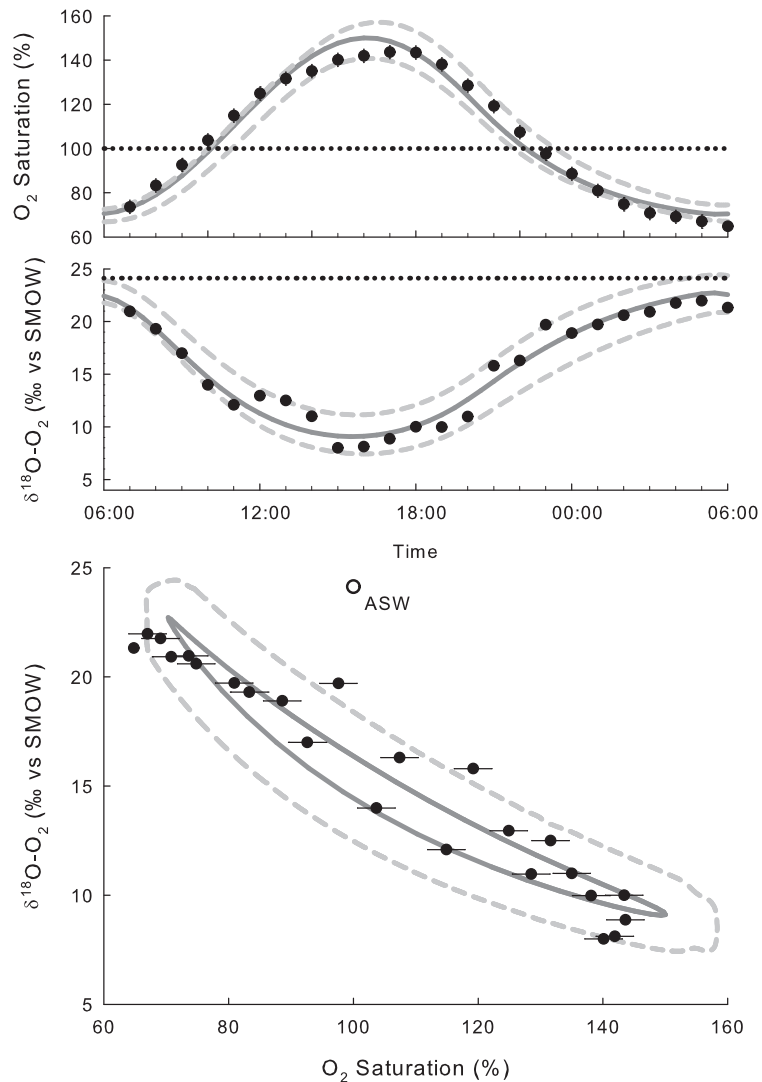


Figure 4.5: Field data (*black dots*) with 1 *SD* error bars ($\pm 0.2\%$ and $\pm 0.2\text{‰}$) and PoRGy model (*grey line*) diel data from the South Saskatchewan River near Saskatoon from from 14 to 15 July 2004 . The frequency of O₂ saturation data is reduced to match the $\delta^{18}\text{O}-\text{O}_2$ data. Equilibrium saturation is shown as dotted lines in the temporal figures and air-saturated water (ASW) is shown in the cross-plot. The ‘sensitivity cloud’ (*light grey dashed line*) around the best-fit was created based on $\pm 5\%$ of the metabolic rates, $\pm 10\%$ of gas exchange coefficient, ± 0.003 of α_R , and ± 0.3 of $\delta^{18}\text{O}-\text{H}_2\text{O}$. For abbreviations, see Figures 4.1 and 4.2.

Table 4.1: PoRGy model input parameters and results for examples shown in Figures 4.3, 4.4, and 4.5. FLUDEX Flooded Upland Dynamics Experiment, P primary production, R community respiration, G gas exchange, k G coefficient, G^* gross G (sum of influx and efflux, not their difference)

Example	Input variables: Independently known	Input variables: Adjusted to improve fit (rates are $\text{mg m}^{-2} \text{h}^{-1}$)	Calculated from model fit (rates are $\text{mg m}^{-2} \text{h}^{-1}$)
FLUDEX Medium C reservoir, Experimental Lakes Area, northwestern, Ontario	$\delta^{18}\text{O-H}_2\text{O} = -6.8 \text{ ‰}$ latitude = 49.6639° longitude = -93.7221° altitude = 424 masl $k = 0.00524 \text{ m h}^{-1}$ temperature = 21–25°C depth = 0.9 m area = 4900 m^2 day of year = 204 year = 2003	$P_{max} = 510$ $R_{20} = 150$ $\alpha_R = 0.979$	$P = 131$ $R = 168$ $G^* = 14$ $P:R = 0.78:1$ $P:R:G = 9.28:11.9:1$
Wetland 50, St. Denis National Wildlife Area	$\delta^{18}\text{O-H}_2\text{O} = 0 \text{ ‰}$ latitude = 51.2167° longitude = -106.267° altitude = 550 masl temperature = 7–17°C depth = 0.165 m area = 11 040 m^2 day of year = 271 year = 2000	$P_{max} = 830$ $R_{20} = 200$ $k = 0.0093 \text{ m h}^{-1}$ $\alpha_R = 0.985$	$P = 105$ $R = 143$ $G^* = 41$ $P:R = 0.73:1$ $P:R:G = 2.5:3.5:1$
South Saskatchewan River, 50 km downstream from Saskatoon	$\delta^{18}\text{O-H}_2\text{O} = -7 \text{ ‰}$ latitude = 52.5104° longitude = -106.4146° altitude = 550 masl temperature = 20.4–24.5°C depth = 0.65 m area = 1 m^2 day of year = 197 year = 2004	$P_{max} = 1640$ $R_{20} = 340$ $k = 0.1072 \text{ m h}^{-1}$ $\alpha_R = 0.998$	$P = 425$ $R = 382$ $G^* = 215$ $P:R = 1.11:1$ $P:R:G = 1.97:1.78:1$

Chapter 5

Aquatic metabolism and ecosystem health assessment using dissolved O₂ stable isotope diel curves

Jason J. Venkiteswaran¹, Sherry L. Schiff¹, Leonard I. Wassenaar²

Ecological Applications 18(4): 965–982 doi: 10.1890/07-0491.1.

© by the Ecological Society of America. Permission to reproduce and statement from the co-authors is found in Appendix B.

Abstract

Dissolved O₂ concentration and $\delta^{18}\text{O}-\text{O}_2$ diel curves can be combined to assess aquatic photosynthesis, respiration, and metabolic balance, and to disentangle some of the confounding factors associated with interpretation of traditional O₂ concentration curves. A dynamic model is used to illustrate how six key environmental and biological parameters interact to affect diel O₂ saturation and $\delta^{18}\text{O}-\text{O}_2$ curves, thereby providing a fundamental framework for the use of $\delta^{18}\text{O}-\text{O}_2$ in ecosystem productivity studies. $\delta^{18}\text{O}-\text{O}_2$ provides information unavailable from concentration alone because $\delta^{18}\text{O}-\text{O}_2$ and saturation curves are not symmetrical and can be used to further constrain gas exchange and isotopic fractionation by eliminating many common assumptions. Changes in key parameters affect diel O₂ saturation and $\delta^{18}\text{O}-\text{O}_2$ curves as follows: (1) an increase in primary production and respiration rates increases the diel range of O₂ saturation and $\delta^{18}\text{O}-\text{O}_2$, and decreases the mean $\delta^{18}\text{O}-\text{O}_2$ value; (2) a decrease in the primary production to respiration ratio ($P:R$) decreases

¹Department of Earth and Environmental Sciences, University of Waterloo, 200 University Avenue West, Waterloo ON, N2L 3G1, Canada.

²Environment Canada, 11 Innovation Boulevard, Saskatoon SK, S7N 3H5, Canada.

the level of O₂ saturation and increases the δ¹⁸O-O₂ values; (3) an increase in the gas exchange rate decreases the diel range of O₂ saturation and δ¹⁸O-O₂ values, and moves the mean O₂ saturation and δ¹⁸O-O₂ values towards atmospheric equilibrium; (4) an decrease in strength of the respiration isotopic fractionation factor (α_R closer to 1) has no effect on O₂ saturation and decreases the δ¹⁸O-O₂ values; (5) an increase in the δ¹⁸O of water has no effect on O₂ saturation and increases the minimum (daytime) δ¹⁸O-O₂ value; and (6) an increase in temperature reduces O₂ solubility and thus increases the diel range of O₂ saturation and δ¹⁸O-O₂ values. Understanding the interplay between these key parameters makes it easier to decipher the controls on O₂ and δ¹⁸O-O₂, compare aquatic ecosystems, and make quantitative estimates of ecosystem metabolism. The photosynthesis to respiration to gas exchange ratio ($P:R:G$) is better than the $P:R$ ratios at describing and assessing the vulnerability of aquatic ecosystems under various environmental stressors by providing better constrained estimates of ecosystem metabolism and gas exchange.

5.1 Introduction

Primary productivity (P) and species richness are commonly used as measures of aquatic ecosystem function. P is the rate of O₂ evolution generated by the photochemical oxidation of water and is associated with the fixation of carbon and energy into plant biomass (*Falkowski and Raven, 1997*). Studies have therefore suggested that dissolved O₂ evolution is a more direct means of estimating P in aquatic systems than conventional carbon-based approaches, since carbon- and O₂-based rates can differ significantly if photorespiratory rates are high or if photosynthetically-derived electrons are used to reduce nitrate (*Falkowski and Raven, 1997*). In aquatic systems, the O₂ evolved from P is added to a pre-existing dissolved O₂ pool that is linked to the atmosphere via air-water gas exchange (G). Aquatic community (plant, animal, microbe) respiration (R) processes also occur in that same environment, consume dissolved O₂ from the water column, and generally produce carbon dioxide (CO₂). Employing O₂ evolution to quantify the aquatic P component of ecosystem function requires disentangling the concomitant processes of P , R , and G that ultimately govern the concentration of dissolved O₂ in aquatic ecosystems. Thus, dissolved O₂ evolution and consumption are inherently linked to carbon-flow and food web structure in freshwater and marine ecosystems (*Carignan et al., 2000*).

Minimum dissolved O₂ concentrations are required for the survival of many aquatic organisms (*Barton and Taylor, 1996; Chapman, 1986*). Thus dissolved O₂ is also a primary indicator of aquatic ecosystem health. Whereas dissolved O₂ concentrations in rivers and lakes naturally seek to attain local equilibrium saturation with atmospheric O₂, the overall metabolic balance between P and R (commonly expressed as a $P:R$ ratio) can be tilted in either

direction (O_2 super- or under-saturation) on a daily to seasonal basis (Carignan *et al.*, 2000; del Giorgio and Peters, 1994; Odum, 1956; Rizzo *et al.*, 1996). Undersaturated and low dissolved O_2 in wetlands, rivers, streams, lakes, and estuaries result from normal biogeochemical processes (e.g., community R) and can be exacerbated by atmospheric reaeration constraints, such as extended ice cover. Human activities, such as industrial or nutrient discharges, may have detrimental impacts on dissolved O_2 concentrations by increasing biological and chemical O_2 demand or by stimulating algal growth (Wetzel, 2001). One adverse outcome of nutrient-driven eutrophication may be temporal anoxia that can result in fish kills or harmful changes in overall community structure either at night, in deeper waters during prolonged thermal stratification, or under sustained ice covered conditions (Carpenter *et al.*, 1998a; Dodds and Welch, 2000; Welch and Jacoby, 2004).

Conventionally, P and R rates in water bodies are determined during the summer growing season using light and dark bottle incubations, by diel dissolved O_2 concentration curve analysis, using ^{14}C - CO_2 incubations, or ^{18}O - H_2O spike incubations (cf. Falkowski and Raven, 1997). Point measurements of O_2 (or CO_2) are ineffective in productive systems because of diel changes in O_2 (and CO_2) concentrations. The analysis of diel dissolved O_2 concentration curves has long been used to estimate P and R in aquatic systems (Chapra and Di Toro, 1991; Odum, 1956; Wetzel, 2001; Wilcock *et al.*, 1998). More recently, the application of natural abundance stable oxygen isotopic ratios (^{18}O : ^{16}O ratio, hereafter in δ -notation relative to Standard Mean Ocean Water) in diel studies of aquatic ecosystems has shown that it is possible to separate some of the confounding factors associated with conventional interpretations of diel concentration curves (Parker *et al.*, 2005; Tobias *et al.*, 2007; Venkiteswaran *et al.*, 2007). While ^{17}O analysis has been proven useful in quantifying gross O_2 production integrated over multi-week timescales and in low productivity or high G environments (e.g., Hendricks *et al.*, 2005; Luz and Barkan, 2000; Sarma and Abe, 2006), this technique has not been applied to ecosystems with diel cycles.

Coupling the analysis of dissolved O_2 concentration and $\delta^{18}O$ - O_2 diel curves is particularly useful in studies of aquatic ecosystem function because the shape, size, and location of dissolved O_2 versus $\delta^{18}O$ - O_2 diel curves provide quantitative information about P , R and G . A non-steady state model (PoRGy) was recently developed to quantify dissolved O_2 and $\delta^{18}O$ - O_2 evolution in aquatic systems (Venkiteswaran *et al.*, 2007). P , R , and G rates, and other key measured environmental parameters were used to generate and fit diel curves to field dissolved O_2 and $\delta^{18}O$ - O_2 data in a variety of aquatic ecosystems. The PoRGy model allows researchers to construct and test O_2 -based hypotheses to decipher aquatic metabolism, metabolic balance, and reaeration under dynamic conditions. Since the natural abundance O_2 isotope approach to aquatic metabolism studies is still relatively new, the pri-

mary objective of this paper is to examine in detail the effects of the key environmental parameters on the shape, size, and magnitude of diel curves of dissolved O_2 and $\delta^{18}O-O_2$ curves, which are intrinsic indicators of ecosystem health. Five generalised $P:R$ stream clusters that cover a majority of the aquatic ecosystem health scenarios likely to be encountered in nature were used to illustrate these effects. These stream clusters were then compared with diel field data from several North American aquatic ecosystems. Importantly, these results provide researchers with a fundamental framework to guide the use of dissolved O_2 and $\delta^{18}O-O_2$ patterns in ecosystem productivity studies of both natural and altered water bodies.

5.2 Methods

$\delta^{18}O-O_2$ fundamentals

Photosynthesis adds dissolved O_2 to aquatic systems. The processes of oxidizing H_2O molecules to produce O_2 does not fractionate between the oxygen isotopes ($\alpha_P = 1.000$, [Guy et al., 1989, 1993](#); [Stevens et al., 1975](#), where α is the isotope fractionation factor defined as the $^{18}O:^{16}O$ ratio of the product to that of the reactant). As a result P generally decreases the ambient $\delta^{18}O-O_2$ value by adding O_2 with the same $\delta^{18}O$ value as the H_2O . The $\delta^{18}O-O_2$ decreases because the $\delta^{18}O-H_2O$ is typically much lower than atmospheric $\delta^{18}O-O_2$. P is controlled by the combination of photosynthetically-active radiation (PAR), temperature, abundance of photosynthetic organisms, and other factors ([Wetzel, 2001](#)).

Conversely, R decreases the dissolved O_2 concentration and increases the $\delta^{18}O-O_2$ value because of the preferential consumption (fractionation) of the light O_2 isotopologue ($^{16}O^{16}O$), and is controlled by many factors including carbon and nutrient availability, temperature, and the abundance of respiring organisms ([Lane and Dole, 1956](#); [Wetzel, 2001](#)). In practice, ecosystem measurements of R include all O_2 consuming pathways such as microbial R , photorespiration, the Mehler-peroxidase reaction, chlororespiration, and chemical and photochemical O_2 demand. All of these pathways preferentially consume the light O_2 isotopologue (cf. [Andrews et al., 2000](#); [Bennoun, 2002](#); [Chomicki and Schiff, 2008](#); [Laws et al., 2000](#); [Miles and Brezonik, 1981](#); [Venkiteswaran et al., 2007](#)). The magnitude of the dissolved O_2 community R isotopic fractionation factor (α_R) is a function of the type of aquatic respiring community and the factors that affect R rates.

While P and R are key expressions of aquatic community structure, G is a physical aeration process that independently drives O_2 and $\delta^{18}O-O_2$ values from under- or super-saturated conditions towards temperature-dependent air-water equilibrium saturation. G is controlled by gas exchange coefficients (k) for each O_2 isotopologue based on the thin boundary layer equation $G = k \times (O_{2 \text{ saturation}} - O_2)$ where the difference between O_2 saturation and

the actual O_2 concentration is multiplied by k . There is a small equilibrium isotope fractionation between the $\delta^{18}O-O_2$ of the atmosphere and the $\delta^{18}O-O_2$ of the dissolved O_2 whereby the latter is about 0.7 ‰ greater than the former ($\alpha_{G-eq} = 1.0007$ [Benson et al., 1979](#)). Since the $\delta^{18}O-O_2$ value of atmospheric O_2 is globally constant at +23.5 ‰ ([Kroopnick and Craig, 1972](#)), dissolved O_2 in saturation equilibrium with the atmosphere and in the absence of P and R will have a $\delta^{18}O-O_2$ value of about +24.2 ‰. The measured kinetic isotopic fractionation factor for O_2 invasion-evasion ($\alpha_{G-k} = 0.9972$ [Knox et al., 1992](#)) means that k for the heavy O_2 isotopologue ($^{18}O^{16}O$) is about 3 ‰ slower than for the light O_2 isotopologue ($^{16}O^{16}O$).

Plots of dissolved O_2 saturation versus $\delta^{18}O-O_2$ are particularly useful for comparing aquatic systems with different P , R , and G because the data are normalised for temperature. The shape, size, and location of a diel curve in a cross-plot of O_2 saturation versus $\delta^{18}O-O_2$ arises from the combined effects of different P , R , and G , and their respective O_2 isotopic fractionation factors that are ecosystem specific (Figure 5.1). Steady-state models have used these cross-plots to display data and estimate $P:R$ (e.g., [Quay et al., 1993](#)). However, transient steady state $P:R$ lines are not linear and the space between them varies as a function of O_2 saturation, $\delta^{18}O-O_2$, and $P:R$ itself. Thus estimating the $P:R$ of an ecosystem or comparing ecosystems without understanding the effects of individual parameters would be very difficult. Three key features of these cross-plots are that $P:R$ lines are curvilinear and not readily apparent from only the O_2 saturation $\delta^{18}O-O_2$ axes, diel curves cross many $P:R$ lines, and the daytime and nighttime portions of the curve are not identical. The effects of six key metabolic and environmental parameters on the shape, size, location, and mean of diel curves are examined: (1) different P and R but the same $P:R$; (2) widely differing $P:R$; (3) different gas exchange coefficients, k ; (4) different community respiration isotopic fractionation factors, α_R ; (5) different $\delta^{18}O-H_2O$ values; and (6) different water temperature regimes.

Diel curves

Diel changes in dissolved O_2 concentration in well-mixed surface water bodies are not sinusoidal. Following sunrise, dissolved O_2 concentrations increase due to photosynthetic inputs and can approach a quasi-steady state plateau where P , R , and G are balanced. However, in reality very few productive aquatic systems reach steady-state conditions during the daytime because of changing PAR and other dynamic factors such as water temperature. As illumination declines and R exceeds P , dissolved O_2 concentrations decline and can approach a steady-state concentration during the nighttime when R is offset by an equal O_2 influx by G (re-aeration). As a result of the dynamic changes in P and R , diel dissolved O_2 concentration curves tend to be saw-toothed, rather than sinusoidal ([Venkiteswaran et al., 2007](#)).

Diel curves of dissolved O_2 and $\delta^{18}O-O_2$ are rarely exact mirror images

of each other. Following sunrise, the addition of O_2 with very low $\delta^{18}O-O_2$ values from P decreases the dissolved $\delta^{18}O-O_2$ value in the water column. The $\delta^{18}O-O_2$ minimum cannot occur before the O_2 concentration maximum unless there is a large water temperature decrease during the day. Following solar noon, P decreases and R causes an increase in the dissolved $\delta^{18}O-O_2$. The $\delta^{18}O-O_2$ value can approach a steady-state value during nighttime that is related not only to the $R:G$ ratio, but is also controlled by α_R . As a result, differences in the diel shape between dissolved O_2 and $\delta^{18}O-O_2$, in addition to the temporal offset between dissolved O_2 and $\delta^{18}O-O_2$ curves, give crucial information that can be exploited to quantify P , R , G , and α_R in aquatic ecosystems.

The environmental conditions and diel depictions in this manuscript are steady-state model solutions using the above parameters and PoRGy (Venkiteswaran *et al.*, 2007). The daytime and nighttime portions of the diel curve follow different trajectories and cross many of the non-diel steady-state $P:R$ lines. Representative values of P , R , and k for the model aquatic ecosystem (Figure 5.1) were chosen to: (1) provide a sufficiently large range of O_2 saturation and $\delta^{18}O-O_2$ to demonstrate the effects; (2) portray a moderate level of metabolic activity typical of natural systems; and (3) represent a moderate gas exchange rate. If P and R are changed, G is also changed even when k is held constant because G depends on O_2 saturation and k . Thus all comparisons of G are presented in terms of k .

5.3 Results

Effect of metabolic rates on diel O_2 and $\delta^{18}O-O_2$

Community metabolic rates control the deviation of diel $\delta^{18}O-O_2$ curves from air-water equilibrium saturation. Increasing P and R , while retaining a constant $P:R$ (Figure 5.2), produces diel curves of O_2 saturation and $\delta^{18}O-O_2$ with a larger amplitude that progressively deviate farther from equilibrium saturation. This finding clearly demonstrates that the common practice of reporting $P:R$ alone reveals very little about the true productivity of an aquatic ecosystem. In O_2 saturation versus $\delta^{18}O-O_2$ space (Figure 5.2), increases in P and R result in (1) an increase the length of the diel curve; (2) an increase in the difference between the daytime and nighttime portions of the curve; and (3) placement of the curve farther away from air-water equilibrium saturation. Higher rates of community metabolism have little effect on the daily mean O_2 saturation, but significantly reduce the daily mean $\delta^{18}O-O_2$ value.

Effect of community respiration rate on diel O_2 and $\delta^{18}O-O_2$

To illustrate the effect of increasing R , P and k were held constant and thus $P:R$ decreased. In water bodies, R may increase relative to P as a result of

warming water temperatures over the course of the day or season, input of allochthonous labile organic carbon from streams or tile drains, and from the seasonal changes in phytoplankton that deliver organic carbon to respiring organisms. R controls several aspects of the shape and location of the diel curve in O_2 saturation versus $\delta^{18}O-O_2$ space (Figure 5.3). The main effect of increasing R relative to P is to (1) decrease the daily mean O_2 saturation level without changing the shape and amplitude of the diel curve; (2) increase the daily mean $\delta^{18}O-O_2$ value and to increase the diel range of $\delta^{18}O-O_2$ values; and (3) enhance the nighttime $\delta^{18}O-O_2$ plateau. The nighttime plateau is much more pronounced than a daytime plateau because of the different effects of $\delta^{18}O-H_2O$ and α_R .

The development of a nighttime plateau is an important feature of diel $\delta^{18}O-O_2$ data because it provides clues about the aquatic ecosystem before any modelling is done. A nighttime plateau in O_2 saturation is the result of R and G being equal. The $\delta^{18}O-O_2$ value of a nighttime plateau is a function of R and α_R . Such a nighttime plateau in $\delta^{18}O-O_2$ only occurs when R is sufficiently large and of similar magnitude as G .

Higher aquatic R affects the O_2 saturation and $\delta^{18}O-O_2$ curves differently. An increase in R affects the amplitude of the diel $\delta^{18}O-O_2$ curve but not the amplitude of the diel O_2 saturation curve. Thus the range of the $\delta^{18}O-O_2$ is an indicator of $P:R$. In O_2 saturation versus $\delta^{18}O-O_2$ space (Figure 5.3), the effect of increasing R is to (1) move the diel curve to the left and upwards; and (2) increase the difference between the daytime and nighttime portions of the diel curve.

Effect of gas exchange coefficient on diel O_2 and $\delta^{18}O-O_2$

The gas exchange coefficient, k , controls several aspects of the shape of the diel O_2 saturation and $\delta^{18}O-O_2$ curves (Figure 5.4). The k values used here (0.12 to 0.36 $m\ h^{-1}$) cover a range from moderate- k environments such as larger lakes and rivers, to higher- k environments such as turbulent streams and rivers (e.g., a large windy lake (12 $m\ s^{-1}$ wind speed at 10 m height; [Wanninkhof, 1992](#)) or a moderately moving stream (1 $m\ s^{-1}$ mean velocity and 1 m depth; [Churchill et al., 1962](#)). In some aquatic ecosystems, k can be estimated via proxy measurements such as wind speed for lakes (e.g., [Cole and Caraco, 1998](#); [Wanninkhof, 1992](#)) or directly by gas tracer and acoustic methods ([Morse et al., 2007](#)). In streams and rivers, numerous empirical equations can be used to estimate k for different hydrologic settings based on easily measured variables, such as channel depth and mean water velocity (cf. [Jha et al., 2004](#)). However, literature k values can vary by up to several orders of magnitude for any given circumstance (e.g., [Churchill et al., 1962](#); [Jha et al., 2004](#); [O'Connor and Dobbins, 1958](#)).

G acts primarily to dampen the magnitude of the diel O_2 saturation and $\delta^{18}O-O_2$ swings driven by P and R . In general, the proximity of the diel

curve to equilibrium saturation conditions is controlled by k , and thus G . The amount of hysteresis exhibited by the diel curves is partially controlled by the $P:G$ ratio, such that if $P:G$ is small, then the difference between the daytime and nighttime portion of the diel curves is small and the total range of O_2 saturation and $\delta^{18}O-O_2$ values is also small. Thus, the net effect of increasing the k value is to: (1) increase G ; (2) move the diel curve closer to air-water equilibrium saturation, (3) decrease the magnitude of the diel curve; (4) change the shape of the diel curve and especially the appearance of a nighttime plateau; and (5) affect the timing of both O_2 saturation and $\delta^{18}O-O_2$ minima and maxima. The temporal offset between solar noon and the O_2 maximum is sometimes used to calculate k from O_2 curve analysis (McBride and Chapra, 2005). Higher k brings the daily mean O_2 saturation and $\delta^{18}O-O_2$ values closer to air-water equilibrium saturation. However, the daily means do not scale linearly with k because G depends on saturation. In O_2 saturation versus $\delta^{18}O-O_2$ space (Figure 5.4), the effects of increasing k are to: (1) decrease the length of the diel curve; and (2) decrease the difference between the daytime and nighttime portions of the curve.

Effect of community respiration isotopic fractionation on diel O_2 and $\delta^{18}O-O_2$

The community R O_2 isotopic fractionation factor (α_R) only affects $\delta^{18}O-O_2$ and not O_2 saturation. Thus α_R controls the placement of the diel curve on the $\delta^{18}O-O_2$ axis and has no effect on O_2 concentration or saturation. Figure 5.5 depict three diel curves with α_R values that range from 0.982 to 1.000. This range of α_R spans the range reported in the literature for natural aquatic systems including those that are O_2 diffusion-limited (cf. Brandes and Devol, 1997; Kiddon et al., 1993). As the respiratory isotopic fractionation becomes weaker (α_R approaches 1), the diel ellipse falls lower on the $\delta^{18}O-O_2$ axis. Also, the slope of the diel ellipse decreases slightly as α_R approaches 1.000. In Figure 5.5, the change in slope produces differences in $\delta^{18}O-O_2$ that are within the measurement error of continuous-flow isotope-ratio mass spectrometry. When $\alpha_R = 1.000$, the steady-state diel curve must fall entirely below the air-water equilibrium saturation $\delta^{18}O$ value of +24.2 ‰. The α_R may approach 1.000 in O_2 diffusion-limited aquatic ecosystems with high R such as those dominated by benthic or sediment respiration (Brandes and Devol, 1997; Hendry et al., 2002).

The diel $\delta^{18}O-O_2$ curve is sensitive to small changes in α_R ; in Figure 5.5, a 0.001 change in α_R shifts the $\delta^{18}O-O_2$ values by at most 0.13 ‰. Although community α_R is unknown for any given aquatic ecosystem, it can be estimated within a reasonable range for water columns and is constrained by a best-fit modelling of the nighttime plateau (the plateau $\delta^{18}O-O_2$ value depends on α_R) and by best-fit modelling of 24 h diel data (Venkiteswaran et al., 2007). Alternately, others have used closed-system bottle incubation experi-

ments to estimate α_R for water bodies (e.g., [Quay et al., 1995](#)) although these results are biased to water column R .

Effect of $\delta^{18}\text{O-H}_2\text{O}$ on Diel O_2 and $\delta^{18}\text{O-O}_2$

The O_2 saturation curve is unaffected by the $\delta^{18}\text{O-H}_2\text{O}$. The $\delta^{18}\text{O-H}_2\text{O}$ instead controls the $\delta^{18}\text{O-O}_2$ minimum and therefore the slope of the entire hysteretic diel curve (Figure 5.6). At a single river station or within a lake it is unlikely that there are significant differences of more than 1 ‰ in $\delta^{18}\text{O-H}_2\text{O}$ over the course of a few diel cycles. Barring large precipitation or reservoir discharge events, evaporation over a few days is insufficient to change the $\delta^{18}\text{O-H}_2\text{O}$ of water bodies such as streams, rivers, and lakes (cf. [Clark and Fritz, 1997](#)). The $\delta^{18}\text{O-H}_2\text{O}$, however, becomes an important variable when comparing results among different water bodies from different geographic locations. Locally, the $\delta^{18}\text{O-H}_2\text{O}$ value may be temporally altered by snowmelt runoff, storm events, and evaporation. Figure 5.6 depicts three diel curves with $\delta^{18}\text{O-H}_2\text{O}$ values ranging from -21 to -7 ‰, representing a range that covers values observed globally in freshwater lakes and rivers ([Bowen et al., 2005](#), <http://www.waterisotopes.org>). The nighttime $\delta^{18}\text{O-O}_2$ maximum is unaffected by the $\delta^{18}\text{O-H}_2\text{O}$ value, acts as a fixed pivot-point for diel curves of different $\delta^{18}\text{O-H}_2\text{O}$ values, and is, instead, controlled by $\alpha_R:\alpha_G$ ratios (i.e., both $\alpha_R:\alpha_{G-k}$ and $\alpha_R:\alpha_{G-eq}$ ratios). The more negative the $\delta^{18}\text{O-H}_2\text{O}$, the more negative the minimum $\delta^{18}\text{O-O}_2$ because of the photosynthetic input of $\delta^{18}\text{O-O}_2$ derived from H_2O . The $\delta^{18}\text{O-H}_2\text{O}$ from many locations can be easily measured or may be estimated from existing databases ([Kendall and Coplen, 2001](#)). However, when comparing among different aquatic ecosystems, diel $\delta^{18}\text{O-O}_2$ curves will be different if the $\delta^{18}\text{O-H}_2\text{O}$ values are different.

Effect of temperature on diel O_2 and $\delta^{18}\text{O-O}_2$

Temperature controls several key aspects of the shape of the diel curve largely because of the role of temperature in the solubility of O_2 and R . Figure 5.7 depicts three diel curves with different water temperature regimes that are typical of the open water season in temperate lakes and rivers. The curves shown include two constant water temperatures and a diel water temperature change with R adjusted by the van 't Hoff–Arrhenius equation. The difference between 8°C and 20°C is a reduced range of O_2 saturation and $\delta^{18}\text{O-O}_2$ values over the diel cycle at the colder temperature. This is solely a result of the difference in solubility of O_2 at different temperatures, which in turn affects G . Although P and R are held constant in this example, the total dissolved O_2 pool is 30% larger at 8°C than at 20°C , thus observed changes in $\delta^{18}\text{O-O}_2$ values are smaller. This is a pool dilution effect whereby the same amount of O_2 is produced by P and consumed by R but as a portion of the total O_2 pool a smaller fraction is metabolically cycled. As a result of the

increased solubility of O₂, a comparatively smaller fraction of the total O₂ is derived from the photosynthetic input of O₂ with very low $\delta^{18}\text{O-O}_2$ values and thus the daytime portion of the concentration curve deviated less from the nighttime portion of the curve. At night, the same R produces a smaller decline in O₂ saturation because of the increased solubility at lower temperatures. The total amount of G (aerial rates of influx and efflux) remains the same because differences in the dissolved O₂ concentration and saturation are balanced by the same k . The slope of the nighttime curve is the same at 8 °C and 20 °C.

The effect of a typical sinusoidal diel temperature change from 8 °C (night) to 20 °C (2.5 h after solar noon) is to increase the diel change in O₂ saturation and decrease the diel change in $\delta^{18}\text{O-O}_2$ relative to the constant temperature regimes. There is only a small effect on the mean O₂ saturation and $\delta^{18}\text{O-O}_2$ values but the shape is changed including: (1) an increased temporal offset of the maximum O₂ saturation and $\delta^{18}\text{O-O}_2$ minimum from solar noon, demonstrating that this offset is not only a function of k ; (2) an earlier minimum O₂ saturation; (3) a decrease in the duration of a night-time plateau; and (4) in a cross-plot of O₂ saturation versus $\delta^{18}\text{O-O}_2$, a reduction in the overall slope of the curve but a greater difference between the daytime and nighttime portions of the curve. Although temperature is not an independent variable, it is important to take diel temperature changes into account because temperature is required to convert measurements of O₂ concentration into saturation. Shallow water bodies, such as ponds and rivers, may exhibit significant diel temperature changes (Venkiteswaran *et al.*, 2007).

Net effects of the key environmental and biological parameters

The overall effect of the key parameters described above on diel O₂ saturation and $\delta^{18}\text{O-O}_2$ curves are not always intuitive, nor are the multiple combinations of these parameters, which are commonly encountered in nature, easily grasped. Table 5.1 contains a generalised framework for initially assessing field diel O₂ and $\delta^{18}\text{O-O}_2$ curves without modelling. P , R , and G affect the diel magnitude of both O₂ saturation and $\delta^{18}\text{O-O}_2$ (the range of values and thus the length of curves). Dissolved O₂ isotopic fractionation factors (α_R and α_G) affect only the $\delta^{18}\text{O-O}_2$ of diels and because they are multiplied by R and k respectively, are only as important as R and k are large. The $\delta^{18}\text{O-H}_2\text{O}$ is similarly expressed relative to P and controls the comparative slope of the diel curve. Temperature controls O₂ solubility, affects R , and thereby modifies both the shape and location of the diel O₂ saturation and $\delta^{18}\text{O-O}_2$ curves in temporal and cross-plot figures. Venkiteswaran *et al.* (2007) provide details about how daily values of P , R , k , and α_R can be estimated from diel O₂ and $\delta^{18}\text{O-O}_2$ curves.

5.4 Discussion

Point measurements are not useful in productive ecosystems

The metabolic balance of productive aquatic ecosystems are not likely to be adequately captured by daytime-only, random, or point measurements of O₂ saturation and $\delta^{18}\text{O-O}_2$ due to diel variation. Diel curves of O₂ concentration have been used previously to estimate metabolic balance ($P:R$) and P and R but have required various assumptions (e.g., assuming constant R and using empirical equations to estimate k). As a result, new methods and approaches to better constrain P and R , lessen the importance of the necessary assumptions, and identify ecosystems at risk from external stressors are required.

Diel $\delta^{18}\text{O-O}_2$ studies can also be useful in aquatic ecosystems that do not exhibit a diel change in every season. The lack of a diel change combined with $\delta^{18}\text{O-O}_2$ sets limits on the P , R , and k required to suppress diel changes in both O₂ and $\delta^{18}\text{O-O}_2$ (e.g., the Amazon River in [Quay et al., 1995](#)). In such ecosystems, P must be low enough that the $\delta^{18}\text{O-O}_2$ value does not change significantly *and* either (1) R and G must be approximately equal if O₂ is undersaturated *or* (2) G must be much greater than R if O₂ is fully saturated.

$P:R:G$ is better than $P:R$

Differences in ecosystem sensitivity to stressors due to the inherent balance between P , R , and G can be easily visualised in a cross-plot. The framework summarised in Table 5.1 was applied to a set of stream clusters for illustration purposes. [Wilcock et al. \(1998\)](#) described five stream clusters based on 23 rural lowland streams in agriculturally developed catchments in order to categorise streams according to their ability to withstand dissolved O₂ stressors and still maintain minimum acceptable environmental dissolved O₂ concentrations, a measure of ecosystem health. To group streams according to the similarity of processes controlling stream dissolved O₂ concentrations, they performed complete linkage cluster analysis of P , R , and k : all determined by analysis of diel dissolved O₂ curves. Here, PoRGy was used to generate steady-state diel $\delta^{18}\text{O-O}_2$ curves for these stream clusters using their values of P , R , and k , information about stream morphometry, and water temperature. A $\delta^{18}\text{O-H}_2\text{O}$ of -7‰ , and an α_R of 0.982 were assumed for all clusters for comparability (Table 5.2; Figure 5.8). The parameters yield either large (clusters 1, 3, and 5) or small (clusters 2 and 4) diel curves. However, the size of the diel curve size is not only related to community structure and metabolic rates, but also to G and thus to sensitivity to external stressors.

The diel curves for each cluster are clearly distinct but represent five snapshots along a continuum of possible diel curves. There is some overlap in the cross-plot between the diel curves (clusters 2 and 3, and clusters 4 and 5) but the lengths of these curves differ greatly.

Two comparisons are made to illustrate that the clusters depends simultaneously on P , R , and G : clusters 1 and 3, and clusters 3 and 5. Clusters 1 and 3 have nearly identical ranges in O_2 saturation: below 60% at night and peaking close to 100% after solar noon. From an O_2 saturation-standpoint these stream clusters are indistinguishable from each other. However, in a cross-plot these clusters are separated in $\delta^{18}O-O_2$ by 5 ‰. This indicates that cluster 1 has a greater $P:G$ ratio and a greater $P:R$ ratio than cluster 3. Thus k is likely much slower in cluster 1 than in cluster 3 and hence cluster 1 is more sensitive to external stressors that affect k than is cluster 3 even though they have identical nighttime minimum O_2 saturation values. Stressors that cause an increase in R , such as increased BOD load or nutrients causing an increase in P , would have a much greater impact on cluster 1 than cluster 3.

Clusters 3 and 5 have very different ranges of O_2 saturation: 60–95% and 75–125% respectively. However their range of $\delta^{18}O-O_2$ values is similar: 20–33 ‰ and 18–30 ‰. In a cross-plot these clusters are separated with cluster 5 being closer to ASW but the mechanism for this separation is not intuitive. Community metabolism rates and k must be higher in cluster 5 than in cluster 3 because the diel curve of cluster 5 has a similar size while being closer to ASW than cluster 3. Stressors that could cause decreases in the nighttime O_2 minimum would have a much greater impact on cluster 3 than cluster 5 because of its slower k . Also, stressors that could reduce k in cluster 5 pose a risk to the nighttime O_2 minimum because of high R .

Diel curves can overlap for reasons other than just P and R (e.g., different k , significant temperature change, or a combination of variables). Field data from other regions can be compared to the [Wilcock et al. \(1998\)](#) clusters in order to generalise about the role of $P:R:G$ in aquatic ecosystems. Field data collected from several North American aquatic ecosystems are presented in [Figure 5.9](#) and [Table 5.3](#) along with best-fit solutions from PoRGy: the South Saskatchewan River 50 km downstream from Saskatoon, Saskatchewan ([Venkiteswaran et al., 2007](#)); the Big Hole River near Dickie Bridge, Montana ([Parker et al., 2005](#)); wetland 50 at the St. Denis National Wildlife Area, Saskatchewan ([Venkiteswaran et al., 2007](#)), and the Red Deer River near Bindloss, Alberta (J. J. Venkiteswaran et al. unpublished data). These data clearly reveal that different types of aquatic ecosystems (in $P:R:G$ terms) fall on different locations on an O_2 saturation versus $\delta^{18}O-O_2$ cross-plot.

The inclusion of $\delta^{18}O-O_2$ in these diel studies makes visually interpreting the diel data easier than O_2 saturation alone, can allow for identifying important effects such as disturbances by following an ecosystem temporally or spatially, presents the clusters and ecosystems as a continuum described by $P:R:G$, and visually relates the ecosystems to each other and perhaps to the environmental influences that would cause them to change with time.

Ultimately, the determinant of O_2 dynamics in aquatic systems is the $P:R:G$ ratio and not the conventional $P:R$ ratio because of the inescapable

connection between the water and the atmosphere in all aquatic ecosystems. Thus, one major advantage of including $\delta^{18}\text{O}-\text{O}_2$ data in diel sampling regimes is the ability to determine the $P:R:G$ ratio with far greater precision than by O_2 saturation alone. Also, since P , R , and G differ between types of aquatic ecosystems (Table 5.4), various ecosystems plot differently in a cross-plot of O_2 saturation versus $\delta^{18}\text{O}-\text{O}_2$. The stream clusters presented above clearly demonstrate that differences between ecosystems (including differences that are not apparent from O_2 saturation curves alone) can become apparent using $\delta^{18}\text{O}-\text{O}_2$ assays.

Measurements of $\delta^{18}\text{O}-\text{O}_2$ also provide a second and independent method of constraining P , R , and k . While P , R , and $P:R$ can be estimated from O_2 saturation alone using conventional methods, the ratios and rates require k to be determined independently or be calculated from empirical models (e.g., *Jha et al., 2004*), numerical solutions (e.g., *McBride and Chapra, 2005*), or nighttime regression (e.g., *Odum, 1956*). This makes O_2 curve comparison between different ecosystems (or the same ecosystem across seasons) very difficult because k is needed to calculate P and R but the sensitivity to k is buried inside the assumptions and calculations. The use of $P:R:G$ ratios explicitly recognises that dissolved O_2 concentration also depends on G and that metabolism is better compared against an independent but ecosystem-relevant variable, k . Determining $P:R:G$ with O_2 saturation and $\delta^{18}\text{O}-\text{O}_2$ data adds a second set of mass balance constraints when determining the rates of P , R , and G . Hence the addition of $\delta^{18}\text{O}-\text{O}_2$ provides a better-constrained estimate of aquatic metabolism and reaeration.

Many processes and factors including P , R , $P:R$, k , temperature, and light simultaneously affect diel curves. For example, both k and temperature will shift the maximum O_2 saturation from solar noon and both R and k will change the level and duration of a nighttime O_2 saturation plateau. Thus both the shape and mean of the diel temporal curves give information on what parameters are important. A confounding issue is that aquatic ecosystems are rarely at daily steady-state (i.e., they do not return to the same point every night) because they are meteorologically dependent (e.g., warming trend, flow-rate changes, cooling trend, cloudy periods). Thus, single diel O_2 studies are best done by including $\delta^{18}\text{O}-\text{O}_2$ and by switching to a transient model so that steady-state assumptions can be removed.

5.5 Conclusions

Six key environmental and biological parameters (P , R , k , α_R , $\delta^{18}\text{O}-\text{H}_2\text{O}$, and temperature) affect the shape, size, and location of diel O_2 saturation and $\delta^{18}\text{O}-\text{O}_2$ curves in complex and interactive ways. Understanding the effect of these key parameters on O_2 saturation and $\delta^{18}\text{O}-\text{O}_2$ elucidates important controls on aquatic ecosystems, allows for comparison between aquatic ecosys-

tems, and aids the use of models (e.g., PoRGy) to determine quantitative estimates of ecosystem metabolic rates using real data. This framework is useful because different combinations of parameters can result in apparently overlapping diel curves. Thus both O₂ saturation and $\delta^{18}\text{O-O}_2$ are needed to disentangle potentially confounding influences.

The sensitivity of aquatic ecosystems to stressors was described in terms of the inherent balance between P , R , and G using five stream clusters described by [Wilcock et al. \(1998\)](#). Diel $\delta^{18}\text{O-O}_2$ curves can be used to identify aquatic ecosystems that may be more vulnerable to external stressors, such as ecosystems where G is small relative to P and R because (1) estimates of k are better constrained with a second mass balance and (2) $P:R:G$ can be inferred from the size, shape, and location of a diel curve in a cross-plot. The general framework of the key parameters and diel O₂ saturation and $\delta^{18}\text{O-O}_2$ curves reported is an important tool for studies of aquatic ecosystem health.

Acknowledgements

This work was funded by a National Science and Engineering Research Council of Canada Strategic Project Grant (SLS and LIW), Environment Canada (LIW), and an Ontario Graduate Scholarship (JJV). R. J. Wilcock kindly provided additional stream morphometry information.

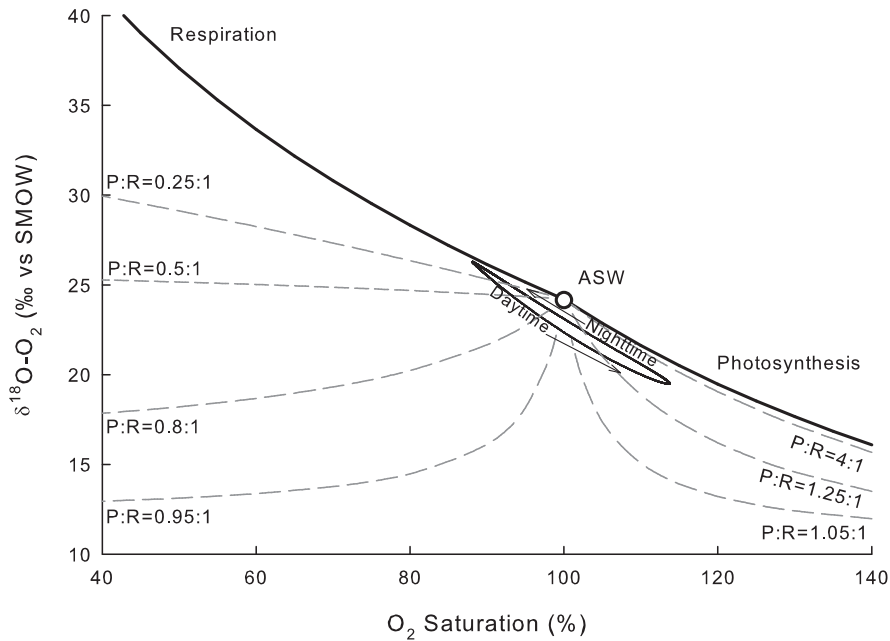


Figure 5.1: A graphical depiction of the primary O_2 processes versus the $\delta^{18}O-O_2$ showing several $P:R$ ratio lines (dashed grey lines) calculated with the steady-state model of [Quay et al. \(1993\)](#) and $\alpha_R = 0.982$ and $\delta^{18}O-H_2O = -7\text{‰}$. The respiration and photosynthesis end-member trajectories (solid black lines) were also calculated with $\alpha_R = 0.982$ and $\delta^{18}O-H_2O = -7\text{‰}$ and are shown as moving away from air-saturated water (ASW). The closed loop is a PoRGy model-generated diel curve with P , R , and G of 288, 300, and 179 $\text{mg m}^{-2} \text{h}^{-1}$ ($P:R:G=1.60:1.68:1$), k of 0.24 m h^{-1} and yields a range of about 25% in saturation and 6‰ in $\delta^{18}O-O_2$. P is the rate of photosynthetic O_2 evolution generated by the photochemical oxidation of water; R is aquatic community (plant, animal, microbe) respiration, G is air–water gas exchange, k is the gas exchange coefficient, and PoRGy is a non-steady-state model that was developed to quantify the dissolved O_2 and $\delta^{18}O-O_2$ evolution in aquatic systems ([Venkiteswaran et al., 2007](#)).

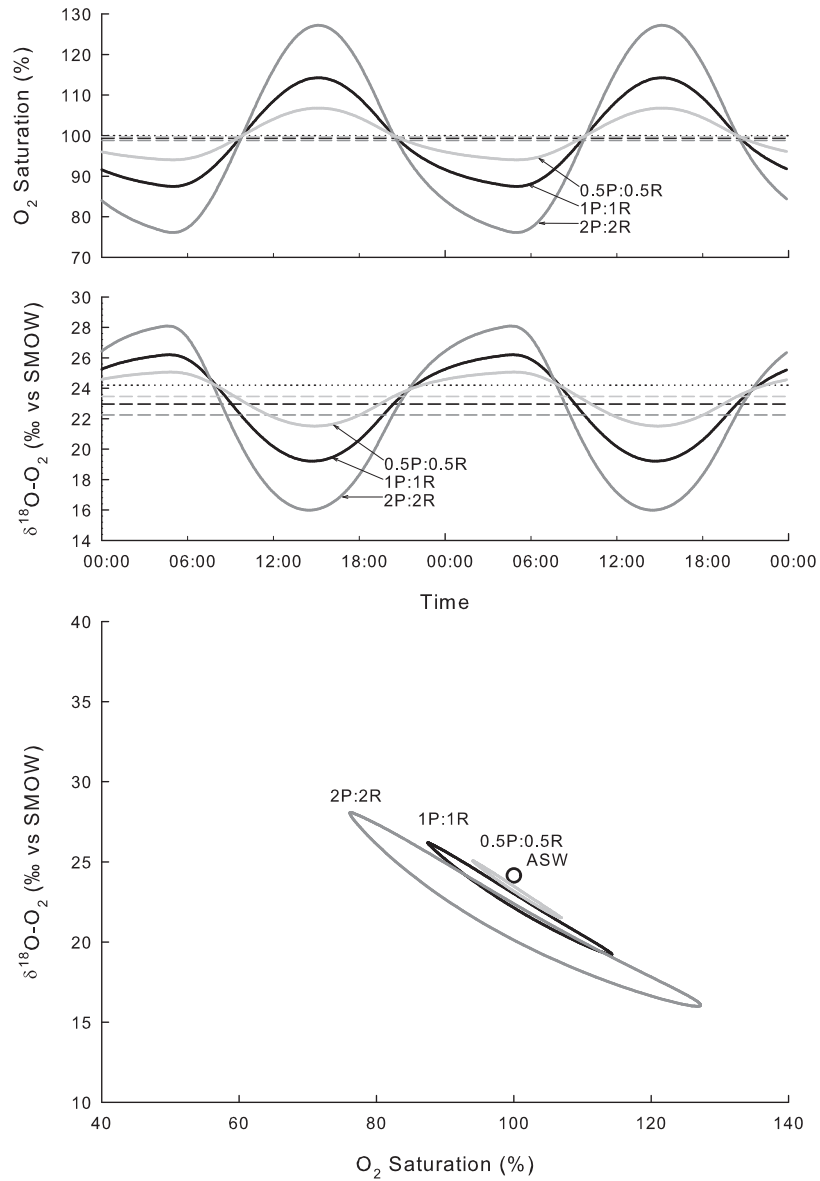


Figure 5.2: Diel curves show how different P and R affect the shape, size, and location of the curves when the $P:R$ ratio is held constant. Three diel curves with the same gas exchange rate and identical $P:R$ ratios, but with different P and R . The solid curve from Figure 5.1 (1P:1R, $288:300 \text{ mg m}^{-2} \text{ h}^{-1}$, black) is compared to curves with half those rates (0.5P:0.5R, $144:350 \text{ mg m}^{-2} \text{ h}^{-1}$, dark grey) and with double those rates (2P:2R, $576:600 \text{ mg m}^{-2} \text{ h}^{-1}$, light grey). Air-saturated water (ASW) is shown as a black circle, and the mean of each diel curve is shown as a dashed line.

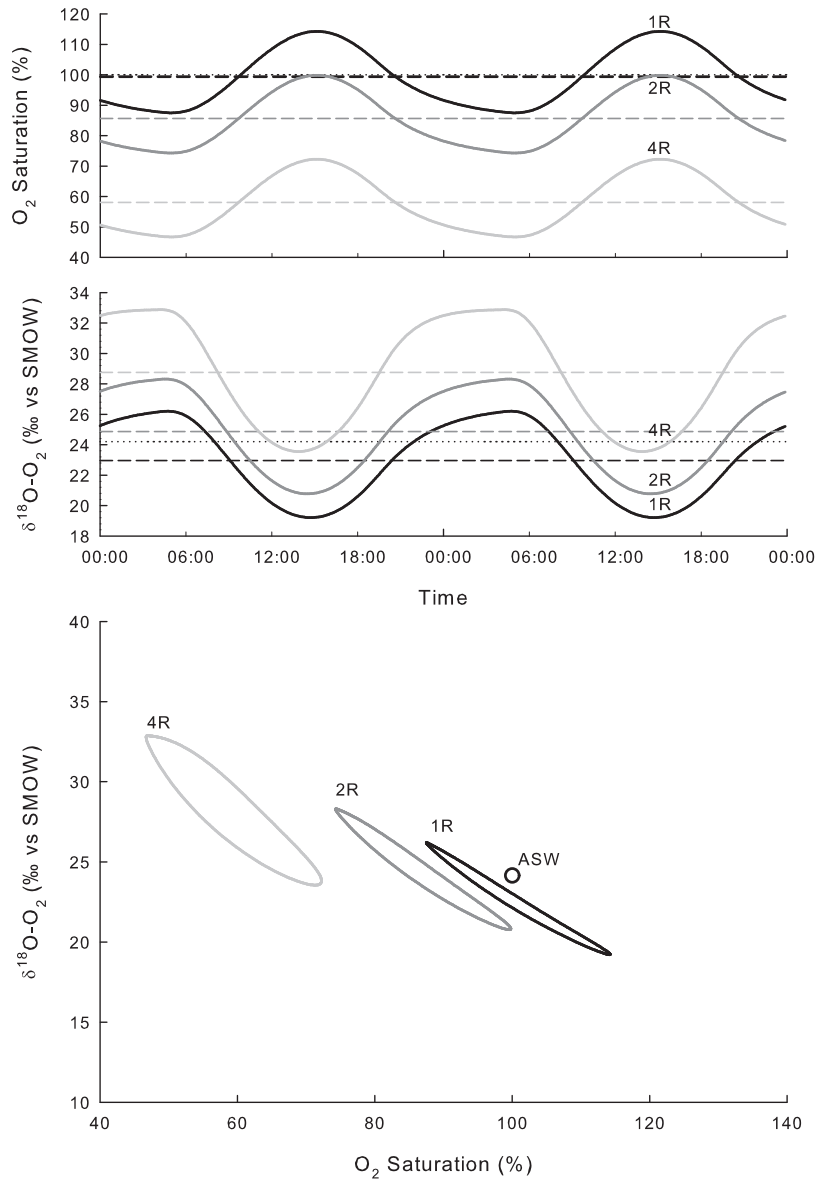


Figure 5.3: Diel curves show how different rates of R affect the shape, size, and location of the curve when the $P:R$ ratio is increased and P and k are held constant. The solid curve from Figure 5.1 (1R, $300 \text{ mg m}^{-2} \text{ h}^{-1}$, black) is compared to curves with double that respiration rate (2R, $600 \text{ mg m}^{-2} \text{ h}^{-1}$, dark grey) and quadruple that respiration rate (4R, $1200 \text{ mg m}^{-2} \text{ h}^{-1}$, light grey). Air-saturated water (ASW) is shown as a black circle, and the mean of each diel curve is shown as a dashed line.

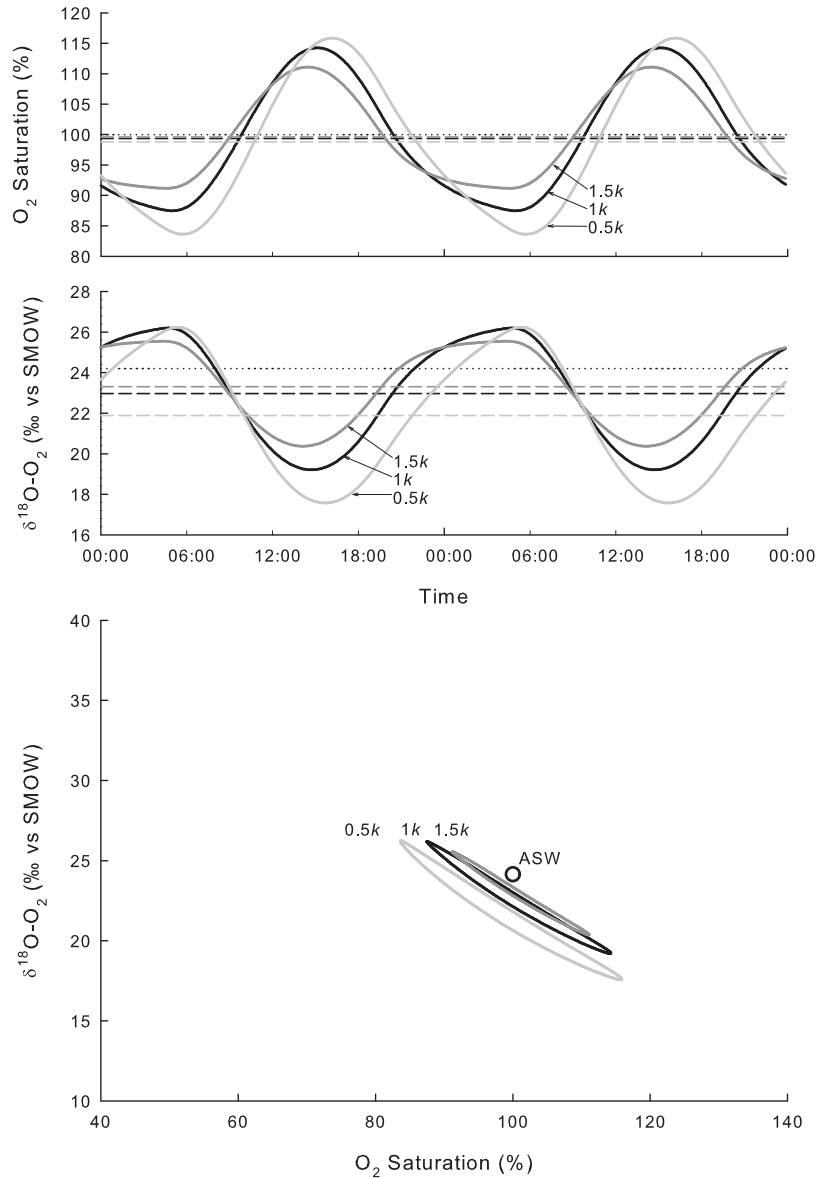


Figure 5.4: Diel curves show how different gas exchange coefficients (k) affect the shape, size, and location of the curve when the $P:R$ ratio and P and R are held constant. The solid curve from Figure 5.1 ($1k$, 0.24 m h^{-1} , black) is compared to curves with increased k ($1.5k$, 0.36 m h^{-1} , dark grey) and decreased k ($0.5k$, 0.12 m h^{-1} , light grey). Air-saturated water (ASW) is shown as a black circle, and the mean of each diel curve is shown as a dashed line.

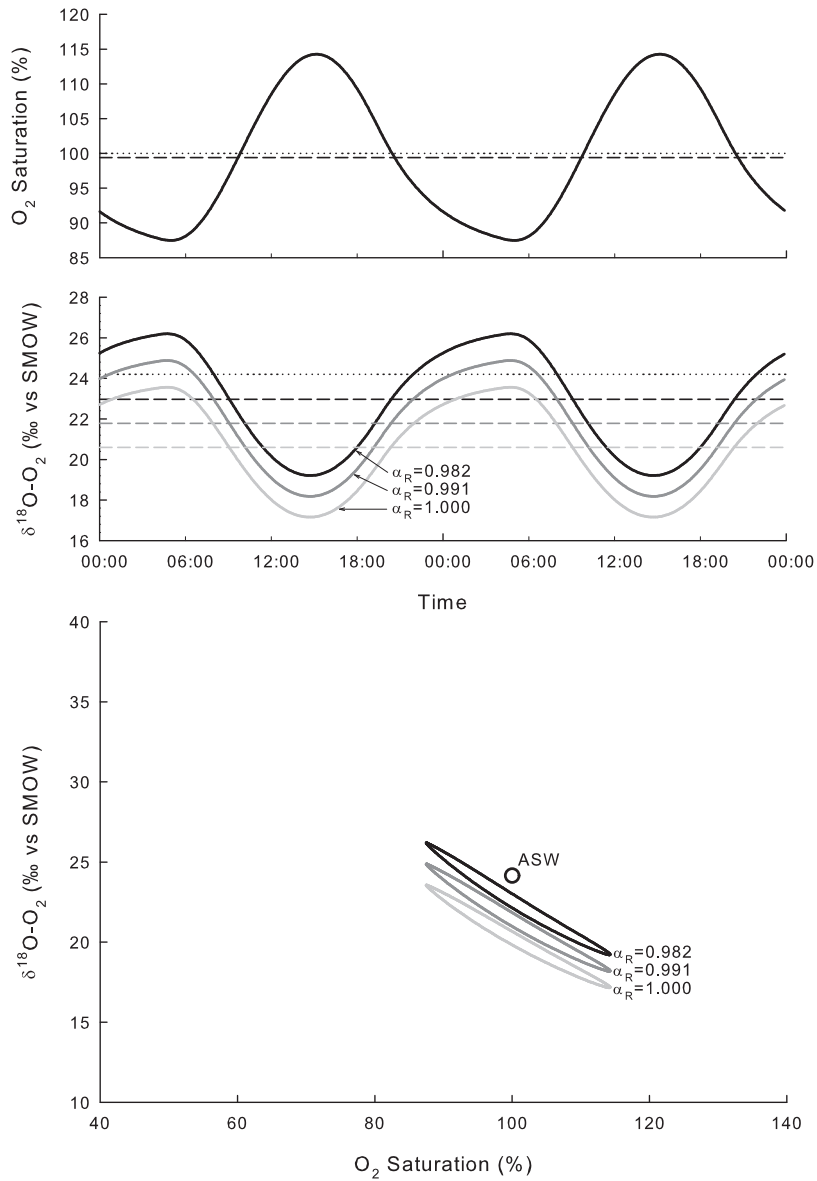


Figure 5.5: Diel curves show how O_2 isotopic fractionation factors (α_R) affect the shape, size, and location of the curve when the $P:R$ ratio, P , R , and k are the held constant. The solid curve from Figure 5.1 ($\alpha_R = 0.982$, black) is compared to curves with $\alpha_R = 0.988$ (dark grey) and $\alpha_R = 0.995$ curve (light grey). Air-saturated water (ASW) is shown as a black circle, and the mean of each diel curve is shown as a dashed line.

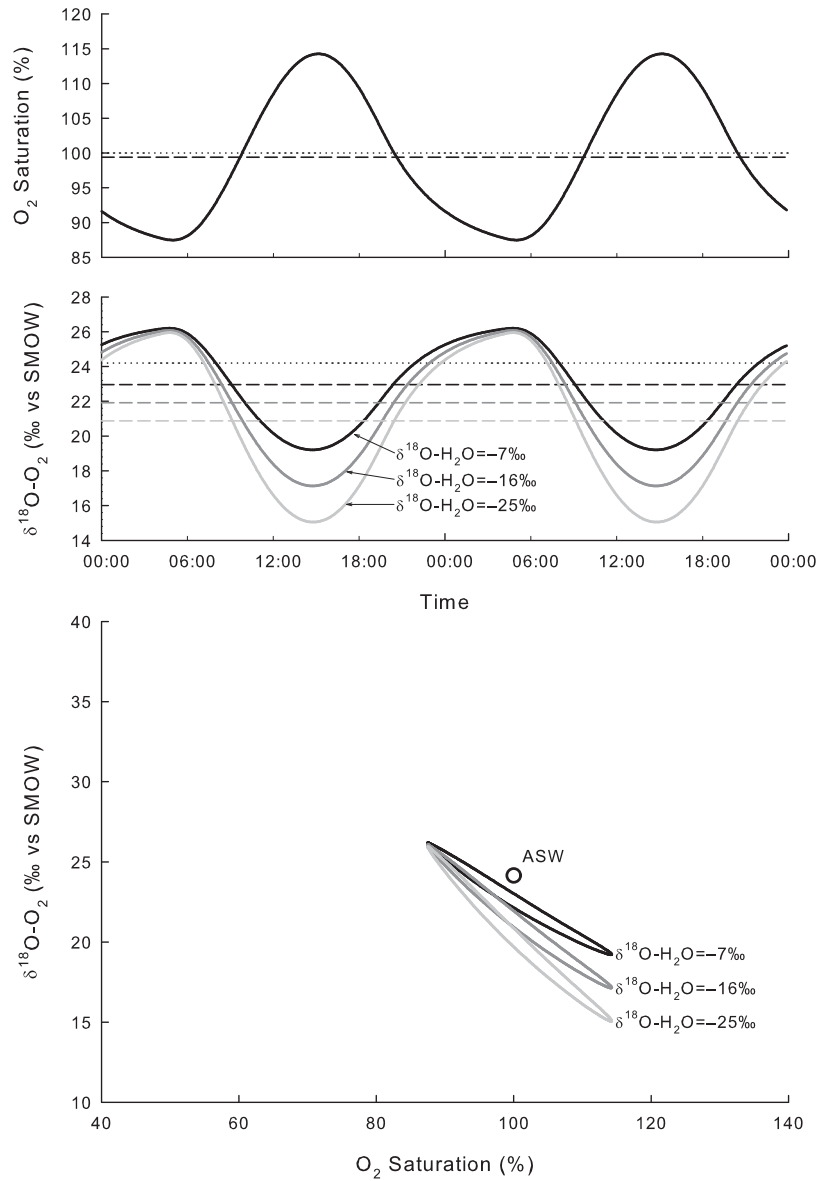


Figure 5.6: Diel curves show how different $\delta^{18}\text{O-H}_2\text{O}$ values affect the shape, size, and location of the curve when the $P:R$ ratio, P , R , and k are held constant. The solid curve from Figure 5.1 ($\delta^{18}\text{O-H}_2\text{O} = -7\text{‰}$, black) is compared to curves with $\delta^{18}\text{O-H}_2\text{O} = -4\text{‰}$ curve (dark grey) and an $\delta^{18}\text{O-H}_2\text{O} = -21\text{‰}$ curve (light grey). Air-saturated water (ASW) is shown as a black circle, and the mean of each diel curve is shown as a dashed line.

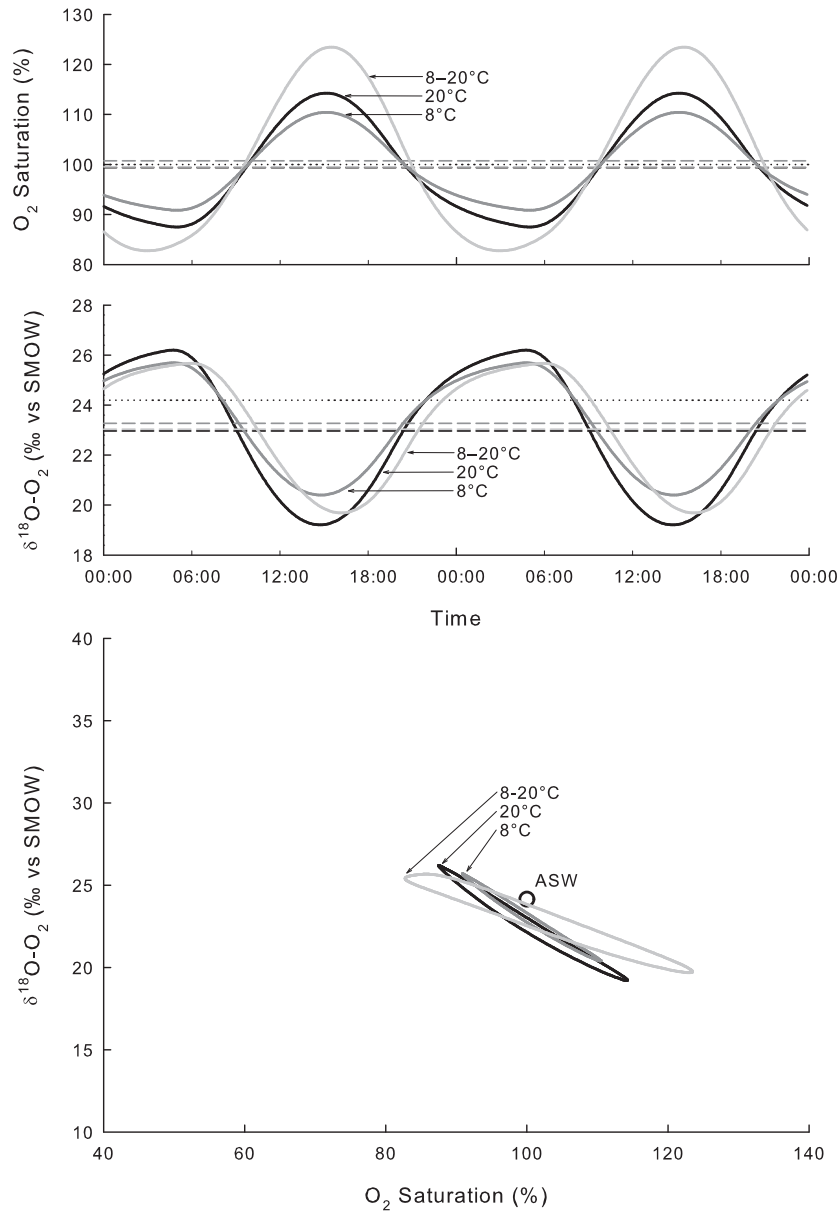


Figure 5.7: Diel curves show how different temperatures affect the shape, size, and location of the curve when the $P:R$ ratio, P , R , and k are held constant. The solid curve from Figure 5.1 (20 °C, black) is compared to curves with a colder water temperature (8 °C, dark grey) and a diel water temperature change (8 °C to 25 °C, light grey). The diel temperature change curve also uses an Arrhenius equation to adjust R rate as a function of temperature. Air-saturated water (ASW) is shown as a black circle, and the mean of each diel curve is shown as a dashed line.

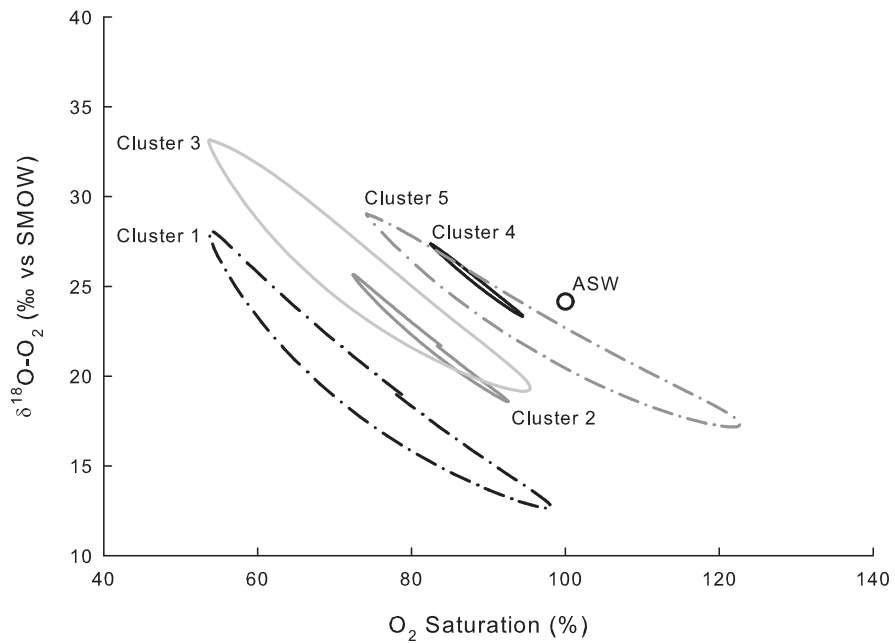


Figure 5.8: Based on a synoptic study of New Zealand streams, [Wilcock et al. \(1998\)](#) organised the ecosystem health of their streams into five clusters based on complete linkage cluster analysis of their P , R , and k values (Table 5.2). Using average P , R , and k for these clusters, PoRGy was employed to generate diel O_2 saturation and $\delta^{18}O-O_2$ curves for each cluster. In order to make the curve more easily comparable, water temperature was set to $20^\circ C$, $\delta^{18}O-H_2O$ value was -7‰ and α_R was set to 0.982 for all clusters, the same as the solid curve from Figure 5.1. Air-saturated water (ASW) is shown as a black circle.

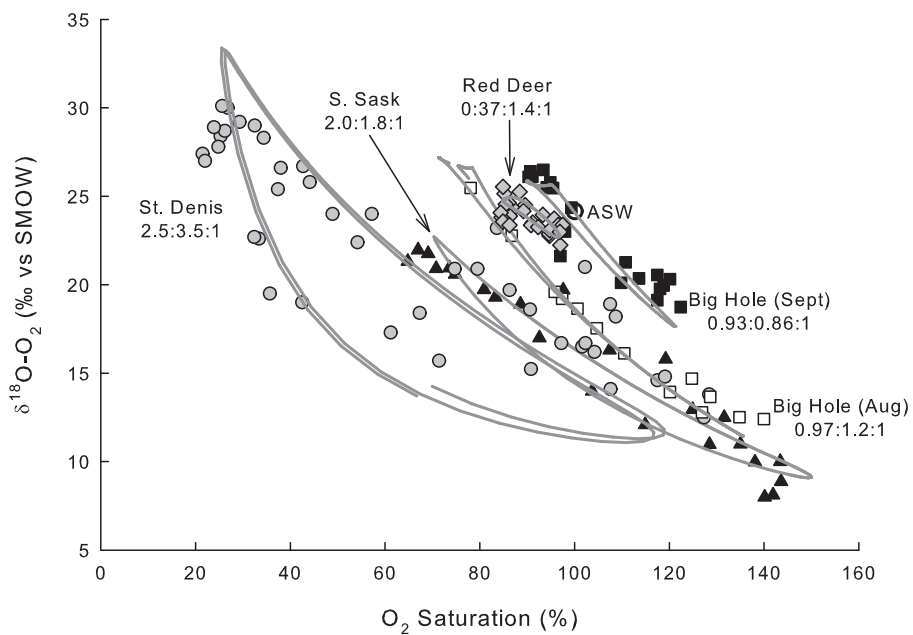


Figure 5.9: Cross-plots of diel O_2 saturation and $\delta^{18}O-O_2$ and $P:R:G$ ratios in three North American rivers and one prairie wetland: South Saskatchewan River 50 km downstream from Saskatoon, Saskatchewan in July (black triangles) (Venkiteswaran *et al.*, 2007); Red Deer River at Bindloss, Alberta in August (gray diamonds) (J. J. Venkiteswaran *et al.* unpublished data); Big Hole River near Dickie Bridge, Montana in August (white squares) and September (black squares) (Parker *et al.*, 2005); and wetland 50 at the St. Denis National Wildlife Area in September (gray circles) (Venkiteswaran *et al.*, 2007). The curves are best-fit solutions calculated with PoRGy. See Table 5.3 for more details. Air-saturated water (ASW) is shown as a black circle.

Table 5.1: Summary of the effect the six key parameters on saturation and values. P is the rate of photosynthetic O_2 evolution generated by the photochemical oxidation of water; R is aquatic community (plant, animal, microbe) respiration, G is air–water gas exchange, k is the gas exchange coefficient, and T is temperature.

Change in variable	O_2 saturation				$\delta^{18}O-O_2$			O_2 saturation (x -axis in the cross-plot)	$\delta^{18}O-O_2$ (y -axis in the cross-plot)	Change in cross-plot shape
	Maximum	Minimum	Mean	Mean	Maximum	Minimum	Mean			
Increase metabolism (P & R)	increase	decrease	no change	no change	increase	decrease	decrease	increases range	increases range and decreased mean	lengthen and broaden
Increase P	increase	decrease	increase	increase	no change	decrease	decrease	moves curve to the right	moves curve down	tilt and lengthen
Increase R	decrease	decrease	decrease	decrease	increase	increase	increase	moves curve to the left	moves curve up	broaden and tilt
Increase G (as k)	decrease	increase	increase (slightly)	increase	decrease	increase	increase	decreases range and moves curve towards 100%	decreases range and moves curve towards +24.2 %	shorten and narrow
Increase k_R (closer to 1)	no change	no change	no change	no change	decrease	decrease	decrease	no effect	moves curve up	very small tilt
Increase T	increase	decrease	decrease	decrease	increase	decrease	decrease	moves left and increases range	increases range	lengthen and broaden
Increase $\delta^{18}O-H_2O$	no change	no change	no change	no change	no change	increase	increase	no effect	increases minimum	tilt and lengthen

Table 5.2: Stream clusters as described by [Wilcock et al. \(1998\)](#) (see [Figure 5.8](#) for diel O_2 saturation and $\delta^{18}O_2$ curves of each cluster). P is the rate of photosynthetic O_2 evolution generated by the photochemical oxidation of water; R is aquatic community (plant, animal, microbe) respiration, G is air–water gas exchange, and k is the gas exchange coefficient. PoRGy is a non-steady-state model that was developed to quantify the dissolved O_2 and $\delta^{18}O_2$ evolution in aquatic systems ([Venkiteswaran et al., 2007](#)).

Cluster	Ecological description (Wilcock et al., 1998)	P ($g\ m^{-3}\ d^{-1}$)	R ($g\ m^{-3}\ d^{-1}$)	G (as k , d^{-1}) ^a	O_2 saturation (x-axis in the cross-plot)	$\delta^{18}O_2$ (y-axis in the cross-plot)	$P:R:G$ and $P:R$ (from PoRGy)
1	Warmer than average; large diel changes in O_2 concentration; high risk of low O_2 concentrations; small changes in flow can effect low O_2 concentrations at night (due to reduced k and increased R); sensitive to temperature change, and nutrient and organic loading ($n = 7$ streams)	$P \gg R$ (24.8)	Below average (9.9)	Below average (1.1)	Low sat at night; large range; always undersaturated	Large range; centered around 20 %	$P:R:G = 4.9:6.0:1$ $P:R = 0.81:1$
2	Low risk for low O_2 concentrations; susceptible to changes in riparian management coupled with low k during droughts ($n = 7$ streams)	High P (38.9)	High R (38.1)	\geq average (8.1)	Low sat at night; large range; always undersaturated	Large range, centered around 26 %	$P:R:G = 0.7:1.7:1$ $P:R = 0.42:1$
3	Warmer than average; large diel changes in O_2 concentration; moderate risk of low O_2 concentrations tempered by high k ($n = 6$ streams)	High P (38.9)	High R (38.1)	\geq average (8.1)	Low sat at night; large range; always undersaturated	Large range, centered around 26 %	$P:R:G = 0.7:1.7:1$ $P:R = 0.42:1$
4	Cooler than average; less productive than average; shady riparian area; low risk of low O_2 concentrations ($n = 6$ streams)	$P \leq R$ (11.2)	\geq average (24.5)	\geq average (11.0)	Small range; always undersaturated	Small range; centered around 26 %	$P:R:G = 0.5:1.5:1$ $P:R = 0.33:1$
5	High k value keeps streams well oxygenated; low risk of low O_2 concentrations ($n = 2$ streams)	High P (63.3)	High R (47.5)	High k (26.5)	Large range; supersaturated during the day; undersaturated at night	Large range; centered around 23 %	$P:R:G = 1.2:1.6:1$ $P:R = 0.75:1$

^a Values of k were converted from units of d^{-1} to $m\ h^{-1}$ (for use in PoRGy) by multiplying by average stream cluster depth.

Table 5.3: Model input parameters and results for field examples shown in Figure 5.9.

Input variables and results	South Saskatchewan River, 50 km downstream from Saskatoon, Saskatchewan, Canada (Venkiteswaran et al., 2007)	Big Hole River, Dickie Bridge Montana, USA (Parker et al., 2005)	Wetland 50, St. Denis National Wildlife Area, Saskatchewan, Canada (Venkiteswaran et al., 2007)	Red Deer River, Blindfloss, Alberta, Canada
Independently known input variables				
$\delta^{18}\text{O-H}_2\text{O}(\text{‰})$	-7	-17.0	-16.1	-17.1
North latitude	52°30'37"	45°51'51"	45°51'51"	50°52'58"
West latitude	106°24'53"	113°5'10"	113°5'10"	110°16'33"
Day of year	197	268	234	230
Year	2004	2004	2004	2003
Input variables adjusted to improve fit				
P_{max} ($\text{mg m}^{-2} \text{h}^{-1}$)	1640	1135	2585	210
R_{30} ($\text{mg m}^{-2} \text{h}^{-1}$)	340	225	885	154
k (m h^{-1})	0.1072	0.2470	0.3479	0.1569
α_R	0.998	0.975	0.987	0.989
Calculations from model fit				
$P:K:G$	1.97:1.78:1	0.93:0.86:1	0.97:1.2:1	2.5:3.5:1
$P:R$	1.11:1	1.08:1	0.79:1	0.73:1
P ($\text{mg m}^{-2} \text{h}^{-1}$)	425	180	584	105
R ($\text{mg m}^{-2} \text{h}^{-1}$)	382	166	740	143
$G^* a$ ($\text{mg m}^{-2} \text{h}^{-1}$)	215	193	600	41
r^2	0.98 and 0.97	0.92 and 0.96	0.95 and 0.93	0.96 and 0.93

^a where G^* is gross G , the total influx and outflux rather than the difference between influx and outflux

Table 5.4: Summary of P , R , and k ranges for different ecosystems. Most metabolic rates were determined directly by measurements of O_2 instead of carbon and subsequent conversion to O_2 . The k values were determined directly via tracer experiments or high-frequency measurements of wind speed combined with mass balance and site-specific equations for converting wind speed; k_{600} is k (in units of distance per time) normalised to a Schmidt number of 600 (the Schmidt number of CO_2 at $20^\circ C$ in freshwater) and is a common format of expressing k for lakes; $k_{2,20^\circ C}$ is the k (in units of per time) normalised to $20^\circ C$ for O_2 (a Schmidt number of 530) and is a common format of expressing k for rivers.

Ecosystem	P (mmol O_2 $m^{-2} d^{-1}$)	R (mmol O_2 $m^{-2} d^{-1}$)	G (as k_{600} cm h^{-1}) or (as $k_{2,20^\circ C}$, h^{-1})	References
Lakes and Ponds: Planktonic	0-620	5-256	k_{600} : 0.5-11	<i>P, R: Carignan et al. (2000); López-Archilla et al. (2004)</i> <i>P: Welch (1968); Wetzel (2001)</i> <i>R: Pace and Prairie (2005); Welch (1974)</i> <i>G: Cole and Caraco (1998); Matthews et al. (2003)</i>
Creeks, Streams, and Rivers	0.3-2000	1-1353	k_{600} : 2-50 $k_{2,20^\circ C}$: 0.0083-300	<i>P, R: Allan (1995)</i> <i>P: Davis (2002); Wetzel (2001)</i> <i>P, G: Wilcock et al. (1999)</i> <i>P, R, G: Mutholland et al. (2001)</i> <i>G: Méling and Flores (1999); Wilcock et al. (1995)</i>

Chapter 6

Determining community respiration and primary production in shallow boreal forest reservoirs with dissolved oxygen isotopes

Abstract

Reservoirs are required to store water for electricity generation, potable water supply, and irrigation. Yet, for these important services, they are an understudied aquatic system with respect to carbon, nutrients, greenhouse gas production, and community metabolism. The biological processes underlying the net cycling of carbon and O₂ in reservoirs are important when deciphering how reservoir creation affects landscapes, water quality, and ecosystem function. The Flooded Upland Dynamics Experiment (FLUDEX) involved the creation of three experimental reservoirs in boreal forest uplands, differing in their amounts of organic matter stored on the landscape, to study changes in greenhouse gas cycling due to flooding. This also provided an opportunity both to study the relationship between carbon and O₂ cycles and to determine rates of community respiration (*CR*) and primary production (*PP*) over the five year life of the experiment by using isotope budgets of dissolved O₂. Rates of *CR* and *PP* depended strongly on the *CR* enrichment factor and as such were determined in three ways: literature values for water-column and sediment *CR*, modelling diel field data, and from carbon-based *NPP*. The diel modelling and benthic respiration results provided upper- and lower-limits on *CR* and *PP* while the carbon-based rates were between those two methods suggesting that O₂-based rates were within those limits.

6.1 Introduction

O₂ is biogeochemically important and fundamental to almost all life (*Falkowski and Raven, 1997*). Globally, O₂ has been used to constrain and estimate primary production and respiration by looking at the O₂:N₂ ratio (*Bender et al., 1994*) and Dole effect (*Blunier et al., 2002; Hoffmann et al., 2004*). The latter is the difference between the isotopic ratio (¹⁸O/¹⁶O, hereafter as δ¹⁸O-O₂) of atmospheric O₂ and ocean water. That the Dole effect is not 0 ‰, i.e., the same as ocean water, is a result of the relative contributions of terrestrial and marine primary production and respiration. Current calculations of the Dole effect are not fully balanced, i.e., the observed value of the atmosphere and calculated values do not match by 2.7 ‰ to 5.5 ‰ (*Bender et al., 1994; Hoffmann et al., 2004*).

At the ecosystem level, O₂ has been used to assess community metabolism rates for oceans, lakes, rivers, and streams (*Allan and Castillo, 2007; Carignan et al., 2000; del Giorgio and Peters, 1994; Odum, 1956; Rizzo et al., 1996; Wilcock et al., 1998*). Diel studies of O₂ and δ¹⁸O-O₂ have been used to reduce the assumptions surrounding these estimates and to constrain gas exchange (*Venkiteswaran et al., 2007*).

O₂ and carbon (C), as CO₂, are related because these gases are linked biochemically (via photosynthesis and respiration) and ecologically (e.g., minimum O₂ concentrations required for most aquatic macrofauna and dissolved and particulate C as fuel for microbial activity). Respiratory and photosynthetic quotients (*RQ* and *PQ*) are often used to convert between molecules of O₂ and CO₂ since the number of moles of O₂ consumed is strongly related to the number of moles of CO₂ produced, and vice versa (e.g., *Carignan et al., 2000*). The range of values of these quotients and their closeness to a 1:1 relationship are variable and depend on several factors such as the source of nitrogen and differences between respiration rates in the dark and light (*Falkowski and Raven, 1997; Wetzel, 2001; Williams and Robertson, 1991*).

As well as being an important biogeochemical element, O₂ may therefore be a useful constraint on dissolved inorganic C (DIC) budgets. Previous studies of greenhouse gas (GHG) fluxes, such as CO₂ and CH₄, from lakes and reservoirs have been based largely on point surface measurements (e.g., *Tremblay et al., 2004*), allometric scaling, and multiple regressions of various easy-to-measure constituents (e.g., *Bastviken et al., 2004*). Another conventional approach to studying community metabolism, although much less common in reservoirs, has been to use diel changes in O₂ (e.g., *Cavalcante et al., 2007*). Neither approach has sought to combine and constrain C- and O₂-based measures of community metabolism.

Considerable effort has been taken to be able to predict mercury cycling in old, new, and proposed reservoirs (e.g., *Bodaly et al., 2007*). Less effort has been expended on predicting or back-casting GHG fluxes from these ecosystems. Community metabolism is the driver of GHG and mercury cycling

and thus metabolic rates are important because predictive models of GHG and mercury cycling require knowledge of biological processes (e.g., [Bodaly et al., 2007](#); [Munthe et al., 2007](#)). These models are required when: estimating GHG emissions from reservoir surfaces; scaling up data from experimental reservoirs to full-size reservoirs; and assessing future or past reservoir construction. Predictive models of GHGs and mercury require knowledge of the rates of and relationships between biological processes. Using measurements of $\delta^{18}\text{O}-\text{O}_2$ contributes a better understanding of community metabolism than previous approaches by providing an additional set of constraints on metabolic rates. With the first whole-ecosystem $\delta^{18}\text{O}-\text{O}_2$ budgets, the objective of this chapter was to use $\delta^{18}\text{O}-\text{O}_2$ to determine rates of community respiration (*CR*) and primary production (*PP*) in the FLUDEX reservoirs.

6.2 Methods

Field site and hydrology budgets

Detailed descriptions of the FLUDEX reservoirs have been presented elsewhere ([Bodaly et al., 2004](#); [Matthews et al., 2005](#), Chapter 2). Briefly, three reservoirs containing upland boreal forest with different amounts of stored organic C (OC) were built at the Experimental Lakes Area in northwestern Ontario. They were named according to their pre-flood OC stores as: High, Medium, and Low C. The vegetation and soils were left intact and were largely dominated by jack pine and paper birch—the regrowth from a severe forest fire in 1980. The reservoirs were flooded to a mean depth of about 1 m by enclosing them on three sides with wooden walls and gravel dykes and leaving them open to the upslope catchment on the fourth side. Reservoirs were between about 0.5 and 0.8 ha in surface area, with a mean depth of 1 m, and a maximum depth of 2 m.

FLUDEX reservoirs were flooded for about 113 d a^{-1} , from late May or early June until late September, for five consecutive years, 1999–2003. Water was continuously pumped into the reservoirs from a nearby lake and reservoir water renewal times were 6–9 d depending on reservoir and year. Hydrologic budgets for each reservoir were calculated each year by measuring inflow, outflow, precipitation, and evaporation. The hydrologic budgets are presented in Chapter 2 (Table 2.2).

Field sampling

Sampling strategies are detailed in Chapter 2 and [Matthews et al. \(2005\)](#). In brief, inflow from Roddy Lake, reservoir outflow, and storage were measured directly. Samples for O_2 concentrations and $\delta^{18}\text{O}-\text{O}_2$ values were collected weekly from a common inflow and the V-notch-weir outflow of each reservoir. To determine the daily values used in budget calculations, weekly data

were linearly interpolated (Chapter 2). To assess the storage of standing O₂ and $\delta^{18}\text{O-O}_2$ at the end of each flood season two vertical profiles of O₂ concentrations and $\delta^{18}\text{O-O}_2$ values were taken per reservoir and averaged and combined with measured depth-to-volume curves.

The original experimental design for the isotope study of FLUDEX did not include $\delta^{18}\text{O-O}_2$ since the analytical capability had not yet been fully established (Roberts *et al.*, 2000; Wassenaar and Koehler, 1999) and for this reason no $\delta^{18}\text{O-O}_2$ samples were collected in the first year. Subsequent analysis of $\delta^{18}\text{O-O}_2$ on samples collected for other purposes was not successful. A comparison between $\delta^{18}\text{O-O}_2$ determined from bottles with butyl blue stoppers (those used for $\delta^{18}\text{O-O}_2$ samples) and $\delta^{18}\text{O-O}_2$ determined from bottles with red Vacutainer stoppers suggests that no simple correlation exists between samples with both stoppers and that red Vacutainer stoppers may be inappropriate for $\delta^{18}\text{O-O}_2$ samples. Thus $\delta^{18}\text{O-O}_2$ values could not be estimated for the first year of flooding and therefore only an O₂ mass budget exists for that year.

Other budget items, precipitation, catchment input, and gas exchange, were estimated or proxy measurements were taken for O₂ concentrations and $\delta^{18}\text{O-O}_2$ values. Precipitation was assumed to be at concentration and isotopic equilibrium with the atmosphere. O₂ concentrations and $\delta^{18}\text{O-O}_2$ values for catchment input were measured in the nearby Lake 114 inflow stream because it could be sampled throughout the flood season since the catchment shape and presence of a V-notch weir was practical for sampling for multiple parameters. The Lake 114 and FLUDEX catchments share a common history: logged in the 1970s, extensively burned in 1980, and similar regrowth patterns. Nevertheless samples of catchment input (as interflow) into the High C reservoir were collected for O₂ concentration because analysis of this parameter could be completed on the small volumes of water that could be practicably collected.

Net gas exchange between the reservoirs and atmosphere was calculated using measured gas flux coefficients (k) and surface O₂ concentrations and $\delta^{18}\text{O-O}_2$ values. The reservoirs were spiked with SF₆ in 2001 and 2003 to determine k (Matthews *et al.*, 2003, Chapter 8), which was subsequently converted for use with O₂ (as per Jähne *et al.*, 1987; Wanninkhof, 1992).

Mass and isotope-mass budgets

Mass and isotope-mass budgets are calculated on a day-by-day basis for each reservoir in each year, as per Chapter 2. Consequently each item in the budgets represents the total mass and mass-weighted $\delta^{18}\text{O-O}_2$ value that entered or exited the reservoirs. The net consumption of O₂ is calculated as the difference between the outputs and inputs of these budgets. Rates of CR and PP are calculated by assigning end-member $\delta^{18}\text{O-O}_2$ values (based on several lines of experimental and literature data) and using a two-end-member

mixing model.

To calculate the mass budgets, daily O₂ concentrations were multiplied by their respective water flux rates (Equation 6.1). Similarly, to calculate the isotope-mass budgets, daily δ¹⁸O-O₂ values were multiplied by their respective O₂ concentrations and water flux rates. Both mass and isotope-mass budgets must be calculated day-by-day rather than with seasonal averages because O₂ concentrations, δ¹⁸O-O₂ values, and water flux rates changed at different rates over the flood season. The daily values of mass and isotope-mass fluxes were summed to determine the seasonal value.

The δ¹⁸O-O₂ value of net O₂ consumption is determined by dividing the difference between the isotope-weighted inputs and outputs by the net consumption of O₂,

$$net = \sum_{i=1}^j (Q_{in} \times C_{in})_i - \sum_{i=1}^j (Q_{out} \times C_{out})_i \quad (6.1)$$

$$\delta_{net} = \frac{\sum_{i=1}^j (Q_{in} \times C_{in} \times \delta_{in})_i - \sum_{i=1}^j (Q_{out} \times C_{out} \times \delta_{out})_i}{net} \quad (6.2)$$

where *net* is net production, *Q* is water flow rate, *C* is O₂ concentration, *i* is day, *j* is the number of flood days, *δ* is the δ¹⁸O-O₂ value, and the subscripts *in* and *out* are reservoir inputs and outputs.

Using isotope-mass budgets to calculate biological processes

The O₂ budgets were used to determine the rates of *CR* (measured as the consumption of O₂) and *PP* (measured as the production of O₂). The enrichment factors¹ associated with *CR* (ε_{CR}) typically range between -21 ‰ and -15 ‰ (Guy *et al.*, 1993; Kiddon *et al.*, 1993; Quay *et al.*, 1995). Water column and benthic O₂ consumption have been reported to have different ε_{CR} values. Where O₂ consumption rates are high but where O₂ is diffusion limited, ε_{CR} may range from -6 ‰ to 0 ‰ (Brandes and Devol, 1997; Hartnett *et al.*, 2005; Hendry *et al.*, 2002). Diel modelling has been used to estimate ε_{CR} in some ecosystems (Venkiteswaran *et al.*, 2007). Here, ε_{CR} was estimated from water column, benthic, diel assessments (see below) and δ¹⁸O-CR was assigned as,

$$\delta^{18}\text{O-CR} = \delta^{18}\text{O-O}_2 + \epsilon_{CR} \quad (6.3)$$

The ε associated with *PP* (ε_{PP}) is 0.00 ‰ (Guy *et al.*, 1989, 1993; Helman *et al.*, 2005; Stevens *et al.*, 1975) and thus δ¹⁸O-O₂ produced by *PP* is equal to δ¹⁸O-H₂O. The δ¹⁸O-H₂O value was measured and, given the flow-through nature of the FLUDEX reservoirs and size of Roddy Lake, was not expected

¹Enrichment factors for different processes are denoted as ε values: ε = $\frac{R_b}{R_a} - 1$ where *R* is the ¹⁸O/¹⁶O ratio of the reactant (*a*) and product (*b*).

to change seasonally. The $\delta^{18}\text{O-PP}$ was assigned the measured $\delta^{18}\text{O-H}_2\text{O}$ value of -6.8‰ . The seasonal effects of increased evaporation in summer were negligible in FLUDEX reservoirs because of their short residence times (Table 2.2).

These two end-member $\delta^{18}\text{O-O}_2$ values were combined with the $\delta^{18}\text{O-O}_2$ value of net O_2 consumption to calculate rates of CR and PP ,

$$net = CR - PP \quad (6.4)$$

$$CR = -\frac{in \times (\delta_{PP} - \delta_{in}) + out \times (\delta_{out} - \delta_{PP})}{\delta_{PP} - \delta_{CR}} \quad (6.5)$$

$$PP = \frac{in \times (\delta_{CR} - \delta_{in}) + out \times (\delta_{out} - \delta_{CR})}{\delta_{CR} - \delta_{PP}} \quad (6.6)$$

where in is the total inputs and out is the total outputs from Equation 6.1, and δ is the isotopic ratio (Equation 6.2).

Diel biological processes

To provide a comparison with the results of the seasonal $\delta^{18}\text{O-O}_2$ mass budgets and to estimate ϵ_{CR} values, diel $\delta^{18}\text{O-O}_2$ sampling was conducted in July-2003. Two days of hourly $\delta^{18}\text{O-O}_2$ samples were collected from each reservoir. O_2 saturation and temperature were measured every 5 min by a Hydrolab MiniSonde 4A. Winkler titrations were performed several times per day to calibrate the sonde. CR and PP rates as well as ϵ_{CR} values from each diel sampling were calculated using a Matlab version of PoRGy (Venkiteswaran *et al.*, 2007) and adjusting for the continuous inflow to the reservoirs (Ho *et al.*, 2000). Best-fits were calculated by minimising the combined sum of squared errors of standardised O_2 saturation and $\delta^{18}\text{O-O}_2$ data. Gas exchange coefficients during the diel sampling were concurrently measured via an SF_6 spike experiment (Chapter 8).

Analytical methods

Samples for O_2 concentration analysis via Winkler titration were collected in 300 mL ground-glass stopper BOD bottles following Carignan *et al.* (1998). Samples were kept cool and dark, fixed within about 30–40 min, and titrated within 8 h. Titration of duplicate samples was within 0.3 mg L^{-1} .

Liquid samples for $\delta^{18}\text{O-O}_2$ analysis were collected in pre-evacuated serum bottles with pre-baked butyl blue stoppers and sodium azide. Analysis was performed at the Environmental Isotope Laboratory at the University of Waterloo on a modified Micromass Isochrom gas chromatograph–isotope ratio mass spectrometer (GC–IRMS). Before analysis, a 5 mL headspace of ultra-high purity helium was added to the sample bottles. Bottles were shaken

at 120 rpm on a reciprocating shaker for at least an hour to equilibrate the dissolved and gaseous phases. The inlet of a μ Gas autosampler was modified with a six-way valve to control gas flows between inlet and IRMS. A subsample of headspace was injected into a T-valve and routed to an in-line Nafion dryer. The counter-current annular flow of dry helium through the Nafion dryer removed H_2O from the sample. The six-way valve routed the sample to the oven where a 5 Å molecular sieve column at 80 °C separated the O_2 , N_2 , and Ar gases. The sample gas was drawn through an open split into the empirically tuned IRMS. Sample gas was bracketed by two pulses of an O_2 monitoring gas ($\delta^{18}\text{O}-\text{O}_2 \approx +24.1 \text{ ‰}$). Sample-size effects were corrected by a calibration curve of air ($\delta^{18}\text{O}-\text{O}_2 \approx +23.5 \text{ ‰}$) versus peak size. Samples were analysed twice. After no more than five samples, one or two internal O_2 working gases ($\delta^{18}\text{O}-\text{O}_2 \approx -8.6 \text{ ‰}$ and $+13.5 \text{ ‰}$) were analysed to ensure consistency. Results are reported as the part per thousand deviation from SMOW ($^{18}\text{O}/^{16}\text{O} \equiv 0.0020052$ as defined by [Hagemann et al., 1970](#)). Precision of $\delta^{18}\text{O}-\text{O}_2$ analysis was $< \pm 0.2 \text{ ‰}$.

6.3 Results

O_2 concentrations and mass budgets

The level of O_2 saturation in reservoir water was lowest in the first year of flooding. It remained both below 100 % saturation and below that of the inflow water in each reservoir for the entire five year experiment (Figures 6.1 and 6.2). In the first two years, O_2 concentrations were lowest in mid-summer when water and flooded soil temperatures were greatest.

The $\delta^{18}\text{O}-\text{O}_2$ values of inflow water ($24.0 \pm 0.4 \text{ ‰}$, $n = 68$) was always close to atmospheric equilibrium (24.2 ‰). Over the four years with data, reservoir outflow values were between 18.7 ‰ and 29.6 ‰ . Both the greatest $\delta^{18}\text{O}-\text{O}_2$ values and greatest difference between reservoirs were measured in the second year of flooding—no samples were collected in the first year (see Methods). The four-year trend in reservoir $\delta^{18}\text{O}-\text{O}_2$ values was that inter-reservoir differences declined and $\delta^{18}\text{O}-\text{O}_2$ values also declined year-after-year.

Since hydrologic residence times varied year-to-year and between reservoirs (Table 2.2), O_2 concentrations and $\delta^{18}\text{O}-\text{O}_2$ values could not be directly compared. Thus isotope-mass budgets were calculated. The O_2 mass budgets indicate that each FLUDEX reservoir was a net consumer of O_2 in each of the five years of flooding (Table 6.1). Only about 40 % of the O_2 added to the reservoirs by inflow and gas exchange was lost via outflow; the rest was consumed within the reservoirs. Since the reservoirs were always undersaturated there was no loss of O_2 by gas exchange and thus all losses were via dissolved O_2 : outflow from the V-notch weir, seepage, and fracture flow. The amount of O_2 added from gas exchange was similar to that added

via the inflow in the High and Low C reservoirs and was typically half that of the inflow in the Medium C reservoir. Precipitation and catchment input were very small components of the O₂ mass budgets (1–6 % of inputs). All FLUDEX reservoirs consumed a large mass of O₂ in all five years of flooding.

Net O₂ consumption was greatest in the first year of flooding. In subsequent years, O₂ consumption was lower, and while the five-year trend was a decline of 35–50 %, there was no general year-to-year trend. Net O₂ consumption declined year-after-year only in the High C reservoir where in the fifth year of flooding it was two-thirds of what it was in the first year. In the Medium C reservoir, net O₂ consumption declined for four years, to a low of 38 % of the first year but increased to 47 % of the first year in the fifth year. In the Low C reservoir, net O₂ consumption declined 50 % from the first to second year. Net O₂ consumption was greater in subsequent years, but remained well below that of the first year. The $\delta^{18}\text{O-O}_2$ of net O₂ consumption also did not show a clear year-to-year trend. It averaged 25.0 ‰ and had a range of 23.0 ‰ to 27.3 ‰ across all reservoirs and years (Table 6.1).

Diel environmental variables

During the diel sampling, reservoir water temperature varied 2.5 °C to 4.3 °C. Water levels did not vary in the reservoirs and thus the constant water level model of *Ho et al. (2000)* was applied with PoRGy to determine metabolic rates and ϵ_{CR} values while accounting for the constant input of O₂ from the inflow and loss of O₂ via the outflow. Water renewal times were 9.6, 7.4, and 6.7 d for the High, Medium, and Low C reservoirs in during the diel sampling. Sunrise and sunset occurred at 05:30 and 21:10 local time.

There was a measured diel change of 1.3–2.5 mg L⁻¹ and 2.7 ‰ to 6.1 ‰ in $\delta^{18}\text{O-O}_2$ for all the reservoirs. Reservoirs were almost always undersaturated in O₂ (the Low C reservoir reached 100.8 % saturation for about 90 minutes) and mostly below the equilibrium saturation $\delta^{18}\text{O-O}_2$ value of 24.2 ‰; four samples at night in the Medium C reservoir were above this value. To account for these observations, *CR* must have been slightly greater than *PP* and gas exchange must have been very slow compared to *CR* and *PP* rates.

6.4 Discussion

Comparing net O₂ consumption to net DIC production

To assess the coherence between the O₂ and DIC mass budgets, net O₂ consumption was compared to net DIC production (Figure 6.3). Both mass budgets were calculated in a similar manner (cf. Chapter 2). Sampling procedures were similar and the underlying hydrology budgets are the same. Rates of O₂ consumption by non-DIC-producing processes are likely small given the paucity of pathways that use O₂ as a terminal electron acceptor

but do not oxidise OC, e.g., Mehler-peroxidase reactions. O₂ production and DIC consumption are tightly linked via *PP*. Methanogenesis can produce both CH₄ and CO₂ and therefore the relationship between net O₂ consumption and net DIC production would be expected to have a slope less than 1.

The strength of the net O₂ consumption to net DIC production relationship ($r^2 = 0.66$, net DIC consumption = $1.3 \times$ net O₂ production – 1.7, Figure 6.3) suggests that (1) rates of O₂ consumption by non-DIC producing processes must be low, and (2) the different simplifying assumptions made while constructing the two mass budgets are adequate for determining budget-based rates of processes.

O₂ processes

Net consumption of O₂ was determined from the O₂ mass budgets. The $\delta^{18}\text{O-O}_2$ and its budgets offered a tool to calculate the rates of these processes but one of the key parameters needed is the $\delta^{18}\text{O}$ of *CR* ($\delta^{18}\text{O-CR}$, Equation 6.3). Although $\delta^{18}\text{O-PP}$ was well constrained with actual measurements of $\delta^{18}\text{O-H}_2\text{O}$, end member values of $\delta^{18}\text{O-CR}$ were estimated based on several lines of evidence. The $\delta^{18}\text{O-CR}$ could not readily be assigned because reported values of ϵ_{CR} range widely (Brandes and Devol, 1997; Chomicki and Schiff, 2008; Kiddon et al., 1993; Quay et al., 1995).

In benthic sediments, the observed magnitude of ϵ_{CR} is small, likely as a result of high rates of respiration relative to diffusion of O₂ into the sediments (Brandes and Devol, 1997; Hartnett et al., 2005; Hendry et al., 2002). This scenario is similar to FLUDEX since in the flooded soils of FLUDEX reservoirs, where O₂ concentrations were very low or zero (O₂ concentrations were typically < 1 mg L⁻¹ or if detectable just 2 cm below the sediment–water interface, data not shown), O₂ consumption rates must have been high relative to O₂ diffusion; and O₂ consumption was often locally going to completion. In contrast, water column *CR* has been suggested to have a much stronger enrichment factor (Kiddon et al., 1993; Quay et al., 1995).

Due to the range of possibilities of ϵ_{CR} , and thus $\delta^{18}\text{O-CR}$, seasonal rates of *CR* and *PP* were calculated from the $\delta^{18}\text{O-O}_2$ budgets via three methods:

1. with literature values of water column ϵ_{CR} (Kiddon et al., 1993; Quay et al., 1995) and average diffusion-limited ϵ_{CR} (Brandes and Devol, 1997);
2. with the ϵ_{CR} determined from diel sampling and modelling; and
3. with average *PQ* values from the literature to convert net primary production (*NPP*) rates from the $\delta^{13}\text{C-DIC}$ budgets presented in Chapter 2 to *PP* rates in O₂.

Method 1: estimating CR and PP from literature values of ϵ_{CR}

The literature provided two end-member ϵ_{CR} values: one for water-column CR and one for O₂-diffusion-limited sediment CR. Water-column incubations suggested ϵ_{CR} values with a magnitude as large as -22‰ (Kiddon *et al.*, 1993). Incubations of sediments and the overlying water column suggested an average of -3‰ (Brandes and Devol, 1997). The magnitude of ϵ_{CR} directly affected the calculated rates of CR and PP such that ϵ_{CR} with a large magnitude produced larger metabolic rates than ϵ_{CR} with a small magnitude (Equations 6.5 and 6.6). The broad assumptions when using these two end-member ϵ_{CR} values were that all of the CR occurs in either: (1) the water column where it is not O₂-diffusion limited, or (2) the flooded soils where it is O₂-diffusion limited. Certainly, these two end-members describe extreme cases (see Appendix A), but given the high rates of decomposition (Chapter 2), using these ϵ_{CR} values served as end-members for the estimated CR and PP rates. The results are summarised in Tables 6.2 and 6.3.

Method 2: estimating CR and PP by comparing measures of seasonal and diel measures of O₂

The ϵ_{CR} values estimated by modelling diel O₂ and $\delta^{18}\text{O-O}_2$ data with PoRGy were similar among reservoirs: -18.6‰ , -20.3‰ , and -18.9‰ in the High, Medium, and Low C reservoirs suggesting that similar processes were governing O₂ consumption in the reservoirs (Table 6.4). However the ϵ_{CR} from diel modelling were greater in magnitude than those observed in Canadian rivers (Venkiteswaran *et al.*, 2007). That their magnitudes were much closer to those observed in whole-water incubations (e.g., $-18 \pm 3\text{‰}$ in Method 1, Quay *et al.*, 1995) than sediment incubations (e.g., -6‰ to 0‰ in Method 1, Brandes and Devol, 1997) suggested that the CR being measured and modelled was mainly pelagic. In all reservoirs, the coefficients of determination (r^2) were better than 0.73 for both O₂ saturation and $\delta^{18}\text{O-O}_2$ except for $\delta^{18}\text{O-O}_2$ in the Low C reservoir.

The strength of the O₂-saturation r^2 values indicates that the modelling reproduced much of the diel change in O₂. However the lower r^2 values for the $\delta^{18}\text{O-O}_2$ and the temporal offsets between the O₂ and $\delta^{18}\text{O-O}_2$ field data and model output indicate that some feature of the field-data curves were not well-captured by PoRGy (Figures 6.4, 6.5, and 6.6).

The temporal offset between field data and model results may have been a result of the weakened match between the sunlight predicted solely from latitude, longitude, and date and the actual sunlight reaching the reservoirs; reservoirs were bound by wooden walls on three sides and were further enclosed by the surrounding forest and hillslope. The sunlight predicted to strike a flat surface without surrounding barriers such as forest or walls matched field data collected at ELA in 2003 very well (J. J. Venkiteswaran,

unpublished data). However, the diel data was modelled as though the reservoirs were a flat surface without any influence from the surrounding catchment or walls. As a result, PoRGy may have induced *PP* too early or too late in the day relative to what the reservoirs experienced.

The diel O₂-saturation data in the Low C reservoir (Figure 6.6) exhibited the characteristic saw-toothed pattern of diel data (Venkiteswaran *et al.*, 2007, 2008) but the $\delta^{18}\text{O-O}_2$ curve did not. The $\delta^{18}\text{O-O}_2$ data appears to have been more sensitive to changes than O₂ saturation; small changes due to uneven mixing may have a greater effect on $\delta^{18}\text{O-O}_2$ than O₂ saturation since *PP* produced $\delta^{18}\text{O-O}_2$ that is much lower than ambient $\delta^{18}\text{O-O}_2$ and *CR* with strong ϵ_{CR} values can quickly increase ambient $\delta^{18}\text{O-O}_2$ values. Further, complex mixing events such as preferential heating of shallow, open areas and daily thermal stratification-destratification events in the half of the reservoir nearest the sampling location may be a cause of the poor fits (cf. Van de Bogert *et al.*, 2007). Also, close coupling of benthic O₂ production by benthic algal mats and O₂ consumption in the flooded soils may not have met the PoRGy-model requirement of complete mixing. As a result, sampling the Low C reservoir at the outflow may have been less representative of whole-reservoir metabolism than planned. Nevertheless the best-fit-derived ϵ_{CR} values for all three reservoirs were similar and served as a good means for estimating *CR* and *PP* rates.

Daily rates of *CR* and *PP* determined from diel modelling were compared to the seasonal rates (Table 6.6). Diel rates would have varied day-to-day and during a flood season depending on factors such as nutrient and substrate supply, temperature, light, and flushing rates (Falkowski and Raven, 1997; Wetzel, 2001), therefore a single diel rate would not have been expected to match exactly the seasonally averaged rates. However, this comparison is useful when assessing whether the ϵ_{CR} from diel modelling is adequate for the seasonal budgets. Both *CR* and *PP* rates calculated from diel modelling and seasonal isotope-mass budgets are generally within 10 % to 25 % in the High and Low C reservoirs. The diel *CR* rate in the Medium C reservoir was 43 % greater than the seasonal rate. Similarly, the diel *PP* rate was 65 % greater than the seasonal rate in the Medium C reservoir. Given the likely differences in daily rates over the 115 d flood season in 2003, these results were acceptable.

Method 3: estimating *CR* and *PP* by comparing carbon and O₂

Conversion between C and O₂ is often used by pelagic researchers who measure *PP* and/or *CR* with one currency and want to apply the data to the other (del Giorgio and Williams, 2005). The photosynthetic quotient (*PQ*) and respiratory quotient (*RQ*) are defined as:

$$PQ = \frac{\Delta O_2}{-\Delta CO_2} \quad (6.7)$$

$$RQ = \frac{\Delta CO_2}{-\Delta O_2} \quad (6.8)$$

and require that O₂ and CO₂ production and consumption are directly related.

Commonly, O₂ is used to measure CR rates and carbon is used at the ecosystem scale. Thus the value assigned to RQ for conversion between O₂ and carbon is important. *del Giorgio and Williams (2005)* describe the theoretical range of RQ as 0.50–1.33 and 0.67–1.24 for organic respiration with O₂ as the electron acceptor. RQ is often assumed to be 0.8–1.2 for aerobic respiration (*Carignan et al., 2000*). But for anaerobic respiration, CO₂ production is not accompanied by O₂ consumption. Where there are significant rates of reactions that differ from this, such as the Mehler-peroxidase reactions, anaerobic respiration (e.g., anaerobic heterotrophic organic respiration), and aerobic and re-oxidation respiration (e.g., chemoautotrophs) the RQ has ‘no useful meaning in these situations’ because the constraints on it are lost (*del Giorgio and Williams, 2005*).

Photosynthetic electron flow, which is frequently determined by O₂ measurements, is often converted to estimates of carbon fixation by the PQ. Although *Williams and Robertson (1991)* report a theoretical range for PQ of 0.5–3.5, it is often assumed to be 1.00–1.25 (e.g., *Carignan et al., 1998*). *Laurs (1991)* calculated PQ to be 1.4 for new production and 1.1 for recycled production, where the former is PP from newly available nitrogen as NO₃⁻ or N₂ and the latter is from NH₄⁺. Given a highly simplified photosynthesis model, one mole of CO₂ is reduced for each mole of O₂ produced. This 1:1 ratio is altered by O₂ consuming processes such as photorespiration and the Mehler-peroxidase reactions as well as NO₃⁻ reduction using electrons that otherwise may have been used for CO₂ fixation. Whereas O₂ is the product of the light-driven oxidation of H₂O and is catalysed by photosystem II, CO₂ fixation is light-independent and is catalysed by RuBisCO. Thus conversion between carbon and O₂ relies on the assumptions inherent in the PQ value and the differences between O₂ production and CO₂ fixation.

If electrons are used to reduce NO₃⁻ as a nitrogen source, instead of NH₄⁺, PQ would be about 1.3. In all reservoirs and all years, measured NO₃⁻ concentrations, when detectable, were ≤ 3 µgNL⁻¹ and measured NH₄⁺ concentrations were 17–24 µgNL⁻¹. Given the ammonium concentrations and the shading provided by the coloured dissolved OC in the reservoirs (cf. Chapter 2 *Schiff, in prep*), photorespiration and the Mehler-peroxidase reactions may not have had a significant effect on O₂ and CO₂ and thus the PQ in FLUDEX reservoirs should have been slightly greater than 1. A PQ value of

1.25 was used since it has commonly been used in softwater Canadian Shield lakes (cf. *Carignan et al., 2000*).

The carbon-based *NPP* rates from the $\delta^{13}\text{C}$ -DIC budgets (Chapter 2) were converted into O_2 -based *PP* rates with a *PQ* of 1.25. Then this *PP* rate was used with the O_2 mass budgets alone to determine both *CR* (Equation 6.4) and ϵ_{CR} :

$$\epsilon_{CR} = \frac{net \times \delta_{net} + PP \times \delta_{PP}}{net + PP} - \delta^{18}\text{O-O}_2 \quad (6.9)$$

where *net* is from the O_2 isotope-mass budgets (Equation 6.4, Table 6.1), *PP* is converted from carbon (Table 2.4) to O_2 , and δ_{PP} is known ($\delta^{18}\text{O-H}_2\text{O}$, see above).

Since these *CR* and *PP* rates relied on *NPP* rates from the $\delta^{13}\text{C}$ -DIC budgets, the year-to-year trends were a combination of both the $\delta^{18}\text{O-O}_2$ and $\delta^{13}\text{C}$ -DIC budgets. The good relationship between net DIC production and net O_2 consumption re-affirmed the use of *NPP* rates together with the O_2 mass budgets (Figure 6.3). One notable advantage was that the O_2 -only mass budget from the first year of flooding can be used to estimate metabolic rates for that year.

The ϵ_{CR} values ranged between -15.5% and $+4.3\%$ (Table 6.7, Equation 6.9). The positive ϵ_{CR} was a result of the negative *NPP* rate propagated from the $\delta^{13}\text{C}$ -DIC budgets for the fifth year in the Low C reservoir. The ϵ_{CR} values generally decreased in magnitude (i.e., became closer to zero) year-after-year as *CR* and *PP* declined.

Comparing rates of *CR* and *PP* and *P:R* ratios

The first method applied the range of literature ϵ_{CR} values from water-column incubations (*Kiddon et al., 1993; Quay et al., 1995*) and sediment incubations *Brandes and Devol (1997)*; this results in an upper- and lower-limit on *CR* and *PP* rates, respectively. The second method applied calculated ϵ_{CR} values with a large magnitude and as a result produced upper limits on *CR* and *PP* rates. The third method allowed for *CR* and ϵ_{CR} to be back-calculated from *PP* rates. This was accomplished by using the *NPP* rates from the $\delta^{13}\text{C}$ -DIC budgets (Chapter 2) and converting them from carbon to O_2 with a *PQ* value. These O_2 -based rates were then combined with the O_2 mass budget (this chapter) to estimate ϵ_{CR} .

The best comparison of metabolic rates was between those calculated with the ϵ_{CR} value of -22% (water-column values from Method 1 and diel modelling values from Method 2) and the $\delta^{13}\text{C}$ -DIC-based *NPP* rates (Method 3) since the magnitude of the O_2 -diffusion limited ϵ_{CR} value was shown to be too small. The metabolic rates calculated with diel modelling ϵ_{CR} values were greater than those calculated from the $\delta^{13}\text{C}$ -DIC budgets: *CR* rates by about two-fold and *PP* rate by about three- to four-fold.

The year-to-year trends in metabolic rates calculated with diel ϵ_{CR} values (Method 2) varied between the reservoirs (Table 6.5, Figure 6.7). *CR* in the High C reservoir remained within 10% over four years. *PP* rates, however, increased 25% over four years. In the Medium C reservoir, *CR* and *PP* increased from the second to third years and decreased from the third to fifth years concomitantly. *CR* and *PP* rates in Low C reservoir increased by more than one-third from the second to third year and then returned to the second-year rate for the last three years.

The net result of these processes is that the *P:R* (*PP:CR*) ratio generally increased from year-to-year in all reservoirs, from about 0.5:1 to 0.6:1 in the second year to about 0.7:1 to 0.8:1 in the fifth year. These *P:R* ratios matched those determined from diel modelling (Table 6.4).

Metabolic rates estimated with Method 3 generally declined over all five years (Table 6.7, Figure 6.8). *CR* rates clearly declined over five years and while *PP* exhibited a peak in the third year, *PP* rates continued to decline in the last two years. In the High C reservoir, the five-year decline in *CR* was greater than 50% and for *PP* was 75%. *CR* in the Medium C reservoir decreased by 25% from the first to the third year and declined a further 40% to the fifth year while *PP* was about constant for three years then declining 58% over the last two years. *CR* and *PP* were most variable in the Low C reservoir. *CR* declined 50% from the first to second year and then increased 33% in the third year. *CR* then declined 60% from the third to fifth years. In the Low C reservoir, *PP* increased 40% from the first to third year. The decline thereafter was very large, by 46% in the fourth year and to $-30 \text{ kg O}_2 \text{ ha}^{-1}$ in the fifth year. Since *PP* rates were calculated from the $\delta^{13}\text{C}$ -DIC-based *NPP* rates and converted to O_2 , the negative rate from the $\delta^{13}\text{C}$ -DIC budget was propagated to these results.

Together these metabolic rates indicated an overall decline in metabolism over five years. The *P:R* ratio decreased in the High C reservoir from 0.3:1 to 0.2:1, exhibited no net change in the Medium C reservoir at 0.3:1, although it peaked at 0.4:1 in the third year, and an overall decline in the Low C reservoir from 0.3:1 to effectively zero with a peak of 0.5:1 in the third year.

Together, metabolic rates calculated from Methods 2 and 3 indicated that *CR* was greater than *PP* in all reservoirs and years. However both *CR* and *PP* rates and *P:R* ratios were greater in Method 2 than Method 3.

Error assessment

The parameter with the greatest level of uncertainty in this whole-ecosystem $\delta^{18}\text{O}$ - O_2 approach was ϵ_{CR} . When determining rates of *CR* and *PP*, the end-member values were very important. Whereas the $\delta^{18}\text{O}$ -*PP* can be determined by measuring the $\delta^{18}\text{O}$ - H_2O , the $\delta^{18}\text{O}$ -*CR* relies on ϵ_{CR} , an enrichment factor that is not well known at the ecosystem scale.

The ϵ_{CR} values determined in these whole ecosystem $\delta^{18}\text{O}$ - O_2 budgets

were not directly comparable to literature values based on bottle incubations and single species (e.g., [Kiddon et al., 1993](#); [Quay et al., 1995](#)). At the ecosystem scale, ϵ_{CR} remained difficult to estimate. CR occurred in the water column, in periphytic communities, and in the flooded soils. Each of these locations was expected to have different ϵ_{CR} values controlled by the factors that control CR such as nutrient availability and recycling ([Wetzel, 2001](#)). Each O_2 consuming pathway, both biotic and abiotic, has different ϵ_{CR} values (cf. [Venkiteswaran et al., 2007](#)). This further confounded calculation of $\delta^{18}O-O_2$ budgets since the whole-reservoir seasonal budgets required a single average ϵ_{CR} value.

In Chapter 2, the potential error in the $\delta^{13}C$ -DIC budgets on rates of CR and NPP was assessed by adjusting the end-member $\delta^{13}C$ values by $\pm 1\text{‰}$, a range that was $> 2 SD$ on $\delta^{13}C$ -DIC measurements. This caused the calculated rates of CR and NPP to change by an average of $\pm 60 \text{ kg C ha}^{-1}$, which was up to $\pm 6\text{--}17\%$ or $\pm 128\text{--}200 \text{ kg O}_2 \text{ ha}^{-1}$ using a PQ of 1.25.

Using a similar approach with the $\delta^{18}O-O_2$ data, both the $\delta^{18}O-CR$ and $\delta^{18}O-PP$ end-members were adjusted by $\pm 1\text{‰}$, a range that was $> 3SD$ on $\delta^{18}O-O_2$ and $\delta^{18}O-H_2O$ measurements. This assessment was done on the results of all three methods. In the water-column estimates in Method 1, the net result was to change the calculated CR and PP rates by $12\text{--}44\%$ (an average of $\pm 930 \text{ kg O}_2 \text{ ha}^{-1}$). In sediment estimates in Method 1, the net result was to change the calculated CR and PP rates by $3\text{--}5\%$ (an average of $\pm 50 \text{ kg O}_2 \text{ ha}^{-1}$). In Method 2, the net result was to change the calculated CR and PP rates by $9\text{--}30\%$ (an average of $\pm 490 \text{ kg O}_2 \text{ ha}^{-1}$). In Method 3, the net result was to change the calculated CR and PP rates by $3\text{--}11\%$ (an average of $\pm 110 \text{ kg O}_2 \text{ ha}^{-1}$). Similar to the $\delta^{13}C$ -DIC budgets, much of the range of these errors was comparable to the errors associated with other budget items such as concentrations, gas exchange, and volumetric measurements of inflow and outflow water (cf. [Matthews et al., 2005](#)). If ϵ_{CR} were known to within $\pm 1\text{‰}$ then these error estimated would have been acceptable. However, ϵ_{CR} was not known to within $\pm 1\text{‰}$ and literature suggests that it may have ranged from -22‰ to 0‰ . Clearly, the error associated with CR and PP rates was directly tied to the error associated with ϵ_{CR} and was thus greater than the $\pm 1\text{‰}$ estimates would suggest.

Reducing the uncertainty around ϵ_{CR} would reduce the error associated with CR and PP rates. The range of ϵ_{CR} values assessed in the three methods was large: from -22‰ to -3‰ . With the -3‰ ϵ_{CR} , PP rates were an order of magnitude smaller than the daily rates (Table 6.6) and one PP rate was below zero. This suggests that the seasonal ϵ_{CR} values were between the diffusion-limited and water-column end-members (Method 1). Further, since rates of CR and PP determined with the -3‰ ϵ_{CR} were very small and the -3‰ end-member could not have reproduced the diel data (cf. [Venkiteswaran et al., 2008](#)) this indicates that the magnitude of ϵ_{CR} must have been much larger (Method 2). That the ϵ_{CR} values determined from $\delta^{13}C$ -DIC-based

NPP rates (Method 3) generally fell between those used in the other methods suggested that: (1) rates from the other methods may be maxima and minima; (2) the C-based rates from the $\delta^{13}\text{C}$ -DIC budgets were of a similar magnitude to the O_2 -based rates; and (3) that the general trends, such as declining *CR* and a small third-year peak in *PP*, observed in the $\delta^{13}\text{C}$ -DIC budgets, are also features found in the $\delta^{18}\text{O}$ - O_2 budgets.

Given this level of uncertainty in ϵ_{CR} and the differences in *CR* and *PP* rates determined by all three methods, the objectives of this chapter have partly been achieved. While *CR* and *PP* rates were determined by three methods, the inability to better constrain ϵ_{CR} and thus constrain metabolic rates limited the usefulness of $\delta^{18}\text{O}$ - O_2 in this study. If ϵ_{CR} were to have been better constrained, $\delta^{18}\text{O}$ - O_2 budgets may have been able to provide independent confirmation of $\delta^{13}\text{C}$ -DIC-based processes (Chapter 2). Nevertheless, it is clear that information about ecosystem-scale processes can be learned from $\delta^{18}\text{O}$ - O_2 budgets. The year-to-year changes in *CR* and *PP* rates and, in future studies, seasonal changes in metabolism, describe how ecosystems evolve. These metrics, broadly described as ecosystem health by Venkiteswaran *et al.* (2008), were only determinable by using $\delta^{18}\text{O}$ - O_2 . Recent ecosystem-scale studies using $\delta^{18}\text{O}$ - O_2 have been successful but have not had the additional complications of elevated *CR* rates in freshly flooded sediments and study periods longer than a few days (Ostrom *et al.*, 2005; Roberts, 2004; Roberts *et al.*, 2000; Venkiteswaran *et al.*, 2007).

6.5 Conclusions

Whole-ecosystem budgets of O_2 and $\delta^{18}\text{O}$ - O_2 were used to determine rates of net O_2 consumption and metabolism in the FLUDEX reservoirs for five years. Net O_2 consumption was greatest in the first year of flooding and declined by 35–50% by the fifth year demonstrating that these reservoirs were sinks of atmospheric O_2 and net decompositional ecosystems.

Metabolic rates were estimated from the $\delta^{18}\text{O}$ - O_2 budgets via three methods, with: end-member literature ϵ_{CR} values from water-column incubations and O_2 -diffusion-limited sediment incubations (Method 1); ϵ_{CR} values from diel modelling (Method 2); and from carbon-based *NPP* rates determined with the $\delta^{13}\text{C}$ -DIC budgets. The literature ϵ_{CR} values provided upper- and lower-bounds on *CR* and *PP* rates. The ϵ_{CR} value from sediment incubations must have been too small in magnitude given the resulting metabolic rates. The ϵ_{CR} values from diel modelling were similar to those from water-column incubations in the literature (Kiddon *et al.*, 1993; Quay *et al.*, 1995) suggesting that pelagic processes were governing O_2 consumption. The ϵ_{CR} values calculated from the $\delta^{13}\text{C}$ -DIC budgets (Method 3) fell between the literature-based end-members (Method 1) suggesting a whole ecosystem ϵ_{CR} that incorporated *CR* occurring in different locations. This study re-confirms the

importance of ϵ_{CR} on the ability to fit diel data and its control on calculated rates of *CR* and *PP* (cf. [Venkiteswaran et al., 2008](#)).

Rates of *CR* and *PP* were generally within two- to three-fold across all methods. Year-to-year trends were slightly different between the methods. All methods indicated that *PP* had a small peak in the third or fourth year of flooding. *CR* rates were variable year-to-year via Method 2, where there was little change in the High C reservoir, a two-year increase and then a two-year decrease, in the Medium C reservoir, and variable in the Low C reservoir. Method 3 indicated that *CR* generally declined from the first-year onward. As a result of differences in ϵ_{CR} values, both *CR* and *PP* rates and *P:R* ratios were greater in Method 2 than Method 3. Estimates from these methods suggest that *CR* was greater than *PP* in all reservoirs and years, rates of *CR* and *PP* slowed year-after-year, and that community metabolism in the three reservoirs was similar. Together, the results successfully demonstrated a method to study O_2 -based metabolism at the whole-ecosystem scale in a way not possible with O_2 concentrations alone.

Acknowledgements

Funding for this research was provided by the Natural Sciences and Engineering Research Council of Canada, the Canada Foundation for Climate and Atmospheric Sciences, the Climate Change Action Fund, Environment Canada's Science Horizons program, the Centre for Research in Earth and Space Technology, and an Ontario Graduate Scholarship. Fisheries and Oceans Canada, Manitoba Hydro, and Hydro-Québec provided funding for FLUDEX. W. A. Mark and D. Hunkeler provided invaluable help with the modifications to the IRMS required for $\delta^{18}O$ - O_2 analysis. Field and laboratory assistance was contributed by R. J. Elgood. A. M. Wojtyniak and K. T. Maurice were enthusiastic field assistants during the diel $\delta^{18}O$ - O_2 sampling. Sampling strategies were improved by many discussions with R. A. Bodaly, K. G. Beaty, and D. Findlay.

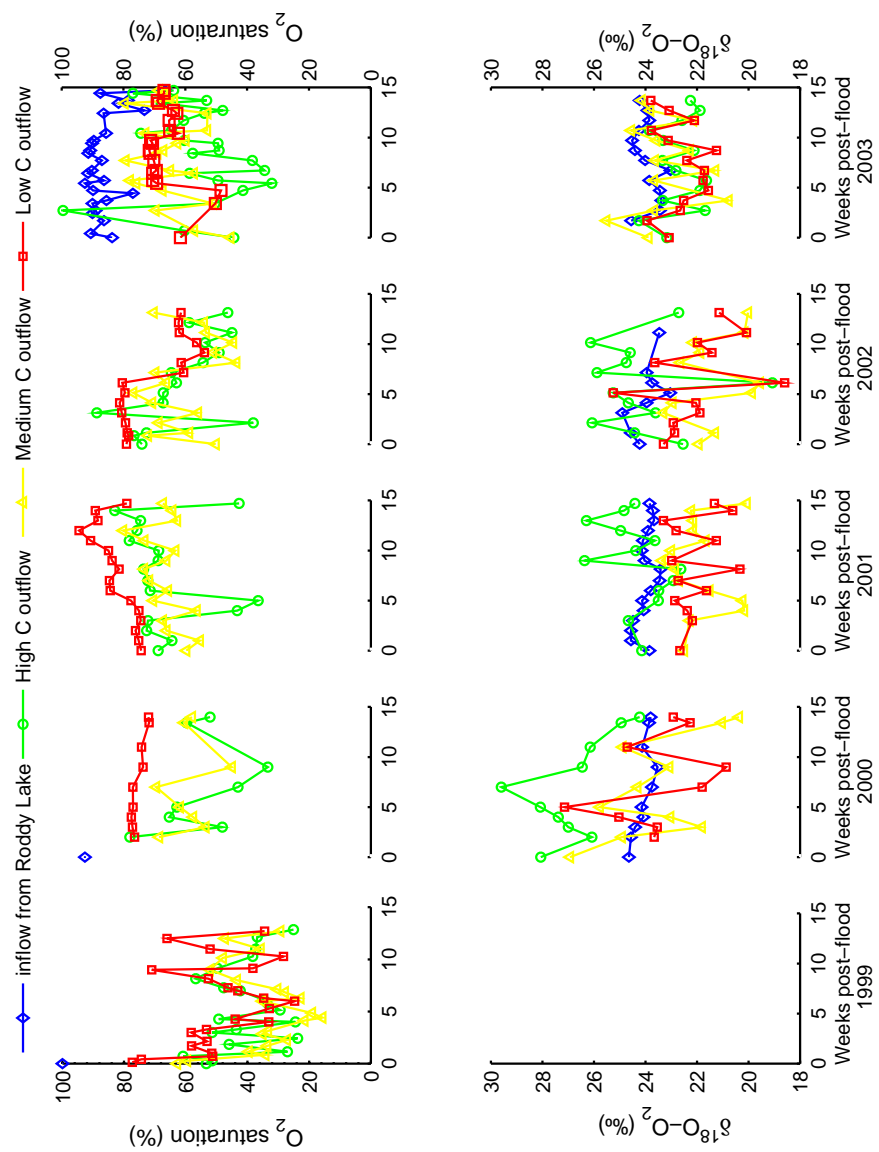


Figure 6.1: O_2 saturation and $\delta^{18}O-O_2$ of FLUDEX reservoir inflow and outflows. Flooding began on 22 June 1999, 30 May 2000, 29 May 2001, 02 June 2002, and 04 June 2003.

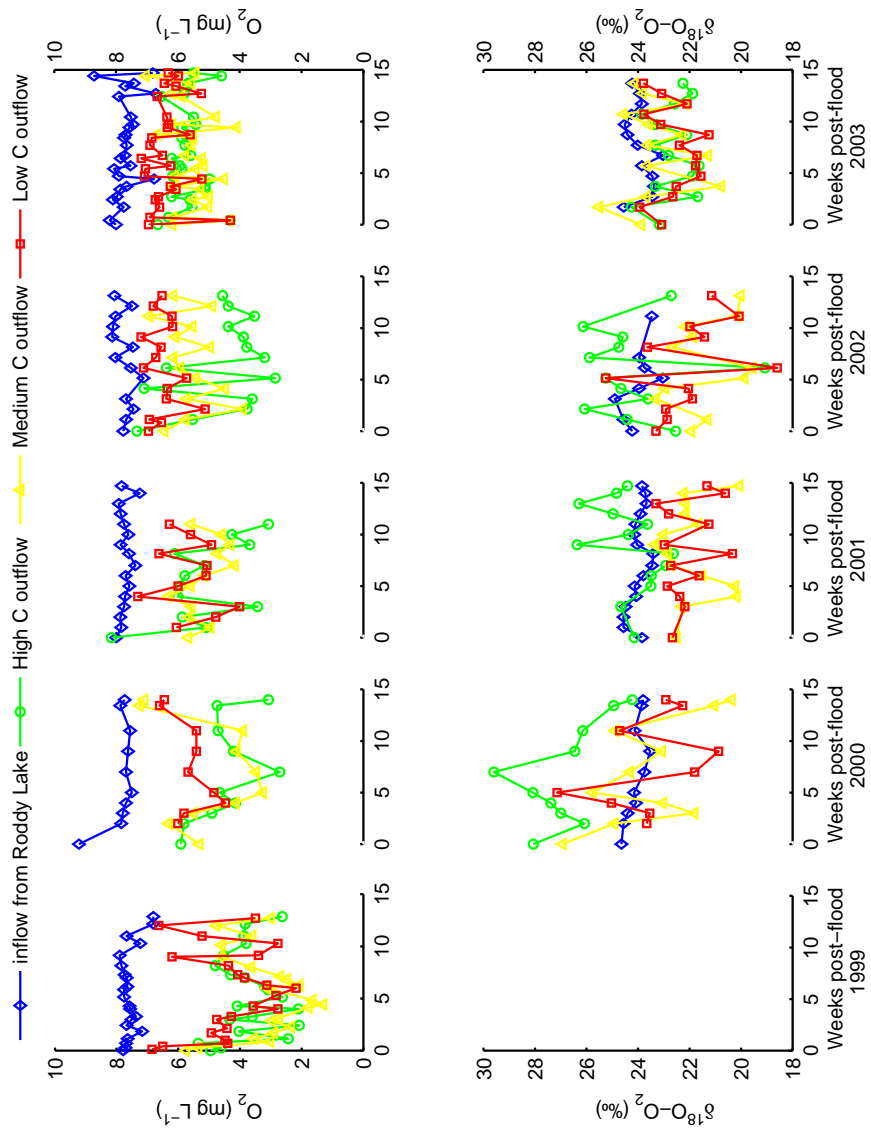


Figure 6.2: O_2 concentrations and $\delta^{18}O-O_2$ of FLUDEX reservoir inflow and outflows. Flooding began on 22 June 1999, 30 May 2000, 29 May 2001, 02 June 2002, and 04 June 2003.

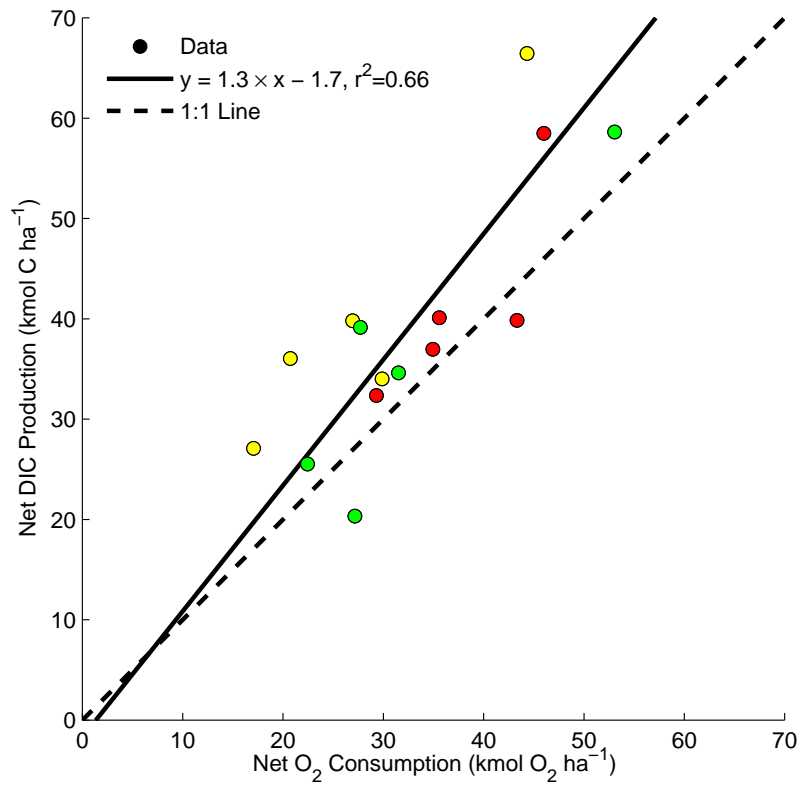


Figure 6.3: Net DIC production versus net O₂ consumption in FLUDEX reservoirs. Reduced-major-axis best-fit line for all data from High (red), Medium (yellow), and Low C (green) reservoirs.

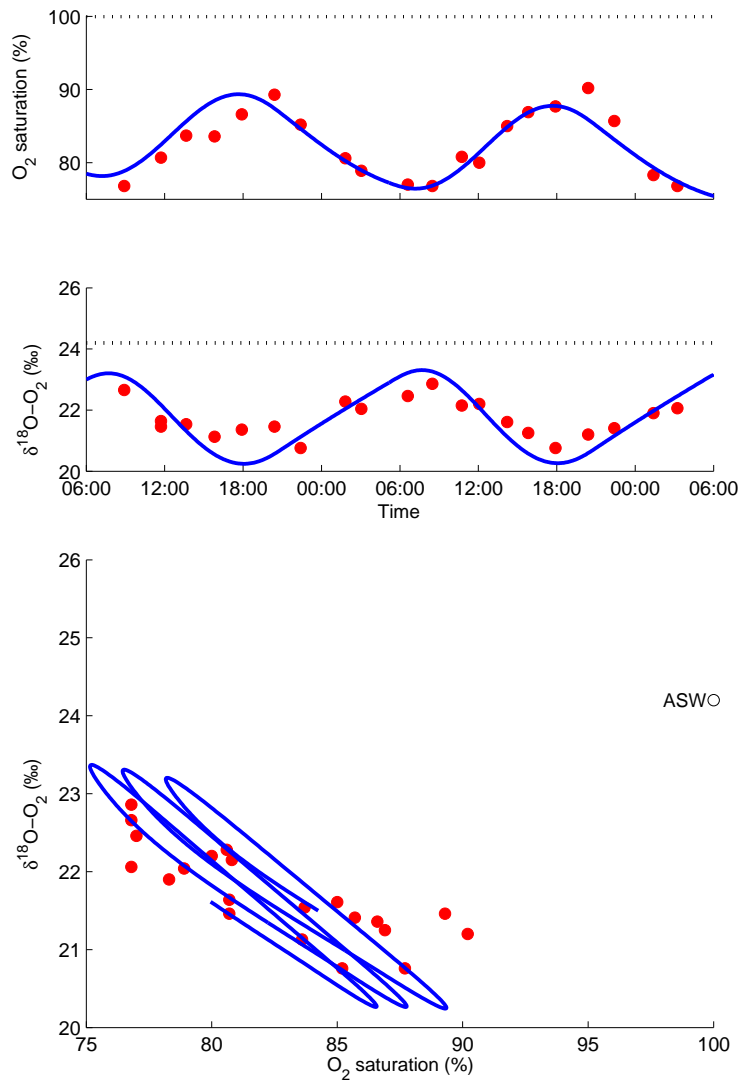


Figure 6.4: Diel field data (*red dots*) with 1 *SD* error bars ($\pm 0.2\%$ and $\pm 0.2\text{‰}$) and PoRGy results (*blue line*) from the FLUDEX High C reservoir from 21 to 23 July 2003. The frequency of O₂ saturation data is reduced to match the $\delta^{18}\text{O}-\text{O}_2$ data. Equilibrium saturation is shown as dotted lines in the temporal figures and air-saturated water (ASW) is shown in the cross-plot.

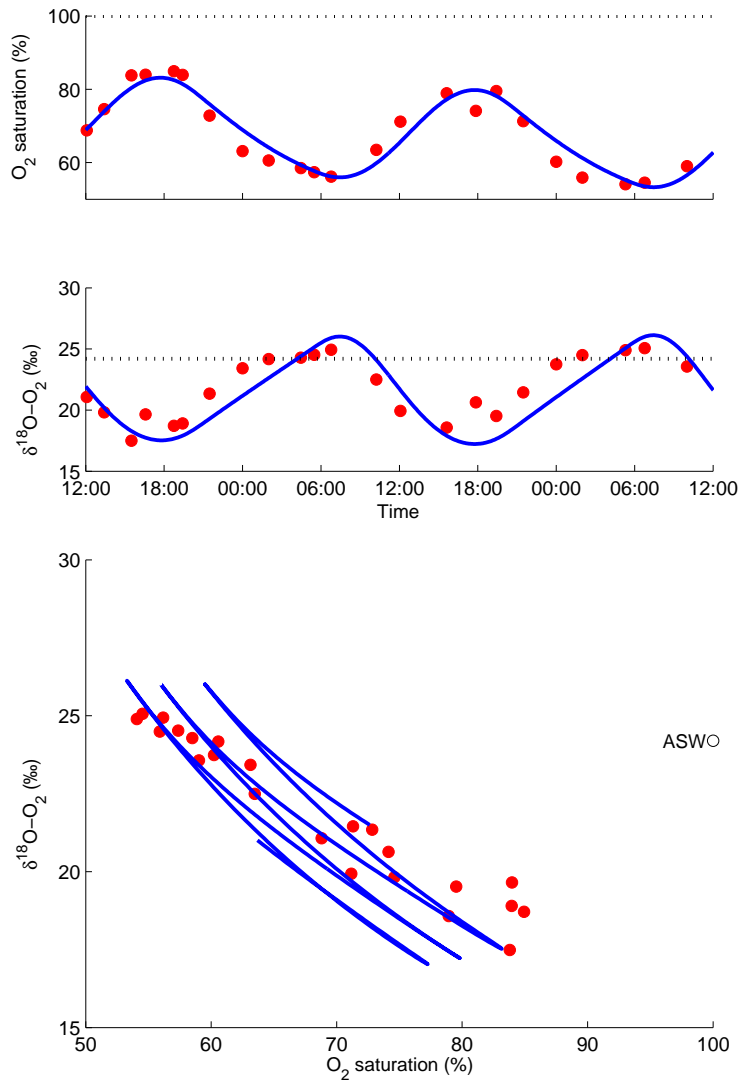


Figure 6.5: Diel field data (*red dots*) with 1 SD error bars ($\pm 0.2\%$ and $\pm 0.2\text{‰}$) and PoRGy results (*blue line*) diel data from the FLUDEX Medium C reservoir from 23 to 25 July 2003. The frequency of O₂ saturation data is reduced to match the $\delta^{18}\text{O-O}_2$ data. Equilibrium saturation is shown as dotted lines in the temporal figures and air-saturated water (ASW) is shown in the cross-plot.

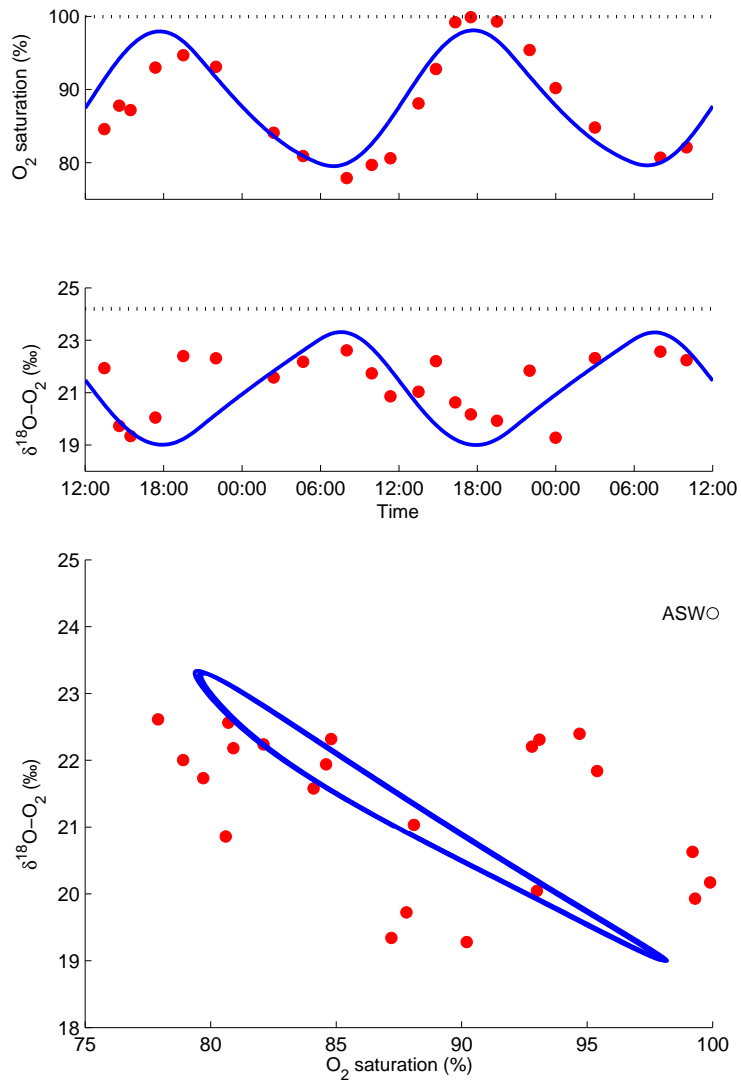


Figure 6.6: Diel field data (*red dots*) with 1 *SD* error bars ($\pm 0.2\%$ and $\pm 0.2\text{‰}$) and PoRGy results (*blue line*) diel data from the FLUDEX Low C reservoir from 25 to 27 July 2003. The frequency of O₂ saturation data is reduced to match the $\delta^{18}\text{O}-\text{O}_2$ data. Equilibrium saturation is shown as dotted lines in the temporal figures and air-saturated water (ASW) is shown in the cross-plot.

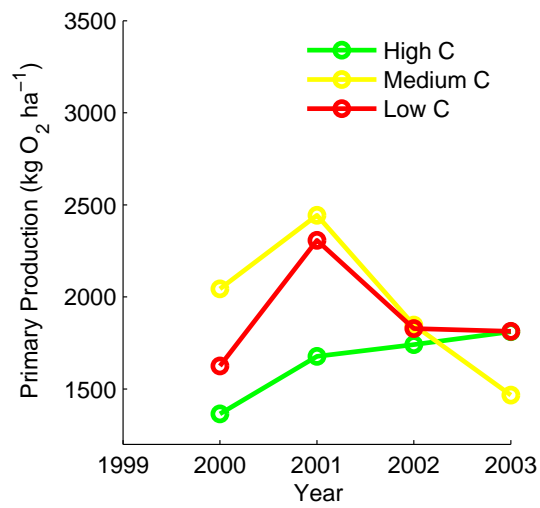
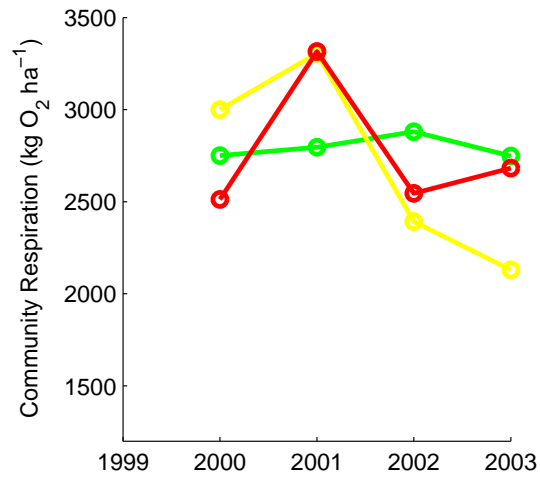


Figure 6.7: Rates of *PP* and *CR* in FLUDEX reservoirs from 1999–2003 calculated with ϵ_{CR} determined by diel modelling.

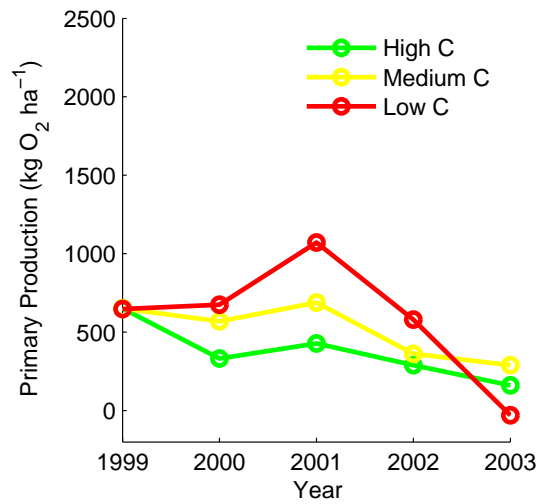
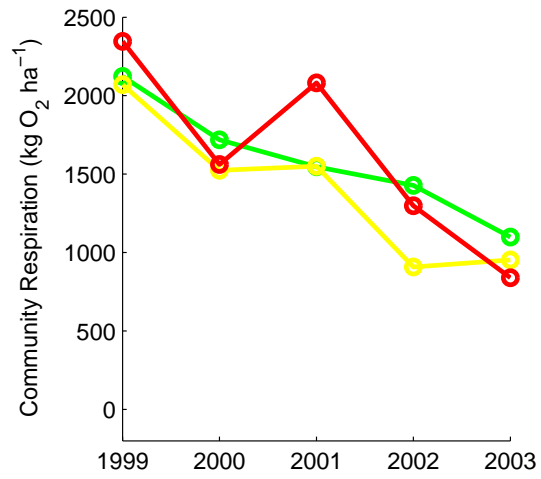


Figure 6.8: Rates of *PP* and *CR* in FLUDEX reservoirs from 1999–2003 calculated by converting *NPP* from the $\delta^{13}\text{C}$ -DIC budgets into O_2 with $PQ = 1.25$.

Table 6.1: The volume- and mass-weighted $\delta^{18}\text{O}$ of dissolved oxygen (O_2) budgets for FLUDEX reservoirs for 1999–2003 (O_2 in $\text{kg O}_2 \text{ ha}^{-1}$ and $\delta^{18}\text{O}$ in ‰).

	High C reservoir												Medium C reservoir												Low C reservoir											
	1999			2000			2001			2002			2003			1999			2000			2001			2002			2003								
	O_2	$\delta^{18}\text{O}$		O_2	$\delta^{18}\text{O}$		O_2	$\delta^{18}\text{O}$		O_2	$\delta^{18}\text{O}$		O_2	$\delta^{18}\text{O}$		O_2	$\delta^{18}\text{O}$		O_2	$\delta^{18}\text{O}$		O_2	$\delta^{18}\text{O}$		O_2	$\delta^{18}\text{O}$										
Inflow	812	994	24.0	896	24.0	872	24.0	931	24.0	1174	1114	24.0	1190	24.0	826	24.0	885	24.0	1173	1137	24.1	1348	24.0	1206	24.0	1421	24.0									
Gas Exchange	999	859	24.2	692	24.2	729	24.2	573	24.2	740	520	24.2	468	24.2	392	24.2	445	24.2	1194	719	24.2	680	24.2	506	24.2	557	24.2									
Precipitation ^a	33	46	24.2	32	24.2	33	24.2	27	24.2	33	46	24.2	32	24.2	33	24.2	28	24.2	33	46	24.2	32	24.2	33	24.2	28	24.2									
Catchment Input	40	126	26.8	54	26.8	46	26.8	21	26.8	8	28	26.8	13	26.8	16	26.8	5	26.8	0	2	26.8	1	26.8	1	26.8	0	26.8									
Total Inputs	1884	2026	24.3	1675	24.2	1681	24.2	1552	24.1	1955	1709	24.1	1702	24.1	1268	24.1	1363	24.1	2400	1904	24.1	2062	24.1	1746	24.1	2006	24.1									
V-notch Outflow	294	491	26.9	425	24.2	407	24.1	471	22.7	398	562	23.5	641	22.1	524	21.4	505	23.3	217	380	23.2	483	22.1	386	21.6	450	22.6									
Wall Seepage	79	96	26.8	90	24.2	76	23.9	90	22.7	100	134	23.6	150	22.0	149	21.4	146	23.3	159	170	23.4	114	22.1	207	21.9	120	22.6									
Fracture Storage	39	53	26.9	43	24.2	60	24.1	53	22.7	38	56	23.5	49	22.1	48	21.4	50	24.4	252	387	23.4	383	22.1	354	21.9	479	22.6									
Total Outputs	412	639	26.9	557	24.2	543	24.1	614	22.7	536	753	23.5	840	22.1	722	21.4	700	23.4	702	1018	23.3	1054	22.1	1028	21.7	1137	22.7									
Net O_2 Consumption	1472	1386	23.1	1118	24.2	1138	24.2	938	25.1	1418	956	24.6	862	26.1	546	27.7	663	24.9	1698	887	25.0	1008	26.2	718	27.4	869	25.9									

^a O_2 input from precipitation was assumed to be at concentration and isotopic equilibrium with the atmosphere.

Table 6.2: The CR and PP rates calculated from volume- and mass-weighted $\delta^{18}\text{O}-\text{O}_2$ budgets and water-column estimates of ϵ_{CR} (Kiddon *et al.*, 1993; Quay *et al.*, 1995) for FLUDEX reservoirs for 1999–2003 (all rates are in $\text{kg O}_2 \text{ ha}^{-1}$).

	High C reservoir				Medium C reservoir				Low C reservoir						
	1999	2000	2001	2002	2003	1999	2000	2001	2002	2003	1999	2000	2001	2002	2003
CR	3553	3852	3984	3998	3998	3613	4122	4122	3052	2573	3471	4800	3752	3794	
PP	2166	2735	2846	3060	3060	2657	3261	3261	2507	1910	2585	3792	3033	2925	
PP:CR	0.61	0.71	0.71	0.77	0.77	0.74	0.79	0.79	0.82	0.74	0.74	0.79	0.81	0.77	
ϵ_{CR}	-22	-22	-22	-22	-22	-22	-22	-22	-22	-22	-22	-22	-22	-22	-22

Table 6.3: The CR and PP rates calculated from volume- and mass-weighted $\delta^{18}\text{O}-\text{O}_2$ budgets and diffusion-limited estimates of ϵ_{CR} (*Brandes and Devol, 1997*) for FLUDEX reservoirs for 1999–2003 (all rates are in $\text{kg O}_2 \text{ ha}^{-1}$).

	High C reservoir					Medium C reservoir					Low C reservoir				
	1999	2000	2001	2002	2003	1999	2000	2001	2002	2003	1999	2000	2001	2002	2003
CR	1351	1238	1238	1268	1129	1100	1096	1096	748	773	1040	1282	961	1073	
PP	-35	120	129	129	191	144	234	203	203	110	154	274	243	203	
PP:CR	-0.03	0.10	0.10	0.10	0.17	0.13	0.21	0.27	0.27	0.14	0.15	0.21	0.25	0.19	
ϵ_{CR}	-3	-3	-3	-3	-3	-3	-3	-3	-3	-3	-3	-3	-3	-3	-3

Table 6.4: PoRGy model input parameters and results for diel O₂ and δ¹⁸O-O₂ modelling of FLUDEX reservoirs in July-2003.

Input variables and results	FLUDEX High C reservoir, Experimental Lakes Area, northwestern, Ontario	FLUDEX Medium C reservoir, Experimental Lakes Area, northwestern, Ontario	FLUDEX Low C reservoir, Experimental Lakes Area, northwestern, Ontario
Independently known input variables			
δ ¹⁸ O-H ₂ O (‰)	-6.8	-6.8	-6.8
North latitude	49.6639°	49.6639°	49.6639°
West latitude	-93.7221°	-93.7221°	-93.7221°
Day of year	203	204	205
Year	2003	2003	2003
k (m h ⁻¹)	0.0061	0.0060	0.0052
Altitude (masl)	424	424	424
Area (m ²)	7400	4900	6300
Depth (m)	0.9	0.9	1.1
Temperature (°C)	20.5-22.9	22.0-25.5	21.0-25.0
Input variables adjusted to improve fit			
P _{max} (mg m ⁻² h ⁻¹)	229	545	349
R ₂₀ (mg m ⁻² h ⁻¹)	73	153	89
α _R	0.9814	0.9797	0.9811
ε _{CR} (‰)	-18.6	-21.3	-18.9
Calculations from model fit			
P:R:G	7.9:9.4:1	7.0:12:1	9.1:11:1
P:R	0.74:1	0.79:1	0.83:1
P (mg m ⁻² h ⁻¹)	59	139	88
R (mg m ⁻² h ⁻¹)	70	176	106
G* ^a (mg m ⁻² h ⁻¹)	8	14	10
r ^{2b}	0.79 and 0.78	0.96 and 0.87	0.73 and 0.32

^a where G* is gross G, the sum of the influx and outflux rather than the difference between influx and outflux

^b where r² values are for the fit between field data and model results for O₂ saturation and δ¹⁸O-O₂

Table 6.5: The CR and PP rates calculated from volume- and mass-weighted $\delta^{18}\text{O}-\text{O}_2$ budgets and diel estimates of ϵ_{CR} (Table 6.4) for FLUDEX reservoirs for 1999–2003 (all rates are in $\text{kg O}_2 \text{ ha}^{-1}$).

	High C reservoir				Medium C reservoir				Low C reservoir						
	1999	2000	2001	2002	2003	1999	2000	2001	2002	2003	1999	2000	2001	2002	2003
CR	2751	2796	2880	2748	2748	3000	3305	2393	2130	2130	2513	3316	2546	2683	2683
PP	1365	1678	1741	1811	1811	2044	2443	1848	1467	1467	1626	2307	1828	1814	1814
PP:CR	0.50	0.60	0.60	0.66	0.66	0.68	0.74	0.77	0.69	0.69	0.65	0.70	0.72	0.68	0.68
ϵ_{CR}	-18.6	-18.6	-18.6	-18.6	-18.6	-20.3	-20.3	-20.3	-20.3	-20.3	-18.9	-18.9	-18.9	-18.9	-18.9

Table 6.6: Diel and seasonal *CR* and *PP* rates in FLUDEX reservoirs 2003 (all rates are in $\text{kg O}_2 \text{ ha}^{-1}$). Diel rates were converted using a 115 d flood season. Seasonal rates are from Table 6.5.

	High C reservoir	Medium C reservoir	Low C reservoir
<i>CR</i> from diel	2180	4858	2926
<i>CR</i> from budget	2748	2754	2683
<i>PP</i> from diel	1628	3809	2429
<i>PP</i> from budget	1811	1336	1814

Table 6.7: The CR and PP Rates calculated from volume- and mass-weighted $\delta^{18}\text{O}-\text{O}_2$ budgets and DIC-based NPP rates for FLUDEX reservoirs for 1999-2003 (all rates are in $\text{kg O}_2 \text{ ha}^{-1}$).

	High C reservoir				Medium C reservoir				Low C reservoir						
	1999	2000	2001	2002	2003	1999	2000	2001	2002	2003	1999	2000	2001	2002	2003
CR	2123	1719	1546	1428	1099	2070	1524	1550	908	953	2346	1562	2081	1298	840
PP	651	332	428	290	161	651	569	688	362	290	648	675	1072	580	-30
PP:CR	0.31	0.19	0.28	0.20	0.15	0.31	0.37	0.44	0.40	0.30	0.28	0.43	0.52	0.45	-0.04
ϵ_{CR}	-15.2	-9.6	-8.6	-6.1	-2.3	-15.5	-10.6	-10.6	-7.4	-8.1	-13.7	-12.1	-13.0	-9.6	4.3

Chapter 7

Methane oxidation: isotopic enrichment factors in freshwater boreal reservoirs

Jason J. Venkiteswaran¹, Sherry L. Schiff¹

Applied Geochemistry 20(4): 683–690 doi: [10.1016/j.apgeochem.2004.11.007](https://doi.org/10.1016/j.apgeochem.2004.11.007).

This article was published in Applied Geochemistry, Vol 20, Venkiteswaran, J.J., Schiff, S.L., Methane oxidation: isotopic enrichment factors in freshwater boreal reservoirs, 683–690, Copyright Elsevier (2005). Permission to reproduce and statement from the co-author is found in Appendix B.

Abstract

Methane oxidation plays a vital role in controlling the flux of CH₄ from many ecosystems. Release of the green house gas CH₄ to the atmosphere during creation and operation of hydro-electric reservoirs is of concern because of the dramatic changes in C and nutrient cycling that result from flooding. Experimentally flooded reservoirs in the boreal forest at the Experimental Lakes Area, northwestern Ontario, Canada, have been under study for a decade. In these large-scale ecosystem experiments, stable C isotopic ratios are used to determine the importance of CH₄ oxidation but quantification requires knowledge of the C isotope enrichment factor associated with CH₄ oxidation under the appropriate environmental conditions. Laboratory incubations were used to assess the CH₄ oxidation enrichment factors in 3 experimental boreal reservoirs with different soil and vegetation, and flood histories. As a result of flooding, new flooded surfaces were created with different temperature

¹Department of Earth Sciences, University of Waterloo, 200 University Avenue West, Waterloo ON, N2L 3G1, Canada.

and hydrologic regimes and the importance of CH₄ oxidation in controlling the flux of CH₄ to the atmosphere changed significantly. However, isotopic ratio data from different systems could not be compared directly because the enrichment factor changed between systems. The enrichment factor in a flooded boreal wetland ecosystem (ELARP) decreased with temperature and the rate of CH₄ oxidation increased with temperature. This was in contrast with two flooded upland boreal forest reservoirs (Flooded Upland Dynamics Experiment) where the enrichment factor was smaller than in ELARP and there was little or no temperature effect on the enrichment factors or rates of CH₄ oxidation.

7.1 Introduction

Methane plays an important role in the C budget of natural and anthropogenically impacted ecosystems. The direction and magnitude of the net ecosystem CH₄ flux is controlled by two microbial processes (CH₄ production and CH₄ oxidation), and factors controlling transport (such as diffusion coefficients and rates of ebullition). A change in the relative importance of these processes can lead to large changes in the magnitude of net ecosystem CH₄ flux.

The microbiology, microbial ecology, and biogeochemistry of CH₄ production pathways have been reviewed at length (e.g., [Garcia, 1990](#); [König, 1992](#)). Briefly, methanogens are obligate anaerobes that ferment only in anoxic, reducing conditions ($E_h < -200$ mV). These archaea cannot tolerate significant O₂, NO₃⁻, or NO₂⁻ levels due to enzyme instability ([Schönheit et al., 1981](#)). Methanogens are often classified by the compounds they utilise as their source of energy and C, e.g., acetate, methylamines, or CO₂. The ultimate mineralization of organic C to CH₄ occurs via a consortia of microbes.

In contrast, CH₄ oxidation can occur aerobically and anaerobically. Methane oxidation occurs in soils (e.g., [Dunfield et al., 1993](#); [Keller et al., 1993](#); [Williams and Crawford, 1984](#)), wetlands (e.g., [Bartlett and Harriss, 1993](#); [Frenzel and Karofeld, 2000](#); [Matthews and Fung, 1987](#)), lakes (e.g., [Rudd and Hamilton, 1975](#); [Whalen and Reeburgh, 1990](#)), marine systems (e.g., [Boehme et al., 1996](#); [Martens et al., 1986](#)), and gas hydrate vents (e.g., [Boetius et al., 2000](#); [Valentine, 2002](#)). Methane oxidisers thrive in soil and peat that fluctuate between saturated and unsaturated conditions ([Shannon and White, 1994](#)), and also respond to an increased O₂ supply from an overlying algal or moss layer and thus, on light availability for photosynthetic production of O₂ ([Frenzel and Karofeld, 2000](#); [King, 1990](#)).

Globally, CH₄ oxidation is a sink for CH₄ and serves to significantly reduce the flux of CH₄ to the atmosphere ([Whiticar, 1993](#)). The greenhouse gas (GHG) budget of ecosystems can be significantly influenced by CH₄ cycling processes since the global warming potential (GWP) of CH₄ is 23 times that of CO₂ on a 100 year time horizon ([Dentener et al., 2001](#)). Wetlands account

for 25 % of non-anthropogenic CH₄ emissions (*Fung et al., 1991*). A change in the fraction of CH₄ oxidised in wetlands would alter the GWP of the GHG flux from wetlands to the atmosphere.

Water reservoirs can serve as a source of GHGs to the atmosphere (*Galy-Lacaux et al., 1997; Huttunen et al., 2002; Kelly et al., 1997; Rudd et al., 1993; St.Louis et al., 2000*). Prior to flooding, the ecosystem GHG flux is dominated by CO₂ and most ecosystems are net GHG sinks on the decadal scale. After flooding, an increase in CH₄ production during anaerobic decomposition, and a reduction in the fraction of CH₄ oxidised combine to increase significantly the GWP of the GHG flux to the atmosphere (Chapter 2).

To study GHG cycling in boreal reservoirs, two large-scale reservoir experiments were initiated at the Experimental Lakes Area (ELA), northwestern Ontario, Canada. In the Experimental Lakes Area Reservoir Project (ELARP), a small boreal wetland complex with large stores of organic C as peat was flooded (*Kelly et al., 1997; McKenzie et al., 1998; Scott et al., 1999*). In the Flooded Upland Dynamics Experiment (FLUDEX), 3 boreal upland areas with lower but differing amounts of stored organic C in soils and vegetation were flooded (*Matthews et al. (2005); Chapter 2*). The before and after flooding GHG budgets of these reservoir systems have been studied intensively and the increased importance of CH₄ to the total GHG flux to the atmosphere after flooding is well documented. The importance of CH₄ oxidation in these systems in mitigating the total flux of CH₄ to the atmosphere has not been well quantified.

Kelly et al. (1997) and *McKenzie et al. (1998)* suggested that increased CH₄ production combined with the reduction of CH₄ oxidation in ELARP were the most important factors contributing to an increase in the CH₄ flux from the wetland to the atmosphere. Stable C isotopic ratios can be employed to determine the importance of CH₄ oxidation to the net ecosystem GHG flux to the atmosphere. Pathways that produce CH₄, and the amount of CH₄ oxidation can be determined because each process affects the C isotopic ratio of CH₄ differently. Thus, C isotopic ratios can be used to investigate processes affecting the net ecosystem GHG flux because they can yield C cycling information unavailable from concentration-only studies. Additionally, CH₄ production and potential GHG flux can be estimated if the isotopic enrichment factor, $\delta^{13}\text{C-CH}_4$ values, and CH₄ concentration are known. However, reported CH₄ oxidation enrichment factors vary widely (e.g., 4–31 ‰; *Whiticar (1999)*). Temperature has been implicated as having a positive relationship with the magnitude of the enrichment factor (*Whiticar and Suess, 1990*).

To determine the enrichment factor for these reservoirs, a series of incubations were performed to address the following: (1) effect of temperature on CH₄ oxidation enrichment factor; (2) difference between FLUDEX and ELARP enrichment factors; (3) implications for the interpretation of GHG cycling in boreal reservoirs.

7.2 Theory

During CH₄ oxidation, ¹²C-CH₄ is preferentially consumed over ¹³C-CH₄ and thus the residual CH₄ becomes isotopically enriched. The magnitude of this preference is defined as the enrichment factor and can be calculated by assuming a simple Rayleigh fractionation in a closed system (*Clark and Fritz, 1997*). Isotopic ratios are reported in δ-‰ notation (relative to the standard VPDB). The enrichment of δ¹³C-CH₄ values and the accompanying decline in CH₄ concentration is used to determine the enrichment factor (ε), which is the slope of the linear regression of 1000 × ln $\frac{R}{R_0}$ plotted against -ln *f*

$$\epsilon = \frac{1000 \times \ln \frac{R}{R_0}}{-\ln f} \quad (7.1)$$

where *R* is the isotopic ratio (¹³C:¹²C) of CH₄ at the time of sampling, *R*₀ is the initial isotopic ratio of CH₄, and *f* is the fraction of CH₄ remaining at the time of sampling.

7.3 Methods

Field sites

The experimental reservoirs were located at the ELA in the boreal forest of northwestern Ontario, Canada (49°40' N 93°45' W). In ELARP, the water level in a small wetland complex (2.39 ha central pond surrounded by 14.4 ha of peatland) was raised by 1.3 m in 1993 (*Kelly et al., 1997*). *Dyck and Shay (1999)* provide a detailed description of plant communities before flooding. Briefly, the peatland had a ground cover of *Sphagnum* mosses with an overstory of shrubs, primarily leatherleaf (*Chamaedaphne calyculata*) and Labrador tea (*Ledum groenlandicum*), and some tree cover of black spruce (*Picea mariana* (Mill) BSP). Maximum and average peat depths were 9.1 and 1.7 m, respectively. The wetland complex was flooded each spring following spring melt, and the water level was lowered to the original pre-flood level each fall to simulate the seasonal water level fluctuations in larger hydroelectric reservoirs.

Three areas of upland boreal forest were flooded in 1999 to a mean depth of approximately 1.0 m as part of FLUDEX. Overburden within the FLUDEX reservoirs ranged from 0 m to more than 1 m of soil and till. *Matthews et al. (2005)* provide a detailed description of plant and soil communities. Briefly, all vegetation and organic soil was burned off during a forest fire in 1980 and regrowth was dominated by a dense, even-aged jack pine (*Pinus banksiana* Lamb.) and paper birch (*Betula papyrifera* Marsh.) forest. The understory contained *Sphagnum* mosses, Labrador tea, and leatherleaf in the moist soil and vegetation community, and *Polytrichum* mosses, alder (*Alnus* spp.), and blue-

berry (*Vaccinium* spp.) in the dry soil and vegetation community. FLUDEX reservoirs were defined on the quantity of organic C in vegetation and soil, High, Medium, and Low C reservoirs. The FLUDEX reservoirs were flooded by continuously having pumped water from a nearby oligotrophic lake into the reservoirs from late spring to early fall to simulate the seasonal water fluctuations in the shallow areas of larger hydroelectric reservoirs.

Field sample collection

Water was collected from 3 locations: 1.5 m depth along a wall of floating peat in ELARP; and 5 cm below the sediment–water interface (SWI) of both the High C and Medium C reservoirs. ELARP samples were collected with a Van Dorn sampler and water from the FLUDEX reservoirs was pumped to the surface via Tygon® tubing. Samples were collected in amber Boston Round bottles covered with Al foil to prevent light intrusion and sealed with black phenolic Poly-Seal™ caps with cone liners to prevent atmospheric contamination during transport to the laboratory.

Pre-evacuated 11 mL Vacutainer® tubes were capped with baked septa (60 °C, 12 h), flushed with N₂, and filled with sample water by displacing the N₂ gas. Tubes were incubated at 3 temperatures (18, 22 and 30 °C) on an orbital shaker in complete darkness. An additional set from each sample location was acidified (0.1 mL of 85% phosphoric acid) to kill the microbes and incubated as a control. See Table 7.1 for a summary of experimental conditions.

Incubation duration was determined in a preliminary experiment at ELA and was approximately 8–10 days. The duration was chosen to span approximately 60% CH₄ oxidation to ensure that the concentration and isotopic ratio changed sufficiently to allow the enrichment factor to be calculated. At each sampling time during the incubation and at the end of each incubation period, 3 tubes from each sample set were removed and killed by acidification. One tube was utilised for CH₄ concentration analysis at ELA and two tubes were archived for subsequent isotopic ratio analysis at the Environmental Isotope Laboratory (EIL) at the University of Waterloo.

Concentration analysis

Methane concentration analysis was performed by gas chromatography at ELA. A N₂ headspace (2 mL) was added to each tube and the tubes were shaken on a wrist-action shaker for 10 min to equilibrate the headspace and liquid CH₄ concentrations. A subsample of headspace gas was analysed using a Varian 3800 gas chromatograph (GC). A Poropak Q column at 80 °C, using ultra-high purity H₂ as the carrier gas, performed separation of CH₄ and CO₂. A flame ionisation detector at 250 °C detected CH₄. All analyses were performed in duplicate on a linear calibration through zero. Analysis

of standards, after no more than 10 samples, during sample runs was always within 3.5%. Methane concentrations were corrected for temperature and barometric pressure differences between initial, incubation, and analysis conditions.

Isotopic ratio analysis

Methane isotopic ratio analysis was performed by gas chromatography combustion isotope ratio mass spectrometry. A He headspace (2 mL) was added to the tubes. Tubes were shaken on a reciprocating shaker at 60 rpm for at least 2 h to equilibrate the headspace and dissolved CH₄ concentrations. A subsample of headspace gas was injected into a HP 6890 GC (injection port at 250 °C). A GS CarbonPlot column (30 m × 0.32 mm) at 45 °C separated CH₄ and CO₂ in a He carrier gas (1.2 mL min⁻¹). Methane was completely combusted to CO₂ in a Micromass combustion furnace (CuO catalyst at 850 °C) fitted to the GC. The CO₂ flows into the mass spectrometer (Micromass Isochrom) through an open split where the relative abundances of masses 44, 45, and 46 were measured. Analysis of each sample was performed in duplicate and a CO₂ gas standard of known isotopic ratio was analysed before and after each sample as a reference standard. Gas samples of an internal standard were analysed after no more than 10 samples. Analytical precision is ± 0.5 ‰.

7.4 Results and discussion

CH₄ oxidation rates and enrichment factors

Methane concentration in the headspace gas of the tubes declined and the $\delta^{13}\text{C-CH}_4$ values enriched over time consistent with CH₄ oxidation by methanotrophs (Figure 7.1). Methane oxidation enrichment factors and the response to temperature were different in the two experimental reservoir systems, ELARP and FLUDEX. Methane oxidation enrichment factors in ELARP incubations ranged from 18.6 ‰ to 21.4 ‰. Increasing incubation temperature had a negative effect on the enrichment factor, confirming reports in the literature (cf. *Whiticar, 1999; Whiticar and Suess, 1990*) (Figure 7.2). The enrichment factor of 21.4 ‰ at 18 °C decreased to 19.6 ‰ at 22 °C and 18.6 ‰ at 30 °C, respectively. These values are in the middle of previously reported values (*Whiticar, 1999*). The effect of temperature on the enrichment factors for the FLUDEX High C and Medium C reservoirs was much smaller. In the FLUDEX High C reservoir, the enrichment factor decreased from 13.9 ‰ at 22 °C to 12.5 ‰ at 30 °C, and in the Medium C reservoir, from 14.3 ‰ at 22 °C to 14.0 ‰ at 30 °C (Table 7.1).

The rates of CH₄ oxidation were similar between replicates; however, rates were slower at lower temperature. Methane oxidation rates in ELARP ranged

from 7.5–50 $\mu\text{mol L}^{-1} \text{h}^{-1}$ (at 18 °C and 30 °C, respectively), and are within the range of rates reported for wetlands (e.g., *Duchemin et al.*, 1995; *Happell et al.*, 1993). Methane oxidation rates were slower in FLUDEX incubations than in ELARP incubations, 11–15 $\mu\text{mol L}^{-1} \text{h}^{-1}$ (at 22 and 30 °C, respectively), with much less difference between rates at different temperature than in ELARP. Whereas temperature has a strong effect on CH_4 oxidation rates and enrichment factors in ELARP, there is much less or no effect on CH_4 oxidation rates and enrichment factors in FLUDEX. Initial incubation CH_4 concentrations were similar in all tubes and therefore the range of CH_4 oxidation rates observed at a given temperature may have been a function of prior in situ conditions such as nutrients and inhibitors, microbial population, and microbial activity.

The enrichment factors determined from 3 reservoir ecosystems at environmentally relevant temperatures differ. Thus, the importance of CH_4 oxidation in a disturbed ecosystem cannot be determined solely by the $\delta^{13}\text{C}\text{-CH}_4$ values. ELARP and FLUDEX reservoirs were vastly different landscapes, both before and after flooding. Prior to flooding, the Sphagnum-dominated ELARP wetland had strong O_2 and CH_4 gradients at the air–water interface. A community of CH_4 oxidisers was well established in the peat and the before flood pond as suggested by highly enriched $\delta^{13}\text{C}\text{-CH}_4$ values and relatively low CH_4 flux to the atmosphere. After flooding in ELARP, the flooded peat was anoxic with low O_2 concentration water above it. Methane oxidiser habitat was initially eliminated in the peat, until the floating peat was revegetated, and the gaseous aerobic zone produced by *Sphagnum* was recreated. In the ELARP pond, water temperature increased and surface O_2 concentration decreased following flooding. However, the pond continued to be seasonally stratified and the summer hypolimnion was anoxic, providing habitat for CH_4 oxidisers in the pond (*Rudd and Hamilton*, 1975, 1978). Before flooding, the soil of FLUDEX reservoirs was dry and unsaturated, except the portion of the High C reservoir vegetated with *Sphagnum*, and was a net sink of CH_4 (*Matthews et al.*, 2005). After flooding, the FLUDEX soil quickly became anoxic and a source of CH_4 to the oxic water column (Chapter 2). Periphyton colonised surfaces in the reservoirs and benthic periphyton was an important source of O_2 to the CH_4 oxidisers (Chapter 2). In both ELARP and FLUDEX, CH_4 oxidiser habitat changed as a result of flooding for reservoir creation. However, CH_4 oxidisers colonised new habitat where environmental conditions were adequate for their growth.

ELARP: Experimental Lakes Area Reservoir Project

In undisturbed peat, a large portion of the potential CH_4 flux to the atmosphere is oxidised in the gaseous aerobic zone above the water table (*Bubier et al.*, 1995; *Saarnio et al.*, 1997; *Sundh et al.*, 1995). The change in water table depth in the peat of ELARP, resulting from flooding, decreased the extent

of the gaseous aerobic zone and thus reduced the habitat for CH₄ oxidisers. Two new peat surfaces were created, flooded peat and floating peat. In flooded peat, the gaseous aerobic zone in the *Sphagnum* spp. was eliminated, and in shallow areas, *Sphagnum* has grown up into the water column. In floating peat, the surface layer of peat (≈ 1 m) detached from the lower layers of peat, and floated at the water surface, reducing the entire gaseous aerobic zone. Floating peat has become revegetated and recreated the gaseous aerobic zone, since ELARP was first flooded in 1993.

The peat surfaces became as warm or warmer than the pond after flooding. The lower layers of peat, below the floating peat, became much warmer and contributed CH₄ to the pond. As a result of flooding, the magnitude and $\delta^{13}\text{C}$ value of the ELARP ecosystem CH₄ flux to the atmosphere changed. Methane flux from the pond to the atmosphere increased about 4-fold, but the $\delta^{13}\text{C}$ -CH₄ value did not change ($\delta^{13}\text{C}$ -CH₄ of -38 ‰) (Kelly *et al.*, 1997). In the pond, the incubations suggest that the CH₄ oxidation rate increased and the enrichment factor decreased as a result of the increased water temperature. The change in peat CH₄ processes was more dramatic. Before flooding, the CH₄ flux from the peat surface was very small and highly oxidised ($\delta^{13}\text{C}$ -CH₄ of -28 ‰ ; 87–91 % oxidised based on the range of enrichment factors observed in ELARP incubations). The CH₄ flux from the floating peat increased greatly and became less oxidised ($\delta^{13}\text{C}$ -CH₄ of -56 ‰; 55 % oxidised based on the ELARP incubation at 30 °C). The CH₄ flux from the submerged peat had also increased greatly and became unoxidised ($\delta^{13}\text{C}$ -CH₄ of -63 ‰) (McKenzie *et al.*, 1998; Poschadel, 1997) because the near surface of the submerged flooded peat was too anoxic to support CH₄ oxidation. The fraction of the CH₄ flux to the atmosphere from the pond that was oxidised changed even though the $\delta^{13}\text{C}$ -CH₄ value did not because temperature and CH₄ oxidation rate increased and the enrichment factor decreased. The CH₄ flux from the floating peat islands and flooded peat was greater and much less oxidised than that of the pond.

The source of the increased CH₄ production is likely the anaerobic decomposition of flooded vegetation (Kelly *et al.*, 1997). As a result of flooding, the vegetation on the peat was submerged, died, and decomposed. While decomposition rates increased at higher temperature, the increase in the CH₄:CO₂ ratio was more important because of the increased insolubility of CH₄ at higher temperatures. This led to increased bubble formation, mostly comprised of CH₄ (Kelly *et al.*, 1997). The floating peat CH₄ flux was higher because ebullitive CH₄ did not diffuse through the water and gaseous aerobic zone before reaching the atmosphere, and thus was not subject to CH₄ oxidation.

The use of ecosystem and temperature specific fractionation factors is important. In ELARP, the difference in fractionation factors, from 18.6 ‰ to 21.4 ‰ (15–30 °C), changes the calculated fraction of CH₄ oxidised by ap-

proximately 20 %. If the smaller enrichment factor of FLUDEX had been used (12.5–14.3 ‰), the role of CH₄ oxidation would have been overestimated by close to 15 %.

FLUDEX: Flooded Upland Dynamics Experiment

The FLUDEX CH₄ oxidation enrichment factors were similar in both reservoirs, and exhibited a small dependence on temperature (Figure 7.2). FLUDEX enrichment factors were 4–8 ‰ smaller than in ELARP. At the reservoir scale, CH₄ concentration and $\delta^{13}\text{C-CH}_4$ values varied widely in FLUDEX and were not the same in the 3 FLUDEX reservoirs (Chapter 2). The role of CH₄ oxidation in controlling the flux of CH₄ from FLUDEX reservoirs to the atmosphere likely varies widely because the range of $\delta^{13}\text{C-CH}_4$ values observed is large, –99 ‰ to –11 ‰ (Chapter 2).

The fraction of CH₄ oxidised in the soil of FLUDEX reservoirs varies widely from reservoir to reservoir and from year to year. Once flooded, the soils became a source of CH₄ to the overlying water column. To quantify the net production of CH₄ in the FLUDEX reservoirs, CH₄ mass and $\delta^{13}\text{C-CH}_4$ budgets were created (Chapter 2). In 1999, little to no CH₄ was oxidised, and $\delta^{13}\text{C-CH}_4$ values of net CH₄ production were very depleted (–92 ‰ to –72 ‰) indicating that CH₄ was produced via CO₂ reduction. Methane produced via CO₂ reduction is more depleted than CH₄ produced via methyl-type fermentation (Whiticar, 1999) and soil porewater profiles indicate a characteristic relationship between CH₄ and DIC concentrations and $\delta^{13}\text{C-DIC}$ and $\delta^{13}\text{C-CH}_4$ (Chapter 2). In 2000 and 2001, soil porewater data indicate that CH₄ was initially produced by CO₂ reduction and later produced by both CO₂ reduction and methyl-type fermentation (Chapter 2). This seasonal shift in 2000 and 2001 made it difficult to assign an initial $\delta^{13}\text{C-CH}_4$ value, though soil porewater profiles were used to estimate the initial $\delta^{13}\text{C-CH}_4$ value.

To compare the fraction of CH₄ oxidised in the FLUDEX reservoirs, the $\delta^{13}\text{C-CH}_4$ of the net production of CH₄ is combined with the enrichment factors. In 2000 in the High C reservoir, 63–67 % of the CH₄ produced in the flooded soils was oxidised, based on the range of FLUDEX enrichment factors. In 2001, in the High C reservoir, 90–93 % of the CH₄ produced was oxidised. The Medium C reservoir showed a similar increase in the fraction of CH₄ oxidised, from 26 % in 2000 to 78 % in 2001. However, a smaller fraction of CH₄ was oxidised in the Medium C reservoir than in the High C reservoir. If a larger enrichment factor had been assumed, such as the ELARP enrichment factors, the role of CH₄ oxidation in mitigating the GHG flux from the ecosystem would have been underestimated by approximately 15 %.

The different fractions of CH₄ oxidised in the High C and Medium C reservoirs may be due to the Sphagnum-based peat found only in the High

C reservoir and the photosynthetic O₂ released from the living *Sphagnum* and benthic periphyton. *King (1990)* suggests that light mediated changes in O₂ distribution within sediments affects the rate of CH₄ oxidation. Variable CH₄ oxidation was caused by this 'photostimulation' and not by changes in CH₄ production. *Frenzel and Karofeld (2000)*, measured high-resolution CH₄ concentration profiles in a bog, and found that the saturated–unsaturated interface in the *Sphagnum* was not always the location of CH₄ oxidation; in locations without vascular plants, CH₄ concentrations were very low where there were green parts of *Sphagnum*. They attributed photosynthetic O₂ from the green parts of *Sphagnum* as providing increased O₂ to CH₄ oxidisers. In FLUDEX, this may have been the case in the High C and to a lesser extent in the Medium C reservoir.

7.5 Conclusions

The relative importance of CH₄ oxidation can be over or underestimated if an inappropriate enrichment factor is chosen. In three experimental reservoir systems, the rates of CH₄ oxidation and CH₄ oxidation enrichment factors were determined in laboratory incubations. In ELARP, increased temperature greatly increased the CH₄ oxidation rates and decreased the enrichment factor. The fractionation factors ranged from 18.6 ‰ to 21.4 ‰. In two FLUDEX reservoirs, the CH₄ oxidation rates and enrichment factors did not vary much with temperature or between reservoirs. The fractionation factors averaged 13.2 ‰ and 14.1 ‰ in the High C and Medium C reservoirs, respectively. As a result of flooding, the importance of CH₄ oxidation changed in the 3 reservoirs. New surfaces were created that were greater sources of CH₄ to the atmosphere than the before flood surfaces and the relative importance of CH₄ at each surface varied widely. Interpretation of δ¹³C-CH₄ data is complicated by the wide range of CH₄ oxidation enrichment factors and the relationship between enrichment factor, rate, and temperature. The laboratory incubations show that the fractionation factor must be determined for each ecosystem. Direct comparison of δ¹³C-CH₄ data between different systems necessitates evaluation of ecosystem- and temperature-specific enrichment factors, before and after ecosystem changes, such as flooding and reservoir creation.

Acknowledgements

Richard Elgood provided logistical support and constructive advice to improve a previous draft of this manuscript. Two reviewers provided helpful suggestions that improved this manuscript. This research was funded by Canada Foundation for Climate and Atmospheric Sciences, Climate Change Action Fund, Centre for Research in Earth and Space Technology, and the

Natural Sciences and Engineering Research Council of Canada (NSERC).
FLUDEX is funded by Fisheries and Oceans Canada, Manitoba Hydro, and
Hydro-Québec.

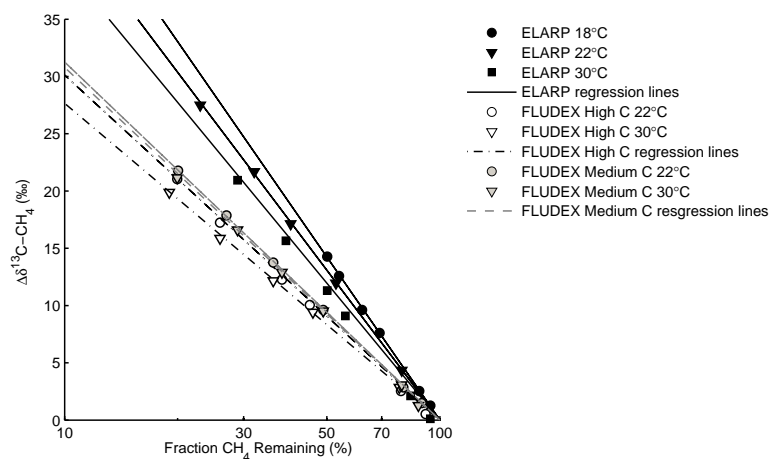


Figure 7.1: Rayleigh fractionation plot of the CH₄ oxidation incubations from ELARP and FLUDEX. The δ¹³C-CH₄ data are plotted as the difference between the initial and final δ¹³C-CH₄ to account for differences in initial δ¹³C-CH₄ between incubations.

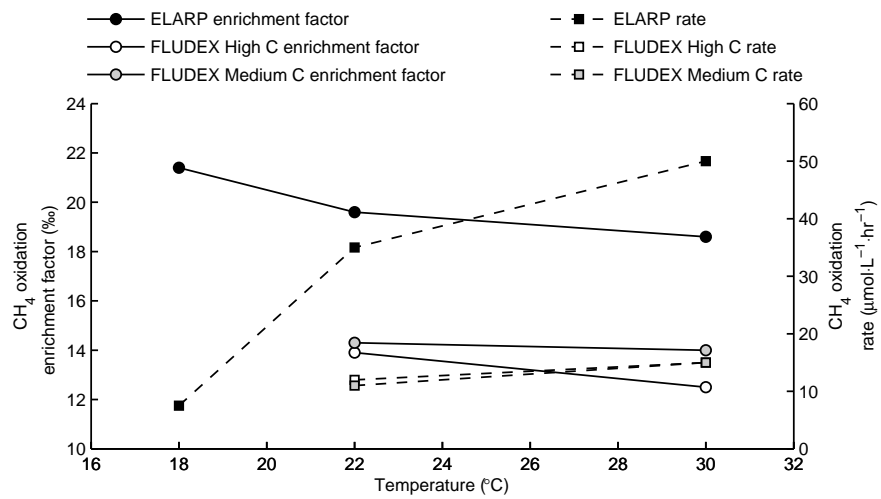


Figure 7.2: Temperature dependency of the CH_4 oxidation enrichment factor in ELARP, and FLUDEX High and Medium C reservoirs.

Table 7.1: Reservoir enrichment factors and fraction of CH₄ oxidised in ELARP and FLUDEX

Reservoir and location ^a	Incubation temperature (°C)	CH ₄ oxidation rate (µmol L ⁻¹ h ⁻¹)	Enrichment factor (‰)	Assumed initial isotopic ratio (‰)	Environmental isotopic ratio (‰) ^b	Fraction of CH ₄ oxidised (%) ^c
ELARP pond	18	7.5	21.4	-70	-38	79
ELARP pond	22	35	19.6	-70	-38	82
ELARP pond	30	50	18.6	-70	-38	84
FLUDEX High C reservoir	22	12	13.9	-70	-57 (2000)	63 (2000)
					-39 (2001)	90 (2001)
FLUDEX High C reservoir	30	15	12.5	-70	-57 (2000)	67 (2000)
					-39 (2001)	93 (2001)
FLUDEX Medium C reservoir	22	11	14.3	-70	-66 (2000)	26 (2000)
					-50 (2001)	78 (2001)
FLUDEX Medium C reservoir	30	15	14.0	-70	-66 (2000)	26 (2000)
					-50 (2001)	78 (2001)

^a $n = 3$ for each.

^b Environmental isotopic ratio observed in the ELARP pond, and as the net production of CH₄ in the FLUDEX reservoirs.

^c Calculated via Rayleigh equation (Equation (7.1)) using assumed initial isotopic ratio of CH₄ produced in site and enrichment factors from laboratory experiments.

Chapter 8

Direct comparison of two diffusive gas exchange methods in a low-wind environment

Abstract

To compare diffusive gas exchange methods, a trace gas was added to three low-wind aquatic ecosystems. Calculating the flux of gases between water and the atmosphere requires an accurate estimate of the gas exchange coefficient (k). The k was calculated using sulfur hexafluoride (SF_6) via both a trace gas spike to the whole ecosystem and by the flux rate of SF_6 into static flux chambers (SFCs). Comparisons of the two methods were made on three experimental boreal reservoirs. In this low-wind environment, k values were low, $< 1 \text{ cm h}^{-1}$ compared to small lakes, from about 1 cm h^{-1} to about 10 cm h^{-1} . SFC-derived k values were $2\text{--}8\times$ greater than whole reservoir k values. SFCs likely overestimated k by disturbing the surface boundary layer and by not being deployed during the lower wind-speed-periods that were typical overnight. SFCs are a poor choice for quantifying the diffusive gas exchange in a treed, low-wind environment.

8.1 Introduction

The radiative forcing of the atmosphere is increasing due to an increasing concentration of greenhouse gases (GHGs) (Farquhar *et al.*, 2001). The flux of these GHGs from natural and anthropogenic surfaces on the Earth to the atmosphere is both changing and increasing. Main freshwater sources of CO_2 and CH_4 to the atmosphere are lakes (Cole *et al.*, 1994), wetlands (Whiting and Chanton, 2001), rice paddies (Sass *et al.*, 1999; Watanabe *et al.*, 1999), and reservoirs (Bodaly *et al.*, 2004; Cullenward and Victor, 2006; St.Louis *et al.*, 2000).

Accurate measurements and reliable techniques are required to quantify the flux of different GHGs from aquatic surfaces to the atmosphere. Additionally, quantifying the flux of O₂ and CO₂ is important for ecosystem metabolism studies (*del Giorgio et al., 1999; Odum, 1956; Venkiteswaran et al., 2007*). There are many techniques used to estimate flux and, depending on conditions, some are better suited than others because each method relies on different sets of assumptions. Four common approaches are (i) trace gas additions, (ii) wind-speed-to-gas-exchange relationships, and (iii) static floating chambers (SFCs).

Trace gases, such as SF₆, have been used to directly measure k in lakes and oceans (*Cole and Caraco, 1998; Crusius and Wanninkhof, 2003; Wanninkhof et al., 1985, 1987*). Trace gases are chosen because they are believed to be biologically and chemically inert and thus only factors affecting gas exchange rates will affect them. The extremely low solubility of SF₆ allows k to be determined over short sampling periods. The out-gassing of SF₆ is used to calculate k for SF₆ over different timescales and the value obtained can then be converted for use with other gases. Trace gas studies are, however, limited to aquatic systems where the water column is well mixed and therefore the surface SF₆ concentration uniform. In aquatic systems where the water column is not well mixed, an advection-dispersion model coupled with an appropriate sampling regime has successfully been applied (*Ho et al., 2000*).

Wind speed to gas exchange relationships have been determined in wind and wave tunnels, large lakes, and the oceans (*Clark et al., 1996; Liss and Merlivat, 1986; Upstill-Goddard et al., 1990*). However, the wind speed to gas exchange relationship does not, by definition, include the influence of other environmental parameters, such as, rain, surface films, and bubble entrainment by large waves. At low wind-speeds (typically < 2–3 m s⁻¹), where these factors exert relatively more control on k , the wind-speed-to-gas-exchange relationship is expected to be less accurate at predicting k (cf. *Cole and Caraco, 1998*).

SFCs are often used to determine the net gas exchange between water and the atmosphere. They can be used to study spatial and temporal variability in gas exchange because of their small size and the brief period of time required for each measurement. However, floating chambers may cause several confounding problems when used to quantify gas flux, such as: changing the environment inside the chamber so that the effects of wind, waves, and rain on gas exchange are altered; depending on chamber design, water turbulence inside and below the chamber can be altered; chambers can trap bubbles escaping from the sediment; chambers can change the atmospheric pressure and temperature inside the chamber; and chambers only measure gas flux over a small surface area so scaling up chamber flux rates can create relatively large errors in estimates of gas exchange between the entire aquatic system and the atmosphere. These problems are often summarised as ‘chamber ef-

fects' and their relative importance varies between ecosystem and chamber design. Also, SFCs may not effectively determine the flux of gases from the atmosphere into the aquatic system, invasion, because the concentration of the trace gas in the chamber may decline significantly during the period the chamber is deployed.

Kremer et al. (2003) describe the debate surrounding SFCs and summarise the conditions under which the SFC method will give estimates of short-term gas exchange that are more reliable than wind speed estimates. Further, they note that scale of interest is critically important since and SFCs are a well-tested method applicable over time scales of 1–3 h. They describe the ideal chamber as having a low profile and large water surface area to chamber volume ratio and note that a drifting chamber can disrupt the aqueous boundary layer. These characteristics do not necessarily describe ELA-style SFCs (cf. *Kelly et al., 1997; Matthews et al., 2003*).

Purpose

To determine the 'chamber effects' associated with ELA-style SFCs (*Kelly et al., 1997; Matthews et al., 2003*), a direct comparison between whole-ecosystem-derived k values and SF_6 flux rates from SFCs was made. This whole-ecosystem experiment presents a unique opportunity to evaluate the ability of SFCs to quantify k of trace gases in a low-wind environment. The experiment permits the introduction of a tracer over a large scale, fast flushing rates promote tracer mixing, and hydrologic budgets can be well constrained.

8.2 Site description and methods

Study sites

The comparison was performed in the three reservoirs of the Flooded Upland Dynamics Experiment (FLUDEX) at the ELA in northwestern, Ontario, Canada. FLUDEX was established to study GHG cycling within three upland boreal reservoirs with differing stores of organic carbon (*Bodaly et al., 2004*). The reservoirs were named based on their pre-flood organic carbon stores and designated as: High, Medium, and Low Carbon (C). Determining the net flux of CO_2 and CH_4 from the reservoirs to the atmosphere was one of the main goals of the experiment (*Matthews et al., 2005*, Chapter 2).

Reservoirs were created by building polypropylene-lined wooden and earthen dikes along three side of the reservoir and thereby allowing flooding against the natural slope. The reservoirs were small (< 1 ha), had a short water residence time (6.0–10.6 d during this study period), and were expected to be low wind-speed environments because of trees remaining in the reservoirs and surrounding forests (Table 8.1). The reservoirs were flooded from late May to late September for five years (about 113 d a^{-1} , 1999–2003) by con-

tinuously pumping water from a nearby oligotrophic lake. The comparison experiment was performed in mid-July 2003 when there was little precipitation and the water level of the reservoirs was constant (K. G. Beaty, unpublished data.).

Collection and Analysis of SF₆ Concentration in Surface Samples

Surface water samples for SF₆ concentration were collected in glass serum bottles fitted with rubber stoppers (previously baked at 60 °C for at least 12 h). Bottles were filled just below the surface (wrist depth) and sealed with the aid of a needle to eliminate any trapped air. A 5 mL headspace of ultra-high purity N₂ gas was added before analysis. To prevent any gas loss, samples were kept inverted. Atmospheric pressure and water temperature were recorded.

Samples for SF₆ concentration were analyzed on the same equipment described by *Matthews et al. (2003)*. Briefly, samples were shaken to equilibrate, and a sub-sample of the headspace was injected into a Varian 3800 gas chromatograph with an electron capture detector at 300 °C and 90 % argon and 10 % CH₄ carrier gas through a 5 Å molecular sieve column at 80 °C. Standardisation was done to ensure that the instrument was performing consistently but not to calculate absolute SF₆ concentration.

Determining k from a whole reservoir SF₆ spike

To determine k , SF₆ is added to a water body and it quickly moves from the water to the atmosphere due to its high insolubility. The resulting decline in concentration has been used to determine k in a variety of systems (*Clark et al., 1994, 1996; Ledwell et al., 1986; Wanninkhof, 1992; Wanninkhof et al., 1985, 1987; Watson et al., 1991*) including lakes and reservoirs at ELA (*Crusius and Wanninkhof, 2003; Matthews et al., 2003*). Since the FLUDEX reservoirs are flow-through systems, SF₆ in the reservoirs is continually diluted by the inflow and lost via the outflow. The effect of dilution has previously been determined for systems with a constant water volume (*Ho et al., 2000*), where the SF₆ concentration is described by an exponential function:

$$C(t) = C_0 \times e^{-\left(\frac{P}{V} + \frac{k}{h}\right)t} \quad (8.1)$$

where $C(t)$ is the SF₆ concentration at time t , C_0 is the initial concentration, P is the pumping rate of water into the reservoirs (mL h⁻¹), V is the volume of the reservoir (mL), k is the gas exchange coefficient (cm h⁻¹), and h is the mean depth of the water (cm). In this case, P was measured daily using an inline flow meter. A continuous stage-level recorder at the outflow V-notch-weirs indicated that V was constant during the experiment in all reservoirs and there was little precipitation during the experiment (K. G. Beaty, unpublished data). Equation 8.1 was solved for k via two methods: (i)

the initial–final method using only initial and final SF₆ concentrations (as per [Matthews et al., 2003](#)) and (ii) the curve-fitting method to minimise the sum of squared errors between the curve and all SF₆ concentrations. The two-point method was used to calculate daily k values and a single 10 day- k .

The k determined for SF₆ evasion from the reservoirs can be converted to use with other relevant gases and at different temperatures. The k of different gases has been shown to be directly related to the inverse of the ratio of their Schmidt numbers (Sc , the ratio of the kinematic viscosity of water to the diffusion coefficient of the gas in water) to some exponent n ([Jähne et al., 1987](#)). The reported value of k is often normalized to a Sc number of 600, the Sc for CO₂ at 20 °C in freshwater:

$$k_{600} = k_{\text{SF}_6} \times \left(\frac{600}{Sc_{\text{SF}_6}} \right)^n \quad (8.2)$$

where k_{600} is the gas exchange coefficient for a Sc of 600, k_{SF_6} is the gas exchange coefficient prior to conversion, 600 is the Sc against which the data are converted, Sc_{SF_6} is the Sc of SF₆, and n is -0.67 . The value of n is related to the surface conditions of the water where n is -0.5 for free surfaces and -0.67 for rigid surfaces ([Jähne et al., 1984](#)). Sc can be estimated from a best-fit formula derived by ([Wanninkhof, 1992](#)):

$$Sc_{\text{SF}_6} = 3255.3 - 217.13T + 6.83707T^2 - 0.086070T^3 \quad (8.3)$$

where T is temperature in degrees Celcius. Reservoir surface temperature was logged at 5 min intervals using thermocouple wire (Cu/Cu-Ni), a CR10 datalogger and CR10TCR thermocouple reference. Temperature data collected 24 h prior to sampling was used to calculate Sc_{SF_6} .

SF₆ addition

Two 2 L polyethylene terephthalate bottles were half-filled with reservoir inflow water and compressed to remove the remaining air. Each bottle was capped with a rubber stopper and the remaining 1 L was filled with pure SF₆. The bottles were shaken for two minutes to dissolve SF₆ into the water. The water was subsequently emptied into the reservoir, approximately 10 cm below the surface, from a canoe as the canoe was paddled around the reservoir. This process was repeated twice for each bottle. Previous SF₆ addition experiments have indicated that SF₆ concentrations at the surface were uniform within 4 d ([Matthews et al., 2003](#)). Surface water samples were collected daily from the same six locations as the SFCs and from the inflow and outflow of each reservoir as described above.

Determining gas exchange with static floating chambers

SFCs (16.4 L) were made from polycarbonate drinking water bottles with the flat bottom removed. The chambers were held afloat by a Styrofoam sheet (45 cm × 45 cm × 3 cm) affixed to the bottom of the bottle so that the bottle was held flush with the surface of the water. The chambers were capped with a rubber stopper and a Vacutainer stopper was fitted into a side port for gas sampling via tubing, needles, 3-way valves, and syringes. Chambers were dried with paper towels and flushed with air before being set on the water surface. Six chambers were placed on the reservoir surface each day for two consecutive days in each reservoir in mid-July 2003. Chambers were deployed for approximately 60 min, longer than in some studies, because k was known to be very low (Matthews *et al.*, 2003). Samples of gas for concentration analysis were drawn from the chambers at approximately 0, 30, and 60 min by a 5 mL syringe with a 3-way valve and needle. Gas samples were stored in 4.5 mL Vacutainers (stoppers were previously baked at 60 °C for at least 12 hr). SFC samples were analyzed within 3 months on the Varian system described above. Previous studies indicate that storage does not affect the sample over this time.

SF₆ chamber concentrations were linearly regressed against time to determine gas flux rates of SF₆ out of the reservoir and the strength (r^2) of that relationship. Data from individual SFCs was not used in overall flux estimates if the r^2 of the regression was < 0.85. Evidence of ebullitive flux of GHGs from the sediments is normally used to omit data from individual SFCs based on the rapid increase in CH₄ and CO₂, however analysis of SF₆ in bubbles probed from the sediments indicate that ebullition did not affect the concentration of SF₆ in SFCs. Also, dilution of SF₆ in the SFC by 10 mL of bubbles would be negligibly small (< 0.1 % of SFC volume).

The initial SFC concentration of SF₆ was expected to be above the average atmospheric concentration, approximately 6×10^{-12} mol/mol based on published annual rates of increase (Maiss and Brenninkmeijer, 1998), due to degassing from the reservoirs. Initial SFC concentrations were deemed acceptable if they were within 20% of the mean initial concentration of all chambers deployed on that reservoir.

To compare the SFCs with the whole reservoir SF₆ spike, the average SFC flux rates were converted to k values. Using the flux rate from the SFCs and the surface concentrations measured concurrent with the SFC, k was determined as:

$$k = \frac{F}{C_{surface}} \quad (8.4)$$

where k is the gas exchange coefficient (cm hr⁻¹), F is the SFC flux rate (SF₆ cm² hr⁻¹), and $C_{surface}$ is the surface SF₆ concentration. The SF₆ concentration in water at solubility equilibrium with the atmosphere is negligibly small

compared to the surface SF₆ concentration after the SF₆ spike and therefore was set to zero.

A comparison between k values is more relevant than flux rates in these reservoirs because k values will ultimately be used to calculate the evasion rates of CO₂ and CH₄ (Matthews *et al.*, 2005, Chapter 2) and the invasion rates of N₂O and O₂ (Hendzel *et al.*, 2005; Venkiteswaran *et al.*, 2007).

8.3 Results

Determining k from Whole Reservoir SF₆ Spike

Three to four days after the SF₆ spike, the surface SF₆ concentrations were generally within 10–20 % of each other in the High and Low C reservoirs and 5–15 % in the Medium C reservoir at the 6 sampling locations in each reservoir. Similar variations have been observed during previous SF₆ spikes of the Medium C reservoir (Matthews *et al.*, 2005). Although spatial variability has been small in some lakes (2 % in the epilimnion of a 12.8 ha lake basin (Crusius and Wanninkhof, 2003) and < 3.2 % in a 15 ha lake (Cole and Caraco, 1998)), it has been larger in other sites (occasionally > 40 % in a 14 ha lake (Upstill-Goddard *et al.*, 1990) and about 15 % along the shore of a 1.7 ha reservoir (Frost and Upstill-Goddard, 2002)). The SF₆ in FLUDEX reservoirs was as well mixed as in other ecosystems and thus determining k from the SF₆ decline is not precluded.

Daily decreases in SF₆ concentration were measured in all reservoirs and the decrease was large enough that after correcting for inflow, all but 3 daily k values were positive (indicating a net flux of SF₆ from the reservoirs to the atmosphere). Over 4–8 d, the decline in SF₆ concentration was about one order of magnitude. The k values determined daily, over 10 d by both initial–final and curve-fitting methods were all < 1 cm hr⁻¹ (Table 8.2) as they were in 2001 (Matthews *et al.*, 2003)

The SF₆ concentrations declined quickly in the first 4 days and then more slowly in the subsequent 5 days (Figure 8.1). As a result, the curve-fitting of the High C reservoir data appears to overestimate the SF₆ concentrations in days 2–4 and underestimate in days 5–9. When the SF₆ data are divided and analyzed as two separate sets of data (days 0–4 and days 4–10) a k_{600} value can be calculated for each set of data (Figure 8.2). The k_{600} for days 0–4 is 1.47 cm hr⁻¹ and for days 4–10 is 0.28 cm hr⁻¹. This first value is twice that from curve-fitting of all the SF₆ data (0.75 cm hr⁻¹), but the second value is 2.6× smaller than the 10 d k_{600} value. However, there were no changes in pumping rate, reservoir volume and depth, or weather during this time.

A comparison of k_{600} values calculated via the initial–final and curve-fitting methods is warranted. In this experiment, the k_{600} values calculated via both methods were different for the Medium and Low C reservoirs (Table 8.2). In 2000–2001, average k_{600} values of 0.70 cm hr⁻¹, 0.49 cm hr⁻¹,

0.91 cm hr⁻¹ for a total of 10 different 4-day spikes in the High, Medium, and Low C reservoirs were calculated using the initial-final method (Matthews *et al.*, 2003). Recalculating the k_{600} values using the curve-fitting method, and thus using all the field data instead of only initial and final data, yielded average k_{600} values of 1.26 ± 0.14 cm hr⁻¹, 0.98 ± 0.14 cm hr⁻¹, 1.66 ± 0.23 cm hr⁻¹ (mean \pm SE, $n = 10$). All but one of the fits had an $r^2 > 0.94$. That these recalculations are 45–50 % higher than the initial-final methods suggested that the calculation was susceptible to small changes in the initial and final concentration measurements and thus curve-fitting with all the data was more appropriate.

Equation 8.1 contains components to account for the constant input of SF₆-free water into the reservoirs. If a large proportion of the decline in SF₆ concentration were due to this constant input and not due to gas exchange, then these experiments would have only been assessing how well reservoir hydrology can be measured. In Equation 8.1, $\frac{P}{V}$ contributed 28, 43, and 56 % to the decline in SF₆ in the High, Medium, and Low C reservoirs.

Determining k from SFCs

More than half of the SFC data met the criteria to be used in determining k . The range of k_{600} from individual SFCs was 0.09–25.1 cm hr⁻¹. When pooled by reservoir, the k_{600} were 1.42 ± 0.35 cm hr⁻¹, 5.52 ± 2.13 cm hr⁻¹, and 5.41 ± 3.67 cm hr⁻¹ (mean \pm SE, $n = 7$, for each reservoir) for the High, Medium, and Low C reservoirs.

8.4 Discussion

Comparing the two SF₆ approaches

The SFC-derived k_{600} was 7.5 to 8× greater than the spike-derived k_{600} in the Medium and Low C reservoirs and twice the spike-derived k_{600} in the High C reservoir (based solely on mean value). Further, the uncertainty associated with the SFC-derived k_{600} was greater than the spike-derived k_{600} .

It has been noted that only SFCs can be used to assess the changes in k over the short terms that are necessary for some types of metabolism studies (Kremer *et al.*, 2003). Since the SF₆ spike required several days for the SF₆ concentration to decline sufficiently, the more variable SFC-derived k_{600} values may be partly a result of the difference in time scales and a measure of the short-term k_{600} . Given the stated goals of FLUDEX—determining GHG fluxes and cycling over five years—a more integrative measure of k_{600} is appropriate.

Sources of error associated with the Whole-Reservoir SF₆ Spike

Whole-reservoir SF₆ spikes require that: the SF₆ tracer is fully mixed; the surface concentration of SF₆ be uniform; and the inflows and outflows be well characterised. If these conditions are met, then the decline in SF₆ concentration will be directly related to gas exchange, thus providing k . The FLUDEX reservoirs were flow-through systems with water renewal times that were slightly shorter than the duration of the SF₆ spike. It is likely that the rate of renewal increased the variability of the surface SF₆ concentrations above that previously reported in small lakes (e.g., *Crusius and Wanninkhof, 2003*). In larger systems, or systems where inflow is much less important than in the FLUDEX reservoirs, the relative error associated with measurement of water inflow and outflow would be much smaller. If the reservoirs were not adequately mixed with respect to SF₆ concentration, then the correction term for dilution would have accounted for too large a portion of the decline in SF₆ concentration. This would effectively underestimate the calculated k value. The uncertainty associated with complete mixing and dilution is reduced in this experiment since the duration of the experiment was close to the flushing rate of the reservoirs and thus the calculated dilution could be estimated.

Significant disruptions to reservoir surfaces such as rain induced turbulence would have increased the k value. However, there was only 34.3 mm of rain recorded at the ELA meteorological site during the experiment and one-third of that fell during one event. The effect of several small precipitation events is likely to be small relative to other sources of error. The effect of the one large (13.9 mm) precipitation event would be to increase the 1 d- k value on that day, however this effect is not seen in the SF₆ data (Figure 8.1). The 10 d- k value would have been much less affected.

Other potential losses of SF₆ are diffusion into sediments and co-ebullition with sediment-formed gases such as CH₄ and CO₂ (*Wanninkhof, 1992; Wanninkhof et al., 1985*). Adsorption of SF₆ to sediments has been demonstrated to be weak (*Wanninkhof et al., 1985; Watson et al., 1991*). The diffusion coefficient of SF₆ into sediments can be estimated as $D \times \phi^2$, where D is the diffusivity of SF₆ and (ϕ) is the average porosity of the soils. At a measured soil temperature of 20 °C, diffusivity is about $1.05 \times 10^{-5} \text{ cm}^2 \text{ s}^{-1}$ (*King and Saltzman, 1995*). Using a conservative average soil porosity of 0.5, the diffusion coefficient would have been $< 0.01 \text{ cm hr}^{-1}$ and smaller than errors associated with the hydrological measurements (*Winter, 1981*). Ebullition rates, measured with bubble traps (cf. Chapter 3), during the SF₆ spike were $44.4 \pm 23.9 \text{ mL m}^{-2} \text{ d}^{-1}$, $37.8 \pm 16.9 \text{ mL m}^{-2} \text{ d}^{-1}$, and $5.2 \pm 3.1 \text{ mL m}^{-2} \text{ d}^{-1}$ of gas (mean \pm SE, $n = 10$, $n = 8$, and $n = 10$), about one order of magnitude smaller than the rate required to alter the k by only 0.01 cm hr^{-1} . Further, analysis of bubbles indicates that SF₆ concentration of bubbles was less than the detection limit ($< 1 \times 10^{-9} \text{ mol/mol}$). In general, the sources of error surrounding the spike-derived k_{600} were relatively small and thus the

spike-derived k_{600} provided a good basis for comparison with SFCs.

Sources of error associated with SFCs

Several factors will affect SFC-derived k_{600} values and they can be summarised as factors affecting the validity of the assumptions inherent in chamber work and climatic factors affecting the chambers. Chamber effects will manifest themselves in different ways and can increase or decrease the SFC-derived k_{600} values. The walls of the ELA-style chamber do not extend below the surface of the water. In chambers where the walls do extend below the surface of the water, the effect can be to either increase turbulence at the air-water interface and thus to increase k or to trap a pocket of water under the chamber and thus to decrease k .

ELA-style chambers are approximately 60 cm tall and thus can easily be disturbed by the wind. To reduce the amount of movement of SFCs on reservoir surfaces, the SFCs were tethered using ties to trees on opposite sides of the SFC. Chamber movement would increase k because of increased turbulence in the water just below the air-water interface. In systems with greater wind speed and larger waves than the FLUDEX reservoirs, chamber-induced turbulence may be unimportant.

The time-of-day when the SFCs were deployed may have skewed the SFC-derived k values upward. Wind speed at the surface of the FLUDEX reservoirs has been shown to be very slow, typically $< 1 \text{ m s}^{-1}$ (Matthews *et al.*, 2003). However, wind speed is lower at night and the SFC data were collected during the late morning and mid-afternoon (Matthews *et al.*, 2003). Nevertheless, this is a potential problem with deploying any manual SFCs because of the logistics and difficulty of nighttime deployment. Also, the SFCs were not shielded from the sun and therefore the temperature of the air in the SFCs may have increased during the 60 min deployment. Solar heating of the surface water may increase turbulence at the surface of the water due to convective currents from evaporation and heating.

For the purpose of this study, wind speed measured at the ELA meteorological site, about 1 km west of the FLUDEX reservoirs, was used to estimate the potential impact of differential wind speed during diel cycles. Although, these wind speeds will be greater than, and may vary more than, at the surface of the FLUDEX reservoirs (since the meteorological anemometer is 10 m above the ground surface in a clearing of $120 \text{ m} \times 55 \text{ m}$), these data provide a means to assess daytime versus nighttime wind speed effects. During the experiment, average hourly daytime (06:00–22:00) wind speed was 2.5 m s^{-1} ($SD = 3.9$, $SE = 0.005$) and average hourly nighttime (23:00–05:00) wind speed was 2.0 m s^{-1} ($SD = 3.6$, $SE = 0.001$). The hourly groupings were chosen based on sunrise and sunset and thereby account for increased wind speed during the daytime caused by differential heating of the landscape. Wind speeds were expected to be much lower at the reservoirs surface due

to the surrounding forest acting as a windbreak. Wind speeds measured previously at 1 m above the reservoir surface were much lower and different between day ($0.24 \pm 0.02 \text{ m s}^{-1}$) and night ($0.080 \pm 0.02 \text{ m s}^{-1}$) (Matthews *et al.*, 2003). This observation suggested that diel wind patterns may be a confounding factor when comparing whole reservoir spikes and SFC-derived k values.

In order to facilitate sampling, transects were cut through the forests of the FLUDEX reservoirs prior to flooding. To reduce the effects of transects, SFCs were placed about 1–2 m into the forest, though some areas of the reservoirs were inaccessible by boat and SFCs could not be deployed there. SFCs were placed in representative shallow and deep areas and in areas of sparse and dense forest in all three reservoirs.

The variability in SFC-derived k values was large even though the surface SF_6 concentrations (and CO_2 and CH_4 concentrations measured at the same time) were relatively uniform across a given reservoir. The SFC flux rates and SFC-derived k values did not correlate with water depth or density of trees.

Estimating k at low wind speeds

Cole and Caraco (1998) compared two well-known wind speed to gas exchange relationships with their low-wind- SF_6 -derived k_{600} values and found that both the tri-linear model of Liss and Merlivat (1986) and the power function of Wanninkhof (1992) underestimated k_{600} at measured wind speeds of $1\text{--}2 \text{ m s}^{-1}$. By combining and binning data from 10 lakes, they developed a power function with a constant offset such that at very low and zero wind speeds k_{600} is approximately 2 cm hr^{-1} .

Crusius and Wanninkhof (2003) assessed three types of relationships between k and wind speed (at 10 m height). Of two bilinear functions, they propose a 0.72-times-wind-speed and a constant k of 1.0 cm hr^{-1} at wind speeds $< 3.7 \text{ m s}^{-1}$. The power function has a small (0.168 cm hr^{-1}) offset for no wind. All provided good fits with the field data but Crusius and Wanninkhof (2003) concluded that there was no strong dependence of k on low wind speeds ($< 3.7 \text{ m s}^{-1}$ at 10 m height). This follows theoretical predictions (Deacon, 1977) and the strong dependence on wind speeds $> 3.7 \text{ m s}^{-1}$ is a result of the onset of capillary waves (Jähne *et al.*, 1984). Using the ELA meteorological-site data and previously measured wind speeds (a range of $1.0\text{--}2.5 \text{ m s}^{-1}$, (Matthews *et al.*, 2003)), the power function predicts k_{600} of $0.4\text{--}1.9 \text{ cm hr}^{-1}$, and the bilinear functions predict k_{600} of $0.7\text{--}1.8 \text{ cm hr}^{-1}$ and simply 1.0 cm hr^{-1} .

The k values from FLUDEX reservoirs in 2000–2001 ($0.98\text{--}1.66 \text{ cm hr}^{-1}$) and 2003 ($0.67\text{--}0.75 \text{ cm hr}^{-1}$) were at the lower end of those predicted by the equations of Crusius and Wanninkhof (2003). Clearly both the present data and those of Matthews *et al.* (2003) indicate that at very low wind speed (about 0.3 cm hr^{-1} at the water surface, $2.0\text{--}2.5 \text{ m s}^{-1}$ at 10 m height) k_{600} is much

lower than 2 cm hr^{-1} (Cole and Caraco, 1998) and closer to the three models of Crusius and Wanninkhof (2003).

Implications for FLUDEX reservoirs

The strength of the goodness-of-fit ($r^2 > 0.94$) of the SF_6 concentration data to the curve fitting of Equation 8.1 indicates that the shallow, flow-through nature of the FLUDEX reservoirs was not an impediment to mixing. In GHG studies of these reservoirs care was taken to measure the variability of concentrations at the reservoir surface and in vertical profiles (Hendzel et al., 2005; Matthews et al., 2005, Chapter 2). A large deviation from the constant-level model of Ho et al. (2000) would have indicated that the reservoirs were not well mixed and as such the model would have been inappropriate for determining k in these reservoirs. The SF_6 data provided good evidence that the FLUDEX reservoirs were, in fact, well mixed and that it was therefore possible to (i) use the model of Ho et al. (2000) and (ii) make simplifying assumptions about GHG fluxes (e.g., Matthews et al., 2005, Chapter 2).

General Conclusions

The trace gas approach for determining k worked well in the FLUDEX reservoirs. It was comparatively easier to perform whole-reservoir spikes of SF_6 rather than repeated SFC measurements. The spike approach was also advantageous as it removed the variabilities of water depth and tree density and integrated diel patterns of wind and water surface conditions. Further, measurement of other important biogeochemical gases such as CO_2 , CH_4 , N_2O and O_2 could be made simultaneously using the sample bottle for surface SF_6 concentration or by collecting a second sample bottle at the same time.

In flow-through systems, the ability to determine daily k values can be compromised by the slow rate of gas exchange and heterogeneity caused by dilution from continuous inflow. This suggests that sampling many locations at a high frequency is a requirement for interpreting the SF_6 data. As long as dilution can be accounted for by adequate measurements, trace gas spikes are a feasible method for determining k in flow-through systems.

SFCs are commonly used in ecosystems similar to FLUDEX reservoirs. However, comparing SFC and whole-reservoir results confirms that ELA-style SFCs over-estimate k in some low wind-speed environments. Although the wind-induced turbulence of the SFCs was likely less in FLUDEX than in small lakes, other factors such as diel wind and temperature changes, differential heating of reservoir water, and greater water turbulence under the SFCs than in the open reservoir likely contributed to the greater k and larger variability associated with SFCs than whole reservoir trace-gas spikes.

Acknowledgments

A. M. Wojtyniak and K. T. Maurice provided enthusiastic field and laboratory assistance. R. J. Elgood provided logistical support. C. J. D. Matthews kindly provided SF₆ concentration data from 2000–2001. This research was funded by the Canadian Foundation for Climate and Atmospheric Sciences, the Natural Sciences and Engineering Research Council of Canada, Fisheries and Oceans Canada, and an Ontario Graduate Scholarship. Environment Canada's Science Horizons Youth Internship Program funded a laboratory assistant. Fisheries and Oceans Canada, Manitoba Hydro, and Hydro-Québec funded FLUDEX.

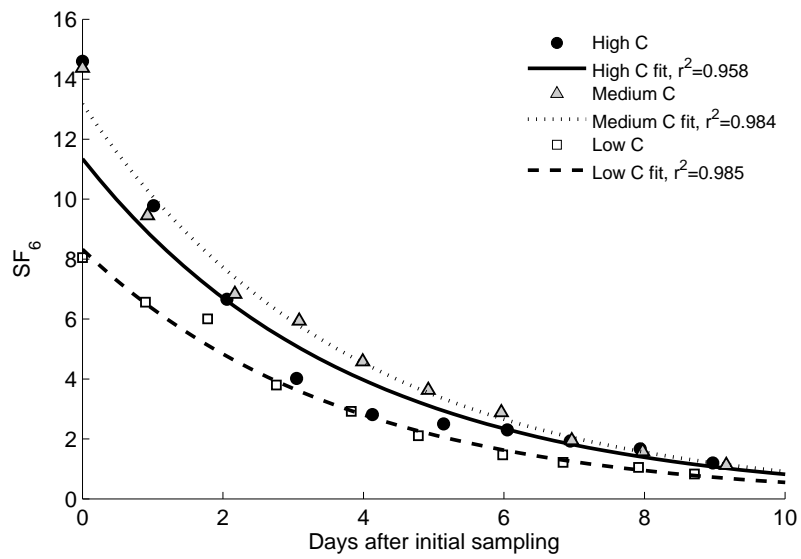


Figure 8.1: Surface water SF_6 concentrations in the three FLUDEX reservoirs in July 2003. Each symbol represents the mean SF_6 concentration measured that day ($n = 6$ per symbol, SE bars are approximately the size of the symbols). Regression curves are based on a best-fit of Equation 8.1.

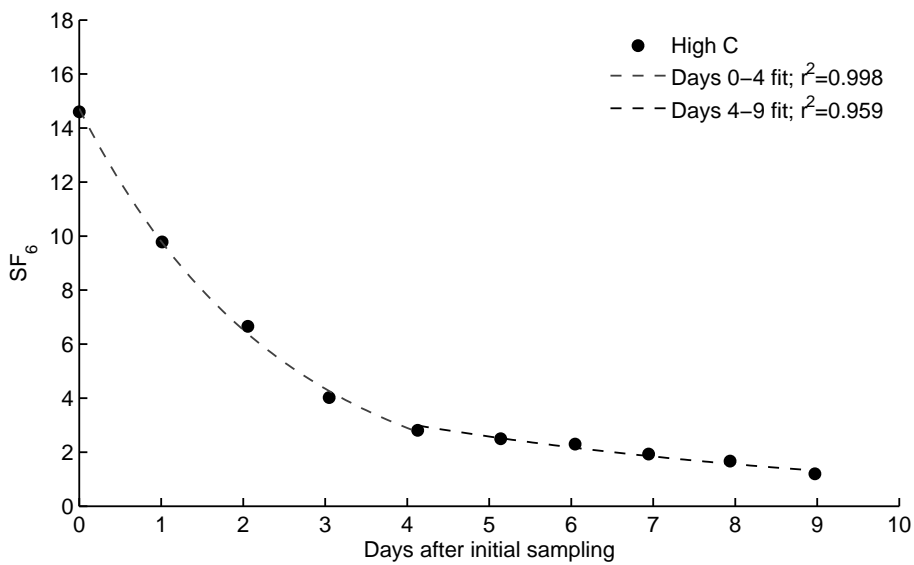


Figure 8.2: Surface water SF₆ concentration in the High C FLUDEX reservoir in July 2003. Each symbol represents the mean SF₆ concentration measured that day ($n = 6$ per symbol, SE bars are approximately the size of the symbols). Regression curves for days 0-4 and days 4-9 are based on best-fits of Equation 8.1.

Table 8.1: Physical characteristics of FLUDEX reservoirs in 2003.

	High C	Medium C	Low C
Water Surface Area (m ²)	6400	5000	6300
Upland Catchment Area (m ²)	47800	7300	900
Reservoir Volume (m ³)	6870	4270	7120
Residence Time (d) ^a	9.6	7.4	6.7
Mean Depth (m) ^b	0.9	0.9	1.1

^a Reservoir Volume ÷ (Total Inputs ÷ Total Days)

^b Reservoir Volume ÷ Water Surface Area

Table 8.2: FLUDEX reservoir k_{600} values.

Reservoir	Whole Reservoir SF ₆ Spike (cm hr ⁻¹) (initial-final method, 10 d)	Whole Reservoir SF ₆ Spike (cm hr ⁻¹) (curve-fitting method, 10 d)	Whole Reservoir SF ₆ Spike (cm hr ⁻¹) (mean ± SE, n = 9, 1 d values)	Static Floating Chamber (cm hr ⁻¹) (mean ± SE, n = 7)
High C	0.83	0.75	0.81 ± 0.24	1.42 ± 0.35
Medium C	0.73	0.67	0.72 ± 0.13	5.52 ± 2.13
Low C	0.65	0.71	0.64 ± 0.21	5.41 ± 3.67

Chapter 9

Greenhouse gas and dissolved organic carbon production in shallow zones of boreal reservoirs

Abstract

Hydroelectric reservoirs provide almost a quarter of Canada's installed electrical generating capacity. Understanding the effects of flooding vast areas of land, particularly in the boreal forest, is an important part of cost-benefit analyses of reservoir construction. The medium-term (10 a and 20 a) fluxes of carbon from boreal reservoirs are not well known. This is due, in part, to a lack of study and the difficulty and expense of in-depth multi-year whole-ecosystem research projects. To determine the changes in carbon fluxes from boreal reservoirs, one wetland (ELARP) and three upland (FLUDEX) experimental reservoirs were studied before and after flooding. Research from these reservoirs on greenhouse gas fluxes, mercury cycling and bioaccumulation, and dissolved organic carbon production has been published. Here, all research on CO₂, CH₄, and dissolved organic carbon from these two reservoir projects was combined to estimate the carbon flux rates from the ecosystems over one to two decades. Flux rates of CO₂ and CH₄ from the wetland reservoir increased several fold as a result of flooding and remained elevated for at least a decade. Upland reservoir flux rates of CO₂ peaked in the first year of flooding and declined thereafter while CH₄ flux rates peaked in the third year of flooding and declined rapidly thereafter. Flux rates of both gases from the upland reservoirs were lower by at least one-third than from the wetland reservoir. The flux rate of dissolved organic carbon was greater from the upland reservoirs than from the wetland reservoir and remained elevated, whereas the dissolved organic carbon flux rates from the wetland reservoir declined to pre-flood levels within a decade. Elevated flux rates of CO₂ and CH₄ from the wetland reservoir are projected to continue for decades while much lower rates were observed from the

upland reservoirs after less than a decade. The proportion of wetland and upland areas and reservoir temperature regime are important factors affecting the magnitude and longevity of CO₂, CH₄, and dissolved organic carbon fluxes from boreal reservoirs.

9.1 Introduction

The flooding of boreal landscapes drastically alters the cycling and storage of carbon (C) and greenhouse gases (GHG). Boreal reservoirs vary in their flooded areas and depths as well as the proportion of flooded upland to flooded wetland. As a result, comparing data from different reservoirs and reservoirs of different ages has been problematic (*St.Louis et al., 2000*).

The construction of reservoirs converts boreal forest and wetland ecosystems that are typically C sinks or C neutral into reservoir surfaces that are GHG sources to the atmosphere. The length of time these reservoirs remain a source of GHGs and the magnitude of that GHG source has been the subject of much study and controversy. Some studies suggest that GHG emissions are short-term and will decrease rapidly with reservoir age as the portion of labile soil and vegetation organic C (OC) decomposes (e.g., *Tremblay et al., 2005*). Whereas other studies suggest that GHG emissions can remain elevated for decades and possibly centuries, related in part to the large stores of OC that were present before flooding (*Kelly et al., 1997; St.Louis et al., 2000; Taddonléké et al., 2005*).

Two whole-ecosystem experiments were conducted in order to study GHG fluxes from and C cycling within boreal reservoirs with different types and amounts of stored OC. The main GHG goal of ELARP (the Experimental Lakes Area Reservoir Project) and FLUDEX (the Flooded Upland Dynamics Experiment) was to test the hypothesis that pre-flood OC stores were predictors of post-flood GHG fluxes. The important processes in the shallow zones of upland boreal reservoirs were extensively studied in FLUDEX for five years (*Bodaly et al., 2004; Matthews et al., 2005*, Chapters 2, 3, and 6,). Similarly, the shallow wetland boreal reservoir, ELARP, was extensively studied for ten years (e.g., *Kelly et al., 1997; St.Louis et al., 2004*). These experiments represented two end-members on the boreal forest landscape: young, upland forests and old peatlands. Together, they can be used to test the hypothesis of OC stores and longevity of GHG fluxes.

In addition to GHGs, the net production of dissolved OC (DOC) and dissolved inorganic C (DIC) will be examined to determine the DIC:DOC ratio produced by upland and wetland flooding. The fate of some portion of DOC produced by reservoirs is microbial and/or photocatalytic decomposition to DIC and is available to be lost to the atmosphere as CO₂. Furthermore, there is a positive relationship between DOC export and methylmercury export (*St.Louis et al., 2004*) and, in drinking water reservoirs, elevated DOC concen-

trations make disinfection by chlorination difficult because of the increased chemical demand for chlorine, the production of carcinogenic organochlorine by-products, and the encouragement of microbial growth (cf. *Davies and Mazumder, 2003*).

Here, the available data from two reservoir experiments were compiled and compared to determine the differences between flooding of uplands and wetlands. Experimental results were used to produce a descriptive model of GHG emissions from ELARP and FLUDEX. The ultimate goal was to develop a series of equations that describe the changes in GHG fluxes with time as a result of flooding. These equations were then used to estimate the medium-term (10 a and 20 a) GHG fluxes to the atmosphere from the ELARP and FLUDEX reservoirs.

9.2 Methods

Field sites

The ELARP and FLUDEX reservoirs have been extensively studied and their descriptions are published elsewhere (*Asada et al., 2005; Bodaly et al., 2004; Kelly et al., 1997*). Detailed GHG research has been published (*Asada et al., 2005; Hesslein et al., 2005; Matthews et al., 2005; McKenzie et al., 1998; Poschadel, 1997; Saquet, 2003; Scott et al., 1999*) and is presented in Chapters 2 and 3. This chapter seeks not to republish data but to extend the GHG and DOC summaries of ELARP (*Asada et al., in prep; St.Louis et al., 2004*) and combine them with the GHG and DOC data of FLUDEX (Chapter 2; *Schiff, in prep*).

Both ELARP and FLUDEX reservoirs were built at the Experimental Lakes Area (ELA) in northwestern Ontario (49°40' N 93°45' W) where the boreal forest typically contains forests, wetlands, and numerous small lakes. ELARP consisted of a 2.39 ha pond (L979) and its surrounding 14.4 ha peatland. Average peat thickness was 1.7 m and radiocarbon dating at the bottom of the 9.1 m of organic sediments in the pond indicated that OC had been accumulating since 9200 radiocarbon years before present. ELARP contained pond and peatland ecosystems that were reliant on inflow from upstream lakes. The water level of the pond was raised 1.3 m by damming the outflow in early-June 1993. To simulate the seasonal fluctuations of many boreal reservoirs, the water level was reduced to just above the pre-flood level each fall after about 150 d of flooding. The water level was raised again each spring for ten years by capturing the Spring freshet from the upstream oligotrophic Lake 240. Large sections of flooded peat began to float as a result of the buoyancy of trapped bubbles, which resulted from peat decomposition (*McKenzie et al., 1998; Scott et al., 1999*). Each successive year a greater portion of peat began to float until about 85 % of the initial peat surface area was floating by the tenth year (*Asada et al., 2005*). ELARP was designed to be a worst-case scenario of reservoir construction: a wetland in a shallow reservoir (*Kelly*

et al., 1997). GHG, DOC, and hydrology budgets for ELARP have been previously reported (*Hesslein et al.*, 2005; *Kelly et al.*, 1997; *Saquet*, 2003; *St.Louis et al.*, 2004).

The three FLUDEX reservoirs, with differing amounts of stored OC but with about 19 times less OC than ELARP, were flooded for about 113 d a^{-1} starting in late-May 1999 for five years (Table 9.1). In total, FLUDEX reservoirs contained five pre-flood soil and vegetation types but all reservoirs were all pond-like and received inflow pumped from a nearby lake at a constant rate. Further, given the similarities of both pre-flood OC stores and total post-flood C fluxes (Chapters 2 and 3), results from the FLUDEX reservoirs are grouped together to represent low OC stores.

Forest fires are a natural feature of the boreal forest. The ELARP catchment was burned in 1974. The FLUDEX catchment was logged in the 1970s. Both catchments were burned extensively in 1980. The effects of forest fires on wetlands, streams, and lakes at ELA have been described (*Bayley et al.*, 1992a,b). Analysis of soil cores indicates that all OC in the litter and fungal-humic layers was completely burned to charcoal in the 1980 forest fire. They were designed to mimic the shallow upland areas of boreal reservoirs where decomposition rates were believed to be greatest. To follow the seasonal water level fluctuations characteristic of the shallow zones of large boreal reservoirs, the reservoirs were completely drawn down each fall (*Bodaly et al.*, 2004). GHG, DOC, and hydrology budgets for FLUDEX reservoirs have been published (*Matthews et al.*, 2005; *Schiff*, in prep) and are presented in Chapters 2 and 3.

Generalised model of carbon cycling

ELARP and FLUDEX were studied at different spatio-temporal resolutions with different sampling methods covering different ecosystems. In ELARP, GHG fluxes from the pond surface to the atmosphere were estimated via concentration and wind speed as well as static floating chambers. GHG fluxes from the peatland surface were estimated via static chambers. These data were combined with hydrology and DOC concentrations to calculate GHG and DOC mass budgets.

In FLUDEX, GHG fluxes from reservoir surfaces to the atmosphere were estimated via concentration and SF_6 -derived gas exchange coefficients (k) (Chapter 8; *Matthews et al.*, 2003). Mass and isotope-mass budgets were calculated for each reservoir by combining GHG and DOC concentrations with $\delta^{13}\text{C}$ values and hydrology to calculate community respiration (CR) and net primary production (NPP), net CH_4 production, and DOC production. The common theme of ELARP and FLUDEX was to collect adequate data to calculate flood-season budgets of DIC, CH_4 , and DOC.

Using previously calculated budgets (Chapters 2 and 3; *Asada et al.*, in prep; *Hesslein et al.*, 2005; *Matthews et al.*, 2005; *Schiff*, in prep; *St.Louis et al.*,

2004), simple regression equations were developed to describe annual fluxes or production. The form of each regression equation was chosen so that major features of the data could easily be matched with a minimum number of parameters and negative values were prevented from being extrapolated. In general, this approach ruled out linear regressions and suggested exponential decay, power functions, and Gaussian regression curves.

A parsimonious approach was used to develop equations that describe the change in carbon fluxes after flooding. FLUDEX data had only five post-flood years and ELARP data five to nine. As a result, FLUDEX data sets with a clear year-after-year decline were modelled with either an exponential function of the form $y = a \times e^{b \times YAF} + c$ or a power function of the form $y = a \times YAF^b$, where y is the C flux, a , b , and c are constants, and YAF is years after flooding. Data sets with a clear up-and-down pattern were modelled with a Gaussian curve of the form $y = a \times e^{-\left(\frac{YAF-b}{c}\right)^2}$.

Flood-season lengths were different for FLUDEX and ELARP as a result of differences in hydrology; FLUDEX received water pumped uphill from a nearby lake, starting in late May or early June, for about 113 d a^{-1} , while ELARP received water from an upstream lake, starting at Spring melt, for about 152 d a^{-1} . Since CO_2 and CH_4 production are greatest occurs in the summer when water and peat temperatures are warmest, a result of the longer flood season in ELARP is that GHG flux rates are likely lower than if the flood seasons were identical between the two reservoir systems. Nevertheless, to compare ELARP and FLUDEX, data from entire flood seasons were used.

In previous publications of ELARP results, the pond and peatland surface were often treated separately (cf. *Asada et al., in prep*) or treated with different data sets at different time scales (cf. *Hesslein et al., 2005*). For FLUDEX, the three reservoirs are treated as upland replicates because their C fluxes over 5a were within in a few percentage points (Chapter 2) and pre-flood stores of total OC were similar relative to that of ELARP (Table 9.1). To estimate medium-term C cycling for both ELARP and FLUDEX, the following ecosystems processes and fluxes were modelled:

- upland community respiration (data from Chapter 2);
- upland net primary production (data from Chapter 2);
- upland net DIC production (data from Chapter 2);
- upland net CH_4 production (data from Chapter 2);
- upland CH_4 ebullition (data from Chapters 2 and 3);
- upland net DOC production (data from *Schiff (in prep)*);

- wetland pond surface CO₂ flux (data from *Hesslein et al. (2005)* and J. W. M. Rudd, C. A. Kelly, and V. L. St.Louis, unpublished data);
- wetland pond net DIC production (data from *Hesslein et al. (2005)*);
- wetland pond surface CH₄ flux (data from J. W. M. Rudd, C. A. Kelly, and V. L. St.Louis, unpublished data);
- wetland pond net DOC production (data from *St.Louis et al. (2004)*);
- wetland peatland surface CO₂ flux (data from *Asada et al. (in prep)*); and
- wetland peatland surface CH₄ flux (data from *Asada et al. (in prep)*).

An attempt to build a long-term predictive model that can be used outside of ELARP and FLUDEX was limited by the current approach that did not include any information about the year-to-year availability of OC for decomposition or direct correlations to pre-flood OC stores. As such, it was not possible to address how OC pools changed with time. Thus extrapolating these equations far beyond the field data is not recommended.

9.3 Results

Upland community respiration

Rates of CR in FLUDEX were greatest in the first year of flooding and steadily declined thereafter (Figure 9.1). By the fifth year, CR rates were half that of the first year. As a result, an exponential decline was used to fit all seasonal CR rates because it best described the general shape of the data and was based on the assumptions that (1) CR continued to decline year-after-year as the amount of easily decomposable OC decreases and (2) CR will not be negative.

Upland net primary production

Unlike CR, NPP rates in FLUDEX were similar in the first three years and peaked in the second or third year of flooding (Figure 9.2). NPP declined by about half from the third to fifth years of flooding. As a result, a Gaussian curve was used to fit all seasonal NPP rates and was based on the ideas that (1) there was a small increase in NPP in the second and third year or at least NPP was constant for three years and (2) NPP will not be negative. NPP was likely stimulated by nutrients released as a result of flooding and declined after nutrients were cycled and flushed from the reservoirs. This trend has been observed in other reservoir studies (*Tremblay et al., 2005*).

Upland net DIC production

Net DIC production was greatest in the first year of flooding and declined thereafter (Figure 9.3). By the fifth year, CR rates were about one-third to one-half that of the first year. As a result, an exponential decline was used to fit all seasonal net DIC production rates because it best described the general shape of the data and was based on the assumptions that (1) net DIC production declined year-after-year as CR slowed and (2) the initial decline in net DIC production was tempered by NPP. Gas exchange between the reservoir surfaces and the atmosphere accounted for 64% (on average) of the DIC exported from the reservoirs.

Upland net CH₄ production and ebullition

While CH₄ production is related to decomposition dynamics in the flooded soils (Chapter 2), unlike CR, net CH₄ production and CH₄ ebullition both peaked in the third year of flooding (Figures 9.4 and 9.5). From the third to fifth year, net CH₄ production fell by about half while CH₄ ebullition decreased by more than two-thirds. Gaussian curves were used to fit both CH₄ data sets based on the ideas that (1) net CH₄ production and CH₄ ebullition peaked in the third year and (2) net CH₄ production and CH₄ ebullition will not be negative.

Upland net DOC production

Rates of net DOC production in FLUDEX were greatest in the first year of flooding and declined quickly thereafter (Schiff, in prep, Figure 9.6). By the third year, net DOC production rates were about half that of the first year and remained fairly constant in the fourth and fifth years. As a result, a power function was used to fit net DOC production rates based on the assumptions that (1) there was a decline in net DOC production in the first few years and (2) net DOC production approached a plateau value above zero by the fifth year.

Wetland pond net DIC production

Net DIC production in the ELARP pond was calculated by combining routine measurements of alkalinity with hydrology data in a small Stella-based model (Hesslein et al., 2005, Figure 9.7). Net DIC production was defined in the same manner as in FLUDEX (cf. Chapter 2) such that it was the difference between all outputs of DIC and all inputs of DIC. Thus, net DIC production included the losses of DIC via the outflow and gas exchange. ELARP results show a marked increase of two- to ten-fold from pre- to post-flood years. Gas exchange accounted for $99 \pm 0.7\%$ (mean \pm SD, for all years presented,

$n = 11$) of net DIC production. Net DIC production can be approximated simply by determining CO₂ gas exchange.

Wetland pond surface CO₂ flux

The ELARP pond p_{CO_2} ¹ values show a distinct seasonal trend and peak during August of each year (Figure 9.8). Despite differences in hydrology and pond temperature in the two pre-flood years, the range of p_{CO_2} data was remarkably similar. After flooding, p_{CO_2} values increased to peak values that were at about three- to five-fold greater than pre-flood values. The net result was a large increase in the flux of CO₂ from the pond surface to the atmosphere.

Average seasonal fluxes of CO₂ from the pond surface to the atmosphere were estimated using measured wind speeds and a wind-speed-to- k relationship (Figure 9.9; J. W. M. Rudd, C. A. Kelly, and V. L. St. Louis, unpublished data; Kelly *et al.*, 1997; Wanninkhof, 1992). Both p_{CO_2} and wind speed data were collected for two pre-flood years and post-flood years 1–3, 5, and 6. In two subsequent post-flood years, 8 and 10, only p_{CO_2} data were collected. As a result, k had to be estimated to calculate the CO₂ flux from the pond to the atmosphere for the latter years. The range of annual temperature-corrected k values was 1.7–3.1 cm h⁻¹ for the seven years with measured data. An average of those seven k values yields the temperature-corrected k value of 2.4 cm h⁻¹ that was used for post-flood years 8 and 10.

As a result of flooding, the CO₂ flux increased from a pre-flood rate of $2.1 \pm 0.5 \text{ kg C ha}^{-1} \text{ d}^{-1}$ to a post-flood rate of $11.9 \pm 0.6 \text{ kg C ha}^{-1} \text{ d}^{-1}$ (mean \pm SD). During the 10 years of flooding, it was not clear if the CO₂ flux rates increased, although a linear regression suggested that possibility ($r^2 = 0.52$ and CO₂ flux rate = $5.0 \times \text{YAF} + 9.4$).

The CO₂ flux rates determined with p_{CO_2} and k data were, on average, less than 15% different from net DIC production rates in Hesslein *et al.* (2005) (pre-flood rate of $2.0 \pm 0.6 \text{ kg C ha}^{-1} \text{ d}^{-1}$ and a post-flood rate of $14.0 \pm 5.3 \text{ kg C ha}^{-1} \text{ d}^{-1}$ (mean \pm SD)). However, since gas exchange accounted for 99% of net DIC production, and in order to use CO₂ and CH₄ flux rates determined by the same methods for both upland and wetland reservoirs, the p_{CO_2} and k data were used.

Wetland pond surface CH₄ flux

Like the p_{CO_2} values, the ELARP pond p_{CH_4} values show distinct seasonal trends and peak during August of each year (Figure 9.8). Data from the two

¹As recommended by the International Union of Pure and Applied Chemistry, the notation here for partial pressure is p_i , where i is the i th constituent (Cohen *et al.*, 2007; Gamsjäger *et al.*, 2008). Some have used P_i (e.g., Stumm and Morgan, 1996), while others have redefined both the minuscule p and majuscule P for other purposes related to partial pressure (e.g., Davies *et al.*, 2003).

pre-flood years were similar despite differences in hydrology and pond temperature. In the first three years after flooding, peak p_{CH_4} values increased from eight- to thirteen-fold over the pre-flood peaks, while average p_{CH_4} values had increased four- to six-fold. Thereafter, peak and average p_{CH_4} values remained much higher than pre-flood values. The net result was a large increase in the flux of CH_4 from the pond surface to the atmosphere.

Average seasonal fluxes of CH_4 from the pond surface to the atmosphere were estimated using the same method as for CO_2 fluxes (Figure 9.11). The range of annual temperature-corrected k values was 1.8–3.2 cm h^{-1} for the years with measured data. Therefore, an average temperature-corrected k value of 2.5 cm h^{-1} was used for post-flood years 8 and 10.

CH_4 flux rates increased more than four-fold as a result of flooding from $0.13 \pm 0.09 \text{ kg C ha}^{-1} \text{ d}^{-1}$ to $0.58 \pm 0.13 \text{ kg C ha}^{-1} \text{ d}^{-1}$ (mean \pm SD). The lack of fit of a linear regression ($r^2 = 0.01$ and CH_4 flux rate = $0.005 \times \text{YAF} + 0.5$) indicates that the post-flood CH_4 flux rates did not exhibit a time trend during the 10 years of flooding.

Wetland basin net DOC production

Net DOC production in the ELARP basin was calculated by combining routine measurements of DOC concentration with hydrology data (St.Louis *et al.*, 2004, Figure 9.12). The results show a marked three-fold increase from pre- to the early post-flood years. Net DOC production generally declined each year after flooding with one low rate in the very dry sixth year of flooding. By the ninth post-flood year, net DOC production was within 10% of the highest pre-flood year. Net DOC production was modelled with an exponential function, to estimate the three years for which there were no data. After the tenth year of flooding the difference between pre- and post-flood net DOC production was estimated as zero since net DOC production rates had declined to near pre-flood rates.

Wetland peatland surface CO_2 flux

Asada *et al.* (in prep) estimated the net flux of CO_2 from the ELARP peatland surface to the atmosphere. They combined measures of living vegetation using standard regression equations (Asada *et al.*, 2005; Dyck and Shay, 1999) and available static flux chamber and flux-gradient methods (Kelly *et al.*, 1997; Saquet, 2003, Figure 9.13; V. L. St.Louis unpublished data). Their data indicate that as a result of flooding, a small CO_2 sink of $0.18 \text{ kg C ha}^{-1} \text{ d}^{-1}$ became a net source of $0.5\text{--}2.0 \text{ kg C ha}^{-1} \text{ d}^{-1}$ to the atmosphere. Although new vegetation established on the peat over 10 years of flooding has replaced the OC in pre-flood living biomass, the peatland surface remained a large source of CO_2 to the atmosphere (Asada *et al.*, 2005).

Wetland peatland surface CH₄ flux

Asada et al. (in prep) also determined that the CH₄ flux from the peatland surface to the atmosphere increased by about 350 times as a result of flooding, from 0.07 kg C ha⁻¹ d⁻¹ to 2.0–2.5 kg C ha⁻¹ d⁻¹ (Figure 9.14). This surface remained a large source of CH₄ at similar levels 10 a after the initial flooding.

Generalised model of carbon cycling

FLUDEX data showed year-to-year trends in rates of GHG and DOC production. As a result, the model equations were used to determine net rates over the medium-term (Table 9.2). Pre-flood net DIC production was estimated from the OC accumulation in the soil, excluding the mineral layer, and vegetation prior to flooding (Table 9.1). Since the OC was fixed from atmospheric CO₂ via photosynthesis, the soil and vegetation OC stores are an integrated measure of net DIC production for the reservoirs since a forest fire razed the sites in 1980. These areal OC densities were divided by 20 a and 365 d a⁻¹ to convert them to a 20-year average rate in mass area⁻¹ d⁻¹; this rate is akin to a 20-year average net ecosystem production rate. Thus the mean rate of net DIC production was -4.8 ± 1.0 kg C ha⁻¹ d⁻¹. This rate was within published ranges of net ecosystem production measured in boreal jack pine forests of similar ages (*Bond-Lamberty et al., 2004; Harden et al., 2000; Howard et al., 2004*). CH₄ oxidation rates by FLUDEX soils were measured with static flux chambers prior to flooding (*Joyce, 2001*). The rate of net CH₄ production was -0.009 ± 0.002 kg C ha⁻¹ d⁻¹. These were very small and similar to rates measured in the boreal forest with similar vegetation (*Savage et al., 1997*).

While ELARP data showed clear differences between pre- and post-flood rates, time-trends were not readily evident in any data sets except net DOC production. Therefore for ten years, post-flood rates were constant. As a result, a pre- versus post-flood model was used for most data sets where average pre-flood rates were subtracted from average post-flood rates to determine net rates over the medium-term (Table 9.3).

9.4 Discussion

CO₂ and DIC

Flooding both uplands and wetlands ecosystems caused them to become net producers of DIC in all years studied. Whereas net DIC production in FLUDEX declined year-after-year from the first year of flooding, in ELARP, both CO₂ flux from the revegetated peatland surface and from the pond surface remained elevated for more than a decade.

DOC

Both FLUDEX and ELARP were net exporters of DOC in all years of flooding. DOC export declined more rapidly and earlier in FLUDEX than in ELARP, but areal rates of DOC export from FLUDEX were three to five times greater than from ELARP. Part of the difference between these ecosystems may be the result of differences in residence time, length of flood season, and the source of DOC.

Residence times in ELARP varied widely between and during each year as a direct result of the rate of water input from the upstream lake and, to a lesser extent, surrounding catchment (*St.Louis et al., 2004*). During some summers, the outflow from ELARP stopped entirely. At other times, the outflow approached the limits of the weir systems on the ELARP dam. Since almost all the water inputs to FLUDEX were controlled from the pumped inflow (see Chapter 2), the residence times did not vary much within or between years. For both ELARP and FLUDEX, differences in residence time may have affected the rate and amount of photobleaching and photochemical loss of DOC as well as other transformations such as microbial decomposition and sedimentation that lead to increased DOC loss rates (*Molot and Dillon, 1997; von Wachenfeldt and Tranvik, 2008*).

ELARP remained a pond for the entire year, regardless of whether the water level was raised to flood level or not, so DOC budgets were calculated for the entire year and then prorated by flow to match the flood-season dates. In FLUDEX, DOC budgets were calculated for only the flood season. This may skew the ELARP rates down since DOC production was slower at colder temperatures in the fall and winter (*Moore, 1997; Moore et al., 2003*).

The sources of DOC added to the two reservoir systems may also have been different. ELARP had a very large store of OC as peat and the flux of DOC from this peat into the pond was the source of most of the DOC (*Moore et al., 2003*). Photosynthetic production of DOC may have been a relatively small source of DOC because of the shading effect of the dark-coloured pond water (*Carpenter et al., 1998b; Jackson and Hecky, 1980; Schindler et al., 1978*).

Although net DOC production in ELARP ($< 1 \text{ kg C ha}^{-1} \text{ d}^{-1}$) is an order of magnitude lower than it is for DIC ($11.9 \text{ kg C ha}^{-1} \text{ d}^{-1}$), these increases in DOC to downstream ecosystems can still have effects on community metabolism and structure as well as the ability of drinking water agencies to disinfect water (*Davies and Mazumder, 2003; Pastor et al., 2003; Schindler, 2001*). DOC export from peatlands downstream exerts controls on primary production (*Carpenter and Pace, 1997*), bacterial production (*Hobbie, 1992; Wetzel, 1992*), biogeochemical cycles (*Driscoll et al., 1980; Guildford et al., 1987; Jackson and Hecky, 1980; St.Louis et al., 2004*), and attenuates visible and ultraviolet (UV) radiation in downstream ecosystems (*Morris et al., 1995; Schindler et al., 1990, 1996b; Williamson et al., 1999*). Drinking water agencies must limit the production of disinfection by-products during water treatment. Elevated

and changing loads of DOC make this difficult when disinfecting by UV radiation and chlorine and chloramine additions ([Chow et al., 2005](#); [Volk et al., 2005](#)).

DIC:DOC ratio

The DIC:DOC ratio, i.e., the ratio of net DIC production to net DOC production, provides information about the degree to which decomposition from OC to DIC has proceeded but also reflects factors such as photosynthetic rates, mineralisation rates, and residence times. If decomposition occurs as OC being degraded by enzymes such as hydrolases to produce DOC, then the amount of that DOC converted to DIC describes the extent to which decomposition of OC has occurred. In addition, the amount of DIC is also controlled by CO₂ consumption by photosynthesis. However, decomposition of OC is not the only source of DOC since photoautotrophs also produce DOC exudates (e.g., [Reche and Pace, 2002](#); [Wetzel, 1992](#)).

In FLUDEX, the DIC:DOC ratio was between 1:1 and 4:1. In ELARP, the pond pre-flood DIC:DOC ratios were 7:1 and 8:1. Post-flood, the pond DIC:DOC ratio ranged between 10:1 and 50:1. The low DIC:DOC ratios in FLUDEX reservoirs suggest that with a short residence time, mineralisation of OC to DIC may not have proceeded as far as in ELARP. Additionally, isotopic ratios suggest that DOC exported from FLUDEX reservoirs is comprised of a significant portion of photosynthetically derived DOC ([Schiff, in prep](#)). The result of flooding ELARP has been to produce a lot more DIC relative to DOC. Increased temperatures in the peat suggest that increased decomposition has fuelled this ([Moore et al., 2003](#); [St.Louis et al., 2004](#)). This comparison emphasised both the differences in DIC and DOC export from FLUDEX and ELARP but also the differing roles of hydrology, photosynthesis, and decomposition in these two ecosystems.

CH₄

ELARP produced much more CH₄ than FLUDEX since the CH₄ flux from the peat to atmosphere was much larger than the flux from the pond. The peatland surface exhibited CH₄ flux rates more than one order of magnitude greater than FLUDEX and the ELARP pond surface exhibited CH₄ flux rates about five times greater than maximum CH₄ production in FLUDEX. The sustained flux of CH₄ from both ELARP surfaces was in stark contrast to FLUDEX where CH₄ fluxes peaked in the third year and declined rapidly thereafter.

Total carbon fluxes from ELARP and FLUDEX

As a result of flooding ELARP, a small CO₂ and CH₄ source to the atmosphere was converted into a large CO₂ and CH₄ source. Prior to flooding, FLUDEX was accumulating OC in new vegetation and soil after a large forest fire and was a very small sink for CH₄. It became a source of both CO₂ and CH₄ to the atmosphere, albeit a source that declined with time. However, given the 19-fold difference in pre-flood OC stores between ELARP and FLUDEX, the differences in measured seasonal flux rates were not that large (Tables 9.2 and 9.3).

Over 10- and 20-year projections, the surface fluxes of GHGs to the atmosphere of ELARP were clearly greater than FLUDEX. To determine the GHG and DOC fluxes from the entire ELARP reservoir, individual peat and pond rates were prorated based on changes in the areal pond:peat ratio over time (cf. *Asada et al.*, 2005) (Table 9.4). This ratio decreased from about 6.3:1 to 0.45:1 over the first ten years of flooding as more peat began to float. An important difference between ELARP and FLUDEX results was that GHG flux rates from FLUDEX declined markedly in only five years and were projected to be at rates less than half of first-year rates within a decade, whereas GHG flux rates from ELARP remained elevated for more than a decade of direct study. This is particularly important for CH₄ fluxes for two reasons: (1) the GWP of CH₄ is 23-times that of CO₂ over a 100-year timeline (*Ehhalt et al.*, 2001); and (2) since OC storages in boreal forest uplands is transient due to forest fires, any conversion of that OC to CH₄ is a clear increase in the GWP of that C.

Changes in DOC export from reservoirs was not part of the initial hypotheses of ELARP and FLUDEX (*Bodaly et al.*, 2004; *Kelly et al.*, 1997). Rather, DOC concentrations and fluxes were studied as part of mercury and general ecosystem processes. In ELARP, DOC flux was small relative to both CO₂ and CH₄ fluxes, but was more than one-third of the GHGs in FLUDEX; in both cases it is important for water 'quality' and mercury export (*Hall et al.*, 2005; *St.Louis et al.*, 2004). While DOC export from temperate catchments is strongly correlated with the fraction of wetland cover and average slope (*Dillon and Molot*, 1997), the effect on DOC export by continuous flooding (as opposed to seasonal or pulsed flooding *Junk et al.*, 1989; *Tockner et al.*, 2000) has not been well studied. In some systems, net production or consumption of DOC depended on hydrology and climate (e.g., *Evans et al.*, 2006; *Schindler et al.*, 1996a) but without other data such as isotopic and molar ratios it is difficult to rule out differences in photosynthetic production of DOC. These factors may explain part of the difference in results from ELARP and FLUDEX since the former had much longer residence times than the latter.

Long-term accumulation rates of OC are much greater in boreal peatlands (0.3–2.2 kg C ha⁻¹ d⁻¹) than in boreal forests (0.03–0.33 kg C ha⁻¹ d⁻¹) (*Schlesinger*, 1997). This indicates that the loss of a boreal peatland represents

a greater long-term loss of a CO₂ sink than a boreal forest. Medium-term CH₄ dynamics also indicate that flooding ELARP caused a greater net change in CH₄ flux rates than flooding FLUDEX in part because of the rapid decline in CH₄ flux rates after the third year of flooding.

When the loss of the pre-flood ecosystems is accounted for, the 10- and 20-year projections for net GHG and DOC fluxes from FLUDEX increased by about 50 % and became as large as or larger than ELARP (Table 9.5). This was the result of the FLUDEX pre-flood C sink being much larger than the ELARP pre-flood flux rates of CH₄ and CO₂. Upland jack pine-dominated boreal forests are C sinks for at least 50 a (*Harden et al., 2000*). Although rates of C accumulation decline as forest stands age (e.g., *Bond-Lamberty et al., 2004*), the estimated pre-flood FLUDEX C sink is appropriate for both the 10- and 20-year projections given measured C sink rates in other parts of the boreal forest (cf. *Bond-Lamberty et al., 2004; Harden et al., 2000; Howard et al., 2004*). These results suggest that the loss of a boreal forest C sink may account for about half of the changes in C cycling as a result of upland reservoir creation and this would not be captured by measures of post-flood surface-water concentrations and gas fluxes.

The flux of GHGs from reservoirs has been suggested to be positively correlated to pre-flood OC stores less tree bole since wood is quite resistant to decomposition under water (*Eijsackers and Zehnder, 1990; St.Louis et al., 2000*). The 10- and 20-year projections of GHG and DOC production rates were compared to pre-flood C stores less tree boles to determine the fraction of pre-flood OC that would be lost. In ELARP, 2 % and 3 % of pre-flood OC would have been lost over 10- and 20-years. In FLUDEX, 47 % and 67 % would have been lost over 10- and 20-years. Assuming calculated rates of net GHG and DOC production can be sustained, ELARP would support 600 to 660 a of fluxes and FLUDEX only 21 to 29 a. These results clearly show that (1) the longevity of GHG fluxes is much greater in ELARP than FLUDEX and (2) projected GHG and DOC flux rates from FLUDEX are likely maxima as a result of assuming an adequate supply of OC for decomposition. Thus GHG fluxes from FLUDEX would likely have declined below model predictions before 20 a and the net result of flooding upland forests would then become only the loss of a forest C sink whereas elevated GHG fluxes from ELARP are likely to continue for at least decades.

Comparing ELARP and FLUDEX as the high and low extremes of landscape OC storage indicated there was a positive relationship between pre-flood OC storage and both the magnitude and longevity post-flood reservoir GHG fluxes. Medium-term GHG fluxes were successfully estimated with the equations of a simple descriptive model suggesting that differences in the longevity of GHG fluxes from ELARP and FLUDEX are key. Quantifying post-flood GHG fluxes in ecosystems with pre-flood OC stores between those of ELARP and FLUDEX would help complete the OC stores and GHG flux

relationship (*St.Louis et al., 2000*). Medium-term GHG fluxes from reservoirs that flood ecosystems with different OC stores may be predictable based on solely pre-flood OC storage. Predictive models of GHG fluxes may ultimately be developed using series of detailed pre- and post-flood data sets.

Acknowledgements

Many people contributed to FLUDEX and ELARP; among them are numerous field and laboratory assistants as well as, alphabetically by surname, R. O. Aravena, T. Asada, K. G. Beaty, P. Bettess, N. Bloom, R. A. Bodaly, N. M. Boudreau, B. A. Branfireun, J. L. Bubier, D. Burton, K. A. Cherewyk, A. Cherry, N. Comer, B. S. Dyck, R. J. Elgood, G. Edwards, J. Embury, R. Flett, R. J. P. Fudge, P. M. Gerrard, B. D. Hall, R. Harris, J. Hebert, R. E. Hecky, L. H. Hendzel, R. H. Hesslein, A. Heyes, M. Hines, P. Humenchuk, J. P. Hurley, E. M. Joyce, C. A. Kelly, M. E. Lyng, C. D. Mackenzie, C. Magura, M. Mailman, A. R. Majewski, D. Malley, C. J. D. Matthews, L. Matos, K. T. Maurice, T. R. Moore, G. K. McCullough, M. J. Paterson, A. Partridge, A. F. Penn, C. D. Poschadel, K. R. Rolfhus, D. M. Rosenberg, N. T. Roulet, J. W. M. Rudd, K. Sandilands, M. A. M. Saquet, S. L. Schiff, K. J. Scott, P. Sellers, J. M. Shay, L. Stepanovich, V. L. St.Louis, G. Thurtell, B. G. Warner, K. Wider, A. Wiens, A. M. Wojtyniak, and J. B. Yavitt. General funding for ELARP was provided by Fisheries and Oceans Canada, Manitoba Hydro, Ontario Hydro, Hydro-Québec, and the Natural Sciences and Engineering Research Council of Canada. General funding for FLUDEX was funded by Fisheries and Oceans Canada, Manitoba Hydro, and Hydro-Québec.

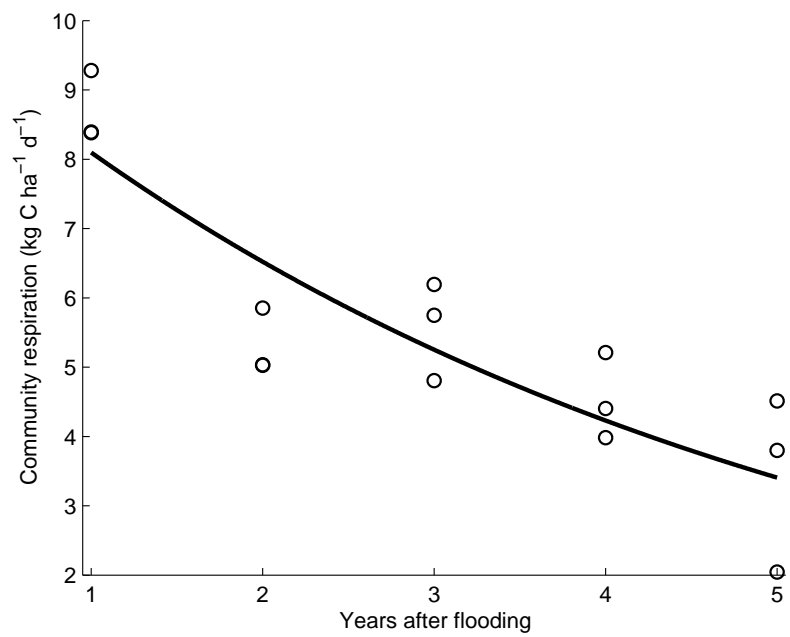


Figure 9.1: Community respiration rates in FLUDEX reservoirs. Regression details are in Table 9.2.

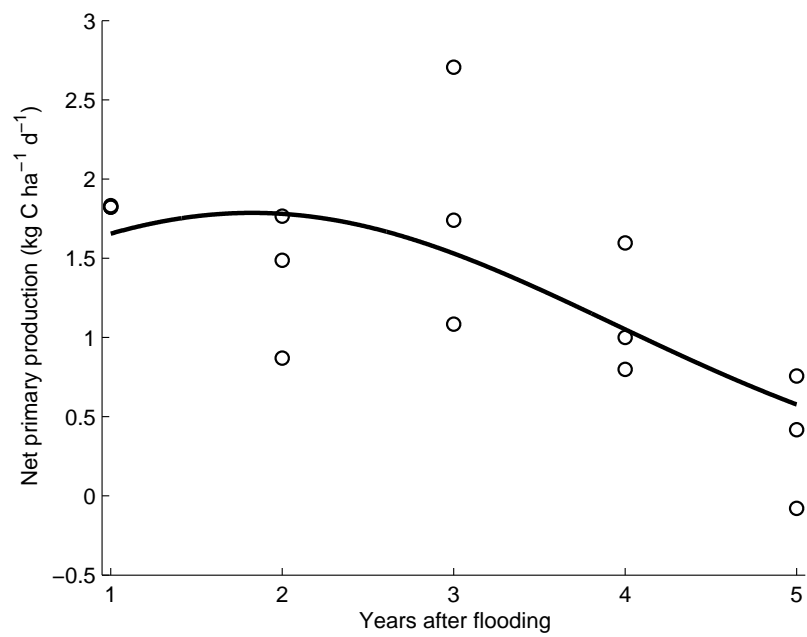


Figure 9.2: Net primary production rates in FLUDEX reservoirs. Regression details are in Table 9.2.

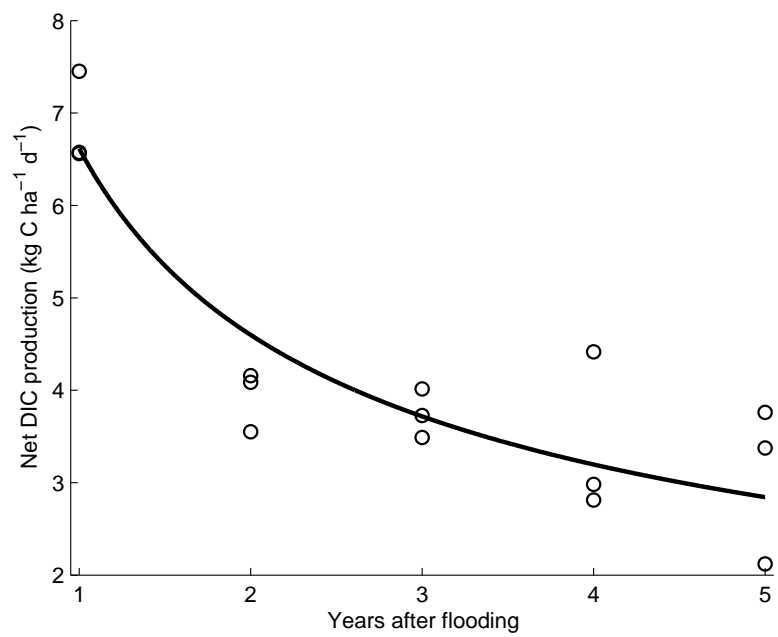


Figure 9.3: Net DIC production rates in FLUDEX reservoirs. Regression details are in Table 9.2.

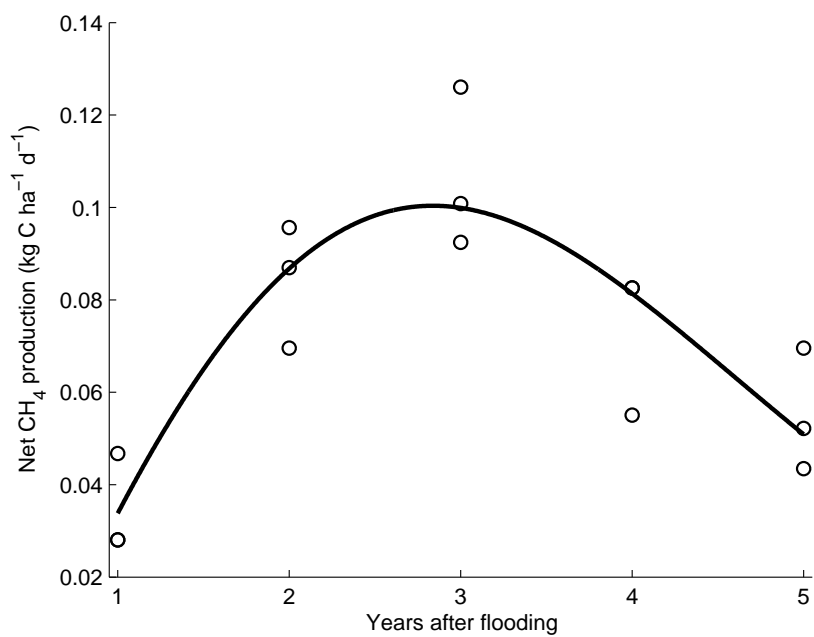


Figure 9.4: Net CH₄ production rates in FLUDEX reservoirs. Regression details are in Table 9.2.

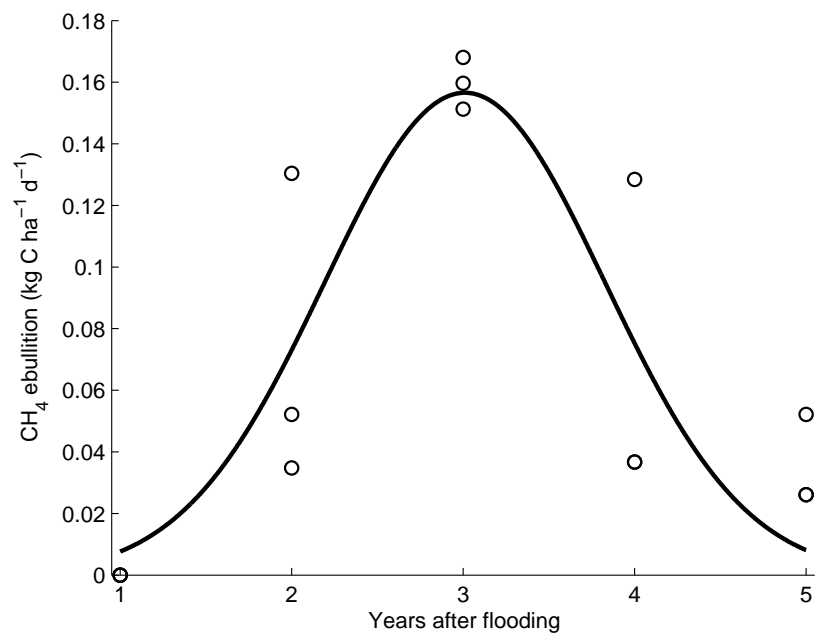


Figure 9.5: CH₄ ebullition rates in FLUDEX reservoirs. Regression details are in Table 9.2.

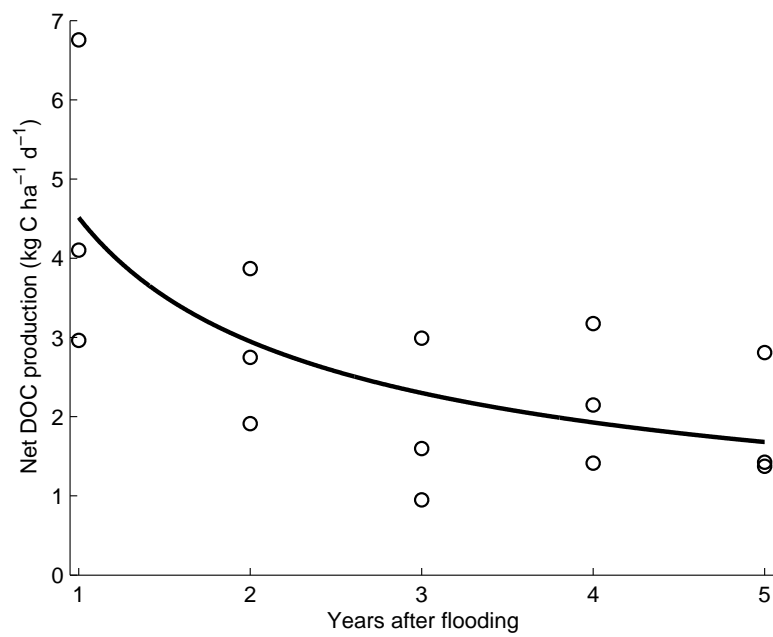


Figure 9.6: Net DOC production rates in FLUDEX reservoirs. Regression details are in Table 9.2.

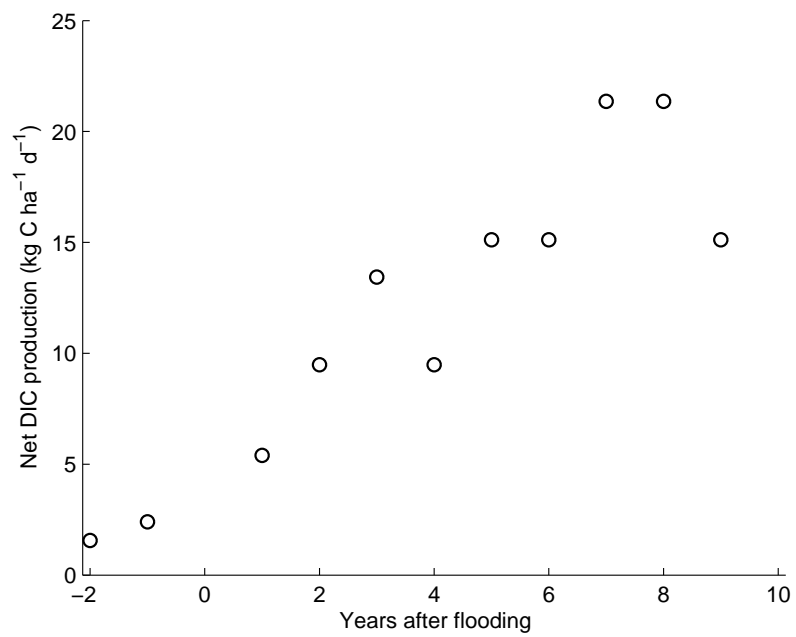


Figure 9.7: Net DIC production rates in the ELARP pond. Flooding began in June 1993.

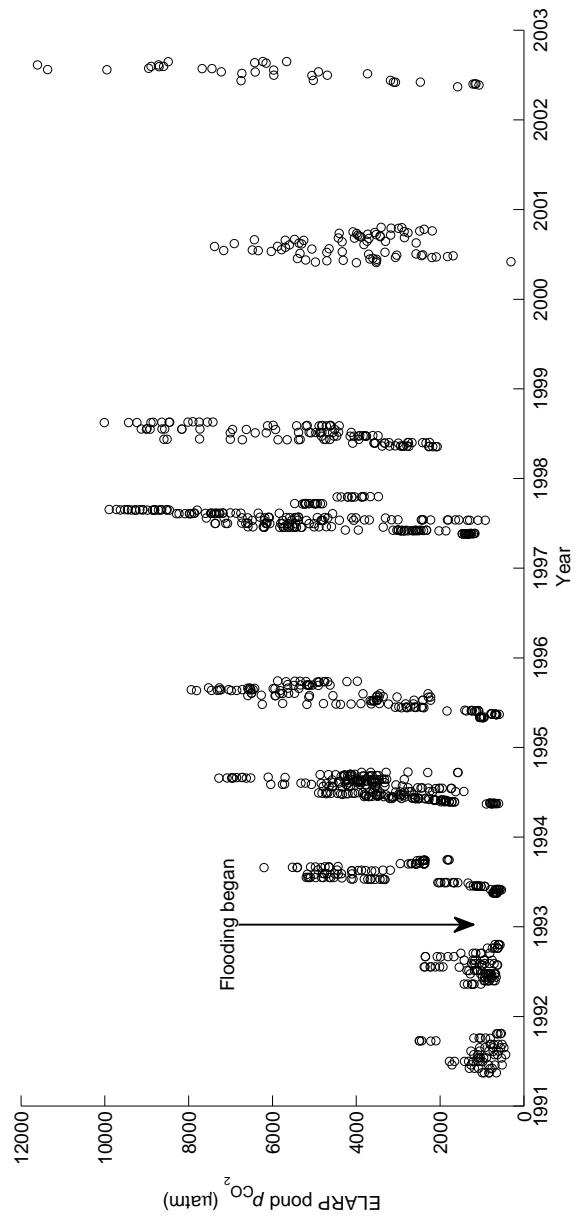


Figure 9.8: p_{CO_2} values in the ELARP pond. Flooding began in June 1993.

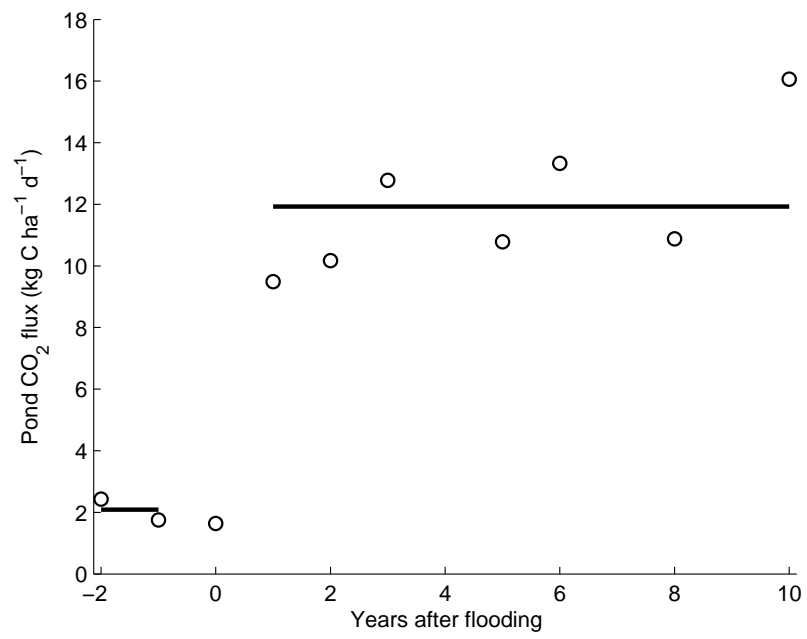


Figure 9.9: CO₂ flux rates from the ELARP pond to the atmosphere. Year 0 is Spring 1993 before flooding began in June.

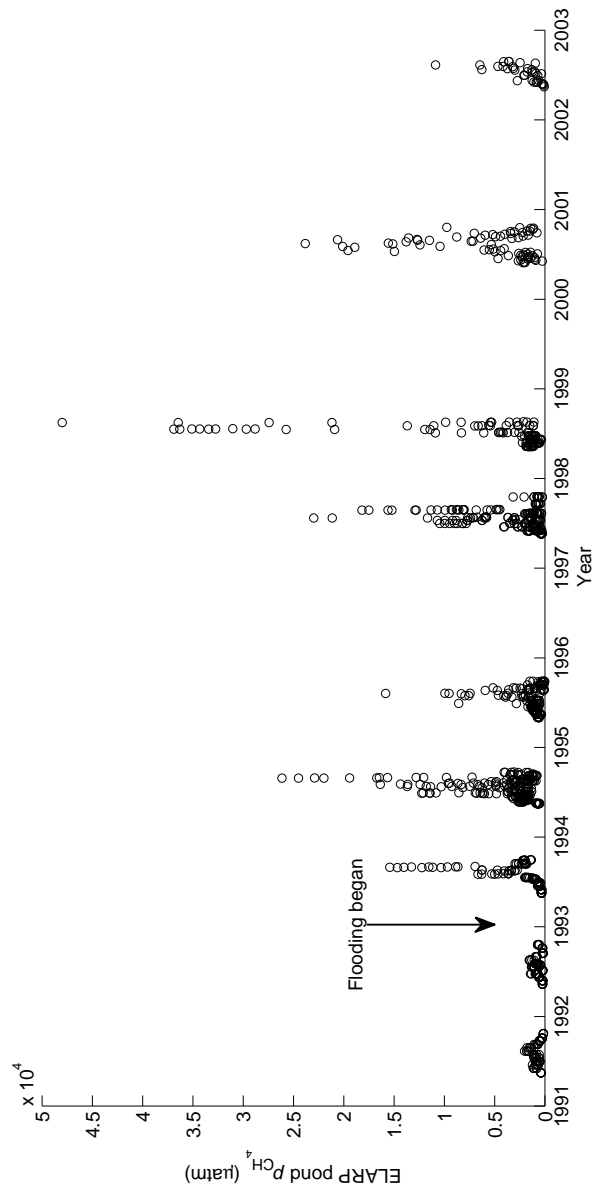


Figure 9.10: p_{CH_4} values in the ELARP pond. Flooding began in June 1993.

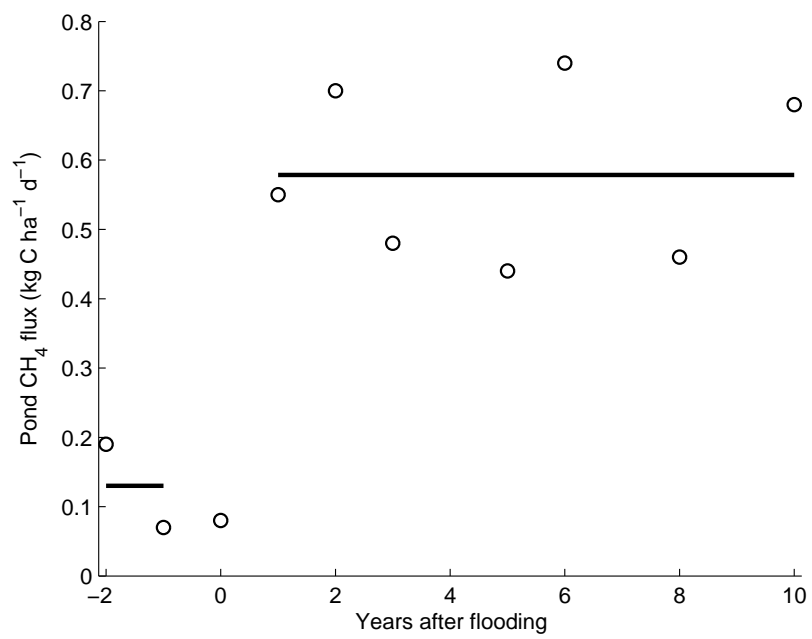


Figure 9.11: CH₄ flux rates from the ELARP pond to the atmosphere. Year 0 is Spring 1993 before flooding began in June.

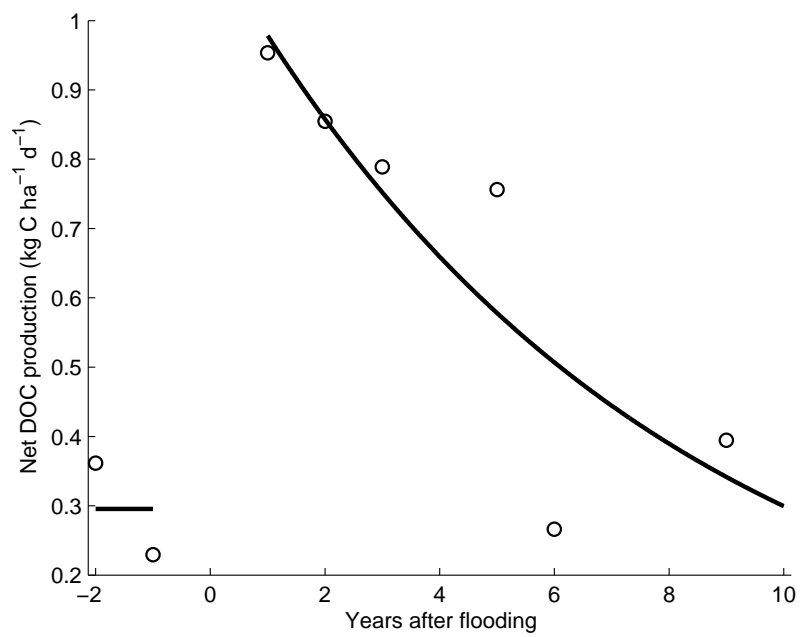


Figure 9.12: Net DOC production rates in the ELARP pond. Flooding began in June 1993.

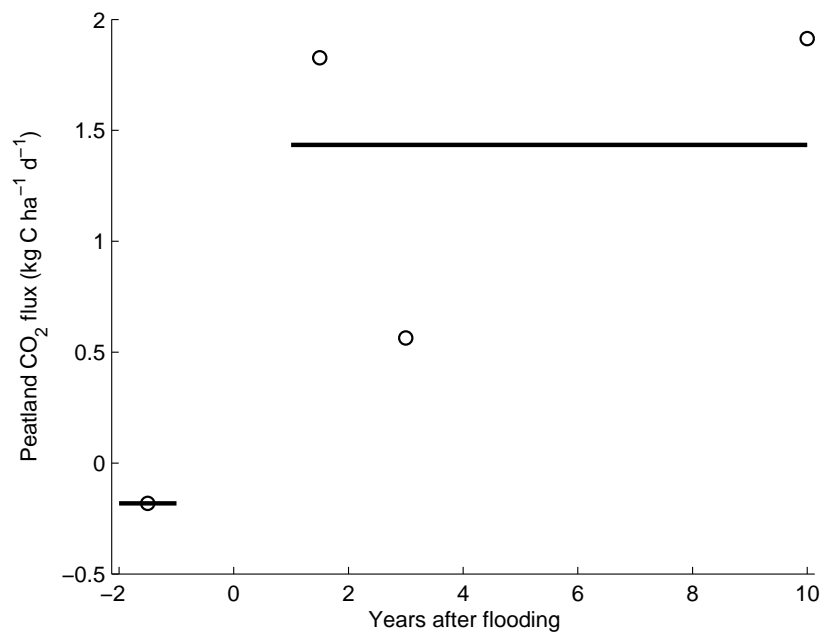


Figure 9.13: CO₂ flux rates from the ELARP peatland to the atmosphere. Flooding began in June 1993.

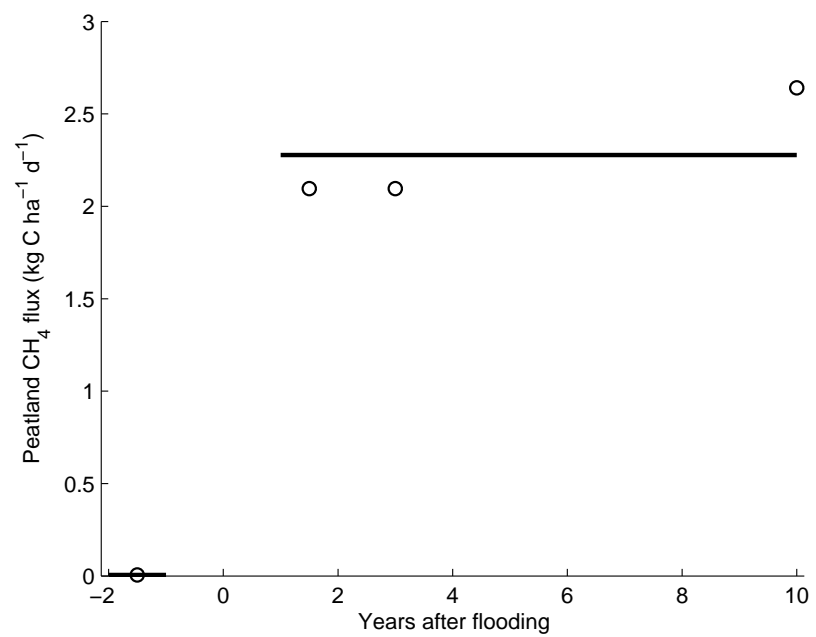


Figure 9.14: CH₄ flux rates from the ELARP peatland to the atmosphere. Flooding began in June 1993.

Table 9.1: Pre-flood organic carbon stores in ELARP and FLUDEX reservoirs. All units are kg C ha⁻¹. ELARP values are from *Asada et al. (in prep)*. FLUDEX values are from Chapter 2.

Organic carbon type	ELARP	FLUDEX High C	FLUDEX Medium C	FLUDEX Low C
Peat	668800	0	0	0
Litter and fungal-humic layer	n/a	15400	5700	8700
Mineral layer	0	2900	1500	2400
Above-ground vegetation less wood and bark	8030	3400	2830	2000
Above-ground wood and bark	12570	24200	24870	17800
Total carbon	689400	45900	34900	30900

Table 9.2: Pre- and post-flood greenhouse gas and dissolved organic carbon (DOC) flux rates and equations from FLUDEX reservoirs. All values are parameterised in terms of years after flooding (YAF) and are in units of $\text{kg C ha}^{-1} \text{d}^{-1}$.

Flux	Pre-flood	Post-flood	Description
Community respiration		$10.05 \times e^{-0.7309 \times \text{YAF}} + 3.699$	Exponential decline describes the general shape and is based on the assumptions that (1) CR will decline year-after-year as the amount of easily decomposable OC decreases and (2) CR will not be negative
Net primary production		$1.786 \times e^{-\left(\frac{\text{YAF}-4.825}{2.367}\right)^2}$	Gaussian curve is based on the ideas that (1) there was a (small) increase in NPP in the second and third year and (2) NPP will not be negative
Net DIC production	-5.9 to -3.9 (-4.8 ± 1.0) ^a	$6.616 \times \text{YAF}^{-0.5247}$	Power function describes the general shape and is based on the assumptions that (1) net DIC production will decline year-after-year as the CR slows, (2) the initial decline in net DIC production is tempered by NPP, and (3) net DIC production will not be negative
Net CH ₄ production	-0.011 to -0.007 (-0.009 ± 0.002) ^b	$0.102 \times e^{-\left(\frac{\text{YAF}-3.075}{2.161}\right)^2}$	Gaussian curve is based on the ideas that (1) there was NMP peaked in the third year and (2) NMP will not be negative
CH ₄ ebullition		$0.1566 \times e^{-\left(\frac{\text{YAF}-3.010}{1.159}\right)^2}$	Gaussian curve is based on the idea that (1) there was ME peaked in the third year and (2) ME will not be negative
Net DOC production		$4.514 \times \text{YAF}^{-0.614}$	Power function is based on the assumptions that (1) there was a decline in net DOC production in the first few years and (2) net DOC production approached a plateau value above zero by the fifth year

^a Pre-flood net DIC production was estimated from the amount of stored OC in the soil, excluding the mineral layer, and vegetation prior to flooding (mean \pm SD, $n = 3$ reservoirs).

^b Pre-flood net CH₄ production was estimated from static flux chamber measurements of soil CH₄ fluxes by [Joyce \(2001\)](#) (mean \pm SD, $n = 3$ reservoirs).

Table 9.3: Pre- and post-flood greenhouse gas and dissolved organic carbon (DOC) flux rates from the ELARP reservoir. All values are parameterised in terms of years after flooding (YAF) and are in units of $\text{kg C ha}^{-1} \text{d}^{-1}$.

Flux	Pre-flood	Post-flood
Pond CO_2	2.1	11.9
Pond CH_4	0.13	0.58
Pond DOC	0.22 to 0.36	0.27 to 0.95 $1.116 \times e^{-0.1315 \times \text{YAF}}$
Peat CO_2	-0.18	0.5 to 2.0 (1.4 ± 0.8) ^a
Peat CH_4	0.07	2.0 to 2.5 (2.3 ± 0.3) ^a

^a mean \pm SD, $n = 3$

Table 9.4: Predictions of 10- and 20-year greenhouse gas and dissolved organic carbon (DOC) post-flood flux rates from ELARP and FLUDEX reservoirs. All are in units of $\text{kg C ha}^{-1} \text{d}^{-1}$ and have *not* been adjusted for differences in global warming potential. Rates were averaged over the stated time and were calculated only as post-flood rates. Rates for ELARP were prorated based on changes in the areal pond:peat ratio over time (cf. *Asada et al., 2005*). These rates were based on seasonal budgets and were not adjusted for differences in flood-season lengths, i.e., 152 d for ELARP and 113 d for FLUDEX.

	ELARP 10-year	ELARP 20-year	FLUDEX 10-year	FLUDEX 20-year
Net DIC production ^a	4.9	6.6	3.2	2.4
Net CH ₄ production ^a	0.24	0.32	0.04	0.02
CH ₄ ebullition			0.03	0.02
Net DOC production ^a	0.37	0.19	2.2	2.0
Peat CO ₂	0.82	0.63		
Peat CH ₄	1.4	1.0		
<i>Total</i>	<i>7.7</i>	<i>8.73</i>	<i>5.3</i>	<i>3.9</i>

^a Represents pond for ELARP

Table 9.5: Predictions of 10- and 20-year net greenhouse gas and dissolved organic carbon (DOC) flux rates from ELARP and FLUDEX reservoirs. All are in units of $\text{kgC ha}^{-1} \text{d}^{-1}$ and have *not* been adjusted for differences in global warming potential. Rates were averaged over the stated time and were calculated as the difference between pre- and post-flood rates. Rates for ELARP were prorated based on changes in the areal pond:peat ratio over time (cf. [Asada et al., 2005](#)). These rates were based on seasonal budgets and were not adjusted for differences in flood-season lengths, i.e., 152 d for ELARP and 113 d for FLUDEX.

	ELARP 10-year	ELARP 20-year	FLUDEX 10-year	FLUDEX 20-year
Net DIC production ^a	4.1	5.4	8.0	7.2
Net CH ₄ production ^a	0.19	0.25	0.04	0.02
CH ₄ ebullition			0.03	0.02
Net DOC production ^a	0.37	0.37	2.0	1.4
Peat CO ₂	0.93	0.71		
Peat CH ₄	1.3	1.0		
<i>Total</i>	6.9	7.6	10.1	8.7

^a Represents pond for ELARP

Chapter 10

Conclusions and recommendations

10.1 General comments

The overall objective of this thesis was to describe the temporal evolution of upland boreal reservoirs (Flooded Upland Dynamics Experiment, FLUDEX) in terms of community respiration (*CR*) and primary production (*PP*) rates using carbon (*C*) and O_2 . To complete this goal, a series of experiments was designed to: (1) determine the importance of ebullition as a conduit of greenhouse gases (GHGs) from upland boreal reservoirs to the atmosphere; (2) measure directly the gas exchange coefficient (*k*) for the FLUDEX reservoirs; (3) perform comparative measurements of carbon and O_2 in incubations of reservoir water; and (4) compare the upland and wetland reservoir experiments at the Experimental Lakes Area (ELA). As a result of the O_2 and $\delta^{18}O-O_2$ research, an improved conceptual model and ultimately a computer model of $\delta^{18}O-O_2$ was required. Development of the PoRGy model led to the publication of two manuscripts (Chapters 4 and 5) wherein diel changes in O_2 and $\delta^{18}O-O_2$ were used to separate community metabolism and gas exchange. This chapter summarises the main conclusions of the research, identifies the major contributions to the scientific community, proposes areas that should remain a focus in future reservoir and GHG studies, and raises questions that can be addressed by future research.

10.2 Main conclusions and contributions to research

The temporal evolution of biological processes in the FLUDEX reservoirs was quantified and described (Chapter 2). *CR* rates declined year-after-year in all reservoirs for all five years of flooding. By the fifth year, *CR* was about half of what it was in the first year. Net *PP* (*NPP*) rates peaked slightly in the third year of flooding and declined much more slowly than *CR*. *NPP* needed to be separated from net dissolved inorganic C (DIC) production so that *CR* could be quantified and applied to other systems. Net CH_4 production peaked in

the third year at more than twice the rate in the first year. By the fifth year, net CH_4 production remained greater than it was in the first year. CH_4 oxidation greatly decreased the potential flux of CH_4 to the atmosphere by oxidising more than three-quarters of the CH_4 produced in the flooded soils. When CO_2 and CH_4 are combined, the annual global warming potential of the GHG flux from the FLUDEX reservoirs declined over five years. However, contrary to one of the initial hypotheses of FLUDEX (cf. [Bodaly et al., 2004](#)), neither CR nor total GHG fluxes were directly related to the quantity of organic C (OC) that was flooded.

Rates of CR and NPP were separated from DIC concentrations by using $\delta^{13}\text{C}$ -DIC. This was a whole-ecosystem application of natural abundance stable isotopes to examine biological processes. Previously, $\delta^{13}\text{C}$ -DIC had been used in whole ecosystem studies to constrain mass budgets (e.g., [Quay et al., 1986](#)) but not to directly determine processes at this scale. By using biological processes to describe the evolution of reservoirs, some of the controls on GHG cycling become more easily understood: the lability and decomposition of OC; and the release of nutrients and changes in NPP. Recently, whole-ecosystem-isotopic-labelling experiments have been conducted allowing easier separation of processes and trophic levels easier ([Bade et al., 2007](#); [Pace et al., 2004](#)). However, this approach suffers from the difficulty of obtaining regulatory approval for the addition of isotopes and the extra care required with isotope spikes so that samples and other field sites are not contaminated. Furthermore, complex modelling is required when $\delta^{13}\text{C}$ values change rapidly (e.g., [Cole et al., 2006](#)).

Ebullition was identified as an important source of CH_4 from reservoir surfaces to the atmosphere (Chapter 3). Bubbles with high concentrations of CH_4 formed in the upper-most part of the flooded soil and were the most important source of CH_4 to the atmosphere after three years. Each year, ebullition rates peaked in late-August when soil temperatures were greatest. Bubbles trapped in the flooded soil at the end of the flood season constituted a significant source of CH_4 . This often unmeasured CH_4 was released directly to the atmosphere when the soils drained during autumn drawdown and was of the same order of magnitude as flood-season ebullition.

Ebullitive fluxes from reservoirs are poorly quantified and infrequently studied. Ebullition is notoriously episodic and factors including changes in barometric pressure, hydrostatic pressure (i.e., water depth), and soil temperature may cause ebullitive releases ([Boudreau et al., 2001a](#); [Fechner-Levy and Hemond, 1996](#)). In the FLUDEX reservoirs, bubbles must have formed, or at least resided sufficiently long, near the top of the flooded soils since bubble $\delta^{13}\text{C}$ - CH_4 values indicated the CH_4 had been partially oxidised. The fate of bubbles trapped in flooded soil at the end of a flood season had never been determined. Soil gas surveys in FLUDEX indicate that this gas was readily available to flux to the atmosphere (the gas was about half CH_4)

and was almost as large as the entire flood season ebullitive flux. Attempts at quantifying ebullitive fluxes in large reservoirs have proven difficult and therefore developing a semi-mechanistic parametric model may be more appropriate. In this way, basic physical controls on bubbles such as pressure can be measured and parameterised against proxies of CH₄ production such as temperature and O₂ gradients.

A dynamic O₂ stable isotope model (PoRGy) that required a minimum number of parameters to quantify daily averaged *P*, *R*, and gas exchange rates under transient field conditions was presented (Chapter 4). PoRGy was the first dynamic δ¹⁸O-O₂ model published that can model ecosystems with diel changes in O₂ concentration and/or δ¹⁸O-O₂. It was a significant advancement in O₂ research because it removed the previous requirement for steady-state assumptions when interpreting δ¹⁸O-O₂ data. The *P*:*R*:*G* ratio was presented as a more ecologically meaningful ratio than *P*:*R* because it compared community metabolism to an independent but ecologically relevant variable, gas exchange.

A framework for interpreting diel δ¹⁸O-O₂ curves was developed using PoRGy (Chapter 5). The effects of six key environmental and biological parameters on diel O₂ and δ¹⁸O-O₂ curves was presented allowing preliminary assessments of aquatic ecosystems before any modelling is done. Understanding these parameters makes it easier to determine the controls on diel curves, compare aquatic ecosystems, quantitatively estimate *CR* and *PP*, and assess ecosystem health. The usefulness of the *P*:*R*:*G* ratio was further explained with examples that assessed the vulnerability of aquatic ecosystems to environmental stressors.

For the first time in a whole ecosystem, O₂ and δ¹⁸O-O₂ budgets were constructed and O₂-based processes were quantified (Chapter 6). Over five years, net O₂ consumption declined in all three reservoirs by about half. At the whole-reservoir scale, the enrichment factor associated with *CR* (ϵ_{CR}) remains the most difficult parameter to determine because of several inter-related factors, these include: separating the several O₂-consuming pathways including abiotic ones; differences between organisms; the potential for diffusion limitation; and various spatio-temporal variables. The uncertainty on all of these factors needs to be reduced as ecosystem-level δ¹⁸O-O₂ studies are conducted. As a result, FLUDEX rates of *CR* and *PP* were calculated from δ¹⁸O-O₂ budgets via three methods. This produced upper- and lower-bounds on *CR* and *PP* rates and provided a constrained estimate of ϵ_{CR} . The methods suggested that rates of *CR* and *PP* slowed year-after-year and that rates in the three reservoirs were likely within 10–20% of each other.

CH₄ oxidation enrichment factors for upland and wetland boreal reservoirs were determined in Chapter 7 so that CH₄ production and oxidation could be individually quantified. The enrichment factors in the boreal wetland reservoir (ELARP) decreased with temperature and the rate of CH₄ ox-

idation increased with temperature. In two FLUDEX reservoirs, the enrichment factor was smaller than in ELARP and there was little or no temperature effect on either the enrichment factor or CH₄ oxidation rate. Together, these enrichment factors indicate that $\delta^{13}\text{C-CH}_4$ values before and after flooding in ELARP are not directly comparable and that $\delta^{13}\text{C-CH}_4$ values in FLUDEX and ELARP cannot be compared to each other. These were the first CH₄ oxidation enrichment factors published for boreal reservoirs and are among the few that have assessed temperature- and rate-dependence of the CH₄ oxidation enrichment factor.

Values of k in the low-wind-speed FLUDEX reservoirs were determined by comparing several methods so that rates of diffusive gas flux could be determined (Chapter 8). The k was calculated using sulfur hexafluoride (SF₆) via both a whole-reservoir trace-gas spike and by the flux rate of SF₆ into static flux chambers (SFCs). SFC-derived k values were 2–8× greater than whole reservoir coefficients. SFCs likely overestimated k by disturbing the surface boundary layer and because they were not deployed during the lower-wind-speed periods overnight. There are few published data on k in low-wind environments particularly because at low wind speeds, wind and wave processes stop being the controlling factors of gas exchange. Given the heterogeneity of the flux rates measured by SFCs, a larger-scale approach to estimate gas fluxes may be more appropriate in small, sheltered ecosystem.

The results of the upland and wetland reservoir experiments were compared (Chapter 9). A series of equations was developed from all available field data to describe the change in CO₂ and CH₄ flux from the flooded ecosystems to the atmosphere. These equations were used to compare 10 a of field data from ELARP with 5 a of data from FLUDEX and to estimate GHG fluxes from those ecosystems for 20 a. Over 10 a, the flux rate of C from ELARP to the atmosphere was only about 3-fold greater than FLUDEX despite the 19-times difference between their pre-flood OC stores. The flux rates of both CO₂ and CH₄ from ELARP to the atmosphere were large and lasting. In FLUDEX, the CO₂ flux rate decreased from the first year onward and the flux rate of CH₄ peaked in the third year and declined rapidly after that. The flux rate of dissolved organic carbon (DOC) from ELARP was small relative to both CO₂ and CH₄ and was negligible by the tenth year of flooding. However, DOC flux rates from FLUDEX were more than one-third of the total C flux rate. When projected over 20 a, the differences between ELARP and FLUDEX became more apparent since the large OC stores in ELARP appear to be able to fuel CO₂, CH₄, and DOC flux rates at levels much elevated above pre-flood levels for decades. In FLUDEX, the CO₂, CH₄, and DOC flux rates declined and plateaued within 5 to 10 years suggesting that slower OC decomposition rates controlled C cycling in the upland reservoirs.

As a means of comparing C- and O₂-based rates of *CR* and *PP*, a series of proof-of-concept experiments were conducted in the same closed system over

time (Appendix A). Concentrations and isotopic ratios (O_2 , DIC, $\delta^{18}O-O_2$, and $\delta^{13}C-DIC$) were measured and used to determine rates and enrichment factors. Results suggested that, within the errors of the measurements, *CR* and *PP* rates were comparable in carbon and O_2 units. Further, isotopic enrichment factors for *CR* and *PP* were within previously determined ranges suggesting that these experiments had not deviated from established models of carbon and O_2 cycling.

10.3 Questions for Future Research

Decomposition dynamics have been studied at different time-scales and by researchers from different disciplines (cf. *Chapin III et al., 2006; Cole and Caraco, 2001; del Giorgio and Williams, 2005; Raich and Tufekcioglu, 2000; Trumbore, 2000*). When using $\delta^{13}C$ to estimate *CR* and decomposition, it became apparent that several important aspects remain unstudied. While litterbag experiments have been conducted in a plethora of forest and field ecosystems (e.g., *Moore et al., 2006*), very few have been done in flooded or seasonally inundated ecosystems (e.g., *Hall and St.Louis, 2004; Oelbermann and Schiff, 2008, in prep*). This lack of study in wet or moist ecosystems became evident during the attempts to understand and discuss *CR* and ϵ_{CR} and when assigning a $\delta^{13}C-CR$ end-member for the isotope-mass budgets (Chapter 2). *Davidson et al. (2006)* proposed moving beyond basic temperature-dependent equations when modelling microbial activity, however, data for flooded soils have not been published.

In general, there are few proxies that can be used for reservoir age when estimating the effects of flooding. As a result, it is imperative to continue monitoring ecosystems that have undergone inundation. In addition to questions of age and decomposition, there are unknowns related to isotopes. The isotope dynamics of decomposition, flooded or not, are not well enough studied and to confound the problem, findings from published studies are contradictory (e.g., *Ehleringer et al., 2000; Lehmann et al., 2002; Nadelhoffer and Fry, 1988; Oelbermann and Schiff, 2008; Schweizer et al., 1999; Šantrůčková et al., 2000*).

The bigger picture of studying flooded ecosystems includes understanding the changes that ecosystems make between ecological steady-states. When uplands and seasonally wet areas are converted into wetlands, ponds, and lakes, some ecological thresholds may be passed and thus the flooded ecosystems may tend toward another steady-state or may oscillate chaotically between states (*Carpenter et al., 1999; Groffman et al., 2006*, and e.g., *Rosenberg et al., 1997*). Using reservoirs, and their associated large-scale changes in hydrology, as proxies for changes such as melting permafrost (*Beilman et al., 2001; Gorham, 1991; Turetsky et al., 2002*), may provide insights for northern Canada and global boreal areas in this century. Similarly, reservoir decom-

missioning may be used as a proxy for predicted declines in the water levels of lakes and subsequent revegetation (e.g., the Penobscot River Mercury Study and Penobscot River Restoration Project).

One of the common and important findings in both FLUDEX and ELARP research was the large flux of CH₄ from the reservoirs to the atmosphere. Understanding the factors that control these fluxes would help develop a model of CH₄ fluxes and enable a determination of whether the controlling factor is: temperature, nutrients, redox conditions, or available substrate. Since CH₄ is produced in anoxic environments like flooded soils or peat, it may be possible to model CH₄ fluxes simply as a net flux from the sediment to the oxic water column while assuming that there are no water column processes. If anoxia and temperature are the drivers of CH₄ production and anoxia can be estimated with temperature data, by combining O₂ diffusion with CR, then CH₄ fluxes would be a function of temperature (R. H. Hesslein, personal communication). Testing this hypothesis with a variety of data sets may prove to be rewarding.

Ebullition from FLUDEX was difficult to measure but was certainly easier to measure than in ELARP. Bubble flux and bubble volumes are notoriously difficult to measure in wetlands (*Fechner-Levy and Hemond, 1996; Walter and Heimann, 2000; Walter et al., 2006*). However, ebullition could be a large source of GHGs, mostly CH₄, to the atmosphere and this flux needs to be quantified. It is possible that to measure bubbles at a large scale may only be achieved by proxies such as estimates of bubble storage volumes and by using continuously deployed static-flux chambers. The former has been performed by measuring bubbles stored in flooded soils (Chapter 3) and by recording the elevation changes in peatlands (e.g., *Fechner-Levy and Hemond, 1996; Strack et al., 2005*). The latter could be done by looking for evidence of rapid changes in CH₄ concentration similar to the methods employed when interpreting static-flux-chamber data. With an automated chamber (e.g., *Carignan, 1998*), both ebullitive events and diffusive fluxes could be measured. In addition to the methods outlined in Chapters 2 and 3, *Huttunen et al. (2001)* described a sediment bubble gas sampler and a subsurface bubble gas collector. Although these were improvements, there remains a need for ebullition research including new sampling techniques.

One question that was never fully addressed in FLUDEX and ELARP was the total composition of bubbles. Measurements of CH₄ and CO₂ concentrations were easily and regularly performed but concentrations never summed to 100%. Nitrogen likely formed the balance of the bubble gas, but it had not been measured and its fraction would have been expected to change during each flood season (cf. *Fechner-Levy and Hemond, 1996*). The sum of CH₄ and CO₂ generally increased during each flood season in FLUDEX (Chapter 3), which could be a result of the decline in nitrogen gas and increases in CH₄ and CO₂ in porewater over time. A basic bubble model including variables

such as the volume of ebullition, and changing CH₄ and CO₂ production rates, only suggests that this may be the case.

The fate of the bubbles trapped in the flooded soils at the end of each flood season was addressed in FLUDEX (Chapter 3) but not in ELARP. The ELARP wetland must have had a large store of bubbles, as indicated by the buoyancy of the floating peat and the change in peat elevation through the flood season (cf. *Strack et al., 2005; Tokida et al., 2005, 2007*), however, the total amount of trapped gas and its ultimate fate is unknown. In mid-winter when the ELARP pond is frozen over, gas forms pools under the ice and this gas is released to the atmosphere in early spring (K. G. Beaty, personal communication). Further, the amount of bubbles that over-winter in the peat is also unknown.

Several decades of research on the relationship between wind speed and gas exchange has provided several equations for estimating the k for open waters (cf. *Cole and Caraco, 1998; Crusius and Wanninkhof, 2003; Wanninkhof, 1992*). However, in low-wind environments, such as FLUDEX reservoirs and parts of the ELARP pond, it is very difficult to estimate the k without direct measurement (*Matthews et al., 2003*, Chapter 8). Wind speeds 1 m above the surface of FLUDEX reservoirs were very low, averaging 0.24 m s⁻¹ during the day and 0.08 m s⁻¹ at night (*Matthews et al., 2003*). Wind speeds above the ELARP pond typically averaged about 2 m s⁻¹ (J. W. M. Rudd, C. A. Kelly, and V. L. St. Louis, unpublished data). Some wind-speed-to-gas-exchange-coefficient relationships have a sharp break around 3.7 m s⁻¹ to account for low and high wind speeds (*Wanninkhof, 1992*) while others suggest a constant k for wind speeds < 2 m s⁻¹ (*Cole and Caraco, 1998; Crusius and Wanninkhof, 2003*). In any case, the agreement between the various wind-speed-to-gas-exchange-coefficient relationships is poor at low wind speeds. An approach that avoids using wind speeds, such as physical limnology, may be appropriate in some ecosystems (*MacIntyre et al., 2001*). Further, the effect of organic films in reducing the k has been noted but not well studied (*Frew et al., 2004*). Such films were evident in FLUDEX reservoirs and may have been a factor that contributed to the slow k values in FLUDEX.

In summary, research on carbon decomposition dynamics and isotopes has not been fully exploited. There are also several areas for research into O₂ respiration that would benefit from further study. The ambiguity around estimates of CR in freshwater, which organisms are respiring, at what rate, and where, has been identified as areas requiring more research (*del Giorgio and Williams, 2005; Pace and Prairie, 2005; Williams and del Giorgio, 2005*). The uncertainty around ϵ_{CR} and O₂ consumption in freshwaters is large enough that constrained best-fit modelling was the approach undertaken in this research (Chapter 4). Determining the differences between benthic and pelagic respiration as well as abiotic O₂ consumption is a logical next step toward understanding biogeochemical cycles in aquatic ecosystems (*Chomicki and Schiff,*

2008, J. J. Venkiteswaran, K. M. Chomicki, and S. L. Schiff, unpublished data).

Recently, a method for estimating the contribution of pelagic and benthic metabolism in small lakes was published (*Van de Bogert et al., 2007*). Adapting this approach for use with $\delta^{18}\text{O}-\text{O}_2$ would provide a means of better understanding the spatio-temporal aspects of CR while using the constraints of $\delta^{18}\text{O}-\text{O}_2$ (*Venkiteswaran et al., 2007*). In stream and river ecosystems, where a large portion of CR likely occurs in benthic and epibenthic communities, there is very little known about ϵ_{CR} . The difficulties in studies of these ecosystems are that while whole-water incubations may not be appropriate, benthic chambers or benthic incubations are very difficult to perform because of the nature and variability of the substrate. Therefore there are excellent opportunities for some creative experimental design and finely tuned research projects to address these issues.

Appendices

Appendix A

Determining water-column metabolism with carbon and oxygen isotopes

Abstract

A series of light and dark sealed chamber experiments were conducted to determine how well DIC, O₂, δ¹³C-DIC, and δ¹⁸O-O₂ could be measured simultaneously. Rates of community respiration (*CR*) and primary production (*PP*) were calculated by measuring these parameters and compiling isotope-mass budgets in the open systems of the FLUDEX reservoirs. The closed systems of sealed chambers offered the opportunity to estimate how well carbon and O₂ budgets matched by removing the confounding influences of gas exchange and hydrology. *CR* rates were comparable (3.8 μmol O₂ L⁻¹ h⁻¹ and 4.5 μmol O₂ L⁻¹ h⁻¹ and 2.9 μmol DIC L⁻¹ h⁻¹ and 3.0 μmol DIC L⁻¹ h⁻¹) and respiratory quotients were similar 0.68 and 0.78. The DIC produced by *CR* had similar δ¹³C-DIC values (-26.7 ‰ and -27.1 ‰) to the dissolved organic carbon (-29.9 ‰). The δ¹⁸O-O₂ enrichment factors for *CR* were between -7.0 ‰ and -1.8 ‰. *PP* rates were comparable (5.1 μmol O₂ L⁻¹ h⁻¹ and 5.9 μmol O₂ L⁻¹ h⁻¹ and 3.0 μmol DIC L⁻¹ h⁻¹ and 3.1 μmol DIC L⁻¹ h⁻¹) and photosynthetic quotients were 0.97 and 1.24. Photosynthetic δ¹³C-DIC enrichment factors were between -5.8 ‰ and -12.2 ‰. These results suggest that, within the errors of measurement, *CR* and *PP* rates were comparable in carbon and O₂ units. Further, enrichment factors could be explained by current models of metabolism and were within previously determined ranges, suggesting that these experiments did not deviate from established models of carbon and O₂ cycling.

A.1 Introduction

Much of the reservoir research at the Experimental Lakes Area (ELA) has focused on the sediment–water interface or across the ecosystem–atmosphere interface because these are the locations where the greatest fluxes of greenhouse gases (GHGs) occur (e.g. *Matthews, 2002; Scott et al., 1999*). A result of this focus is that studies of pelagic carbon (C) cycling and metabolism have often been secondary. Collecting representative samples of the open-water is easier than studying surfaces and interfaces. This experiment provided the opportunity to study pelagic metabolism at the same time as testing assumptions about isotopic methods in a simplified closed system.

Whole-reservoir research on the Flooded Upland Dynamics Experiment (FLUDEX) has included determination of net dissolved inorganic C (DIC) production (*Matthews et al., 2005*, Chapter 2) and net O₂ consumption (Chapter 6). Additionally, stable isotopic ratios of C and oxygen (¹³C/¹²C, hereafter as $\delta^{13}\text{C}$; and ¹⁸O/¹⁶O, hereafter as $\delta^{18}\text{O}$) were used to determine rates of community respiration (CR) and primary production (PP) (Chapters 2 and 6). Determining CR and PP requires several assumptions about isotopic enrichment, details of which are outlined in Chapters 2 and 6.

To determine how well DIC and O₂ could be measured in the same closed system over time, a series of sealed-chamber experiments were conducted in 2002. Rates of DIC and O₂ change were compared and enrichment factors were calculated from changes in $\delta^{13}\text{C}$ -DIC and $\delta^{18}\text{O}$ -O₂. Given the unreliable results obtained using benthic chambers (*Joyce, 2001; Matthews, 2002*), the ability to reconcile DIC and O₂ was paramount for interpreting whole reservoir budgets (see Chapters 2, 3 and 6).

A.2 Methods

FLUDEX reservoirs

In 1999, three upland boreal forest reservoirs were built at the (ELA) to study the changes in the cycles of GHGs and mercury as a result of flooding (*Bodaly et al., 2004*). These reservoirs differed in their amounts and types of pre-flood organic C (OC) stores and were named accordingly: High, Medium, Low C reservoirs. Reservoir surface areas were between 0.5 and 0.8 ha and mean depths were about 1 m (Table 2.1). Reservoir water chemistry was well characterised and DIC concentrations were always greater than those of the inflow (Chapter 2). Similarly, reservoir O₂ concentrations were consistently less than those of the inflow (Chapter 6). More detailed information about the reservoirs is provided elsewhere (*Bodaly et al., 2004*, Chapter 2).

Sealed chambers

Three 18.9 L plastic bottles, the same type of bottle used for benthic chambers, were filled with Medium C reservoir water and 240 mL of periphyton. The periphyton was collected from the sheets of algae that grew attached to the flooded trees by either slowly drawing in periphyton to a syringe or breaking twigs and allowing most of the water to drain from the periphyton. Chambers were deployed in an open, shallow part of the Medium C reservoir in late-July for about 33 h covering a day–night–day cycle to emphasise the changes expected by *PP*. Chambers were again deployed in late-August for 12 d to allow a greater total of *CR* and *PP* to alter the concentration and δ values than in July. Each time, a second set of three chambers was concurrently deployed in the same manner but was darkened to prevent any light from entering the chamber. Based on initial results, the second deployment of dark sealed chambers was limited to 30 h to prevent them from becoming anoxic. Initial and final samples for DIC and O₂ concentrations and $\delta^{13}\text{C}$ -DIC and $\delta^{18}\text{O}$ -O₂ were collected from all chambers.

Analytical methods

Samples for DIC concentration were collected in 50 mL Wheaton serum bottles, capped the pre-baked Vacutainer stoppers, killed by acidification, and analysed via gas chromatography as per (Chapter 2). Samples were kept cool and dark, and were analysed within two weeks. Precision of DIC concentration analysis was $\pm 5\%$. $\delta^{13}\text{C}$ -DIC samples were collected in the same manner, killed with sodium azide, and analysed at the Environmental Isotope Laboratory (EIL) at the University of Waterloo as per Chapter 2. Precision of $\delta^{13}\text{C}$ -DIC analysis was $\pm 0.3\%$. Samples for O₂ concentration were collected in 300 mL BOD bottles with ground-glass stoppers. Samples were fixed within one hour and titrated the same day following the methods described in *Carignan et al. (1998)*. Titration of duplicate samples was within 0.3 mg O₂/L. $\delta^{18}\text{O}$ -O₂ samples were collected in pre-evacuated 125 mL serum bottles with butyl blue stoppers and killed with sodium azide. Samples were analysed at EIL as per Chapter 6. Precision of $\delta^{18}\text{O}$ -O₂ analysis was $< \pm 0.2\%$.

Theory and equations

Five variables were calculated using samples collected from dark sealed chambers. *CR* rate was calculated from the change in O₂ and DIC concentrations (Equations A.1 and A.2). The respiratory quotient (*RQ*), the ratio of DIC produced to O₂ consumed by *CR*, was calculated (Equation A.3) and should be about 0.67–1.24 (cf. Chapter 6). The O₂ enrichment factor for *CR* ($\epsilon_{\text{CR O}_2}$) was calculated based on the change in both O₂ concentration and $\delta^{18}\text{O}$ -O₂ (Equa-

tion A.4) and should be between -25‰ and 0‰ (cf. [Venkiteswaran et al., 2007](#)). The $\delta^{13}\text{C-DIC}$ added to the dark chamber, an estimate of the $\delta^{13}\text{C-DIC}$ produced by CR , was calculated from the change in DIC concentration and $\delta^{13}\text{C-DIC}$ (Equation A.5) and should be about -27‰ (Chapter 2).

$$CR_{O_2} = \frac{C_{initial} - C_{final}}{\Delta t} \quad (\text{A.1})$$

$$CR_{DIC} = \frac{C_{final} - C_{initial}}{\Delta t} \quad (\text{A.2})$$

$$RQ = \frac{CR_{DIC}}{CR_{O_2}} \quad (\text{A.3})$$

$$\epsilon_{CR_{O_2}} = \frac{\ln \frac{\delta_{final} + 1000}{\delta_{initial} + 1000}}{\ln \frac{C_{final}}{C_{initial}}} \quad (\text{A.4})$$

$$\delta^{13}\text{C-DIC}_{added} = \frac{C_{final} \times \delta_{final} - C_{initial} \times \delta_{initial}}{C_{final} - C_{initial}} \quad (\text{A.5})$$

In light sealed chambers, net ecosystem production (NEP) was calculated (Equations A.6 and A.7). NEP was defined as $PP - CR$ ([Lovett et al., 2006](#)) and thus:

$$NEP_{O_2} = \frac{C_{final} - C_{initial}}{\Delta t} \quad (\text{A.6})$$

$$NEP_{DIC} = \frac{C_{final} - C_{initial}}{\Delta t} \quad (\text{A.7})$$

By combining data from light and dark sealed chambers, four variables related to PP were calculated. PP rate was calculated for both O_2 and DIC (Equations A.8 and A.9). The photosynthetic quotient (PQ), the ratio of O_2 produced to DIC consumed by PP , was calculated (Equation A.10) and should be about 1.0–1.4 (cf. Chapter 6). The DIC enrichment factor for PP ($\epsilon_{PP_{DIC}}$) was calculated based on the change in both DIC concentration and $\delta^{13}\text{C-DIC}$ (Equation A.11) and should be between -20‰ and $< 0\text{‰}$ ([Hecky and Hesslein, 1995](#), Chapter 2).

$$PP_{O_2} = NEP_{O_2} - CR_{O_2} \quad (\text{A.8})$$

$$PP_{DIC} = CR_{DIC} - NEP_{DIC} \quad (\text{A.9})$$

$$PQ = \frac{PP_{O_2}}{PP_{DIC}} \quad (\text{A.10})$$

$$\epsilon_{PP_{DIC}} = \frac{C_{final,light} \times \delta_{final,light} - C_{initial,light} \times \delta_{initial,light} - CR_{DIC} \times \delta^{13}\text{C-DIC}_{added}}{C_{final,light} - C_{initial,light} - CR_{DIC}} - \delta_{initial,light} \quad (\text{A.11})$$

A.3 Results and discussion

Dark chambers

All dark sealed chambers exhibited an increase in DIC concentration and a decrease in O₂ concentration (Figure A.1). This is consistent with CR (cf. *Falkowski and Raven, 1997*) (Equations A.1 and A.2). The late-July chambers exhibited CR rates of 4.5 μmol O₂ L⁻¹ h⁻¹ and 2.9 μmol DIC L⁻¹ h⁻¹. CR rates in late August were slightly slower in O₂ and similar in DIC: 3.8 μmol O₂ L⁻¹ h⁻¹ and 3.0 μmol DIC L⁻¹ h⁻¹. Water column CR rates were two to three orders of magnitude slower than seasonal whole reservoirs rates calculated from the isotope-mass budgets, 167 μmol DIC L⁻¹ h⁻¹ and 1074 μmol O₂ L⁻¹ h⁻¹ (Chapters 3 and 6.) Given the large stores of OC in the flooded soils, rates of CR would be expected to be much greater in the soils than in the flooded water column.

One way to assess how well rates based on DIC and O₂ can be reconciled is to calculate the RQ observed in the dark sealed chambers (Equation A.3). This requires that only aerobic CR affects CO₂ and O₂ concentrations. In practical applications, RQ is often assumed to be 0.8–1.0 (*Duarte and Agustí, 1998*) and *del Giorgio and Williams (2005)* suggest 0.67–1.24. The late-July and late-August dark sealed chambers had RQ values of 0.65 and 0.78 (Figure A.2). While these RQ values fell within the expected ranges, it is difficult to describe the composition of a carbon source (e.g., carbohydrates versus lipid) based on these quotients because of the magnitude of error surrounding DIC and O₂ concentration measurements.

The δ¹³C-DIC in all dark sealed chambers decreased by more than 0.5 ‰. Given adequate supplies of decomposable organic carbon and nutrients, CR was expected to add δ¹³C-DIC of about –27 ‰ based on the assumption outlined in Chapter 2 and the δ¹³C-DIC of dark sealed chambers should therefore have tended toward that value. Using Equation A.5, the δ¹³C-DIC added was calculated to be –26.7 ‰ and –27.1 ‰ in the late-July and late-August incubations. These results are consistent with incubations of FLUDEX soils and vegetation (*Baril, 2001; Boudreau, 2000; Ferguson, 2000; Oelbermann and Schiff, 2008*).

The δ¹⁸O-O₂ in all dark sealed chambers increased by more than 1.6 ‰ (Figure A.1). This increase and the measured decrease in O₂ is characteristic of CR (cf. *Venkiteswaran et al., 2007*). Using initial and final O₂ concentrations and δ¹⁸O-O₂ values, enrichment factors for CR were calculated (Equation A.4). Enrichment factors ranged between –7.0 ‰ and –1.8 ‰. There was very little relationship between O₂ consumption rates and enrichment factors ($r^2 = 0.16$, Figure A.3). Enrichment factors this weak (i.e., close to zero) have been observed in systems with low O₂ concentrations and/or those with diffusion limitation (*Brandes and Devol, 1997; Hartnett et al., 2005; Hendry et al., 2002*). These enrichment factors were much weaker than those

determined by whole reservoir diel $\delta^{18}\text{O}\text{-O}_2$ measurements in 2003 (Chapter 6) and those of rivers in North America (Venkiteswaran *et al.*, 2007, 2008).

Light Chambers

The light sealed chambers exhibited an average decrease in DIC and an increase in O_2 concentrations (Figure A.1). Given the day-and-night combination experienced by the chambers, the magnitude of concentration change (NEP) was expected to be less than that of the dark sealed chambers. NEP rates in the late-July chambers incubated for 33 h were $0.62 \mu\text{mol O}_2 \text{ L}^{-1} \text{ h}^{-1}$ and $-3.0 \mu\text{mol DIC L}^{-1} \text{ h}^{-1}$. The late-August light chambers incubated for 288 h had NEP rates of $0.16 \mu\text{mol O}_2 \text{ L}^{-1} \text{ h}^{-1}$ and $-0.21 \mu\text{mol DIC L}^{-1} \text{ h}^{-1}$.

PP was calculated by combining data from the light and dark chambers (Equations A.8 and A.9). In late-July, PP was $5.9 \mu\text{mol DIC L}^{-1} \text{ h}^{-1}$ and $3.2 \mu\text{mol O}_2 \text{ L}^{-1} \text{ h}^{-1}$. In late-August, PP was $5.1 \mu\text{mol DIC L}^{-1} \text{ h}^{-1}$ and $3.0 \mu\text{mol O}_2 \text{ L}^{-1} \text{ h}^{-1}$. Given the periphyton that covered the drowned trees and the biofilm on the flooded soils, water column PP was expected to be much lower than whole-reservoir PP because the latter included periphyton and biofilm (Chapters 2, 3, and 6). Seasonal whole-reservoir PP was $42 \mu\text{mol DIC L}^{-1} \text{ h}^{-1}$ and $791 \mu\text{mol O}_2 \text{ L}^{-1} \text{ h}^{-1}$.

Another way to assess how well rates based on DIC and O_2 can be measured concurrently was to calculate the PQ (Equation A.10). The PQ was 0.97 in late-July and 1.26 in late-August. These quotients are within the range of about 1.0–1.4 commonly calculated and used by other researchers (cf. Chapter 6).

If the $\epsilon_{PP_{DIC}}$ was known for these sealed chambers, then ' $\delta^{13}\text{C}$ -inferred' CR and PP could be calculated directly from the $\delta^{13}\text{C}$ -DIC values in a manner similar to the whole-reservoir estimates in Chapter 2. Given the possible range of $\epsilon_{PP_{DIC}}$ (cf. Hecky and Hesslein, 1995) and lack of independent information to narrow this range for the sealed chambers, this was not possible. However, based on a few assumptions, the change in DIC concentration and $\delta^{13}\text{C}$ was used to estimate $\epsilon_{PP_{DIC}}$. Since $C_{final} - C_{initial} = CR - PP$ in the light sealed chambers (a rewritten NEP Equation A.7) and assuming both an average CR and $\delta^{13}\text{C}\text{-DIC}_{added} = -27 \text{‰}$ from the dark sealed chambers (Equation A.5), an estimate of $\epsilon_{PP_{DIC}}$ can be made (Equation A.11).

The $\epsilon_{PP_{DIC}}$ values were calculated to be an average of -5.8‰ in late-July and -12.2‰ in late-August. Hecky and Hesslein (1995) describe $\epsilon_{PP_{DIC}}$ as decreasing in magnitude as PP rate increased in a shape similar to a hyperbolic tangent where small changes in PP and low PP rates caused the largest change in $\epsilon_{PP_{DIC}}$ values. This pattern occurs in the data from the sealed chambers. At low rates of PP , around $3 \mu\text{mol DIC L}^{-1} \text{ h}^{-1}$ the $\epsilon_{PP_{DIC}}$ was -12.2‰ and as PP rate increased to 4–5 and $9 \mu\text{mol DIC L}^{-1} \text{ h}^{-1}$, the magnitude of $\epsilon_{PP_{DIC}}$ decreased to -6‰ and -4‰ (Figure A.4).

The $\delta^{18}\text{O}\text{-O}_2$ in all light sealed chambers decreased during the incubations

(Figure A.1). The average rate of decline was larger in the shorter late-July incubations than in the longer late-August incubations, averaging -1.5‰ and -3.6‰ respectively. Given the nature of $\delta^{18}\text{O}\text{-O}_2$ systematics (cf. [Venkiteswaran et al., 2007](#)), it would not have been unexpected to observe a greater decline in $\delta^{18}\text{O}\text{-O}_2$ values in the longer incubations since O_2 production from *PP* affects the $\delta^{18}\text{O}\text{-O}_2$ more than O_2 consumption by *CR*. However, when the change in $\delta^{18}\text{O}\text{-O}_2$ is considered against the net rate of O_2 change, there is no relationship ($r^2 = 0.09$).

Unlike many benthic chambers where CH_4 concentrations were adequately large to calculate rates and to determine $\delta^{13}\text{C}\text{-CH}_4$ values, CH_4 concentrations in sealed chambers were low, $< 3\text{--}4\ \mu\text{mol/L}$. These concentrations were typical of the reservoir water column.

Comparing the rates of *CR* and *PP* in the incubations and from the whole-reservoir isotope-mass budgets indicated that water column processes were a much smaller component of DIC and O_2 cycling than were flooded soil or periphyton processes. In retrospect, a simple series of incubations to measure DIC and O_2 in the light and dark would have provided more information about water column processes than the larger and cumbersome sealed chambers (e.g., see methods described by [Carignan et al., 1998](#); [Davies et al., 2003](#)).

A.4 Conclusions

Both *RQ* and *PQ* values were within expected ranges indicating that, given the level of precision of DIC and O_2 concentration measurements, both *CR* and *PP* rates were adequately measured in both C and O_2 currencies. The $\delta^{13}\text{C}\text{-DIC}_{\text{added}}$ was close to -27‰ , confirming the results from previous laboratory incubations ([Baril, 2001](#); [Boudreau, 2000](#); [Ferguson, 2000](#); [Oelbermann and Schiff, 2008](#)) and the assumptions made in Chapter 2 that $\epsilon_{\text{CR}_{\text{DIC}}}$ was very small.

The magnitude of the $\epsilon_{\text{CR}_{\text{O}_2}}$ values was within the wide range reported in the literature (cf. [Venkiteswaran et al., 2007](#)). Although the values were smaller than average, this was not unexpected in sealed chambers without mechanical stirring. Values were comparable to the lake-water incubations conducted in 2004 at ELA and Dorset, central Ontario (J. J. Venkiteswaran, K. M. Chomicki, and S. L. Schiff, unpublished data). The magnitude of $\epsilon_{\text{PP}_{\text{DIC}}}$ was variable but within the expected range and broadly followed the pattern versus rate relationship described by [Hecky and Hesslein \(1995\)](#) (Figure A.4).

Together, these results indicate that multiple, simultaneous measures of *CR* and *PP* were successful and comparable. The enrichment factors determined by changes in $\delta^{13}\text{C}$ and $\delta^{18}\text{O}$ values were within expected ranges and were comparable to results from other incubation experiments. The $\delta^{13}\text{C}\text{-DIC}$ production by decomposition, as estimated by $\delta^{13}\text{C}\text{-DIC}_{\text{added}}$, independently confirmed previous assumptions about DOC decomposition. Thus these

sealed-chamber experiments were successful and support the assumptions and calculations made when estimating whole-reservoir rates of *CR* and *PP* by both $\delta^{13}\text{C-DIC}$ and $\delta^{18}\text{O-O}_2$ (Chapters 2 and 6).

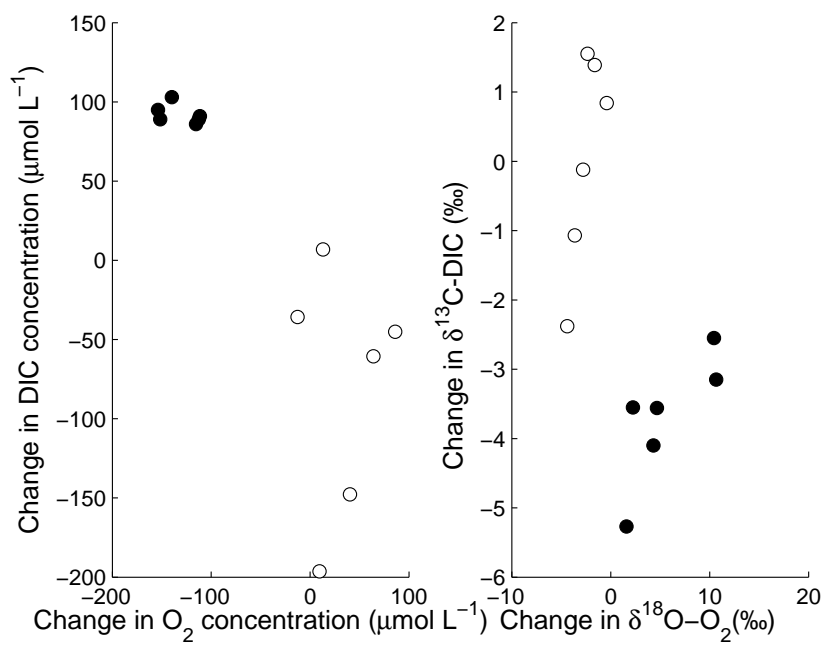


Figure A.1: Change in O_2 and DIC concentrations and $\delta^{18}\text{O-O}_2$ and $\delta^{13}\text{C-DIC}$ values of the FLUDEX light (open circles) and dark (closed circles) sealed chambers in late-July and late-August 2002.

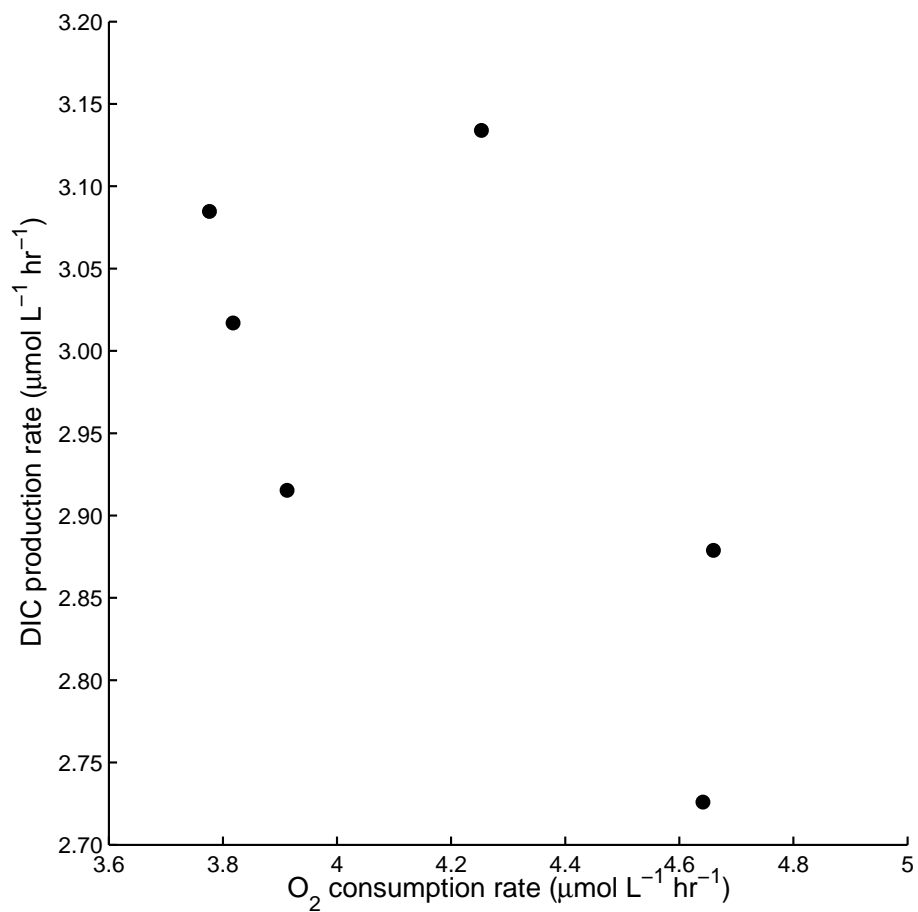


Figure A.2: DIC- and O₂-based CR rates in dark, sealed chambers in FLUDEX in late-July and late-August 2002. A positive relationship between DIC- and O₂-based measures of respiration was expected and any offset between the two would be a function of the respiratory quotient (equation 6.8).

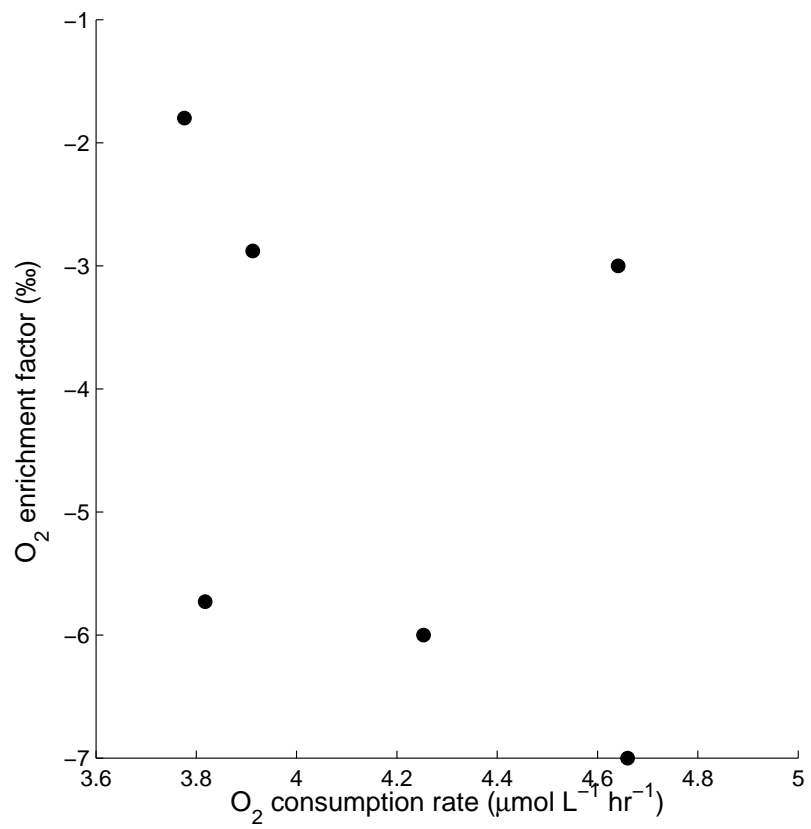


Figure A.3: Respiratory $\delta^{18}\text{O}\text{-O}_2$ enrichment factors ($\epsilon_{\text{CR}\text{O}_2}$) in sealed chambers in FLUDEX as a function of CR rate in late-July and late-August 2002.

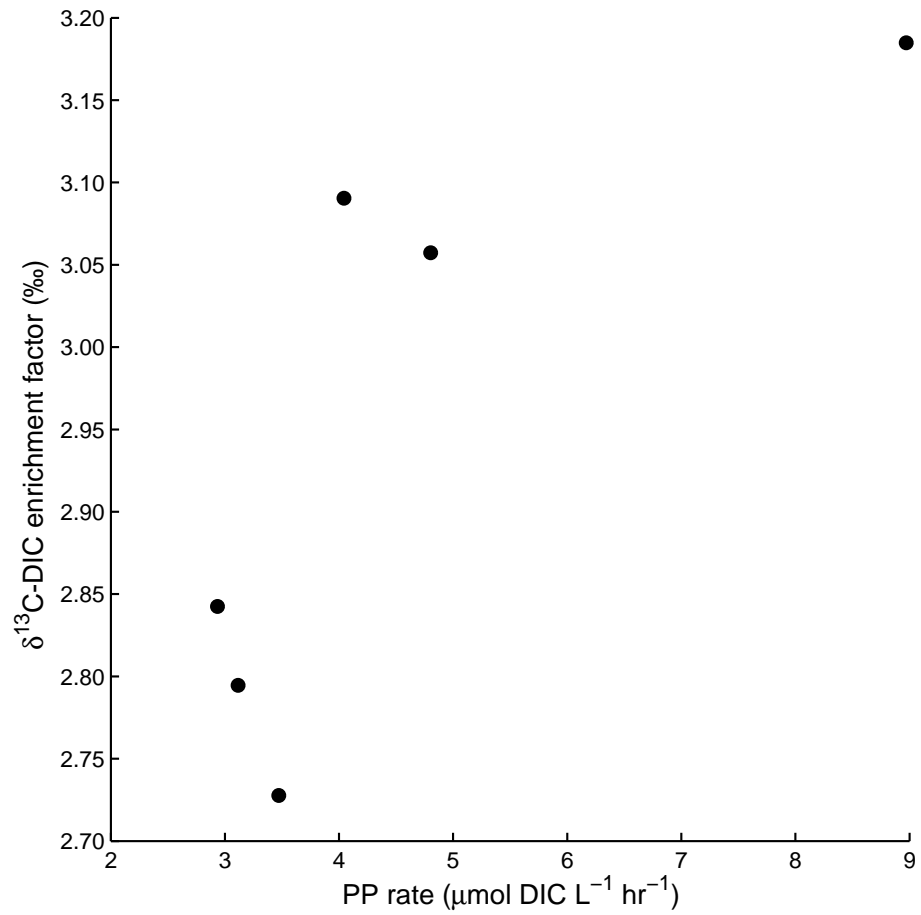


Figure A.4: Photosynthetic $\delta^{13}\text{C}$ -DIC enrichment factors ($\epsilon_{PP_{DIC}}$) in sealed chambers in FLUDEX as a function of PP rate in late-July and late-August 2002.

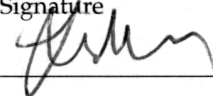
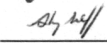
Appendix B

Permission to include and republish copyrighted materials

B.1 Permission to include and republish Chapter 4

We, the undersigned, as co-authors of *Venkiteswaran et al. (2007)*, permit the inclusion of this material in Jason Venkiteswaran's Ph.D. thesis and grant permission for the microfilming of this thesis and its use by Library and Archives Canada as worded in the 'Thesis Non-Exclusive License' (form NL/BN 59/02).

Venkiteswaran, J. J., L. I. Wassenaar, and S. L. Schiff (2007), Dynamics of dissolved oxygen isotopic ratios: a transient model to quantify primary production, community respiration, and air-water exchange in aquatic ecosystems, *Oecologia*, 153(2), 385–398, doi: [10.1007/s00442-007-0744-9](https://doi.org/10.1007/s00442-007-0744-9).

Name	Signature	Date
Leonard I. Wassenaar		Nov 6, 2008
Sherry L. Schiff		20 Nov 2008

Permission B.1: License from Springer for Chapter 4.

SPRINGER LICENSE
TERMS AND CONDITIONS

Jun 27, 2007

This is a License Agreement between Jason J Venkiteswaran ("You") and Springer ("Springer"). Please note that you are liable to account for Value Added Tax (VAT). The license consists of your order details, the terms and conditions provided by Springer, and the payment terms and conditions.

License Number 1719500696897

License date May 31, 2007

Licensed content publisher Springer

Licensed content publication Oecologia

Licensed content title Dynamics of dissolved oxygen isotopic ratios: a transient model to quantify primary production, community respiration, and air—water exchange in aquatic ecosystems

Licensed content author Jason J. Venkiteswaran

Licensed content date May 22, 2007

Volume number

Issue number

Pages 1 – 14

Type of Use Thesis / Dissertation

Details of use Print

Portion of the article Full text

Title of your thesis / dissertation Greenhouse gas cycling in experimental boreal reservoirs

Expected completion date Sep 2008

Total 0.00 USD

Terms and Conditions

Introduction

The publisher for this copyrighted material is Springer Science + Business Media. By clicking "accept" in connection with completing this licensing transaction, you agree that the following terms and conditions apply to this transaction (along with the Billing and Payment terms and conditions established by Copyright Clearance Center, Inc. ("CCC"), at the time that you opened your Rightslink account and that are available at any time at <http://myaccount>.

copyright.com).

Limited License

With reference to your request to reprint in your thesis material on which Springer Science and Business Media control the copyright, permission is granted, free of charge, for the use indicated in your enquiry.

Licenses are for one–time use only with a maximum distribution equal to the number that you identified in the licensing process.

This License includes use in an electronic form, provided its password protected or on the university's intranet. For any other electronic use, please contact Springer at (permissions.dordrecht@springer.com or permissions.heidelberg@springer.com)

The material can only be used for the purpose of defending your thesis, and with a maximum of 100 extra copies in paper.

Although Springer holds copyright to the material and is entitled to negotiate on rights, this license is only valid, provided permission is also obtained from the (co) author (address is given with the article/chapter) and provided it concerns original material which does not carry references to other sources (if material in question appears with credit to another source, authorization from that source is required as well). Permission free of charge on this occasion does not prejudice any rights we might have to charge for reproduction of our copyrighted material in the future.

Altering/Modifying Material: Not Permitted

You may not alter or modify the material in any manner. Abbreviations, additions, deletions and/or any other alterations shall be made only with prior written authorization of the author(s) and/or Springer Science + Business Media. (Please contact Springer at (permissions.dordrecht@springer.com or permissions.heidelberg@springer.com)

Reservation of Rights

Springer Science + Business Media reserves all rights not specifically granted in the combination of (i) the license details provided by you and accepted in the course of this licensing transaction, (ii) these terms and conditions and (iii) CCC's Billing and Payment terms and conditions.

Copyright Notice: Disclaimer

You must include the following copyright and permission notice in connection with any reproduction of the licensed material:

"Springer and the original publisher /journal title, volume, year of publication, page, chapter/article title, name(s) of author(s), figure number(s), original copyright notice) is given to the publication in which the material was originally published, by adding; with kind permission from Springer Science and Business Media"

Warranties: Springer Science + Business Media makes no representations or warranties with respect to the licensed material.

Indemnity

You hereby indemnify and agree to hold harmless Springer Science + Business Media and CCC, and their respective officers, directors, employees and agents, from and against any and all claims arising out of your use of the licensed material other than as specifically authorized pursuant to this license.

No Transfer of License

This license is personal to you and may not be sublicensed, assigned, or transferred by you to any other person without Springer Science + Business Media's written permission.

No Amendment Except in Writing

This license may not be amended except in a writing signed by both parties (or, in the case of Springer Science + Business Media, by CCC on Springer Science + Business Media's behalf).

Objection to Contrary Terms

Springer Science + Business Media hereby objects to any terms contained in any purchase order, acknowledgment, check endorsement or other writing prepared by you, which terms are inconsistent with these terms and conditions or CCC's Billing and Payment terms and conditions. These terms and conditions, together with CCC's Billing and Payment terms and conditions (which are incorporated herein), comprise the entire agreement between you and Springer Science + Business Media (and CCC) concerning this licensing transaction. In the event of any conflict between your obligations established by these terms and conditions and those established by CCC's Billing and Payment terms and conditions, these terms and conditions shall control.

Jurisdiction

All disputes that may arise in connection with this present License, or the breach thereof, shall be settled exclusively by the country's law in which the work was originally published.

v1.0

Permission B.2: License from Springer for Chapter 4 in an electronic thesis.

De: Permissions Heidelberg, Springer DE <Permissions.Heidelberg@springer.com>

À: Jason Venkiteswaran <jjvenkit@uwaterloo.ca>

Cc: customercare@copyright.com

Sujet: AW: Thesis/Disseration

Date: Mon, 04 Jun 2007 08:25:10 +0200 (02:25 EDT)

Dear Mr. Venkiteswaran,

Thank you for your e-mail.

Permission is given to use the material requested for the thesis.

We wish you much success.

With kind regards,

Alice Essenpreis
Springer
Rights and Permissions

-

Tiergartenstrasse 17 | 69121 Heidelberg GERMANY

FAX: +49 6221 487 8223

Alice.Essenpreis@springer.com

www.springer.com/rights

-

-----Ursprüngliche Nachricht-----

Von: Jason Venkiteswaran [mailto:jjvenkit@uwaterloo.ca]

Gesendet: Freitag, 1. Juni 2007 17:19

An: Permissions Heidelberg, Springer DE

Cc: customercare@copyright.com

Betreff: Thesis/Disseration

Hello,

I recently went through the process of requesting the right to reproduce a paper from the Springer publication *Oecologia* in my PhD thesis (see license number 1719500696897). However during the application process I noted that the options for "Details of use" are:

1. Print
2. Restricted access internet
3. University intranet

However, since October 2006, my university, the University of Waterloo, requires and accepts only electronic theses. See here for more details:

http://www.grad.uwaterloo.ca/students/current/thesis_regulations.asp

Therefore I need to confirm that the following clauses in the Springer License Terms and Conditions are not incompatible with the requirements of my university:

--Licenses are for one-time use only with a maximum distribution equal to the number that you identified in the licensing process.

--This License includes use in an electronic form, provided its password protected or on the university's intranet.

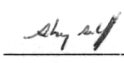
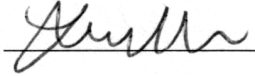
Additionally, my university (as do all other universities in Canada) requires a Theses Non-Exclusive License with the Library and Archives of Canada: <http://www.collectionscanada.ca/obj/s4/f2/frm-nl59-2.pdf>

Thank you for your attention to this matter,
Jason Venkiteswaran.

B.2 Permission to include and republish Chapter 5

We, the undersigned, as co-authors of [Venkiteswaran et al. \(2008\)](#), permit the inclusion of this material in Jason Venkiteswaran's Ph.D. thesis and grant permission for the microfilming of this thesis and its use by Library and Archives Canada as worded in the 'Thesis Non-Exclusive License' (form NL/BN 59/02).

Venkiteswaran, J. J., S. L. Schiff, and L. I. Wassenaar (2008), Aquatic metabolism and ecosystem health assessment using dissolved O₂ stable isotope diel curves, *Ecological Applications*, 18(4), 965–982, doi: [10.1890/07-0491.1](https://doi.org/10.1890/07-0491.1).

Name	Signature	Date
Sherry L. Schiff		<u>20 Nov 2008</u>
Leonard I. Wassenaar		<u>Nov 6, 2008</u>

Permission B.3: License from Ecological Society of America for Chapter 5.

De: Cliff Duke <CSDuke@esa.org>
À: Jason Venkiteswaran <jjvenkit@uwaterloo.ca>
Subject: RE: Request for permission to republish
Date: Mar, 27 Mai 2008 14:27:19 -0400

Mr. Venkiteswaran,

ESA permits students to reprint their articles in their theses. This email confirms that you have permission to do.

Regards,

Clifford S. Duke, Ph.D.
Permissions Editor/Director of Science Programs
Ecological Society of America
1990 M Street NW, Suite 700
Washington, DC 20036

Phone: (202) 833-8773
Fax: (202) 833-8775
Mobile: (202) 320-0905
E-mail: csduke@esa.org
www.esa.org/science

-----Original Message-----

From: Jason Venkiteswaran [mailto:jjvenkit@uwaterloo.ca]
Sent: Monday, May 26, 2008 2:06 PM
To: Cliff Duke
Subject: Request for permission to republish

Hello,

Recently, a manuscript of mine was published in Ecological Applications (18(4): 965--982, doi : 10.1890/07-0491.1).

I wish to republish this manuscript in my doctoral thesis. Since October 2006, my university, the University of Waterloo, requires electronic theses. See here for more details: http://www.grad.uwaterloo.ca/students/current/thesis_regulations.asp

Therefore I am requesting permission to republish this manuscript in my thesis with terms that are not incompatible with the requirements of my university. Additionally, my university (as do all other universities in Canada) requires a Theses Non-Exclusive License with the Library and Archives of Canada: <http://www.collectionscanada.ca/obj/s4/f2/frm-nl59-2.pdf>

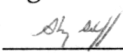
I would, of course, include a statement that the manuscript had previously been published in Ecological Applications with a full citation and that the copyright is held by the Ecological Society of America.

Thank you for your attention to this matter,
Jason Venkiteswaran.

B.3 Permission to include and republish Chapter 7

I, the undersigned, as co-author of *Venkiteswaran and Schiff (2005)*, permit the inclusion of this material in Jason Venkiteswaran's Ph.D. thesis and grant permission for the microfilming of this thesis and its use by Library and Archives Canada as worded in the 'Thesis Non-Exclusive License' (form NL/BN 59/02).

Venkiteswaran, J. J., and S. L. Schiff (2005), Methane oxidation: isotopic enrichment factors in freshwater boreal reservoirs, *Applied Geochemistry*, 20(4), 683–690, doi: [10.1016/j.apgeochem.2004.11.007](https://doi.org/10.1016/j.apgeochem.2004.11.007).

Name	Signature	Date
SherryL.Schiff		20 Nov. 2008

Permission B.4: License from Elsevier for Chapter 7.

De: Jones, Jennifer (ELS–OXF) <J.Jones@elsevier.co.uk>

À: jjvenkit@uwaterloo.ca

Sujet: RE: Obtain Permission

Date: Fri, 8 Jun 2007 12:15:25 +0100 (07:15 EDT)

Dear Jason J Venkiteswaran

We hereby grant you permission to reproduce the material detailed below at no charge in your thesis, in print and on the University of Waterloo web site subject to the following conditions:

1. If any part of the material to be used (for example, figures) has appeared in our publication with credit or acknowledgement to another source, permission must also be sought from that source. If such permission is not obtained then that material may not be included in your publication/copies.
2. Suitable acknowledgment to the source must be made, either as a footnote or in a reference list at the end of your publication, as follows:

"This article was published in Publication title, Vol number, Author(s), Title of article, Page Nos , Copyright Elsevier (or appropriate Society name) (Year)."

3. Your thesis may be submitted to your institution in either print or electronic form.
4. Reproduction of this material is confined to the purpose for which permission is hereby given.
5. This permission is granted for non–exclusive world English rights only. For other languages please reapply separately for each one required. Permission excludes use in an electronic form other than as specified above. Should you have a specific electronic project in mind please reapply for permission.
6. This includes permission for the Library and Archives of Canada to supply single copies, on demand, of the complete thesis. Should your thesis be published commercially, please reapply for permission.

Yours sincerely

Jennifer Jones

Rights Assistant

Your future requests will be handled more quickly if you complete the online form at www.elsevier.com/permissions

Elsevier Limited, a company registered in England and Wales with company number 1982084, whose registered office is The Boulevard, Langford Lane, Kidlington, Oxford, OX5 1GB, United Kingdom.

References

- Abril, G., F. Guérin, S. Richard, R. Delmas, C. Galy-Lacaux, P. Gosse, A. Tremblay, L. Varfalvy, M. A. Dos Santos, and B. Matvienko (2005), Carbon dioxide and methane emissions and the carbon budget of a 10-year old tropical reservoir (Petit Saut, French Guiana), *Global Biogeochemical Cycles*, 19(4), doi: [10.1029/2005GB002457](https://doi.org/10.1029/2005GB002457). 7, 38
- Allan, J. D. (1995), *Stream Ecology: Structure and function of running waters*, first ed., Chapman and Hall. 113
- Allan, J. D., and M. M. Castillo (2007), *Stream Ecology: Structure and function of running waters*, second ed., Springer, doi: [10.1007/978-1-4020-5583-6](https://doi.org/10.1007/978-1-4020-5583-6). 116
- Andrews, S. S., S. Caron, and O. C. Zafiriou (2000), Photochemical oxygen consumption in marine waters: A major sink for colored dissolved organic matter?, *Limnology and Oceanography*, 45(2), 267–277. 69, 90
- Asada, T., B. G. Warner, and S. L. Schiff (2005), Effects of shallow flooding on vegetation and carbon pools in boreal peatlands, *Applied Vegetation Science*, 8(2), 199–208, doi: [10.1658/1402-2001\(2005\)008\[0199:EOSFOV\]2.0.CO;2](https://doi.org/10.1658/1402-2001(2005)008[0199:EOSFOV]2.0.CO;2). 4, 181, 187, 191, 211, 212
- Asada, T., S. L. Schiff, B. G. Warner, C. A. Kelly, V. L. St.Louis, J. W. M. Rudd, M. A. M. Saquet, C. D. Mackenzie, R. H. Hesslein, J. J. Venkiteswaran, R. J. Elgood, B. S. Dyck, J. M. Shay, N. Roulet, K. G. Beaty, T. R. Moore, , and R. O. Aravena (in prep), Change in a carbon pools and fluxes caused by experimental flooding of a boreal peatland-pond complex. 181, 182, 183, 184, 187, 188, 208
- Bade, D. L., S. R. Carpenter, J. J. Cole, M. L. Pace, E. Kritzberg, M. C. Van de Bogert, R. M. Cory, and D. M. McKnight (2007), Sources and fates of dissolved organic carbon in lakes as determined by whole-lake carbon isotope additions, *Biogeochemistry*, 84(2), 115–129, doi: [10.1007/s10533-006-9013-y](https://doi.org/10.1007/s10533-006-9013-y). 214
- Baril, M. (2001), ^{13}C in dissolved inorganic carbon from the decomposition of flooded reservoirs: stable carbon isotope ratios. Bachelor's thesis, University of Waterloo. 18, 24, 227, 229

- Barkan, E., and B. Luz (2003), Measurements of $^{17}\text{O}/^{16}\text{O}$ and $^{18}\text{O}/^{16}\text{O}$ of O_2 and O_2/Ar ratio in air, *Rapid Communications in Mass Spectrometry*, 17(24), 2809–2814, doi: [10.1002/rcm.1267](https://doi.org/10.1002/rcm.1267). 67
- Barth, J. A. C., A. Tait, and M. Bolshaw (2004), Automated analyses of $^{18}\text{O}/^{16}\text{O}$ ratios in dissolved oxygen from 12-mL water samples, *Limnology and Oceanography: Methods*, 2, 35–41. 67
- Bartlett, K. B., and R. C. Harriss (1993), Review and assessment of methane emissions from wetlands, *Chemosphere*, 26(1-4), 261–320. 148
- Barton, B. A., and B. R. Taylor (1996), Oxygen requirements of fishes in northern Alberta rivers with a general review of the adverse effects of low dissolved oxygen, *Water Quality Research Journal of Canada*, 31, 361–409. 88
- Bastviken, D., J. Cole, M. Pace, and L. Tranvik. (2004), Methane emissions from lakes: Dependence of lake characteristics, two regional assessments, and a global estimate, *Global Biogeochemical Cycles*, 18(4), GB4009, doi: [10.1029/2004GB002238](https://doi.org/10.1029/2004GB002238). 38, 116
- Battle, M., M. L. Bender, P. P. Tans, J. W. C. White, J. T. Ellis, T. Conway, and R. J. Francey (2000), Global carbon sinks and their variability inferred from atmospheric O_2 and $\delta^{13}\text{C}$, *Science*, 287(5462), 2467–2470, doi: [10.1126/science.287.5462.2467](https://doi.org/10.1126/science.287.5462.2467). 13
- Bayley, S. E., D. W. Schindler, K. G. Beaty, B. R. Parker, and M. P. Stainton (1992a), Effects of multiple fires on nutrient yields from streams draining boreal forest and fen watersheds: nitrogen and phosphorus, *Canadian Journal of Fisheries and Aquatic Sciences*, 49(3), 584–596. 6, 182
- Bayley, S. E., D. W. Schindler, B. R. Parker, M. P. Stainton, and K. G. Beaty (1992b), Effects of forest-fire and drought on acidity of a base-poor boreal forest stream: similarities between climatic warming and acidic precipitation, *Biogeochemistry*, 17(3), 191–204, doi: [10.1007/BF00004041](https://doi.org/10.1007/BF00004041). 6, 182
- Beilman, D. W., D. H. Vitt, and L. A. Halsey (2001), Localized permafrost peatlands in western Canada: Definition, distributions, and degradation, *Arctic Antarctic and Alpine Research*, 33(1), 70–77, doi: [10.1016/S0038-0717\(02\)00022-6](https://doi.org/10.1016/S0038-0717(02)00022-6). 217
- Bender, M., T. Sowers, and L. Labeyrie (1994), The Dole effect and its variations during the last 130,000 years as measured in the Vostok ice core, *Global Biogeochemical Cycles*, 8(3), 363–376, doi: [10.1029/94GB00724](https://doi.org/10.1029/94GB00724). 67, 116
- Bennoun, P. (2002), The present model for chlororespiration, *Photosynthesis Research*, 73(1-3), 273–277, doi: [10.1023/A:1020479920622](https://doi.org/10.1023/A:1020479920622). 69, 90

- Benson, B. B., D. Krause, Jr, and M. A. Peterson (1979), Solubility and isotopic fractionation of gases in dilute aqueous-solution. 1. Oxygen, *Journal of Solution Chemistry*, 8(9), 655–690. [70](#), [91](#)
- Bird, R. E., and R. L. Hulstrom (1981), A simplified clear sky model for direct and diffuse insolation on horizontal surfaces, *Tech. Rep. SERI/TR-642-761*, Solar Energy Research Institute. [71](#)
- Blunier, T., B. Barnett, M. L. Bender, and M. B. Hendricks (2002), Biological oxygen productivity during the last 60,000 years from triple oxygen isotope measurements, *Global Biogeochemical Cycles*, 16(3), [doi: 10.1029/2001GB001460](#). [116](#)
- Bodaly, R. A., R. E. Hecky, and R. J. P. Fudge (1984), Increases in fish mercury levels in lakes flooded by the Churchill River diversion, northern Manitoba, *Canadian Journal of Fisheries and Aquatic Sciences*, 41(4), 682–691. [2](#)
- Bodaly, R. A., V. L. St.Louis, M. J. Paterson, R. J. P. Fudge, B. D. Hall, D. M. Rosenberg, and J. W. M. Rudd (1997), Bioaccumulation of mercury in the aquatic food chain in newly flooded areas, in *Metal Ions in Biological Systems*, Vol 34, *Metal Ions in Biological Systems*, vol. 34, pp. 259–287. [2](#)
- Bodaly, R. A., K. G. Beaty, L. H. Hendzel, A. R. Majewski, M. J. Paterson, K. R. Rolffhus, A. F. Penn, V. L. St.Louis, B. D. Hall, C. J. D. Matthews, K. A. Cherewyk, M. Mailman, J. P. Hurley, S. Schiff, and J. J. Venkiteswaran (2004), The use of experimental reservoirs to explore the mercury and greenhouse gas impacts of hydro-electric developments: The FLUDEX experiment, *Environmental Science & Technology*, 38(18), 337A–352A. [5](#), [7](#), [10](#), [23](#), [38](#), [76](#), [117](#), [161](#), [163](#), [180](#), [181](#), [182](#), [191](#), [214](#), [224](#)
- Bodaly, R. A., W. A. Jansen, A. R. Majewski, R. J. P. Fudge, N. E. Strange, A. J. Derksen, and D. J. Green (2007), Postimpoundment time course of increased mercury concentrations in fish in hydroelectric reservoirs of northern Manitoba, Canada, *Archives of Environmental Contamination and Toxicology*, 53(3), 379–389, [doi: 10.1007/s00244-006-0113-4](#). [2](#), [116](#), [117](#)
- Boehme, S. E., N. E. Blair, J. P. Chanton, and C. S. Martens (1996), A mass balance of ^{13}C and ^{12}C in an organic-rich methane-producing marine sediment, *Geochimica et Cosmochimica Acta*, 60(20), 3835–3848, [doi: 10.1016/0016-7037\(96\)00204-9](#). [148](#)
- Boetius, A., K. Ravenschlag, C. J. Schubert, D. Rickert, F. Widdel, A. Gieseke, R. Amann, B. B. Jørgensen, U. Witte, and O. Pfannkuche (2000), A marine microbial consortium apparently mediating anaerobic oxidation of methane, *Nature*, 407(6804), 623–626, [doi: 10.1038/35036572](#). [148](#)

- Bond-Lamberty, B., C. K. Wang, and S. T. Gower (2004), Net primary production and net ecosystem production of a boreal black spruce wildfire chronosequence, *Global Change Biology*, 10(4), 473–487, doi: [10.1111/j.1529-8817.2003.0742.x](https://doi.org/10.1111/j.1529-8817.2003.0742.x). 188, 192
- Borsuk, M. E., C. A. Stow, and K. H. Reckhow (2004), Confounding effect of flow on estuarine response to nitrogen loading, *Journal of Environmental Engineering*, 130(6), 605–614, doi: [10.1061/\(ASCE\)0733-9372\(2004\)130:6\(605\).72](https://doi.org/10.1061/(ASCE)0733-9372(2004)130:6(605).72)
- Boudreau, B. P., B. S. Gardiner, and B. D. Johnson (2001a), Rate of growth of isolated bubbles in sediments with a diagenetic source of methane, *Limnology and Oceanography*, 46(3), 616–622. 41, 214
- Boudreau, B. P., B. S. Gardiner, and B. D. Johnson (2001b), Rate of growth of isolated bubbles in sediments with a diagenetic source of methane (vol 46, pg 616, 2001), *Limnology and Oceanography*, 46(6), 1578–1578. 41
- Boudreau, N. M. (2000), Soil carbon, carbon dioxide, and methane in three experimentally flooded upland boreal forest reservoirs: a $\delta^{13}\text{C}$ inventory of sources and processes, Master's thesis, University of Waterloo. 5, 18, 39, 45, 54, 59, 227, 229
- Bowen, G. J., L. I. Wassenaar, and K. A. Hobson (2005), Global application of stable hydrogen and oxygen isotopes to wildlife forensics, *Oecologia*, 143(3), 337–348, doi: [10.1007/s00442-004-1813-y](https://doi.org/10.1007/s00442-004-1813-y). 95
- Bowie, G. L., W. B. Mills, D. B. Porcella, C. L. Campbell, J. R. Pagenkopf, G. Rupp, K. M. Johnson, P. W. H. Chan, S. A. Gherini, and C. C.E. (1985), Rates, constants, and kinetic formulations in surface water quality modelling, *Tech. Rep. EPA/600/3-85/040*, USEPA. 72
- Brandes, J. A., and A. H. Devol (1997), Isotopic fractionation of oxygen and nitrogen in coastal marine sediments, *Geochimica et Cosmochimica Acta*, 61(9), 1793–1801, doi: [10.1016/S0016-7037\(97\)00041-0](https://doi.org/10.1016/S0016-7037(97)00041-0). 69, 71, 94, 119, 123, 124, 127, 142, 227
- Brenna, J. T., T. N. Corso, H. J. Tobias, and R. J. Caimi (1997), High-precision continuous-flow isotope ratio mass spectrometry, *Mass Spectrometry Reviews*, 16(5), 227–258, doi: [10.1002/\(SICI\)1098-2787\(1997\)16:5<227::AID-MAS1>3.0.CO;2-J](https://doi.org/10.1002/(SICI)1098-2787(1997)16:5<227::AID-MAS1>3.0.CO;2-J). 6
- Broecker, W. S. (1985), *How to build a habitable planet*, Eldigo Press. 66
- Brunskill, G. J., and D. W. Schindler (1971), Geography and bathymetry of selected lake basins, Experimental Lakes Area, northwestern Ontario, *Journal of the Fisheries Research Board of Canada*, 28(2), 139–155. 6

- Bubier, J. L., T. R. Moore, L. Bellisario, N. T. Comer, and P. M. Crill (1995), Ecological controls on methane emissions from a northern peatland complex in the zone of discontinuous permafrost, Manitoba, Canada, *Global Biogeochemical Cycles*, 9(4), 455–470. [153](#)
- Carignan, R. (1998), Automated determination of carbon dioxide, oxygen, and nitrogen partial pressures in surface waters, *Limnology and Oceanography*, 43(5), 969–975. [218](#)
- Carignan, R., A. M. Blais, and C. Vis (1998), Measurement of primary production and community respiration in oligotrophic lakes using the Winkler method, *Canadian Journal of Fisheries and Aquatic Sciences*, 55(5), 1078–1084. [120](#), [126](#), [225](#), [229](#)
- Carignan, R., D. Planas, and C. Vis (2000), Planktonic production and respiration in oligotrophic Shield lakes, *Limnology and Oceanography*, 45(1), 189–199. [66](#), [88](#), [89](#), [113](#), [116](#), [126](#), [127](#)
- Carpenter, S., W. Brock, and H. P. (1999), Ecological and social dynamics in simple models of ecosystem management, *Conservation Ecology*, 3(2), 4. [217](#)
- Carpenter, S. R., and M. L. Pace (1997), Dystrophy and eutrophy in lake ecosystems: Implications of fluctuating inputs, *Oikos*, 78(1), 3–14. [189](#)
- Carpenter, S. R., N. F. Caraco, D. L. Correll, R. W. Howarth, A. N. Sharpley, and V. H. Smith (1998a), Nonpoint pollution of surface waters with phosphorus and nitrogen, *Ecological Applications*, 8(3), 559–568, doi: [10.1890/1051-0761\(1998\)008\[0559:NPOSWW\]2.0.CO;2](#). [89](#)
- Carpenter, S. R., J. J. Cole, J. F. Kitchell, and M. L. Pace (1998b), Impact of dissolved organic carbon, phosphorus, and grazing on phytoplankton biomass and production in experimental lakes, *Limnology and Oceanography*, 43(1), 73–80. [189](#)
- Cavalcante, P. R. S., M. do S. Rodrigues, M. F. S. Barroso, R. Barbieri, S. C. L. M., and R. C. A. Oliveira (2007), Diel variation of limnological parameters in a reservoir in northeastern Brazil (Boa Esperança, Maranhão/Piauí): Rainy period, *Lakes and Reservoirs: Research and Management*, 12(1), 35–42, doi: [10.1111/j.1440-1770.2007.00319.x](#). [116](#)
- Chanton, J. P., C. S. Martens, and C. A. Kelley (1989), Gas-transport from methane-saturated, tidal fresh-water and wetland sediments, *Limnology and Oceanography*, 34(5), 807–819. [42](#)
- Chapin III, F. S., G. M. Woodwell, J. T. Randerson, E. B. Rastetter, G. M. Lovett, D. D. Baldocchi, D. A. Clark, M. E. Harmon, D. S. Schimel, R. Valentini, C. Wirth, J. D. Aber, J. J. Cole, M. L. Goulden, J. W. Harden, M. Heimann,

- R. W. Howarth, P. A. Matson, A. D. McGuire, J. M. Melillo, H. A. Mooney, J. C. Neff, R. A. Houghton, M. L. Pace, M. G. Ryan, S. W. Running, O. E. Sala, W. H. Schlesinger, and E. D. Schulze (2006), Reconciling carbon-cycle concepts, terminology, and methods, *Ecosystems*, 9(7), 1041–1050, doi: [10.1007/s10021-005-0105-7](https://doi.org/10.1007/s10021-005-0105-7). 217
- Chapman, R. (1986), Ambient water quality criteria for dissolved oxygen, *Tech. Rep. US EPA 440/5-86-003*, US EPA. 88
- Chapra, S. C., and D. M. Di Toro (1991), Delta method for estimating primary production, respiration, and reaeration in streams, *Journal of Environmental Engineering*, 117(5), 640–655, doi: [10.1061/\(ASCE\)0733-9372\(1991\)117:5\(640\)](https://doi.org/10.1061/(ASCE)0733-9372(1991)117:5(640)). 66, 89
- Chevalier, G., C. Dumont, C. Langlois, and A. Penn (1997), Mercury in northern Québec: Role of the mercury agreement and status of research and monitoring, *Water Air and Soil Pollution*, 97(1-2), 75–84, doi: [10.1007/BF02409646](https://doi.org/10.1007/BF02409646). 2
- Chomicki, K. M., and S. L. Schiff (2008), Stable oxygen isotopic fractionation during dissolved organic carbon photodegradation in stream waters, *Science of the Total Environment*, 404(2-3), 236–244, doi: [10.1016/j.scitotenv.2008.04.024](https://doi.org/10.1016/j.scitotenv.2008.04.024). 90, 123, 219
- Chow, A. T., S. Gao, and R. A. Dahlgren (2005), Physical and chemical fractionation of dissolved organic matter and trihalomethane precursors: A review, *Journal of Water Supply Research and Technology—Aqua*, 54(8), 475–507. 190
- Churchill, M. A., H. L. Elmore, and R. A. Buckingham (1962), The prediction of stream reaeration rates, *Journal of Environmental Engineering*, 88(SA4), 1–46. 77, 93
- Clark, I., and P. Fritz (1997), *Environmental Isotopes in Hydrology*, CRC Press. 13, 21, 35, 43, 95, 150
- Clark, J. F., R. Wanninkhof, P. Schlosser, and H. J. Simpson (1994), Gas-exchange rates in the tidal hudson river using a dual tracer technique, *Tellus*, 46(4), 274–285. 164
- Clark, J. F., P. Schlosser, M. Stute, and H. J. Simpson (1996), SF₆-³He tracer release experiment: A new method of determining longitudinal dispersion coefficients in large rivers, *Environmental Science & Technology*, 30(5), 1527–1532, doi: [10.1021/es962016o](https://doi.org/10.1021/es962016o). 162, 164
- Cleugh, T. R., and B. W. Hauser (1971), Results of the initial survey of the Experimental Lakes Area northwestern Ontario, *Journal of the Fisheries Research Board of Canada*, 28(2), 129–137. 6

- Cohen, E. R., T. Cvitaš, J. G. Frey, B. Holström, K. Kuchitsu, R. Marquardt, I. Mills, F. Pavese, M. Quack, J. Stohner, H. L. Strauss, M. Takami, and A. J. Thor (2007), *Quantities, Units and Symbols in Physical Chemistry*, third ed., RSC Publishing. 186
- Cole, J. J., and N. F. Caraco (1998), Atmospheric exchange of carbon dioxide in a low-wind oligotrophic lake measured by the addition of SF₆, *Limnology and Oceanography*, 43(4), 647–656. 93, 113, 162, 167, 171, 172, 219
- Cole, J. J., and N. F. Caraco (2001), Carbon in catchments: connecting terrestrial carbon losses with aquatic metabolism, *Marine and Freshwater Research*, 52(1), 101–110, doi: 10.1071/MF00084. 217
- Cole, J. J., N. F. Caraco, G. W. Kling, and T. K. Kratz (1994), Carbon-dioxide supersaturation in the surface waters of lakes, *Science*, 265(5178), 1568–1570, doi: 10.1126/science.265.5178.1568. 161
- Cole, J. J., S. R. Carpenter, M. L. Pace, M. C. Van de Bogert, J. L. Kitchell, and J. R. Hodgson (2006), Differential support of lake food webs by three types of terrestrial organic carbon, *Ecology Letters*, 9(5), 558–568, doi: 10.1111/j.1461-0248.2006.00898.x. 214
- Compeau, G. C., and R. Bartha (1985), Sulfate-reducing bacteria: principal methylators of mercury in anoxic estuarine sediment, *Applied and Environmental Microbiology*, 50(2), 498–502. 2
- Coplen, T. B., J. A. Hopple, J. K. Böhlke, H. S. Peiser, S. E. Rieder, H. R. Krouse, K. J. R. Rosman, T. Ding, R. D. Vocke, Jr, K. M. Révész, A. Lamberty, P. Taylor, and P. De Bièvre (2001), Compilation of minimum and maximum isotope ratios of selected elements in naturally occurring terrestrial materials and reagents, *Tech. Rep. US Geological Survey Water-Resources Investigations Report 01-4222*, USGS. 68
- Crusius, J., and R. Wanninkhof (2003), Gas transfer velocities measured at low wind speed over a lake, *Limnology and Oceanography*, 48(3), 1010–1017. 77, 78, 162, 164, 167, 169, 171, 172, 219
- Cullenward, D., and D. G. Victor (2006), The dam debate and its discontents, *Climatic Change*, 75(1-2), 81–86, 21. 3, 4, 7, 161
- Davidson, E. A., I. A. Janssens, and Y. Q. Luo (2006), On the variability of respiration in terrestrial ecosystems: moving beyond Q₁₀, *Global Change Biology*, 12(2), 154–164, doi: 10.1111/j.1365-2486.2005.01065.x. 217
- Davies, J. M., and A. Mazumder (2003), Health and environmental policy issues in Canada: the role of watershed management in sustaining clean drinking water quality at surface sources, *Journal of Environmental Management*, 68(3), 273–286, doi: 10.1016/S0301-4797(03)00070-7. 181, 189

- Davies, J.-M., R. H. Hesslein, C. A. Kelly, and R. E. Hecky (2003), PCO_2 method for measuring photosynthesis and respiration in freshwater lakes, *Journal of Plankton Research*, 25(4), 385–395, doi: [10.1093/plankt/25.4.385](https://doi.org/10.1093/plankt/25.4.385). 186, 229
- Davis, J. F. (2002), Factors affecting photosynthetic rates of periphyton in shallow streams of southeastern Pennsylvania, *Water Environment Research*, 74(4), 370–376, doi: [10.2175/106143002X140134](https://doi.org/10.2175/106143002X140134). 113
- Deacon, E. L. (1977), Gas transfer to and across an air–water interface, *Tellus*, 29(4), 363–374. 171
- del Giorgio, P. A., and R. H. Peters (1994), Patterns in planktonic P:R ratios in lakes: influence of lake trophic and dissolved organic carbon, *Limnology and Oceanography*, 39(4), 772–787. 66, 89, 116
- del Giorgio, P. A., and P. Williams (2005), Respiration in aquatic ecosystems, chap. The global significance of respiration in aquatic ecosystems: from single cells to the biosphere, pp. 267–303, Oxford University. 125, 126, 217, 219, 227
- del Giorgio, P. A., J. J. Cole, N. F. Caraco, and R. H. Peters (1999), Linking planktonic biomass and metabolism to net gas fluxes in northern temperate lakes, *Ecology*, 80(4), 1422–1431, doi: [10.1890/0012-9658\(1999\)080\[1422:LPBAMT\]2.0.CO;2](https://doi.org/10.1890/0012-9658(1999)080[1422:LPBAMT]2.0.CO;2). 162
- Delmas, R., C. Galy-Lacaux, and S. Richard (2001), Emissions of greenhouse gases from the tropical hydroelectric reservoir of Petit Saut (French Guiana) compared with emissions from thermal alternatives, *Global Biogeochemical Cycles*, 15(4), 993–1003, doi: [10.1029/2000GB001330](https://doi.org/10.1029/2000GB001330). 38
- Dentener, F., R. Derwent, E. Dlugokencky, I. Holland, E. Isaksen, J. Katima, V. Kirchhoff, P. Matson, and M. Midgley, P. Wang (2001), Climate Change 2001: The Scientific Basis Contribution of Working Group I to the Third Assessment Report of the Intergovernmental Panel on Climate Change, chap. Atmospheric chemistry and greenhouse gases, Cambridge University Press. 148
- Dillon, P. J., and L. A. Molot (1997), Effect of landscape form on export of dissolved organic carbon, iron, and phosphorus from forested stream catchments, *Water Resources Research*, 33(11), 2591–2600. 191
- Dodds, W. K., and E. B. Welch (2000), Establishing nutrient criteria in streams, *Journal of the North American Benthological Society*, 19(1), 186–196, doi: [10.1043/0887-3593\(2000\)019<0186:ENCIS>2.0.CO;2](https://doi.org/10.1043/0887-3593(2000)019<0186:ENCIS>2.0.CO;2). 89

- Driscoll, C. T., J. P. Baker, J. J. Bisogni, and C. L. Schofield (1980), Effect of aluminum speciation on fish in dilute acidified waters, *Nature*, 284(5752), 161–164, doi: [10.1038/284161a0](https://doi.org/10.1038/284161a0). 189
- Duarte, C. M., and S. Agustí (1998), The CO₂ balance of unproductive aquatic ecosystems, *Science*, 281(5374), 234–236, doi: [10.1126/science.281.5374.234](https://doi.org/10.1126/science.281.5374.234). 227
- Duchemin, É., M. Lucotte, R. Canuel, and A. Chamberland (1995), Production of the greenhouse gases CH₄ and CO₂ by hydroelectric reservoirs of the boreal region, *Global Biogeochemical Cycles*, 9(4), 529–540. 10, 21, 38, 153
- Dudgeon, D. (2000), Large-scale hydrological changes in tropical Asia: Prospects for riverine biodiversity, *Bioscience*, 50(9), 793–806, doi: [10.1641/0006-3568\(2000\)050\[0793:LSHCIT\]2.0.CO;2](https://doi.org/10.1641/0006-3568(2000)050[0793:LSHCIT]2.0.CO;2). 1
- Dunfield, P., R. Knowles, R. Dumont, and T. R. Moore (1993), Methane production and consumption in temperate and sub-arctic peat soils—response to temperature and pH, *Soil Biology & Biochemistry*, 25(3), 321–326. 148
- Dyck, B. S., and J. M. Shay (1999), Biomass and carbon pool of two bogs in the Experimental Lakes Area, northwestern Ontario, *Canadian Journal of Botany*, 77(2), 291–304, doi: [10.1139/cjb-77-2-291](https://doi.org/10.1139/cjb-77-2-291). 4, 11, 39, 150, 187
- Ehhalt, D., M. Prather, F. Dentener, R. G. Derwent, E. Dlugokencky, E. Holland, I. Isaksen, J. Katima, V. Kirchhoff, P. Matson, P. Midgley, and M. Wang (2001), Climate Change 2001: The Scientific Basis Contribution of Working Group I to the Third Assessment Report of the Intergovernmental Panel on Climate Change, chap. Atmospheric chemistry and greenhouse gases, Cambridge University Press. 10, 24, 40, 191
- Ehleringer, J. R., N. Buchmann, and L. B. Flanagan (2000), Carbon isotope ratios in belowground carbon cycle processes, *Ecological Applications*, 10(2), 412–422, doi: [10.1890/1051-0761\(2000\)010\[0412:CIRIBC\]2.0.CO;2](https://doi.org/10.1890/1051-0761(2000)010[0412:CIRIBC]2.0.CO;2). 217
- Eijsackers, H., and A. J. B. Zehnder (1990), Litter decomposition: a Russian matriochka doll, *Biogeochemistry*, 11(3), 153–174, doi: [10.1007/BF00004495](https://doi.org/10.1007/BF00004495). 192
- Evans, C. D., P. J. Chapman, J. M. Clark, D. T. Monteith, and M. S. Cresser (2006), Alternative explanations for rising dissolved organic carbon export from organic soils, *Global Change Biology*, 12(11), 2044–2053, doi: [10.1111/j.1365-2486.2006.01241.x](https://doi.org/10.1111/j.1365-2486.2006.01241.x). 191
- Falkowski, P. G., and J. A. Raven (1997), *Aquatic photosynthesis*, Blackwell. 16, 66, 71, 74, 88, 89, 116, 125, 227

- Farquhar, G. D., M. J. R. Fasham, M. L. Goudlen, M. Heimann, V. J. Jaramillo, H. S. Khashgi, C. Le Quéré, S. R. J., and D. W. R. Wallace (2001), Climate Change 2001: The Scientific Basis Contribution of Working Group I to the Third Assessment Report of the Intergovernmental Panel on Climate Change, chap. The Carbon Cycle and Atmospheric Carbon Dioxide, Cambridge University Press. 161
- Fearnside, P. M. (1995), Global warming response options in Brazil's forest sector: Comparison of project-level costs and benefits, *Biomass and Bioenergy*, 8(5), 309–322, doi: [10.1016/0961-9534\(95\)00024-0](https://doi.org/10.1016/0961-9534(95)00024-0). 7
- Fearnside, P. M. (2002), Greenhouse gas emissions from a hydroelectric reservoir (Brazil's Tucuruí dam) and the energy policy implications, *Water Air and Soil Pollution*, 133(1-4), 69–96, doi: [10.1016/S0140-6701\(03\)90852-6](https://doi.org/10.1016/S0140-6701(03)90852-6). 7
- Fearnside, P. M. (2004), Greenhouse gas emissions from hydroelectric dams: Controversies provide a springboard for rethinking a supposedly 'clean' energy source. An editorial comment, *Climatic Change*, 66(1-2), 1–8, doi: [10.1023/B:CLIM.0000043174.02841.23](https://doi.org/10.1023/B:CLIM.0000043174.02841.23). 7
- Fearnside, P. M. (2006), Greenhouse gas emissions from hydroelectric dams: Reply to Rosa et al., *Climatic Change*, 75(1-2), 103–109, doi: [10.1007/s10584-005-9016-z](https://doi.org/10.1007/s10584-005-9016-z). 7
- Fechner-Levy, E. J., and H. F. Hemond (1996), Trapped methane volume and potential effects on methane ebullition in a northern peatland, *Limnology and Oceanography*, 41(7), 1375–1383. 42, 44, 214, 218
- Ferguson, G. A. G. (2000), *Sources of dissolved organic carbon in flooded uplands. Bachelor's thesis*, University of Waterloo. 24, 227, 229
- Fogel, M. L., and L. A. Cifuentes (1993), Isotope fractionation during primary production, in *Organic geochemistry*, edited by H. M. Engel and S. A. Macko, Plenum Press. 18
- Frenzel, P., and E. Karofeld (2000), CH₄ emission from a hollow-ridge complex in a raised bog: The role of CH₄ production and oxidation, *Biogeochemistry*, 51(1), 91–112. 148, 156
- Frew, N. M., E. J. Bock, U. Schimpf, T. Hara, H. Haussecker, J. B. Edson, W. R. McGillis, R. K. Nelson, S. P. McKenna, B. M. Uz, and B. Jahne (2004), Air-sea gas transfer: Its dependence on wind stress, small-scale roughness, and surface films, *Journal of Geophysical Research-Oceans*, 109(C8), doi: [10.1029/2003JC002131](https://doi.org/10.1029/2003JC002131). 219
- Frost, T., and R. C. Upstill-Goddard (2002), Meteorological controls of gas exchange at a small English lake, *Limnology and Oceanography*, 47(4), 1165–1174. 167

- Fry, B. (2006), *Stable Isotope Ecology*, Springer. 67
- Fung, I., J. John, J. Lerner, E. Matthews, M. Prather, L. P. Steele, and P. J. Fraser (1991), 3-dimensional model synthesis of the global methane cycle, *Journal of Geophysical Research*, 96(D7), 13,033–13,065. 149
- Galy-Lacaux, C., R. Delmas, C. Jambert, J. F. Dumestre, L. Labroue, S. Richard, and P. Gosse (1997), Gaseous emissions and oxygen consumption in hydroelectric dams: A case study in French Guyana, *Global Biogeochemical Cycles*, 11(4), 471–483. 7, 38, 149
- Galy-Lacaux, C., R. Delmas, G. Kouadio, S. Richard, and P. Gosse (1999), Long-term greenhouse gas emissions from hydroelectric reservoirs in tropical forest regions, *Global Biogeochemical Cycles*, 13(2), 503–517, doi: [10.1029/1998GB900015](https://doi.org/10.1029/1998GB900015). 7, 38
- Gamsjäger, H., J. W. Lorimer, P. Scharlin, and G. G. Shaw (2008), Glossary of terms related to solubility (IUPAC recommendations 2008), *Pure and Applied Chemistry*, 80(2), 233–276, doi: [10.1351/pac200880020233](https://doi.org/10.1351/pac200880020233). 186
- Garcia, J. L. (1990), Taxonomy and ecology of methanogens, *FEMS Microbiology Reviews*, 87(3-4), 297–308. 148
- Gelda, R. K., M. T. Auer, S. W. Effler, S. C. Chapra, and M. L. Storey (1996), Determination of reaeration coefficients: Whole-lake approach, *Journal of Environmental Engineering*, 122(4), 269–275, doi: [10.1061/\(ASCE\)0733-9372\(1996\)122:4\(269\)](https://doi.org/10.1061/(ASCE)0733-9372(1996)122:4(269)). 70
- Gilmour, C. C., and E. A. Henry (1991), Mercury methylation in aquatic systems affected by acid deposition, *Environmental Pollution*, 71(2-4), 131–169, doi: [10.1016/0269-7491\(91\)90031-Q](https://doi.org/10.1016/0269-7491(91)90031-Q). 2
- Gorham, E. (1991), Northern peatlands—role in the carbon-cycle and probable responses to climatic warming, *Ecological Applications*, 1(2), 182–195. 217
- Groffman, P., J. Baron, T. Blett, A. Gold, I. Goodman, L. Gunderson, B. Levinson, M. Palmer, H. Paerl, G. Peterson, N. Poff, D. Rejeski, J. Reynolds, M. Turner, K. Weathers, and J. Wiens (2006), Ecological thresholds: The key to successful environmental management or an important concept with no practical application?, *Ecosystems*, 9(1), 1–13, doi: [10.1007/s10021-003-0142-z](https://doi.org/10.1007/s10021-003-0142-z). 217
- Guildford, S. J., F. P. Healey, and R. E. Hecky (1987), Depression of primary production by humic matter and suspended sediment in limnocorral experiments at Southern Indian Lake, northern Manitoba, *Canadian Journal of Fisheries and Aquatic Sciences*, 44(8), 1408–1417. 189

- Guy, R. D., J. A. Berry, M. L. Fogel, and T. C. Hoering (1989), Differential fractionation of oxygen isotopes by cyanide-resistant and cyanide-sensitive respiration in plants, *Planta*, 177(4), 483–491, doi: [10.1007/BF00392616](https://doi.org/10.1007/BF00392616). 68, 90, 119
- Guy, R. D., M. L. Fogel, and J. A. Berry (1993), Photosynthetic fractionation of the stable isotopes of oxygen and carbon, *Plant Physiology*, 101(1), 37–47. 68, 69, 90, 119
- Hagemann, R., G. Nief, and E. Roth (1970), Absolute isotopic scale for deuterium analysis of natural waters. absolute D/H ratio for SMOW, *Tellus*, 22(6), 712–715. 121
- Hall, B. D., and V. L. St.Louis (2004), Methylmercury and total mercury in plant litter decomposing in upland forests and flooded landscapes, *Environmental Science & Technology*, 38(19), 5010–5021, doi: [10.1021/es049800q](https://doi.org/10.1021/es049800q). 5, 24, 217
- Hall, B. D., V. L. St.Louis, and R. A. Bodaly (2004), The stimulation of methylmercury production by decomposition of flooded birch leaves and jack pine needles, *Biogeochemistry*, 68(1), 107–129, doi: [10.1023/B:BI0G.0000025745.28447.8b](https://doi.org/10.1023/B:BI0G.0000025745.28447.8b). 5
- Hall, B. D., V. L. St.Louis, K. R. Rolffhus, R. A. Bodaly, K. G. Beaty, M. J. Paterson, and K. A. Cherewyk (2005), Impacts of reservoir creation on the biogeochemical cycling of methyl mercury and total mercury in Boreal Upland Forests, *Ecosystems*, 8(3), 248–266, doi: [10.1007/s10021-003-0094-3](https://doi.org/10.1007/s10021-003-0094-3). 5, 11, 191
- Happell, J. D., J. P. Chanton, G. J. Whiting, and W. J. Showers (1993), Stable isotopes as tracers of methane dynamics in everglades marshes with and without active populations of methane-oxidizing bacteria, *Journal of Geophysical Research*, 98(D8), 14,771–14,782. 153
- Harden, J. W., S. E. Trumbore, B. J. Stocks, A. Hirsch, S. T. Gower, K. P. O'Neill, and E. S. Kasichke (2000), The role of fire in the boreal carbon budget, *Global Change Biology*, 6(Suppl. 1), 174–184, doi: [10.1046/j.1365-2486.2000.06019.x](https://doi.org/10.1046/j.1365-2486.2000.06019.x). 188, 192
- Hartnett, H., A. Devol, J. Brandes, and B. Chang (2005), Oxygen isotope fractionation in marine sediments during respiration, *Geochimica et Cosmochimica Acta*, 69(10), A579, suppl. 1. 69, 119, 123, 227
- Hecky, R. E., and R. H. Hesslein (1995), Contributions of benthic algae to lake food webs as revealed by stable isotope analysis, *Journal of the North American Benthological Society*, 14(4), 631–653. 10, 17, 226, 228, 229

- Hecky, R. E., D. J. Ramsey, R. A. Bodaly, and N. E. Strange (1991), Advances in mercury toxicology, chap. Increased methylmercury contamination in fish in newly formed freshwater reservoirs, pp. 33–51, Plenum Press. 2
- Helman, Y., E. Barkan, D. Eisenstadt, B. Luz, and A. Kaplan (2005), Fractionation of the three stable oxygen isotopes by oxygen-producing and oxygen-consuming reactions in photosynthetic organisms, *Plant Physiology*, 138(4), 2292–2298, doi: [10.1104/pp.105.063768](https://doi.org/10.1104/pp.105.063768). 68, 119
- Hendricks, M. B., M. L. Bender, B. A. Barnett, P. Strutton, and F. P. Chavez (2005), Triple oxygen isotope composition of dissolved O₂ in the equatorial Pacific: A tracer of mixing, production, and respiration, *Journal of Geophysical Research*, 110(C12), C12,021, doi: [10.1029/2004JC002735](https://doi.org/10.1029/2004JC002735). 67, 89
- Hendry, M. J., L. I. Wassenaar, and T. K. Birkham (2002), Microbial respiration and diffusive transport of O₂, ¹⁶O₂, and ¹⁸O¹⁶O in unsaturated soils: A mesocosm experiment, *Geochimica et Cosmochimica Acta*, 66(19), 3367–3374, doi: [10.1016/S0016-7037\(02\)00949-3](https://doi.org/10.1016/S0016-7037(02)00949-3), 48. 69, 72, 94, 119, 123, 227
- Hendzel, L. L., C. J. D. Matthews, J. J. Venkiteswaran, V. L. St.Louis, D. Burton, E. M. Joyce, and R. A. Bodaly (2005), Nitrous oxide fluxes in three experimental boreal forest reservoirs, *Environmental Science & Technology*, 39(12), 4353–4360, doi: [10.1021/es049443j](https://doi.org/10.1021/es049443j). 5, 38, 43, 167, 172
- Hesslein, R. H., R. A. Dwilow, K. G. Beaty, and M. E. Lyng (2005), Greenhouse gas emissions – fluxes and processes, chap. Comparison of Carbon Dioxide Net Production in Three Flooded Uplands (FLUDEX, 1999–2002) and a Flooded Wetland (ELARP, 1991–2002) Using a Dynamic Model, pp. 251–265, Springer-Verlag, Berlin Heidelberg, doi: [10.1007/3-540-26643-7_10](https://doi.org/10.1007/3-540-26643-7_10). 181, 182, 183, 184, 185, 186
- Heubert, D. (1999), Experimental Lakes Area upland flooding experiment: Vegetation analysis, *Tech. rep.*, Fisheries and Oceans Canada. 11, 39
- Ho, D. T., W. E. Asher, L. F. Bliven, P. Schlosser, and E. L. Gordan (2000), On mechanisms of rain-induced air–water gas exchange, *Journal of Geophysical Research*, 105(C10), 24,045–24,057, doi: [10.1029/1999JC000280](https://doi.org/10.1029/1999JC000280). 120, 122, 162, 164, 172
- Hobbie, J. E. (1992), Microbial control of dissolved organic carbon in lakes: research for the future, *Hydrobiologia*, 229, 169–180, doi: [10.1007/BF00006999](https://doi.org/10.1007/BF00006999). 189
- Hoffmann, G., M. Cuntz, C. Weber, P. Ciais, P. Friedlingstein, M. Heimann, J. Jouzel, J. Kaduk, E. Maier-Reimer, U. Seibt, and K. Six (2004), A model of the Earth’s Dole effect, *Global Biogeochemical Cycles*, 18(1), GB1008, doi: [10.1029/2003GB002059](https://doi.org/10.1029/2003GB002059). 67, 116

- Horita, J., and C. Kendall (2004), Handbook of stable isotope analytical techniques, chap. Stable isotope analysis of water and aqueous solutions by conventional dual-inlet mass spectrometry, pp. 1–37, Elsevier. [71](#), [78](#)
- Hornberger, G. M., and M. G. Kelly (1975), Atmospheric reaeration in a river using productivity analysis, *Journal of the Environmental Engineering*, 101(5), 729–739. [66](#)
- Hornig, J. F. (1999), *Social and Environmental Impacts of the James Bay Hydroelectric Project*, McGill-Queen's Press–MQUP. [2](#)
- Houghton, J. T., L. G. Meira Filho, B. A. Callender, N. Harris, A. Kattenberg, and K. Maskell (Eds.) (1995), *Climate Change 1995: The Science of Climate Change. Contribution of Working Group I to the Second Assessment of the Intergovernmental Panel on Climate Change*, Cambridge University Press. [3](#)
- Houghton, J. T., Y. Ding, D. J. Griggs, M. Noguer, P. J. van der Linden, and D. Xiaosu (Eds.) (2001), *Climate Change 2001: The Science of Climate Change. Contribution of Working Group I to the Third Assessment Report of the Intergovernmental Panel on Climate Change*, Cambridge University Press. [3](#)
- Howard, E. A., S. T. Gower, J. A. Foley, and C. J. Kucharik (2004), Effects of logging on carbon dynamics of a jack pine forest in Saskatchewan, Canada, *Global Change Biology*, 10(8), 1267–1284, doi: [10.1111/j.1529-8817.2003.00804.x](#). [188](#), [192](#)
- Huttunen, J. T., K. M. Lappalainen, E. Saarijärvi, T. Väisänen, and P. J. Martikainen (2001), A novel sediment gas sampler and a subsurface gas collector used for measurement of the ebullition of methane and carbon dioxide from a eutrophied lake, *Science of the Total Environment*, 266(1-3), 153–158, doi: [10.1016/S0048-9697\(00\)00749-X](#). [218](#)
- Huttunen, J. T., T. S. Väisänen, S. K. Hellsten, M. Heikkinen, H. Nykänen, H. Jungner, A. Niskanen, M. O. Virtanen, O. V. Lindqvist, O. S. Nenonen, and P. J. Martikainen (2002), Fluxes of CH₄, CO₂, and N₂O in hydroelectric reservoirs Lokka and Porttipahta in the northern boreal zone in Finland, *Global Biogeochemical Cycles*, 16(1), doi: [10.1029/2000GB001316](#). [7](#), [38](#), [149](#)
- Ingvorsen, K., and T. D. Brock (1982), Electron flow via sulfate reduction and methanogenesis in the anaerobic hypolimnion of Lake Mendota, *Limnology and Oceanography*, 27(3), 559–564. [43](#)
- Jackson, T. A., and R. E. Hecky (1980), Depression of primary productivity by humic matter in lake and reservoir waters of the boreal forest zone, *Canadian Journal of Fisheries and Aquatic Sciences*, 37(12), 2300–2317, doi: [10.1139/f80-277](#). [189](#)

- Jha, R., C. S. P. Ojha, and K. K. S. Bhatia (2001), Refinement of predictive reaeration equations for a typical Indian river, *Hydrological Processes*, 15(6), 1047–1060, doi: [10.1002/hyp.177](https://doi.org/10.1002/hyp.177). 70, 78
- Jha, R., C. S. P. Ojha, and K. K. S. Bhatia (2004), A supplementary approach for estimating reaeration rate coefficients, *Hydrological Processes*, 18(1), 65–79, doi: [10.1002/hyp.1312](https://doi.org/10.1002/hyp.1312). 70, 93, 99
- Joyce, E. M. (2001), The impact of experimental reservoir creation on greenhouse gas fluxes from forested uplands, Master's thesis, University of Alberta. 39, 57, 58, 188, 209, 224
- Junk, W. J., P. B. Bayley, and R. E. Sparks (1989), The flood pulse concept in river-floodplain system, in *Canadian special publication of fisheries and aquatic sciences*, vol. 106, edited by D. P. Dodge. 191
- Juranek, L. W., and P. D. Quay (2005), In vitro and in situ gross primary and net community production in the North Pacific Subtropical Gyre using labeled and natural abundance isotopes of dissolved O₂, *Global Biogeochemical Cycles*, 19(3), GB3009, doi: [10.1029/2004GB002384](https://doi.org/10.1029/2004GB002384). 70, 72, 76, 78
- Jähne, B., W. Huber, A. Dutzi, T. Wais, and J. Ilmberger (1984), Gas transfer at water surfaces, chap. Wind/wave-tunnel experiments on the Schmidt number and wave field dependence of air–water gas exchange, pp. 303–309, Riedel, Hingham MA US. 165, 171
- Jähne, B., K. O. Münnich, R. Bössinger, A. Dutzi, W. Huber, and P. Libner (1987), On the parameters influencing air–water gas-exchange, *Journal of Geophysical Research*, 92(C2), 1937–1949. 118, 165
- Keller, M., and R. F. Stallard (1994), Methane emission by bubbling from Gatun Lake, Panama, *Journal of Geophysical Research*, 99(D4), 8307–8319, doi: [10.1029/92JD02170](https://doi.org/10.1029/92JD02170). 7, 38
- Keller, M., E. Veldkamp, A. M. Weitz, and W. A. Reiners (1993), Effect of pasture age on soil trace-gas emissions from a deforested area of Costa Rica, *Nature*, 365(6443), 244–246, doi: [10.1038/365244a0](https://doi.org/10.1038/365244a0). 148
- Kelly, C. A., J. W. M. Rudd, V. L. St.Louis, and T. Moore (1994), Turning attention to reservoir surfaces, a neglected area in greenhouse studies, a neglected area in greenhouse gas studies, *Eos*, 75(29), 332–333. 2, 4, 38
- Kelly, C. A., J. W. M. Rudd, R. A. Bodaly, N. P. Roulet, V. L. St.Louis, A. Heyes, T. R. Moore, S. Schiff, R. Aravena, K. J. Scott, B. Dyck, R. Harris, B. Warner, and G. Edwards (1997), Increases in fluxes of greenhouse gases and methyl mercury following flooding of an experimental reservoir, *Environmental Science & Technology*, 31(5), 1334–1344, doi: [10.1021/ES9604931](https://doi.org/10.1021/ES9604931). 2, 4, 10, 23, 38, 149, 150, 154, 163, 180, 181, 182, 186, 187, 191

- Kendall, C., and T. B. Coplen (2001), Distribution of oxygen-18 and deuterium in river waters across the United States, *Hydrological Processes*, 15(7), 1363–1393, doi: [10.1002/hyp.217](https://doi.org/10.1002/hyp.217). 95
- Kiddon, J., M. L. Bender, J. Orchardo, D. A. Caron, J. C. Goldman, and M. Dennett (1993), Isotopic fractionation of oxygen by respiring marine organisms, *Global Biogeochemical Cycles*, 7(3), 679–694. 69, 71, 78, 94, 119, 123, 124, 127, 129, 130, 141
- King, D. B., and E. S. Saltzman (1995), Measurement of the diffusion coefficient of sulfur hexafluoride in water, *Journal of Geophysical Research*, 100(C4), 7083–7088. 169
- King, G. M. (1990), Regulation by light of methane emissions from a wetland, *Nature*, 345(6275), 513–515, doi: [10.1038/345513a0](https://doi.org/10.1038/345513a0). 148, 156
- Kirschbaum, M. U. F. (1995), The temperature dependence of soil organic-matter decomposition, and the effect of global warming on soil organic C storage, *Soil Biology & Biochemistry*, 27(6), 753–760, doi: [10.1016/0038-0717\(94\)00242-S](https://doi.org/10.1016/0038-0717(94)00242-S). 72
- Knox, M., P. D. Quay, and D. Wilbur (1992), Kinetic isotopic fractionation during air-water gas transfer of O₂, N₂, CH₄, and H₂, *Journal of Geophysical Research*, 97(C12), 20,335–20,343. xviii, 13, 70, 72, 75, 82, 91
- Konikow, L. F., and J. D. Bredehoeft (1992), Groundwater models cannot be validated, *Advances in Water Resources*, 15(1), 75–83, doi: [10.1016/0309-1708\(92\)90033-X](https://doi.org/10.1016/0309-1708(92)90033-X). 75
- Koskenniemi, E. (1987), Development of floating peat and macrophyte vegetation in a newly created, polyhumic reservoir, western Finland, *Aqua Fennica*, 17(2), 165–173. 4
- Kremer, J. N., S. W. Nixon, B. Buckley, and P. Roques (2003), Technical note: Conditions for using the floating chamber method to estimate air-water gas exchange, *Estuaries*, 26(4A), 985–990. 163, 168
- Kroopnick, P., and H. Craig (1972), Atmospheric oxygen: Isotopic composition and solubility fractionation, *Science*, 175(4017), 54–55, doi: [10.1126/science.175.4017.54](https://doi.org/10.1126/science.175.4017.54). 70, 91
- König, H. (1992), Bacterial gases, chap. Microbiology of methanogens, Éditions Technip. 148
- Lamontagne, S., S. L. Schiff, and R. J. Elgood (2000), Recovery of ¹⁵N-labelled nitrate applied to a small upland boreal forest catchment, *Canadian Journal of Forest Research*, 30(7), 1165–1177, doi: [10.1139/cjfr-30-7-1165](https://doi.org/10.1139/cjfr-30-7-1165). 6

- Lane, G. A., and M. Dole (1956), Fractionation of oxygen isotopes during respiration, *Science*, 123(3197), 574–576, doi: [10.1126/science.123.3197.574](https://doi.org/10.1126/science.123.3197.574). 90
- Langbein, W. B., and W. H. Durum (1967), The aeration capacity of streams, *Tech. Rep. USGS Circular No. 542*. USGS, USGS. 77
- Laws, E. A. (1991), Photosynthetic quotients, new production and net community production in the open ocean, *Deep-Sea Research Part A*, 38(1), 143–167, doi: [10.1016/0198-0149\(91\)90059-O](https://doi.org/10.1016/0198-0149(91)90059-O). 126
- Laws, E. A., M. R. Landry, R. T. Barber, L. Campbell, M. L. Dickson, and J. Marra (2000), Carbon cycling in primary production bottle incubations: inferences from grazing experiments and photosynthetic studies using ^{14}C and ^{18}O in the Arabian Sea, *Deep-Sea Research Part II*, 47(7-8), 1339–1352, doi: [10.1016/S0967-0645\(99\)00146-0](https://doi.org/10.1016/S0967-0645(99)00146-0). 69, 90
- Ledwell, J. R., A. J. Watson, and W. S. Broecker (1986), A deliberate tracer experiment in Santa Monica Basin, *Nature*, 323(6086), 322–324, doi: [10.1038/323322a0](https://doi.org/10.1038/323322a0). 164
- Lehmann, M. F., S. M. Bernasconi, A. Barbieri, and J. A. McKenzie (2002), Preservation of organic matter and alteration of its carbon and nitrogen isotope composition during simulated and in situ early sedimentary diagenesis, *Geochimica et Cosmochimica Acta*, 66(20), 3573–3584, doi: [10.1016/S0016-7037\(02\)00968-7](https://doi.org/10.1016/S0016-7037(02)00968-7). 217
- Liss, P. S., and L. Merlivat (1986), Geochemical cycling, chap. The Role of Air-Sea Exchange, pp. 113–129, Reidel, Hingham, MA US. 162, 171
- Lovett, G., J. Cole, and M. Pace (2006), Is net ecosystem production equal to ecosystem carbon accumulation?, *Ecosystems*, 9(1), 152–155, doi: [10.1007/s10021-005-0036-3](https://doi.org/10.1007/s10021-005-0036-3). 226
- Luz, B., and E. Barkan (2000), Assessment of oceanic productivity with the triple-isotope composition of dissolved oxygen, *Science*, 288(5473), 2028–2031, doi: [10.1126/science.288.5473.2028](https://doi.org/10.1126/science.288.5473.2028). 67, 89
- Luz, B., E. Barkan, M. L. Bender, M. H. Thiemens, and K. A. Boering (1999), Triple-isotope composition of atmospheric oxygen as a tracer of biosphere productivity, *Nature*, 400(6744), 547–550, doi: [10.1038/22987](https://doi.org/10.1038/22987). 67, 68
- López-Archilla, A. I., S. Mollá, M. C. Coletto, M. C. Guerrero, and C. Montes (2004), Ecosystem metabolism in a mediterranean shallow lake (Laguna de Santa Olalla, Doñana National Park, SW Spain), *Wetlands*, 24(4), 848–858, doi: [10.1672/0277-5212\(2004\)024\[0848:EMIAMS\]2.0.CO;2](https://doi.org/10.1672/0277-5212(2004)024[0848:EMIAMS]2.0.CO;2). 113

- MacIntyre, S., W. Eugster, and G. W. Kling (2001), Gas transfer at water surfaces, chap. The Critical Importance of Buoyancy Flux for Gas Flux Across the Air-water Interface, American Geophysical Union. 219
- Mailman, M., and R. A. Bodaly (2005), Total mercury, methyl mercury, and carbon in fresh and burned plants and soil in Northwestern Ontario, *Environmental Pollution*, 138(1), 161–166, doi: [10.1016/j.envpol.2005.02.005](https://doi.org/10.1016/j.envpol.2005.02.005). 6
- Mailman, M., and R. A. Bodaly (2006), The burning question: Does burning before flooding lower methyl mercury production and bioaccumulation?, *Science of the Total Environment*, 368(1), 407–417, doi: [10.1016/j.scitotenv.2005.09.070](https://doi.org/10.1016/j.scitotenv.2005.09.070). 6
- Maiss, M., and C. A. M. Brenninkmeijer (1998), Atmospheric SF₆: Trends, sources, and prospects, *Environmental Science & Technology*, 32(20), 3077–3086, doi: [10.1021/es9802807](https://doi.org/10.1021/es9802807). 166
- Martens, C. S., N. E. Blair, C. D. Green, and D. J. Desmarais (1986), Seasonal-variations in the stable carbon isotopic signature of biogenic methane in a coastal sediment, *Science*, 233(4770), 1300–1303, doi: [10.1126/science.11536566](https://doi.org/10.1126/science.11536566). 148
- Marzolf, E. R., P. J. Mulholland, and A. D. Steinman (1994), Improvements to the diurnal upstream-downstream dissolved-oxygen change technique for determining whole-stream metabolism in small streams, *Canadian Journal of Fisheries and Aquatic Sciences*, 51(7), 1591–1599. 66
- Matthews, C. J. D. (2002), Greenhouse gas production in experimental reservoirs flooding upland boreal forest, Master's thesis, University of Alberta. [39](#), [49](#), [50](#), [53](#), [57](#), [58](#), [224](#)
- Matthews, C. J. D., V. L. St.Louis, and R. H. Hesslein (2003), Comparison of three techniques used to measure diffusive gas exchange from sheltered aquatic surfaces, *Environmental Science & Technology*, 37(4), 772–780, doi: [10.1021/es0205838](https://doi.org/10.1021/es0205838). [13](#), [113](#), [118](#), [163](#), [164](#), [165](#), [166](#), [167](#), [168](#), [170](#), [171](#), [182](#), [219](#)
- Matthews, C. J. D., E. M. Joyce, V. L. St.Louis, S. L. Schiff, J. J. Venkiteswaran, B. D. Hall, R. A. Bodaly, and K. G. Beaty (2005), Carbon dioxide and methane production in small reservoirs flooding upland Boreal Forest, *Ecosystems*, 8(3), 267–285, doi: [10.1007/s10021-005-0005-x](https://doi.org/10.1007/s10021-005-0005-x). [5](#), [6](#), [10](#), [11](#), [12](#), [14](#), [20](#), [25](#), [38](#), [39](#), [117](#), [129](#), [149](#), [150](#), [153](#), [163](#), [167](#), [172](#), [180](#), [181](#), [182](#), [224](#)
- Matthews, E., and I. Fung (1987), Methane emission from natural wetlands: global distribution, area, and environmental characteristics of sources, *Global Biogeochemical Cycles*, 1(1), 61–86. 148

- McBride, G. B. (2002), Calculating stream reaeration coefficients from oxygen profiles, *Journal of Environmental Engineering*, 128(4), 384–386. 70
- McBride, G. B., and S. C. Chapra (2005), Rapid calculation of oxygen in streams: Approximate delta method, *Journal of Environmental Engineering*, 131(3), 336–342, doi: [10.1061/\(ASCE\)0733-9372\(2005\)131:3\(336\)](https://doi.org/10.1061/(ASCE)0733-9372(2005)131:3(336)). 94, 99
- McKenzie, C., S. Schiff, R. Aravena, C. Kelly, and V. L. St.Louis (1998), Effect of temperature on production of CH₄ and CO₂ from peat in a natural and flooded boreal forest wetland, *Climatic Change*, 40(2), 247–266, doi: [10.1023/A:1005416903368](https://doi.org/10.1023/A:1005416903368). 38, 149, 154, 181
- Melching, C. S., and H. E. Flores (1999), Reaeration equations derived from US Geological Survey database, *Journal of Environmental Engineering*, 125(5), 407–414, doi: [10.1061/\(ASCE\)0733-9372\(1999\)125:5\(407\)](https://doi.org/10.1061/(ASCE)0733-9372(1999)125:5(407)). 113
- Miles, C. J., and P. L. Brezonik (1981), Oxygen consumption in humic-colored waters by a photochemical ferrous-ferric catalytic cycle, *Environmental Science & Technology*, 15(9), 1089–1095, doi: [10.1021/es00091a010](https://doi.org/10.1021/es00091a010). 69, 90
- Molot, L. A., and P. J. Dillon (1997), Photolytic regulation of dissolved organic carbon in northern lakes, *Global Biogeochemical Cycles*, 11(3), 357–365. 189
- Moog, D. B., and G. H. Jirka (1998), Analysis of reaeration equations using mean multiplicative error, *Journal of Environmental Engineering*, 124(2), 104–110, doi: [10.1061/\(ASCE\)0733-9372\(1998\)124:2\(104\)](https://doi.org/10.1061/(ASCE)0733-9372(1998)124:2(104)). 70
- Moore, T. R. (1997), Soil processes and the carbon cycle, chap. Dissolved organic carbon: sources, sinks, and fluxes and role in the soil carbon cycle, CRC Press. 189
- Moore, T. R., L. Matos, and N. T. Roulet (2003), Dynamics and chemistry of dissolved organic carbon in precambrian shield catchments and an impounded wetland, *Canadian Journal of Fisheries and Aquatic Sciences*, 60(5), 612–623, doi: [10.1139/F03-050](https://doi.org/10.1139/F03-050). 189, 190
- Moore, T. R., J. A. Trofymow, C. E. Prescott, J. Fyles, and B. D. Titus (2006), Patterns of carbon, nitrogen and phosphorus dynamics in decomposing foliar litter in Canadian forests, *Ecosystems*, 9(1), 46–62, doi: [10.1007/s10021-004-0026-x](https://doi.org/10.1007/s10021-004-0026-x). 217
- Morris, D. P., H. Zagarese, C. E. Williamson, E. G. Balseiro, B. R. Hargreaves, B. Modenutti, R. Moeller, and C. Queimalinos (1995), The attenuation of solar UV radiation in lakes and the role of dissolved organic carbon, *Limnology and Oceanography*, 40(8), 1381–1391. 189

- Morse, N., W. B. Bowden, A. Hackman, C. Pruden, E. Steiner, and E. Berger (2007), Using sound pressure to estimate reaeration in streams, *Journal of the North American Benthological Society*, 26(1), 28–37, doi: [10.1899/0887-3593\(2007\)026\[0028:USPTER\]2.0.CO;2](https://doi.org/10.1899/0887-3593(2007)026[0028:USPTER]2.0.CO;2). 93
- Mulholland, P. J., C. S. Fellows, J. L. Tank, N. B. Grimm, J. R. Webster, S. K. Hamilton, E. Marti, L. Ashkenas, W. B. Bowden, W. K. Dodds, W. H. McDowell, M. J. Paul, and B. J. Peterson (2001), Inter-biome comparison of factors controlling stream metabolism, *Freshwater Biology*, 46(11), 1503–1517, doi: [10.1046/j.1365-2427.2001.00773.x](https://doi.org/10.1046/j.1365-2427.2001.00773.x). 113
- Mulholland, P. J., J. N. Houser, and K. O. Maloney (2005), Stream diurnal dissolved oxygen profiles as indicators of in-stream metabolism and disturbance effects: Fort Benning as a case study, *Ecological Indicators*, 5(3), 243–252, doi: [10.1016/j.ecolind.2005.03.004](https://doi.org/10.1016/j.ecolind.2005.03.004). 66
- Munthe, J., R. A. Bodaly, B. A. Branfireun, C. T. Driscoll, C. C. Gilmour, R. Harris, M. Horvat, M. Lucotte, and O. Malm (2007), Recovery of mercury-contaminated fisheries, *Ambio*, 36(1), 33–44, doi: [10.1579/0044-7447\(2007\)36\[33:ROMF\]2.0.CO;2](https://doi.org/10.1579/0044-7447(2007)36[33:ROMF]2.0.CO;2), munthe, John Bodaly, R. A. (Drew) Branfireun, Brian A. Driscoll, Charles T. Gilmour, Cynthia C. Harris, Reed Horvat, Milena Lucotte, Marc Malm, Olaf. 117
- Myers, G. J., P. W. Davidson, C. Cox, C. Shamlaye, E. Cernichiari, and T. W. Clarkson (2000), Twenty-seven years studying the human neurotoxicity of methylmercury exposure, *Environmental Research*, 83(3), 275–285, doi: [10.1006/enrs.2000.4065](https://doi.org/10.1006/enrs.2000.4065). 2
- Nadelhoffer, K. F., and B. Fry (1988), controls on natural nitrogen-15 and carbon-13 abundances in forest soil organic matter, *Soil Science Society of America Journal*, 52(6), 1633–1640. 18, 217
- Nilsson, C., and K. Berggren (2000), Alterations of riparian ecosystems caused by river regulation, *Bioscience*, 50(9), 783–792, doi: [10.1641/0006-3568\(2000\)050\[0783:AORECB\]2.0.CO;2](https://doi.org/10.1641/0006-3568(2000)050[0783:AORECB]2.0.CO;2). 1
- O'Connor, D. J., and W. Dobbins (1958), Mechanism of reaeration in natural streams, *American Society of Civil Engineering*, 123, 641–684. 77, 93
- Odum, H. T. (1956), Primary production in flowing waters, *Limnology and Oceanography*, 1(2), 102–117. 66, 67, 89, 99, 116, 162
- Oelbermann, M., and S. L. Schiff (2008), Quantifying carbon dioxide and methane emissions and carbon dynamics from flooded boreal forest soil, *Journal of Environmental Quality*, 37(6), 2037–2047, doi: [10.2134/jeq2008.0027](https://doi.org/10.2134/jeq2008.0027). 18, 217, 227, 229

- Oelbermann, M., and S. L. Schiff (in prep), CO₂ and CH₄ production rates from episodic inundations of boreal forest soil. 217
- Oreskes, N., K. Belitz, and K. Shraderfrechette (1994a), The meaning of models—response, *Science*, 264(5157), 331–331, doi: [10.1126/science.264.5157.331](https://doi.org/10.1126/science.264.5157.331). 75
- Oreskes, N., K. Shraderfrechette, and K. Belitz (1994b), Verification, validation, and confirmation of numerical models in the earth sciences, *Science*, 263(5147), 641–646, doi: [10.1126/science.263.5147.641](https://doi.org/10.1126/science.263.5147.641). 74
- Osmond, C. B. (1981), Photorespiration and photoinhibition some implications for the energetics of photosynthesis, *Biochimica et Biophysica Acta*, 639(2), 77–98, doi: [10.1016/0304-4173\(81\)90006-9](https://doi.org/10.1016/0304-4173(81)90006-9). 69
- Ostrom, N. E., M. E. Russ, A. Field, L. Piwinski, M. R. Twiss, and H. J. Carrick (2005), Ratios of community respiration to photosynthesis and rates of primary production in Lake Erie via oxygen isotope techniques, *Journal of Great Lakes Research*, 31, 138–153, suppl. 2. 130
- Owens, M., R. W. Edwards, and J. W. Gibbs (1964), Some reaeration studies in streams, *Air and Water Pollution*, 8(8-9), 469–486. 78
- Pace, M. L., and Y. T. Prairie (2005), Respiration in aquatic ecosystems, chap. Respiration in lakes, pp. 103–121, Oxford University. 74, 113, 219
- Pace, M. L., J. J. Cole, S. R. Carpenter, J. F. Kitchell, J. R. Hodgson, M. C. Van de Bogert, D. L. Bade, E. S. Kritzberg, and D. Bastviken (2004), Whole-lake carbon-13 additions reveal terrestrial support of aquatic food webs, *Nature*, 427(6971), 240–243, doi: [10.1038/nature02227](https://doi.org/10.1038/nature02227). 214
- Parker, S. R., S. R. Poulson, C. H. Gammons, and M. D. Degrandpre (2005), Biogeochemical controls on diel cycling of stable isotopes of dissolved O₂ and dissolved inorganic carbon in the Big Hole River, Montana, *Environmental Science & Technology*, 39(18), 7134–7140, doi: [10.1021/es0505595](https://doi.org/10.1021/es0505595). 67, 72, 78, 89, 98, 109, 112
- Pastor, J., J. Solin, S. D. Bridgham, K. Updegraff, C. Harth, P. Weishampel, and B. Dewey (2003), Global warming and the export of dissolved organic carbon from boreal peatlands, *Oikos*, 100(2), 380–386, doi: [10.1034/j.1600-0706.2003.11774.x](https://doi.org/10.1034/j.1600-0706.2003.11774.x). 189
- Poschadel, C. D. (1997), Floating peat island formation at an experimentally flooded: impacts on methane and carbon dioxide production and flux rates to the atmosphere, Master's thesis, University of Waterloo. 154, 181
- Prairie, Y. T., D. F. Bird, and J. J. Cole (2002), The summer metabolic balance in the epilimnion of southeastern Quebec lakes, *Limnology and Oceanography*, 47(1), 316–321. 66

- Quay, P., J. Stutsman, D. Wilbur, A. Snover, E. Dlugokencky, and T. Brown (1999), The isotopic composition of atmospheric methane, *Global Biogeochemical Cycles*, 13(2), 445–461. [14](#)
- Quay, P. D., S. R. Emerson, B. M. Quay, and A. H. Devol (1986), The carbon cycle for Lake Washington—a stable isotope study, *Limnology and Oceanography*, 31(3), 596–611. [10](#), [214](#)
- Quay, P. D., S. Emerson, D. O. Wilbur, C. Stump, and M. Knox (1993), The $\delta^{18}\text{O}$ of dissolved O_2 in the surface waters of the subarctic Pacific: A tracer of biological productivity, *Journal of Geophysical Research*, 98(C5), 8447–8458, doi: [10.1029/92JC03017](#). xviii, [67](#), [91](#), [101](#)
- Quay, P. D., D. O. Wilbur, J. E. Richey, A. H. Devol, R. Benner, and B. R. Forsberg (1995), The $^{18}\text{O}:^{16}\text{O}$ of dissolved-oxygen in rivers and lakes in the Amazon Basin: determining the ratio of respiration to photosynthesis rates in fresh-waters, *Limnology and Oceanography*, 40(4), 718–729. [67](#), [69](#), [71](#), [76](#), [78](#), [95](#), [97](#), [119](#), [123](#), [124](#), [127](#), [129](#), [130](#), [141](#)
- Raghoebarsing, A. A., A. Pol, K. T. van de Pas-Schoonen, A. J. P. Smolders, K. F. Ettwig, W. I. C. Rijpstra, S. Schouten, J. S. S. Damste, H. J. M. Op den Camp, M. S. M. Jetten, and M. Strous (2006), A microbial consortium couples anaerobic methane oxidation to denitrification, *Nature*, 440(7086), 918–921, doi: [10.1038/nature04617](#). [43](#)
- Raich, J. W., and A. Tufekcioglu (2000), Vegetation and soil respiration: Correlations and controls, *Biogeochemistry*, 48(1), 71–90, doi: [10.1023/A:1006112000616](#). [217](#)
- Ramaswamy, V., O. Boucher, J. Haigh, D. Hauglustaine, J. Haywood, G. Myhre, T. Nakajima, S. G. Y., and S. Solomon (2001), Climate Change 2001: The Scientific Basis Contribution of Working Group I to the Third Assessment Report of the Intergovernmental Panel on Climate Change, chap. Radiative Forcing of Climate Change, Cambridge University Press. [3](#)
- Reche, I., and M. L. Pace (2002), Linking dynamics of dissolved organic carbon in a forested lake with environmental factors, *Biogeochemistry*, 61(1), 21–36, doi: [10.1023/A:1020234900383](#). [190](#)
- Rizzo, W. M., S. K. Dailey, G. J. Lackey, R. R. Christian, B. E. Berry, and R. L. Wetzel (1996), A metabolism-based trophic index for comparing the ecological values of shallow-water sediment habitats, *Estuaries*, 19(2A), 247–256. [89](#), [116](#)
- Roberts, B. J. (2004), Assessing diel respiration in pelagic ecosystems using oxygen stable isotopes: when do the highest rates occur and who is respiring under different light and nutrient regimes?, Ph.D. thesis, Cornell University. [130](#)

- Roberts, B. J., M. E. Russ, and N. E. Ostrom (2000), Rapid and precise determination of the $\delta^{18}\text{O}$ of dissolved and gaseous dioxygen via gas chromatography-isotope ratio mass spectrometry, *Environmental Science & Technology*, 34(11), 2337–2341, doi: [10.1021/es991109d](https://doi.org/10.1021/es991109d). 118, 130
- Roebuck, B. D. (1999), Social and environmental impacts of the James Bay hydroelectric project, chap. Elevated mercury in fish as a result of the James Bay hydroelectric development: perception and reality, McGill-Queen's Press—MQUP. 2
- Rosa, L. P., and R. Schaeffer (1994), Greenhouse-gas emissions from hydroelectric reservoirs, *Ambio*, 23(2), 164–165. 7
- Rosa, L. P., R. Schaeffer, and M. A. dos Santos (1996), Are hydroelectric dams in the Brazilian Amazon significant sources of 'greenhouse' gases?, *Environmental Conservation*, 23(1), 2–6. 7
- Rosa, L. P., M. A. Dos Santos, B. Matvienko, E. Sikar, and E. O. Dos Santos (2006), Scientific errors in the Fearnside comments on greenhouse gas emissions (ghg) from hydroelectric dams and response to his political claiming, *Climatic Change*, 75(1-2), 91–102, doi: [10.1007/s10584-005-9046-6](https://doi.org/10.1007/s10584-005-9046-6). 7
- Rosenberg, D. M., R. A. Bodaly, and P. J. Usher (1995), Environmental and social impacts of large-scale hydroelectric development: who is listening?, *Global Environmental Change*, 5(2), 127–148, doi: [10.1016/0959-3780\(95\)00018-J](https://doi.org/10.1016/0959-3780(95)00018-J). 1
- Rosenberg, D. M., F. Berkes, R. A. Bodaly, H. R. A., K. C. A., and R. J. W. M. (1997), Large-scale impacts of hydroelectric development, *Environmental Reviews*, 5, 27–54. 1, 2, 217
- Rosenberg, D. M., P. McCully, and C. M. Pringle (2000), Global-scale environmental effects of hydrological alterations: Introduction, *Bioscience*, 50(9), 746–751, doi: [10.1641/0006-3568\(2000\)050\[0746:GSEEOH\]2.0.CO;2](https://doi.org/10.1641/0006-3568(2000)050[0746:GSEEOH]2.0.CO;2). 1
- Rudd, J. W. M., and R. D. Hamilton (1975), Factors controlling rates of methane oxidation and distribution of methane oxidizers in a small stratified lake, *Archiv Für Hydrobiologie*, 75(4), 522–538. 21, 148, 153
- Rudd, J. W. M., and R. D. Hamilton (1978), Methane cycling in a eutrophic shield lake and its effects on whole lake metabolism, *Limnology and Oceanography*, 23(2), 337–348. 153
- Rudd, J. W. M., R. Harris, C. A. Kelly, and R. E. Hecky (1993), Are hydroelectric reservoirs significant sources of greenhouse gases?, *Ambio*, 22(4), 246–248. 2, 3, 4, 7, 24, 38, 149

- Russ, M. E., N. E. Ostrom, H. Gandhi, P. H. Ostrom, and N. R. Urban (2004), Temporal and spatial variations in R:P ratios in Lake Superior, an oligotrophic freshwater environment, *Journal of Geophysical Research*, 109, C10S12, doi: [10.1029/2003JC001890](https://doi.org/10.1029/2003JC001890). 67
- Saarnio, S., J. Alm, J. Silvola, A. Lohila, H. Nykänen, and P. J. Martikainen (1997), Seasonal variation in CH₄ emissions and production and oxidation potentials at microsites on an oligotrophic pine fen, *Oecologia*, 110(3), 414–422, doi: [10.1007/s004420050176](https://doi.org/10.1007/s004420050176). 153
- Sander, R. (1999), Compilation of Henry's Law constants for inorganic and organic species of potential importance in environmental chemistry, version 3. 42
- Saquet, M. A. M. (2003), Greenhouse gas flux and budget from an experimentally flooded wetland using stable isotopes and geochemistry, Master's thesis, University of Waterloo. 4, 181, 182, 187
- Sarma, V. V. S. S., and O. Abe (2006), Short-term variation of triple oxygen isotopes and gross oxygen production in the Sagami Bay, central Japan, *Limnology and Oceanography*, 51(3), 1432–1442. 67, 89
- Sarma, V. V. S. S., O. Abe, S. Hashimoto, A. Hinuma, and T. Saino (2005), Seasonal variations in triple oxygen isotopes and gross oxygen production in the Sagami Bay, central Japan, *Limnology and Oceanography*, 50(2), 544–552. 67
- Sass, R. L., F. M. Fisher, A. Ding, and Y. Huang (1999), Exchange of methane from rice fields: National, regional, and global budgets, *Journal of Geophysical Research*, 104(D21), 26,943–26,951, doi: [10.1029/1999JD90008](https://doi.org/10.1029/1999JD90008). 161
- Savage, K., T. R. Moore, and P. M. Crill (1997), Methane and carbon dioxide exchanges between the atmosphere and northern boreal forest soils, *Journal of Geophysical Research*, 102(D24), 29,279–29,288. 188
- Schiff, S. L. (in prep). 126, 181, 182, 183, 185, 190
- Schindler, D. W. (1987), Detecting ecosystem responses to anthropogenic stress, *Canadian Journal of Fisheries and Aquatic Sciences*, 44(Suppl. 1), 6–25. 66
- Schindler, D. W. (2001), The cumulative effects of climate warming and other human stresses on Canadian freshwaters in the new millennium, *Canadian Journal of Fisheries and Aquatic Sciences*, 58(1), 18–29, doi: [10.1139/cjfas-58-1-18](https://doi.org/10.1139/cjfas-58-1-18). 189

- Schindler, D. W., E. J. Fee, and T. Ruszczynski (1978), Phosphorus input and its consequences for phytoplankton standing crop and production in Experimental Lakes Area and in similar lakes, *Journal of the Fisheries Research Board of Canada*, 35(2), 190–196. 189
- Schindler, D. W., K. G. Beaty, E. J. Fee, D. R. Cruikshank, E. R. Debruyne, D. L. Findlay, G. A. Linsey, J. A. Shearer, M. P. Stainton, and M. A. Turner (1990), Effects of climatic warming on lakes of the central boreal forest, *Science*, 250(4983), 967–970, doi: [10.1126/science.250.4983.967](https://doi.org/10.1126/science.250.4983.967). 189
- Schindler, D. W., S. E. Bayley, B. R. Parker, K. G. Beaty, D. R. Cruikshank, E. J. Fee, E. U. Schindler, and M. P. Stainton (1996a), The effects of climatic warming on the properties of boreal lakes and streams at the Experimental Lakes Area, northwestern Ontario, *Limnology and Oceanography*, 41(5), 1004–1017. 6, 191
- Schindler, D. W., P. J. Curtis, B. R. Parker, and M. P. Stainton (1996b), Consequences of climate warming and lake acidification for UV-B penetration in North American boreal lakes, *Nature*, 379(6567), 705–708, doi: [10.1038/379705a0](https://doi.org/10.1038/379705a0). 189
- Schlesinger, W. H. (1997), *Biogeochemistry. An Analysis of Global Change*, second ed., Academic Press. 191
- Schönheit, P., H. Keweloh, and R. K. Thauer (1981), Factor F420 degradation in methanobacterium-thermoautotrophicum during exposure to oxygen, *FEMS Microbiology Letters*, 12(4), 347–349. 148
- Schweizer, M., J. Fear, and G. Cadisch (1999), Isotopic (^{13}C) fractionation during plant residue decomposition and its implications for soil organic matter studies, *Rapid Communications in Mass Spectrometry*, 13(13), 1284–1290, doi: [10.1002/\(SICI\)1097-0231\(19990715\)13:13<1284::AID-RCM578>3.0.CO;2-0](https://doi.org/10.1002/(SICI)1097-0231(19990715)13:13<1284::AID-RCM578>3.0.CO;2-0). 217
- Scott, K. J., C. A. Kelly, and J. W. M. Rudd (1999), The importance of floating peat to methane fluxes from flooded peatlands, *Biogeochemistry*, 47(2), 187–202, doi: [10.1023/A:1006142026171](https://doi.org/10.1023/A:1006142026171). 4, 38, 149, 181, 224
- Shannon, R. D., and J. R. White (1994), 3-year study of controls on methane emissions from 2 Michigan peatlands, *Biogeochemistry*, 27(1), 35–60, doi: [10.1007/BF00002570](https://doi.org/10.1007/BF00002570). 148
- Statistics Canada (2005), Electric power generation, transmission and distribution, *Tech. Rep. 57-202-XIE*, Statistics Canada, Manufacturing, Construction and Energy Division. 1

- Stevens, C. L. R., D. Schultz, C. Vanbaalen, and P. L. Parker (1975), Oxygen isotope fractionation during photosynthesis in a blue-green and a green-alga, *Plant Physiology*, 56(1), 126–129. [68](#), [90](#), [119](#)
- St.Louis, V. L., C. A. Kelly, É. Duchemin, J. W. M. Rudd, and D. M. Rosenberg (2000), Reservoir surfaces as sources of greenhouse gases to the atmosphere: A global estimate, *Bioscience*, 50(9), 766–775. [1](#), [7](#), [10](#), [16](#), [24](#), [38](#), [149](#), [161](#), [180](#), [192](#), [193](#)
- St.Louis, V. L., J. W. M. Rudd, C. A. Kelly, R. A. Bodaly, M. J. Paterson, K. G. Beaty, R. H. Hesslein, A. Heyes, and A. R. Majewski (2004), The rise and fall of mercury methylation in an experimental reservoir, *Environmental Science & Technology*, 38(5), 1348–1358, doi: [10.1021/es001924p](https://doi.org/10.1021/es001924p). [2](#), [4](#), [23](#), [180](#), [181](#), [182](#), [184](#), [187](#), [189](#), [190](#), [191](#)
- Strack, M., E. Kellner, and J. M. Waddington (2005), Dynamics of biogenic gas bubbles in peat and their effects on peatland biogeochemistry, *Global Biogeochemical Cycles*, 19(1), doi: [10.1029/2004GB002330](https://doi.org/10.1029/2004GB002330). [218](#), [219](#)
- Stumm, W., and J. J. Morgan (1996), *Aquatic chemistry*, third ed., Wiley-Interscience. [66](#), [69](#), [186](#)
- Sundh, I., C. Mikkilä, M. Nilsson, and B. H. Svensson (1995), Potential aerobic methane oxidation in a sphagnum-dominated peatland—controlling factors and relation to methane emission, *Soil Biology & Biochemistry*, 27(6), 829–837. [153](#)
- Tadonlélé, R. D., D. Planas, and S. Paquet (2005), Greenhouse gas emissions—fluxes and processes: Hydroelectric reservoirs and natural environments, chap. Bacterial Activity in the Water Column and Its Impact on the CO₂ Efflux, pp. 467–482, Springer-Verlag, Berlin Heidelberg, doi: [10.1007/3-540-26643-7_19](https://doi.org/10.1007/3-540-26643-7_19). [180](#)
- Taylor, B. E., M. C. Wheeler, and D. K. Nordstrom (1984), Stable isotope geochemistry of acid-mine drainage—experimental oxidation of pyrite, *Geochimica et Cosmochimica Acta*, 48(12), 2669–2678, doi: [10.1016/0016-7037\(84\)90315-6](https://doi.org/10.1016/0016-7037(84)90315-6). [69](#)
- Thauer, R. K. (1998), Biochemistry of methanogenesis: a tribute to Marjory Stephenson, *Microbiology*, 144(9), 2377–2406. [41](#), [43](#)
- Tobias, C. R., J. K. Böhlke, and J. W. Harvey (2007), The oxygen-18 isotope approach for measuring aquatic metabolism in high-productivity waters, *Limnology and Oceanography*, 52(4), 1439–1453. [89](#)
- Tockner, K., F. Malard, and J. V. Ward (2000), An extension of the flood pulse concept, *Hydrological Processes*, 14(16-17), 2861–2883, doi: [0.1002/1099-1085\(200011/12\)14:16/17<2861::AID-HYP124>3.0.CO;2-F](https://doi.org/10.1002/1099-1085(200011/12)14:16/17<2861::AID-HYP124>3.0.CO;2-F). [191](#)

- Tokida, T., T. Miyazaki, and M. Mizoguchi (2005), Ebullition of methane from peat with falling atmospheric pressure, *Geophysical Research Letters*, 32(13), doi: [10.1029/2005GL022949](https://doi.org/10.1029/2005GL022949). 219
- Tokida, T., T. Miyazaki, M. Mizoguchi, O. Nagata, F. Takakai, A. Kagemoto, and R. Hatano (2007), Falling atmospheric pressure as a trigger for methane ebullition from peatland, *Global Biogeochemical Cycles*, 21(2), doi: [10.1029/2006GB002790](https://doi.org/10.1029/2006GB002790), tokida, T. Miyazaki, T. Mizoguchi, M. Nagata, O. Takakai, F. Kagemoto, A. Hatano, R. 219
- Tremblay, A., M. Lambert, and L. Gagnon (2004), Do hydroelectric reservoirs emit greenhouse gases?, *Environmental Management*, 33, S509–S517, doi: [10.1007/s00267-003-9158-6](https://doi.org/10.1007/s00267-003-9158-6), suppl. 1. 38, 116
- Tremblay, A., M. Lambert, and C. Demers (2005), Greenhouse gas emissions—fluxes and processes: Hydroelectric reservoirs and natural environments, chap. Introduction, pp. 21–34, Springer-Verlag, Berlin Heidelberg, doi: [10.1007/3-540-26643-7_9](https://doi.org/10.1007/3-540-26643-7_9). 1, 180, 184
- Trumbore, S. (2000), Age of soil organic matter and soil respiration: Radiocarbon constraints on belowground C dynamics, *Ecological Applications*, 10(2), 399–411, doi: [10.1890/1051-0761\(2000\)010\[0399:AOSOMA\]2.0.CO;2](https://doi.org/10.1890/1051-0761(2000)010[0399:AOSOMA]2.0.CO;2). 217
- Turetsky, M. R., R. K. Wieder, and D. H. Vitt (2002), Boreal peatland C fluxes under varying permafrost regimes, *Soil Biology and Biochemistry*, 34(7), 907–912, doi: [10.1016/S0038-0717\(02\)00022-6](https://doi.org/10.1016/S0038-0717(02)00022-6). 217
- Turner, M. A., E. T. Howell, G. G. C. Robinson, P. Campbell, R. E. Hecky, and E. U. Schindler (1994), Roles of nutrients in controlling growth of epilithon in oligotrophic lakes of low alkalinity, *Canadian Journal of Fisheries and Aquatic Sciences*, 51(12), 2784–2793. 17
- UNFCCC (Ed.) (1988), *Report of the Conference of the Parties on its third session, Kyoto, 1 to 11 December 1997. Addendum. Part two: Action taken by the Conference of the Parties at its third session*, FCCC/CP/1997/7/Add.1, UNFCCC, UNFCCC. 3
- Upstill-Goddard, R. C., A. J. Watson, P. S. Liss, and M. I. Liddicoat (1990), Gas transfer velocities in lakes measured with SF₆, *Tellus*, 42, 364–377. 162, 167
- Valentine, D. L. (2002), Biogeochemistry and microbial ecology of methane oxidation in anoxic environments: a review, *Antonie Van Leeuwenhoek*, 81(1–4), 271–282, doi: [10.1023/A:1020587206351](https://doi.org/10.1023/A:1020587206351). 148
- van Dam, O. (2001), Forest filled with gaps. effects of gap size on water and nutrient cycling in tropical rain forest. a study in Guyana, Ph.D. thesis, Utrecht University. 71

- Van de Bogert, M. C., S. R. Carpenter, J. J. Cole, and M. L. Pace (2007), Assessing pelagic and benthic metabolism using free water measurements, *Limnology and Oceanography: Methods*, 5, 145–155. [125](#), [220](#)
- Vannote, R. L., G. W. Minshall, K. W. Cummins, J. R. Sedell, and C. E. Cushing (1980), River continuum concept, *Canadian Journal of Fisheries and Aquatic Sciences*, 37(1), 130–137. [1](#)
- Venkiteswaran, J. J. (2002), A process-based stable isotope approach to carbon cycling in recently flooded upland boreal forest reservoirs, Master's thesis, University of Waterloo, Waterloo. [39](#)
- Venkiteswaran, J. J., and S. L. Schiff (2005), Methane oxidation: isotopic enrichment factors in freshwater boreal reservoirs, *Applied Geochemistry*, 20(4), 683–690, doi: [10.1016/j.apgeochem.2004.11.007](#). [14](#), [21](#), [243](#)
- Venkiteswaran, J. J., L. I. Wassenaar, and S. L. Schiff (2007), Dynamics of dissolved oxygen isotopic ratios: a transient model to quantify primary production, community respiration, and air–water exchange in aquatic ecosystems, *Oecologia*, 153(2), 385–398, doi: [10.1007/s00442-007-0744-9](#). [89](#), [90](#), [91](#), [92](#), [94](#), [96](#), [98](#), [101](#), [109](#), [111](#), [112](#), [116](#), [119](#), [120](#), [124](#), [125](#), [129](#), [130](#), [162](#), [167](#), [220](#), [226](#), [227](#), [228](#), [229](#), [236](#)
- Venkiteswaran, J. J., S. L. Schiff, and L. I. Wassenaar (2008), Aquatic metabolism and ecosystem health assessment using dissolved O₂ stable isotope diel curves, *Ecological Applications*, 18(4), 965–982, doi: [10.1890/07-0491.1](#). [68](#), [125](#), [129](#), [130](#), [131](#), [228](#), [241](#)
- Volk, C., L. A. Kaplan, J. Robinson, B. Johnson, L. Wood, H. W. Zhu, and M. Lechevallier (2005), Fluctuations of dissolved organic matter in river used for drinking water and impacts on conventional treatment plant performance, *Environmental Science & Technology*, 39(11), 4258–4264, doi: [10.1021/es040480k](#). [190](#)
- von Wachenfeldt, E., and L. J. Tranvik (2008), Sedimentation in boreal lakes—the role of flocculation of allochthonous dissolved organic matter in the water column, *Ecosystems*, doi: [10.1007/s10021-008-9162-z](#). [189](#)
- Šantrůčková, H., M. I. Bird, and J. Lloyd (2000), Microbial processes and carbon-isotope fractionation in tropical and temperate grassland soils, *Functional Ecology*, 14(1), 108–114, doi: [10.1046/j.1365-2435.2000.00402.x](#). [217](#)
- Walter, B. P., and M. Heimann (2000), A process-based, climate-sensitive model to derive methane emissions from natural wetlands: Application to five wetland sites, sensitivity to model parameters, and climate, *Global Biogeochemical Cycles*, 14(3), 745–765, doi: [10.1029/1999GB001204](#). [218](#)

- Walter, K. M., S. A. Zimov, J. P. Chanton, D. Verbyla, and F. S. Chapin III (2006), Methane bubbling from Siberian thaw lakes as a positive feedback to climate warming, *Nature*, 443(7107), 71–75, doi: [10.1038/nature05040](https://doi.org/10.1038/nature05040). 44, 218
- Wang, X. F., and J. Veizer (2000), Respiration–photosynthesis balance of terrestrial aquatic ecosystems, Ottawa area, Canada, *Geochimica et Cosmochimica Acta*, 64(22), 3775–3786, doi: [10.1016/S0016-7037\(00\)00477-4](https://doi.org/10.1016/S0016-7037(00)00477-4). 67, 76
- Wang, X. F., and J. Veizer (2004), Erratum to Xuefeng Wang and Jan Veizer (2000), respiration–photosynthesis balance of terrestrial aquatic ecosystems, Ottawa area, Canada. *Geochimica et Cosmochimica Acta* 64(22), 3775–3786, *Geochimica et Cosmochimica Acta*, 68(4), 933–934, doi: [10.1016/S0016-7037\(03\)00490-3](https://doi.org/10.1016/S0016-7037(03)00490-3). 67
- Wanninkhof, R. (1992), Relationship between wind-speed and gas-exchange over the ocean, *Journal of Geophysical Research*, 97(C5), 7373–7382, doi: [10.1029/92JC00188](https://doi.org/10.1029/92JC00188). 93, 118, 164, 165, 169, 171, 186, 219
- Wanninkhof, R., J. R. Ledwell, and W. S. Broecker (1985), Gas exchange–wind speed relation measured with sulfur hexafluoride on a lake, *Science*, 227(4691), 1224–1226, doi: [10.1126/science.227.4691.1224](https://doi.org/10.1126/science.227.4691.1224). 162, 164, 169
- Wanninkhof, R., J. R. Ledwell, W. S. Broecker, and M. Hamilton (1987), Gas-exchange on Mono Lake and Crowley Lake, California, *Journal of Geophysical Research*, 92(C13), 14,567–14,580. 162, 164
- Warner, S. (1999), Social and environmental impacts of the James Bay hydroelectric project, chap. The Cree People of James Bay: Assessing the Social Impact of Hydroelectric Dams and Reservoirs, McGill-Queen’s Press—MQUP. 2
- Wassenaar, L. I., and G. Koehler (1999), An on-line technique for the determination of the $\delta^{18}\text{O}$ and $\delta^{17}\text{O}$ of gaseous and dissolved oxygen, *Analytical Chemistry*, 71(21), 4965–4968, doi: [10.1021/ac9903961](https://doi.org/10.1021/ac9903961). 67, 118
- Watanabe, A., T. Takeda, and M. Kimura (1999), Evaluation of origins of CH_4 carbon emitted from rice paddies, *Journal of Geophysical Research*, 104(D19), 23,623–23,629, doi: [10.1029/1999JD900467](https://doi.org/10.1029/1999JD900467). 161
- Watson, A. J., R. C. Upstill-Goddard, and P. S. Liss (1991), Air–sea gas exchange in rough and stormy seas measured by a dual-tracer technique, *Nature*, 349(6305), 145–147, doi: [10.1038/349145a0](https://doi.org/10.1038/349145a0). 164, 169
- Weiss, R. F. (1970), Solubility of nitrogen, oxygen and argon in water and seawater, *Deep-Sea Research*, 17(4), 721–735. 70, 72

- Welch, E. B., and J. M. Jacoby (2004), *Pollutant Effects in Freshwater: Applied Limnology*, third ed., Spon Press. 89
- Welch, H. E. (1968), Use of modified diurnal curves for measurement of metabolism in standing water, *Limnology and Oceanography*, 13(4), 679–687. 113
- Welch, H. E. (1974), Metabolic rates of arctic lakes, *Limnology and Oceanography*, 19(1), 65–73. 113
- Wetzel, R. G. (1992), Gradient-dominated ecosystems—sources and regulatory functions of dissolved organic matter in freshwater ecosystems, *Hydrobiologia*, 229, 181–198, doi: 10.1007/BF00007000. 189, 190
- Wetzel, R. G. (2001), *Limnology—Lake and River Ecosystems*, Academic Press. 16, 66, 69, 89, 90, 113, 116, 125, 129
- Whalen, S. C., and W. S. Reeburgh (1990), Consumption of atmospheric methane by tundra soils, *Nature*, 346(6280), 160–162, doi: 10.1038/346160a0. 148
- Whiticar, M. J. (1993), Atmospheric methane: Sources, sinks and role in global change, chap. Stable isotopes and global budgets, pp. 138–167, NATO ASI. 148
- Whiticar, M. J. (1999), Carbon and hydrogen isotope systematics of bacterial formation and oxidation of methane, *Chemical Geology*, 161(1-3), 291–314, doi: 10.1016/S0009-2541(99)00092-3. 10, 15, 20, 21, 40, 43, 44, 56, 149, 152, 155
- Whiticar, M. J., and E. Suess (1990), Hydrothermal hydrocarbon gases in the sediments of the King George Basin, Bransfield Strait, Antarctica, *Applied Geochemistry*, 5(1-2), 135–147. 149, 152
- Whiticar, M. J., E. Faber, and M. Schoell (1986), Biogenic methane formation in marine and fresh-water environments: CO₂ reduction vs. acetate fermentation—*isotope evidence*, *Geochimica et Cosmochimica Acta*, 50(5), 693–709, doi: 10.1016/0016-7037(86)90346-7. 10
- Whiting, G. J., and J. P. Chanton (2001), Greenhouse carbon balance of wetlands: methane emission versus carbon sequestration, *Tellus*, 53(5), 521–528, doi: 10.1034/j.1600-0889.2001.530501.x. 161
- Wilcock, R. J., G. B. McBride, J. W. Nagels, and G. L. Northcott (1995), Water-quality in a polluted lowland stream with chronically depressed dissolved oxygen—causes and effects, *New Zealand Journal of Marine and Freshwater Research*, 29(2), 277–288. 113

- Wilcock, R. J., J. W. Nagels, G. B. McBride, K. J. Collier, B. T. Wilson, and B. A. Huser (1998), Characterisation of lowland streams using a single-station diurnal curve analysis model with continuous monitoring data for dissolved oxygen and temperature, *New Zealand Journal of Marine and Freshwater Research*, 32(1), 67–79. [xv](#), [xviii](#), [66](#), [89](#), [97](#), [98](#), [100](#), [108](#), [111](#), [116](#)
- Wilcock, R. J., J. W. Nagels, H. J. E. Rodda, M. B. O'Connor, B. S. Thorold, and J. W. Barnett (1999), Water quality of a lowland stream in a New Zealand dairy farming catchment, *New Zealand Journal of Marine and Freshwater Research*, 33(4), 683–696. [113](#)
- Williams, P., and P. A. del Giorgio (2005), Respiration in aquatic ecosystems, chap. Respiration in aquatic ecosystems: history and background, pp. 1–17, Oxford University. [219](#)
- Williams, P. J. I., and J. E. Robertson (1991), Overall planktonic oxygen and carbon-dioxide metabolisms: the problem of reconciling observations and calculations of photosynthetic quotients, *Journal of Plankton Research*, 13, 153–169, suppl. 1. [116](#), [126](#)
- Williams, R. T., and R. L. Crawford (1984), Methane production in Minnesota peatlands, *Applied & Environmental Microbiology*, 47(6), 1266–1271. [148](#)
- Williamson, C. E., D. P. Morris, M. L. Pace, and A. G. Olson (1999), Dissolved organic carbon and nutrients as regulators of lake ecosystems: Resurrection of a more integrated paradigm, *Limnology and Oceanography*, 44(3), 795–803. [189](#)
- Winter, T. C. (1981), Uncertainties in estimating the water-balance of lakes, *Water Resources Bulletin*, 17(1), 82–115, [doi: 10.1111/j.1752-1688.1981.tb02593.x](#). [169](#)
- Woo, M.-K., and R. D. Rowsell (1993), Hydrology of a prairie slough, *Journal of Hydrology*, 146(1-4), 175–207. [77](#)
- Yan, N. D. (2005), Research needs for the management of water quality issues, particularly phosphorus and oxygen concentrations, related to salmonid cage aquaculture in Canadian freshwaters, *Environmental Reviews*, 13(1), 1–19, [doi: 10.1139/A05-001](#). [66](#)

Colophon

All typesetting was done by the author with \LaTeX using Peter Wilson's memoir class. \LaTeX is a document preparation and typesetting system originally written by Leslie Lamport and is based on Donald Knuth's \TeX typesetting language. The memoir class is an exceptionally well-documented and extensible class that focusses on document design.

The text was set in 11-point URW Palladio L. The original Palatino, designed by Hermann Zapf in 1948–1950, was based on the humanist faces of the Italian Renaissance. These faces typically resemble the characters formed by a broad-nibbed calligraphic pen. Part of the Palatino's beauty is that its proportions are larger than those of Renaissance faces thus making Palatino easy to read. Palatino was digitised and released in 1996 as URW Palladio L. Maths were set in Pazo Math, the symbol font family designed by Diego Puga in 2000–2002 for use with the Palatino family.

Sans serif text in the figures and illustrations is a combination of Nimbus Sans L outlines and unembedded Helvetica, one of the Standard PostScript typefaces. Helvetica is a grotesque face designed in 1957 by Max Miedinger with Edouard Hoffmann. Nimbus Sans L was also designed by Miedinger and released in 1996.

All typefaces embedded in the by PDF file of this thesis (URW Palladio L, Pazo Math, and Nimbus Sans L) were released under the GNU General Public License with the exception of a few mathematical characters of Computer Modern, which was released by the American Mathematical Society under a liberal license.

Illustrations were created with The Gimp and Inkscape. Most graphs were created with MATLAB although some were done with SIGMAPLOT. In retrospect, Octave or Grace may have been equally good choices for graphs, considering that neither MATLAB nor SIGMAPLOT could properly export EPS or PDF files with both the δ and $\%$ characters fully intact. The Gimp, Inkscape, Octave, and Grace were released under the GNU General Public License.

Perhaps paper versions of this thesis will be printed on Forest Stewardship Council certified, or comparably certified, paper.